



HAL
open science

Statistical analysis and modeling of soft or flexible antennas in fluctuating conditions

Jinxin Du

► **To cite this version:**

Jinxin Du. Statistical analysis and modeling of soft or flexible antennas in fluctuating conditions. Electromagnetism. Télécom ParisTech, 2018. English. NNT : 2018ENST0036 . tel-04501004

HAL Id: tel-04501004

<https://telecom-paris.hal.science/tel-04501004v1>

Submitted on 12 Mar 2024

HAL is a multi-disciplinary open access archive for the deposit and dissemination of scientific research documents, whether they are published or not. The documents may come from teaching and research institutions in France or abroad, or from public or private research centers.

L'archive ouverte pluridisciplinaire **HAL**, est destinée au dépôt et à la diffusion de documents scientifiques de niveau recherche, publiés ou non, émanant des établissements d'enseignement et de recherche français ou étrangers, des laboratoires publics ou privés.



Distributed under a Creative Commons Attribution 4.0 International License



EDITE ED 130

Doctorat ParisTech

THÈSE

pour obtenir le grade de docteur délivré par

Télécom ParisTech

Spécialité “Communications & Electronique”

présentée et soutenue publiquement par

Jinxin DU

Le 03/07/2018

Statistical analysis and modeling of soft or flexible antennas in fluctuating conditions

Directeur de thèse : **Christophe ROBLIN**

Jury

M. Ala SHARAIHA , Professeur, IETR - Université de Rennes 1	Président du jury
M. Philippe BESNIER , Directeur de Recherche CNRS, IETR	Rapporteur
M. Hendrik ROGIER , Professeur, Université de Ghent	Rapporteur
M^{me} Shermila MOSTARSHEDI , Maître de conférence, Université Paris-Est Marne-La-Vallée	Examinatrice
M^{me} Odile PICON , Professeur émérite, Université Paris-Est Marne-La-Vallée	Examinatrice
M. Joe WIART , Titulaire de la chaire C2M, Télécom ParisTech	Examineur
M. Christophe ROBLIN , Maître de conférence, Télécom ParisTech	Directeur de thèse

T
H
È
S
E

Télécom ParisTech

école de l'Institut Mines Télécom – membre de ParisTech

46, rue Barrault – 75634 Paris Cedex 13 – Tél. + 33 (0)1 45 81 77 77 – www.telecom-paristech.fr

Statistical Analysis and Modeling of Soft or Flexible Antennas in Fluctuating Conditions

Jinxin DU

Supervisor: Prof. Christophe ROBLIN

Département Communications et Electronique (COMELEC)
Télécom ParisTech (Institut Mines-Télécom and LTCI), Université Paris-Saclay
46 rue Barrault, Paris CEDEX 13, 75634, France

Acknowledgement

I wish to begin this dissertation by expressing my sincere thanks to people who have helped me a lot during the past three and a half years. Without their help, I cannot fulfill my thesis in such an enthusiastic and pleasant way. This thesis was conducted in the RFM (Radio-Fréquences et Micro-ondes) group of the COMELEC (Communications et Electronique) department at Télécom ParisTech.

First of all, I would like to express my greatest gratitude to my supervisor, Prof. Christophe Roblin, who offered me this interesting subject, accompanied me and supported me throughout this important period of my life. He is always available with great patience for discussions whenever I encountered any kind of question or confusion. His encouragement and confidence motivate me to keep moving forward. His rigorous research attitude, extensive expertise and good personal character have impressed me deeply and will also have a far-reaching impact on my future career.

I would also like to thank Prof. Alain Sibille, Prof. Joe Wiart, and Prof. David Lautru who shared their valuable time, experiences and vast knowledge in many fruitful discussions. My appreciation also goes to M. Karim Ben Kalaia and M. Antoine Khy, who helped me a lot in prototyping and experiments. I am especially grateful to Prof. Bruno Sudret' team who offered me the opportunity to use their mathematical toolbox UQLab for academic purpose, which saves me a lot of time for the implementation of numerical algorithms.

I would like to thank the reviewers Prof. Hendrik Rogier and Prof. Philippe Besnier for their extremely admirable work in reviewing my manuscript and writing very relevant evaluation reports. I would also like to thank the examiners Prof. Ala Sharaiha, Prof. Joe Wiart, Prof. Shermila Mostarshedi, and Prof. Odile Picon for their constructive remarks and suggestions on my manuscript, as well as for their valuable discussions in numerous occasions during my thesis.

I am also very grateful to my colleagues in RFM group, M. Xavier Begaud, M. Jean-Christophe Cousin, Mme. Anne-Claire Lepage, M. Bernard Huyart, Mme. Florence Besnard, Mme. Chantal Cadiat and Mme. Yvonne Bansimba for their kind help in a number of ways. I will forever be thankful to my friends Heming Huang, Xin You, Cheng Wang, Wei Wei, Longguang Li, Mengdi Song, Jianan Duan, Jose Enriquez Gonzalez, Chetan Joshi, Taguhi Chalumyan, and Wasyhun Gemechu for their warm company and encouragements during my PhD study.

Finally, I would like to express my deepest gratitude to my family who always accompanies and supports me with unconditional love and care.

Table of contents

List of Figures	VI
List of Tables	IX
List of Acronyms	X
1. Introduction	1
1.1 Motivations.....	1
1.2 Thesis contributions.....	3
1.3 Organization of the thesis	3
2. State of the art	5
2.1 Soft or flexible antennas	5
2.1.1 Mainstream design technologies	5
2.1.2 Advantages and application prospects.....	6
2.1.3 Stochastic characteristics and arising concerns	7
2.1.4 Increasing demand for efficient modeling methods	9
2.2 Literature review for antenna modeling.....	10
2.2.1 FoMs modeling.....	10
2.2.2 Trend of <i>complete</i> FF modeling	12
2.3 Aims to be achieved by our work	12
3. Methodologies for modeling the ATF of variable antennas	14
3.1 Introduction.....	14
3.2 Field parsimony	16
3.2.1 Methods for parsimoniously representing scalar spherical functions.....	17
3.2.1.1 Double Fourier Series (DFS) expansion	17
3.2.1.2 Scalar Spherical Harmonics (SSH) expansion.....	17
3.2.2 Vector Spherical Harmonics (VSH) expansion.....	20
3.2.2.1 Principle	20
3.2.2.2 Test of the performance of VSH.....	21
3.3 Deterministic modeling of ATF: PS	23
3.3.1 Modeling procedures.....	24
3.3.2 Application to a canonical dipole antenna - with one input variable	25
3.3.2.1 Design of a deformable dipole	25
3.3.2.2 Field parsimony with VSH expansion	27
3.3.2.3 Surrogate model extraction	28

3.3.2.4	Model accuracy assessment	28
3.3.2.5	Verification based on interpolation and extrapolation	29
3.3.2.6	Modeling results for severer deformations	30
3.3.3	Application to a canonical dipole antenna - with two input variables.....	32
3.3.4	Discussion	33
3.4	Statistical modeling of the ATFs: PCE.....	34
3.4.1	Introduction	34
3.4.2	Principle of the Polynomial Chaos Expansion (PCE)	35
3.4.2.1	Formulation.....	35
3.4.2.2	Construction of the orthonormal polynomial basis	36
3.4.2.3	Computation of the PCE coefficients.....	37
3.4.2.4	Error indicator for assessing the model accuracy	45
3.4.2.5	Post-processing with PCE model	47
3.4.2.6	Experimental design (ED).....	47
3.4.3	Methodology based on VSH expansion and PCE	49
3.4.3.1	Iterative procedure	50
3.4.3.2	Validation on a canonical dipole antenna	51
3.5	Improvements of the statistical method	54
3.5.1	Frequency behavior	54
3.5.2	Enhanced parsimony	55
3.5.2.1	Sparse VSH expansion.....	56
3.5.2.2	Correlation analysis on the selected dominant VSH modes	57
3.5.3	Appropriate metrics	58
3.5.4	Iterative modeling procedure.....	59
3.5.5	Application to a realistic deformable textile patch antenna.....	60
3.5.5.1	Design of the textile patch antenna	61
3.5.5.2	Joint distribution of the random input parameters	61
3.5.5.3	Pre-evaluation of the ATFs.....	70
3.5.5.4	Prototyping and control measurements	71
3.5.5.5	Preliminary study: sensitivity analysis.....	72
3.5.5.6	Modeling procedure and results	73
3.5.5.7	Validation of the surrogate model.....	75
3.5.5.8	Application examples of the surrogate model.....	77
3.5.5.9	Discussion about the model accuracy	78
3.5.5.10	Discussion about the computational cost	79
3.6	Conclusion	80

4. Antenna surrogate models in radio links analysis	82
4.1 Introduction.....	82
4.2 Effective performance of terminal antenna.....	83
4.3 Local propagation environments	84
4.4 Effective performance and discussion	86
4.4.1 Relative Effective Gain (REG).....	86
4.4.2 Relative Average EG (RAEG) in sub-bands	89
4.4.3 RAEG for restricted azimuthal DoAs.....	91
4.5 Conclusion	93
5. Statistical modeling of the reflection coefficient of variable antennas	94
5.1 Introduction.....	94
5.2 Identification.....	95
5.2.1 Technique 1: Polynomial fitting.....	95
5.2.2 Technique 2: Levy's complex curve fitting with rational functions.....	96
5.3 Surrogate model extraction.....	96
5.4 Applications	97
5.4.1 Application to a canonical dipole	97
5.4.2 Application to a textile patch.....	99
5.5 Conclusion	102
6. Conclusions and Perspectives	104
6.1 Conclusions.....	104
6.2 Perspectives	105
References	107
Publications.....	119
Annex.....	120
I. Introduction.....	120
II. CPW-Fed IIFA on FR4 Substrate.....	122
a. Design of the antenna	122
b. Simulation and measurement results	122
III. CPW-Fed IIFA on FR4 Substrate	125
a. Design of the antenna	125
b. Simulation results	126
c. Test on a body phantom	127
IV. Conclusion	128

Reference	128
Résumé français.....	131

List of Figures

Figure 1.1: IoT electronic devices growth forecasted by IHS (Information Handling Services) 2016.	1
Figure 2.1: Some existing application examples of wearable antennas: (a) health monitoring; (b) smart T-shirt for athletes; (c) smart garment for fire fighters; (d) smart gloves for remote controlling.	7
Figure 2.2: Schematic of a transmitting antenna, fed by a source of internal impedance Z_g , via a transmission line of characteristic impedance Z_c . a_I, b_I are respectively the incident and reflected partial wave. P_{inc}, P_r , and P_a are respectively the incident, reflected, and received power by the antenna. P_{loss} is the conductive & dielectric power loss of the antenna, and P_{rad} is the radiated power by the antenna. k is the vector wave number. $\mathbf{r} = (\theta, \varphi)$ is the unit radial vector. $E_{rad}(\mathbf{r})$ is the electric FF.	10
Figure 2.3: Antenna surrogate models for higher lever analysis.	13
Figure 3.1: Principle of the “Two-Step” approach for modeling the ATF of variable antennas..	15
Figure 3.2: Patch antenna used for field parsimony test.	19
Figure 3.3: SSH expansion applied on the total realized gain $G_r(\theta, \varphi)$ of a patch antenna: (a) initial G_r ; (b) reconstructed G_r with the SSH modes ($N_{SSH} = 5$).	19
Figure 3.4: SSH expansion applied on the polarimetric realized gain $G_{r\varphi}(\theta, \varphi)$ of a patch antenna: (a) initial $G_{r\varphi}$; (b)-(e) reconstructed $G_{r\varphi}$ with the SSH modes ($N_{SSH} = 5, 10, 20$ and 30 respectively).	20
Figure 3.5: VSH expansion applied on the ATF of a patch antenna: (a) initial G_r ; (b) reconstructed G_r with the VSH modes ($N_{VSH} = 5$).	22
Figure 3.6: VSH expansion applied on the ATF of a patch antenna: (a) initial $G_{r\varphi}$; (b) reconstructed $G_{r\varphi}$ with the VSH modes ($N_{VSH} = 5$).	22
Figure 3.7: Surrogate model relating the random input variables and the parsimonious ATF..	23
Figure 3.8: Algorithm flowchart of the parametric study procedure.	25
Figure 3.9: Illustration of the bending phenomenon of a dipole antenna.	26
Figure 3.10: Reflection coefficient $ S_{11} $ of the dipole in different bending states (R_b in mm).	26
Figure 3.11: $RRMSE$ of the reconstructed fields with different approaches.	27
Figure 3.12: Polynomial fitting of the VSH coefficients $H1, 11$ and $H3, 02$	28
Figure 3.13: $RRMSE$ of reconstructed fields with different approaches for 150 random values of the parameter $\kappa \in [0, 1/30]$ mm^{-1}	29
Figure 3.14: G_r patterns of the initial field (both for the straight and curved dipole with $R_b = 10$ mm) and the reconstructed fields with different approaches (only for the curved dipole with $R_b = 10$ mm).	30
Figure 3.15: Polynomial fitting of the VSH coefficient $H1, 01$ (severe bendings: $\kappa \in [0, 1/10]$ mm^{-1}).	31
Figure 3.16: $RRMSE$ of reconstructed fields with different approaches for the most severe bending state.	31

Figure 3.17: <i>RRMSE</i> of reconstructed fields with different approaches for 200 random values of the parameter $\kappa \in [0, 1/10]$ mm ⁻¹	32
Figure 3.18: Illustration of the joint bending & torsion phenomenon of a dipole antenna.....	32
Figure 3.19: <i>RRMSE</i> of reconstructed fields with different approaches for bivariate case.	33
Figure 3.20: The LARS algorithm in the case of $M = 2$ covariates.....	44
Figure 3.21: An example showing the overfitting problem when approximating an empirical sample with high order polynomials.	46
Figure 3.22: Illustration of a dipole undergoing different deformations: (a) original dipole; (b) stretched dipole; (c) curved dipole; (d) curved and twisted dipole.	51
Figure 3.23: Joint effect of stretching, bending, and torsion (ξ, κ, α) on the dipole: (a) reflection coefficient $ S_{11} $; (b) radiation patterns (in E/H plane) at $f = 2.3$ GHz.....	52
Figure 3.24: e_{LLOO} of the PCE models derived from the iteratively enriched EDs.	52
Figure 3.25: (a) Radiation patterns (in E/H plane) of the initial, reconstructed and generated fields for the most deformed case at $f = 2.3$ GHz; (b) <i>RRMSE</i> of 500 generated dipoles for random values of (ξ, κ, α).	53
Figure 3.26: Wearable textile patch antenna: (a) un-deformed plane patch; (b) patch undergoing the joint effect of crumpling, bending and thickness variation.	60
Figure 3.27: Experimental setup (a) and simulation design (b) for bending analysis.	63
Figure 3.28: Center frequency shift under bending ($R_b = 31.75$ mm) for increasing substrate compression $\Delta h/h_0$ (by simulation).	65
Figure 3.29: Statistic of the medium human arm radius, derived from the database 2015-2016 provided by the US National Center for Health Statistics.....	69
Figure 3.30: Experimental setup for measuring the ATFs.	71
Figure 3.31: Three representative patches for which: the prototypes, the simulated/measured reflection coefficient $ S_{11} $, and the simulated/measured G_r at 2.45 GHz in principal cut-planes for the co-polarization and cross-polarization components are presented in columns.....	72
Figure 3.32: S_{WT} of the 6 random input parameters.....	73
Figure 3.33: ATF reconstruction errors for different power threshold $E_{c,\text{th}}$	74
Figure 3.34: Prediction error e_{WTLOO} of surrogate models iteratively constructed by enriching the ED.....	75
Figure 3.35: Comparison between the errors of two successive surrogate models for different EDs.	75
Figure 3.36: Error of the model-generated ATFs w.r.t. the reference MC sample.	76
Figure 3.37: EM-simulated (left column) and model-generated (right column) G_r patterns for a representative average-error configuration.....	77
Figure 3.38: EM-simulated (left column) and model-generated (right column) G_r patterns for a representative maximal-error configuration.	77
Figure 3.39: Comparison between the CDFs of: (a) -10 dB beamwidth, (b) maximal G_{r0} computed from the model and EM-simulations from the MC sample.....	78

Figure 3.40: Prediction error e_{WTLOO} of surrogate models iteratively constructed by enriching the ED till large cardinal.	79
Figure 3.41: Comparison between the CDFs of the model-generated and the EM-simulated dominant VSH coefficients from the MC sample.	79
Figure 4.1: Illustration of the radio link of a wireless communication system.	83
Figure 4.2: CDFs of the relative effective gain of the textile patch antenna in different propagation environments: color thin lines – partial CDFs; red thick line – global CDF.	87
Figure 4.3: Allowable sub-bands for WiFi standard in the 2.4 – 2.5 GHz range.	89
Figure 4.4: CDFs of the relative average effective gain of the textile patch antenna in different propagation environments: color thin lines – partial CDFs; red thick line – global CDF.	90
Figure 4.5: CDFs of the relative average effective gain of the textile patch antenna ($\mu_\varphi \sim \mathcal{U}([-90^\circ, 90^\circ])$) in different propagation environments: color thin lines – partial CDFs; red thick line – global CDF.	92
Figure 5.1: Dipole – Approach I: (a) e_{LOO} of the PCE models of characteristic parameters for different ED; (b) err of reconstruction in case of $N_{ED} = 260$	98
Figure 5.2: Dipole – Approach I: comparison of the frequency responses of the initial, the identified (with polynomial fitting), and the final surrogate model for: (a) the worst case (i.e. with maximal err); (b) the median case (i.e. with median err).	98
Figure 5.3: Dipole – Approach II: (a) e_{LOO} of the PCE models of characteristic parameters for different ED; (b) err of reconstruction in case of $N_{ED} = 120$	99
Figure 5.4: Dipole – Approach II: comparison of the frequency responses of the initial, the identified (with Levy's), and the final surrogate model for: (a) the worst case (i.e. with maximal err); (b) the median case (i.e. with median err).	99
Figure 5.5: Textile patch undergoing random variations in length, bending radius, substrate height and permittivity.	100
Figure 5.6: Patch – Approach I: (a) e_{LOO} of the PCE models of characteristic parameters for different ED; (b) err of reconstruction in case of $N_{ED} = 200$	100
Figure 5.7: Patch – Approach II: (a) e_{LOO} of the PCE models of characteristic parameters for different ED; (b) err of reconstruction in case of $N_{ED} = 280$	100
Figure 5.8: Patch – Approach I: comparison of the frequency responses of the initial, the identified (with polynomial fitting), and the final surrogate model for: (a) the worst case (i.e. with maximal err); (b) the median case (i.e. with median err).	101
Figure 5.9: Patch – Approach II: comparison of the frequency responses of the initial, the identified (with Levy's), and the final surrogate model for: (a) the worst case (i.e. with maximal err); (b) the median case (i.e. with median err).	101

List of Tables

Table I: Some examples of planar soft/flexible antennas [24]-[27], [4].	6
Table II: Parametric study of a deformable dipole: input parameters, modeling parameters and results.	33
Table III: Random input parameters of the textile patch.	61
Table IV: K-S test on the 27 dominant VSH coefficients.	79
Table V: Characteristics of 4 WINNER2/+ propagation environments.	86
Table VI: Statistics of the relative effective gains.	87
Table VII: Statistics of the relative average effective gains.	90
Table VIII: Statistics of the relative average effective gains ($\mu_\varphi \sim \mathcal{U}([-90^\circ, 90^\circ])$).	92
Table IX: Design parameters and variability range for the textile patch.	100

List of Acronyms

AMPS	Advanced Mobile Phone System
ANN	Artificial Neural Networks
ANOVA	Analysis of Variance
ATF	Antenna Transfer Function
AUT	Antenna Under Test
CAD	Computer Aided Design
CDF	Cumulative Density Function
CP	Co-Polarization
DFS	Double Fourier Series
DoA	Directions of Arrival
ED	Experimental Design
EG	Effective Gain
EM	Electromagnetic
FDTD	Finite-Difference Time-Domain
FEM	Finite Element Method
FF	Far Field
FoM	Figures of Merit
GNSS	Global Navigation Satellite Systems
gPCE	generalized Polynomial Chaos Expansion
GPR	Gaussian Process Regression
GPS	Global Positioning System
GQ	Gaussian Quadrature
HLARS	Hybrid Least Angle Regression Sampling
IFA	Inverted F-shape Antenna
IIFA	Integrated IFA
IoT	Internet of Things
ISM	Industrial Scientific Medical
LARS	Least Angle Regression Sampling
LCP	Liquid-Crystal Polymer
LHS	Latin Hypercube Sampling
LOOE	Leave-One-Out Error
LOS	Line-Of-Sight
LTI	Linear Time Invariant
MC	Monte-Carlo
MCS	Monte Carlo Sampling
MEG	Mean Effective Gain
MIMO	Multiple-Input and Multiple Output
NB	Narrow-Band
NLOS	Non-Line-Of-Sight
OLS	Ordinary Least Square
PCE	Polynomial Chaos Expansion
PDF	Probability Density Function
PDMS	Polydimethylsiloxane
PEC	Perfect Electrical Conductor

PET	Polyethylene Terephthalate
PS	Parametric Study
PTFE	Polytetrafluoroethene
QoS	Quality of Service
RAEG	Relative Average Effective Gain
REG	Relative Effective Gain
RMSE	Root Mean Square Error
RRMSE	Relative Root Mean Square Error
SCM	Stochastic Collocation Method
SEM	Singularity Expansion Method
SSH	Scalar Spherical Harmonics
ST	Stochastic Testing
SVR	Support Vector Regression
TE	Transverse Electric
TF	Transfer Function
TM	Transverse Magnetic
TSI	Total Sobol's Indices
UE	User End
UWB	Ultra-Wideband
VNA	Vector Network Analyzer
VSH	Vector Spherical Harmonics
WBAN	Wireless Body Area Network
WLAN	Wireless Local Area Network
XP	Cross-Polarization
XPR	Cross-Polarization power Ratio

Chapter 1

1. Introduction

1.1 Motivations

Since 1980s when the first generation (1G) of mobile communication standard (i.e. Advanced Mobile Phone System, AMPS, developed by Bell Labs) came out, wireless communication technologies have achieved leaping growth and have brought great convenience into people's life. Today, people are highly dependent on all kinds of wireless services such as the cellular networks (e.g. 2G, 3G, 4G), the GNSS (Global Navigation Satellite Systems, e.g. the Global Positioning System or GPS), the Wireless Local Area Networks (WLANs, e.g. Wi-Fi), and the Wireless Body Area Networks (WBANs, e.g. Wi-Fi, Bluetooth, ZigBee). The pace of revolution has never stopped and is even much faster than ever before. We are now almost ready to welcome the 5G technology thanks to which not only people but also many "things" (e.g. machines, vehicles, sensors...) will be connected, forming an immense Internet of Things (IoT). The IoT is supposed to contribute to an "intelligent" world (e.g. smart grid, intelligent transportation, real-time health care, intelligent home, office, factory, etc.) and to improve the quality of people's life to a large extent. With the pervasive expansion of wireless technologies, the requirement for wireless electronic devices will certainly experience explosive growth in coming years. Figure 1.1 shows the prediction of IoT devices growth in the next 10 years [1].

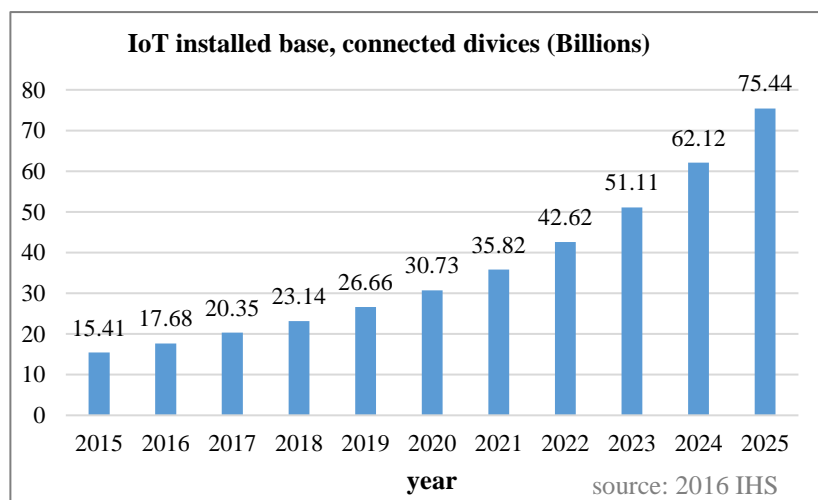


Figure 1.1: IoT electronic devices growth forecasted by IHS (Information Handling Services) 2016.

Being the unique interface to communicate with the outside, antenna is extremely vital component for all wireless electronic devices. Successes in wireless communication industry would have not been achieved without the continuing advances in antenna technology. In recent years, antennas have the trend to be highly integrated, miniaturized, and arrayed in order to meet with the challenging demand of massive deployment, short R&D cycle, low cost and high performance. Moreover, some other advantageous properties are also indispensable in specific application scenarios. In particular, in the context of WBANs where antennas should be integrated into garments or pasted directly onto the human body, softness or flexibility permitting them to conform to various body shapes and sizes would be really useful.

However, softness or flexibility implies geometric deformation (e.g. bending, torsion, crumpling...) which can drastically perturb the behavior (e.g. radiation pattern, impedance...) of antennas. The perturbed antennas are no longer *fixed* or *static*, but *varying* or *dynamic* seeing that their behavior is varying randomly during the operation. In addition to self-deformations, external randomness from the close (possibly fluctuating) environment can also disturb antennas. For example, variation of the temperature and humidity may cause changes of antennas' material properties such as the permittivity and conductivity; nearby surroundings, notably the human body, could perturb antennas' nearfield zone resulting in strong absorption, reflection, scattering, or the joint effect of them. This effect becomes remarkable as antennas become miniaturized.

Nowadays, with the widespread use of *flexible electronics* (such as textile electronics) and the increasing complexity of operating environments, the presence of randomness and uncertainties on the antennas is more realistic than ever before in almost all application contexts. This brings severe challenges in antenna design as well as radio links analysis. How to characterize antennas' *in situ* performance becomes an inescapable concern and is attracting increasing attention. Moreover, in order to guarantee the *in situ* functionality of antennas, the traditional solution is to add an ad hoc gain margin to roughly account for those random effects that can be encountered in real world. However, this usually induces high cost and waste of precious space and/or power resources. To avoid excessive margin values, quantitatively and precisely characterizing the behavior of perturbed antennas is indispensable and is attracting increasing attention of antenna engineers.

Conventionally, the characterization of a classical deterministic antenna (e.g. rigid or large sized, or clearly isolated, etc.) can be carried out by means of measurements or full-wave simulations. Yet, this approach becomes inappropriate for antenna problems under uncertain conditions where a large number of random sources intervene. Indeed, the combinatory of situations can be so explosive that executing measurements or simulations

one by one would be too time-consuming and even physically impossible for us at this time. Under such circumstances, more efficient characterization approaches are urgently required.

This thesis is dedicated to investigate efficient methodologies for quantitatively analyzing and modeling the random effects on the “*overall*” behavior, i.e. the *complete* radiated Far Field (FF) as well as the reflection coefficient, of soft or flexible antennas in fluctuating conditions. Notably, statistical methodologies which provide good modeling accuracy while minimizing the modeling cost are presented. The principle is to try to carry out only very limited number of pre-evaluations (by measurement or simulation), and make full use of them to extract efficient surrogate models for the prediction in other possible situations. The applicative perspectives of such surrogate models are to substitute real antennas or cumbersome full-wave simulations in various types of analyses, notably when the *complete* knowledge (including polarization, amplitude and phase of the field) of the antenna under study is mandatory. Such application contexts comprise for example, joint antenna/directional channel modeling, antenna plugged-in asymptotic simulators (e.g. ray tracing), radio links analysis, MIMO (Multiple-Input and Multiple Output) systems characterization, and beamforming designs.

1.2 Thesis contributions

This thesis is focused on the investigation of efficient methodologies for quantitatively characterizing the “*overall*” behavior of soft/flexible or disturbed antennas that are subject to random uncertainties. The main topics covered are:

- Parsimonious description of the antenna’s *complete* radiated Far Field (FF) or its equivalent, the Antenna Transfer Function (ATF).
- Deterministic methodology for quantitatively modeling the ATF.
- Statistical methodology for quantitatively modeling the ATF in multivariate cases.
- Statistical methodology for quantitatively modeling the antenna’s reflection coefficient $S_{11}(f)$ in multivariate cases.
- Investigation of the usage of antenna surrogate models for radio links analysis, where antenna models are implemented in typical stochastic propagation environments.

1.3 Organization of the thesis

The organization of this thesis is as follows:

Chapter 2 introduces the state of the art of soft or flexible antennas. In the first part, the design technologies, the advantages and broad application prospects, as well as the arising concerns of soft or flexible antennas are briefly introduced. In the second part, the state of the

art on antenna modeling is reviewed, and the aims that we want to achieve in this thesis are outlined.

Chapter 3 proposes methodologies for modeling the antenna's *complete* radiated FF or ATF. First, the field parsimony technique based on the Vector Spherical Harmonics (VSH) expansion is introduced. Then, deterministic as well as stochastic modeling methodologies are proposed. All methodologies have a *Two-Step* process, that is, field parsimony followed by surrogate model extraction. The deterministic methodology is a combination of the VSH expansion and the conventional parametric study; and the statistical methodology is a combination of the VSH expansion and the advanced Polynomial Chaos Expansion (PCE) method.

Chapter 4 investigates the utility of accurate antenna surrogate models for radio links analysis, where the antenna's effective performance is quantified by taking into account both the inherent uncertainties of the antenna itself and those from the stochastic local propagation environments.

Chapter 5 presents a statistical methodology for modeling the complex reflection coefficient $S_{11}(f)$ of narrow-band (NB) variable antennas. This approach is splitted into two steps: identification, and model extraction using the PCE method.

Chapter 6 summarizes the work realized during this thesis and presents some perspectives for future researches.

Chapter **2**

2. State of the art

This chapter presents the research context of this thesis. Firstly, the soft or flexible antennas technology and their broad application prospects are briefly introduced. The arising concerns related to the stochastic characteristics of soft/flexible antennas are also explained. Then, the increasing demand for efficient modeling methods is discussed. Finally, the state of the art on antenna modeling is reviewed, and the aims that we want to achieve in this thesis are outlined.

2.1 Soft or flexible antennas






2.1.1 Mainstream design technologies

“Soft/flexible antennas” is a relative concept with respect to classical non-deformable rigid antennas. Generally, this term refers to a broad category of antennas made of soft or flexible materials whose geometric shape can be more or less changed for purpose of gaining some flexibility during usage. Such kind of flexibility is in high demand not only in a priori unknown application contexts (e.g. uncertainty due to the morphological distribution of the user population), but also for “dynamic” situations where real-time flexibility is mandatory (e.g. time-varying geometric deformations due to movement).

Typical representatives of soft/flexible antennas are those planar shape antennas designed for wearable communications. These antennas are composed of thin soft/flexible conductive layers as their ground plane and radiating part, and dielectric layers as their substrate part. Popularly adopted conductive materials include copper foil, conductive fibers (or *E-fibers*, e.g. copper-, silver- or nickel-plated), conductive inks, and graphene, etc. [2]-[7]. As for the dielectric material, textiles such as denim, cotton, yarn, fleece, etc. are the most common used because of their low-cost, drapability and biocompatibility [8]. In addition, paper, rubber, polymers (e.g. LCPs (liquid-crystal polymers), PDMS (polydimethylsiloxane), PET (polyethylene terephthalate) and PTFE (polytetrafluoroethene), etc.) are also good candidates for dielectric materials [9]-[13]. These thin layers are integrated to realize the specified structure using proper assemblage technologies such as adhesive laminating, sewing, embroidery, screen-printing, ink-jet, and evaporation deposition [2], [14], [15]. In recent years, studies addressing such antennas are more than abundant. Some examples are given in Table I.

Other types of soft/flexible antennas include those classic bendable or foldable wire antennas, as well as those recently emerging micro-fluidic antennas which encapsulate conductive liquids in flexible plastic structures [16]-[19]. Tunable antennas (or antenna arrays) whose “electrical shape” is reconfigurable may also be considered as somewhat “soft/flexible” [20]-[23].

Table I: Some examples of planar soft/flexible antennas [24]-[27], [4].

Photo	Conducting part	Dielectric part	Assemblage
	copper tape	denim	adhesive
	single-walled carbon nanotube composite	paper	inkjet printing
	silver loaded epoxy	PDMS	inkjet printing
	copper and nickel coated fibers	felt	adhesive
	E-fibers	polymer composites	embroidery

2.1.2 Advantages and application prospects

Compared with traditional non-deformable rigid antennas, soft/flexible antennas have some unparalleled advantages namely:

- Deformability/conformability (e.g. stretchability, flexibility, compressibility, drapability) or re-configurability.
- Lightness.
- Low-profile (non-protruding, unobtrusiveness).
- Washability and long-lasting.
- Low-cost.

All these benefits greatly improve the user experience of electronic devices in terms of comfort, beauty and economy, hence making them ideal candidates notably for the explosively emerging *on-body/off-body* WBAN applications. Figure 2.1 illustrates some existing or developing applications of soft/flexible antennas in the framework of WBANs [28]-[31]. It can be seen that many human activity domains are covered: health care – monitoring of the physiological signals such as heart rate, breathing rate, brain wave, blood

pressure, and body temperature, etc. of patients; sportive activities – monitoring of those fitness parameters of the athletes; security/emergency – positioning, and monitoring of the vital signals of fire fighters; and entertainment – remote controlling in virtual reality and computing games.

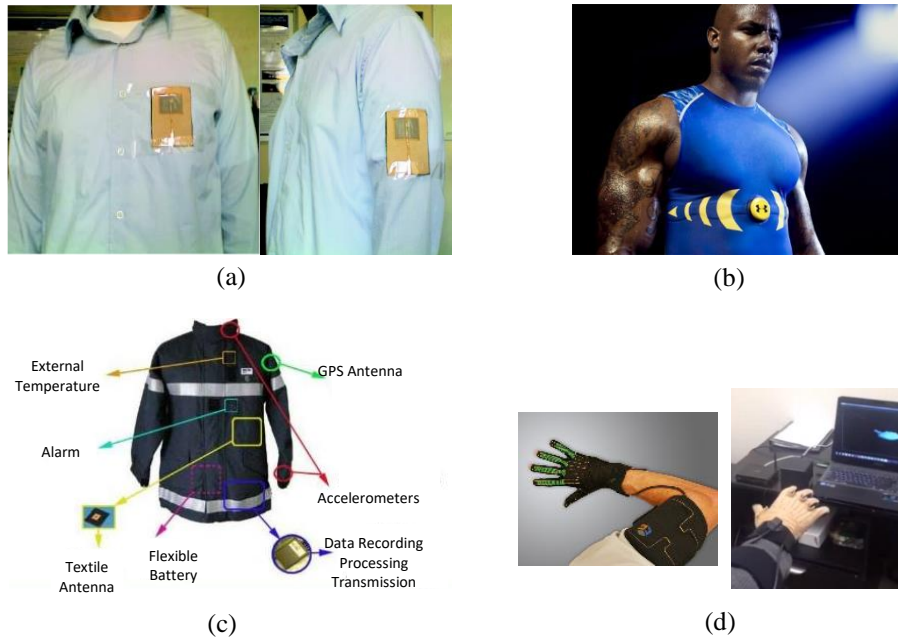


Figure 2.1: Some existing application examples of wearable antennas: (a) health monitoring; (b) smart T-shirt for athletes; (c) smart garment for fire fighters; (d) smart gloves for remote controlling.

2.1.3 Stochastic characteristics and arising concerns

However, just as everything has its two sides, despite the advantages mentioned above, the softness/flexibility is accompanied by negative effects that would not occur (at least not significantly) for non-deformable rigid antennas. In fact, the performance of the latter is conventionally considered to be totally determined by the directivity and the radiation patterns of the transmitting & receiving antennas once they are aligned. By contrast, under the condition of softness/flexibility, the electromagnetic (EM) characteristics of antennas are no longer fixed, but are time-varying, often in a stochastic manner, with regard to the uncertainties coming from some intrinsic and/or external sources. Typically, such random uncertainties can take place in both the fabrication and the usage phase. In the former phase, random uncertainties are introduced due to:

- The imprecision of the characterization of material properties. Note that for most of the soft/flexible materials, their EM properties are not as stable as those of the materials used for non-deformable rigid antennas due to the inhomogeneity and variability, hence they can only be quantified statistically and globally, inevitably introducing some uncertainties.

- The fabrication tolerances. On the one hand, the geometrical precision that can be achieved by existing technologies for soft/flexible materials is far less than that for rigid materials; on the other hand, the fabrication procedure particularly the assemblage step would exert parasite stresses (e.g. compression, creasing, stretching, etc.) inside the material, causing random variability in the material properties as well as on antennas' geometric shape.

And during the usage phase, random uncertainties are caused by:

- The global geometric deformations (e.g. bending, torsion, crumpling, thinning, elongation, etc.) which are caused by external forces and which induce variations in the current distribution and possibly of the material properties of the considered antenna.
- The morphological distribution of the user population, in terms of age (baby, child, teen, adult, senior), gender (male/female), posture (sitting, standing, walking...), device placement (arm, wrist, chest, shoulders, back...), etc.
- The fluctuating environment, whose influence is twofold: first, the temperature and humidity (from moisture, rain, etc.) may cause significant variations in material properties (e.g. conductivity and permittivity); second, the proximity effect of immediate surroundings notably the human body could drastically perturb the reactive near-field of the considered antenna, causing strong effect of absorption, blockage, and reflection, etc. [32], [33]. In such situation, the immediate environment cannot be discriminated from the antenna itself. In other words, the antenna plus its immediate surroundings turn into a new "effective antenna". Therefore, all randomness due to the interaction between the antenna and its neighboring surroundings must be considered as inherent stochastic characteristics of the new "effective antenna".
- The operational frequencies. Apparently, when an antenna operates over different frequency bands its behavior can be quite different. This effect can be considered as a stochastic influence seeing that nowadays many electronic devices support multi-bands (even the so-called "full bands") allowing to switch between frequencies (or even to use carrier aggregation of the signal over non-contiguous spectrum allocations, e.g. in LTE Advanced) according to the supervised real-time channel quality, while the sub-band selection is by essence random.

Additionally, it is worth pointing out that the stochastic properties of the local propagation environment of a considered antenna, that's to say, the spatial and polar distribution of the multipath incoming waves, also have strong influence on the effective performance of the antenna. However, this aspect of uncertainty can be discriminated from those *inherent* antennas uncertainties, and can be characterized separately by stochastic

channel models (cf. Chapter 4 for more thorough discussion). Therefore, this aspect of uncertainty will not be included in our investigations. Henceforward, for sake of clarity, we call the antennas whose behavior/characteristics vary randomly during their operation due to their *inherent* uncertainties as “*Variable antennas*”. This would include those soft/flexible antennas and other types of deformable antennas, as well as those proximity-interacted/disturbed antennas.

Those aforementioned inherent uncertainties can result in drastic changes in the behavior of a given variable antenna, for example:

- Impedance mismatch or detuning.
- Radiation efficiency degradation (due to absorption).
- Re-direction or distortion of the radiation pattern (polarization, amplitude and phase).

Clearly, to ensure the reliable operation of a variable antenna, we have to quantitatively characterize those random effects.

2.1.4 Increasing demand for efficient modeling methods

Conventionally, for designing or characterizing a “classical” deterministic antenna (such as a non-deformable rigid, or large-sized, or clearly isolated one), a canonical process combining full-wave simulations with prototyping & measurements is often adopted. Concretely, preliminary analyses based on full-wave simulations (using some commercially available simulators e.g. HFSS, CST, etc. or self-implemented numeric algorithms e.g. FEM (Finite Element Method), FDTD (Finite-Difference Time-Domain), etc.) are firstly carried out to visualize the behavior of the antenna under study and eventually, a parametric analysis can be applied for a rough search of the optimal parameters. Then, some prototypes are fabricated, and their typical characteristics (e.g. radiation pattern, reflection coefficient S_{11}) are measured to bring to light the realistic performance of the antenna. After that, modifications on design parameters can be made if necessary, and eventually a new round of test could be launched.

However, this process becomes completely incapable for variable antenna problems since the combinatory of random-uncertainties-involved situations can be so explosive that the characterization cost could immediately surpass one’s affordability. Therefore, more appropriate modeling methods which allow to efficiently characterizing those random effects with good precision are of paramount importance, especially in the application contexts of:

- Predicting the real *in situ* performance of variable antennas.
- Acquiring better precision in the assessment of end-to-end radio links performance.
- Saving the cost of maintenance.
- Accelerating the design cycle of an application-dependent variable antenna.

2.2 Literature review for antenna modeling

Antenna modeling aims to efficiently characterize the impact of those random uncertainties on the antenna's behavior. The modeling of variable antennas date as early as the pioneering work of Shifrin in late sixties [34]. More attention has been paid to these issues notably during the last decade (see e.g. [35]). Most of the existing researches had focused on the modeling of some primary relevant characteristics of antennas, for example, the total efficiency, reflection coefficient/impedance, resonant frequency, beamwidth, axe ratio, maximal realized gain, etc. These scalar quantities, also referred as Figures of Merit (FoMs) of interest, describe either partially or averagely the behavior of a given antenna, and a good knowledge on them is often sufficient for most of classical application contexts. Recently, with the increasing demand for *complete* antenna models (i.e. containing the precise information of polarization, amplitude and phase of the field) in e.g. joint directional channel/antenna, MIMO (Multiple-Input and Multiple Output) system or beamforming analysis, an *overall* modeling that must comprise both the *complete* radiated Far Field (FF) and the reflection coefficient (which describe respectively the full transmission and reflection properties of the considered antenna, see Figure 2.2) becomes a highly relevant and timely topic.

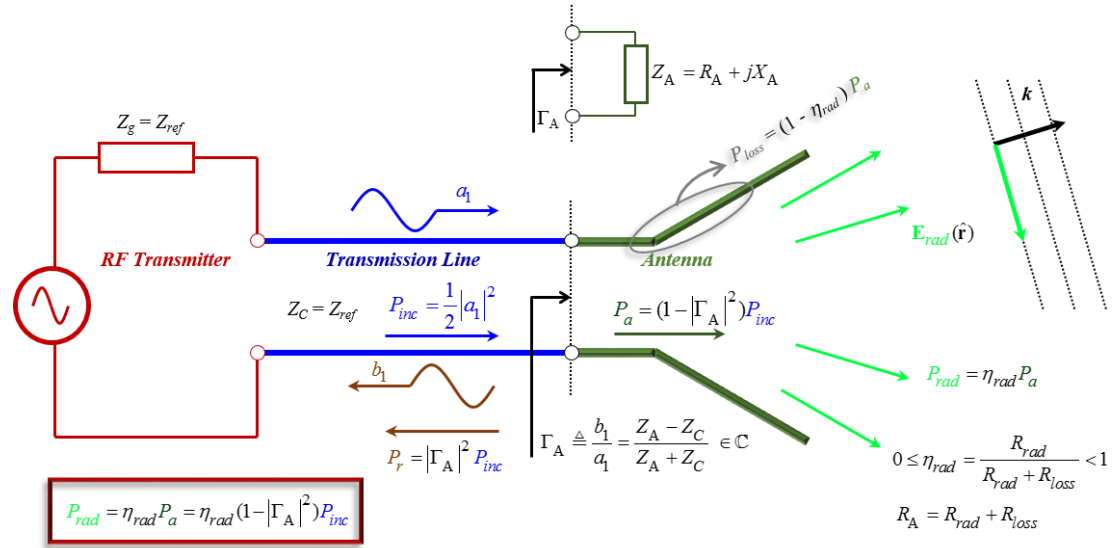


Figure 2.2: Schematic of a transmitting antenna, fed by a source of internal impedance Z_g , via a transmission line of characteristic impedance Z_c . a_1 , b_1 are respectively the incident and reflected partial wave. P_{inc} , P_r , and P_a are respectively the incident, reflected, and received power by the antenna. P_{loss} is the conductive & dielectric power loss of the antenna, and P_{rad} is the radiated power by the antenna. \mathbf{k} is the vector wave number. $\hat{\mathbf{r}} = (\theta, \varphi)$ is the unit radial vector. $\mathbf{E}_{rad}(\hat{\mathbf{r}})$ is the electric FF.

2.2.1 FoMs modeling

The Monte-Carlo (MC) method, due to its simplicity, was first used, e.g. in [36], to assess the statistics of some FoMs of interest for the considered problems. However, the computational cost of MC is high, even prohibitive for some EM problems as it requires a

large number of realizations due to its slow convergence ($\mathcal{O}(1/\sqrt{N})$, N being the number of realizations). Moreover, MC is not effective for sensitivity analysis, i.e. for quantifying the significance of each random effect.

Quite recently, more efficient statistical approaches have been proposed, allowing to quantitatively account for those random effects.

For instance, in [37] the analysis of variance (ANOVA) method combined with a regression technique is used to characterize the individual and joint effect of bending, shearing and stretching on the bandwidth of a textile antenna.

In [38], the randomness in antenna design parameters was addressed by means of small signal analysis, which expands the FoMs of interest as a Taylor series of the design parameters. This approach is mainly suited for relatively small random variations of the input parameters.

Support Vector Regression (SVR) had also been used for antenna modeling. FoMs that have been characterized in this manner include e.g. the impedance (at the resonant frequency) of a microstrip patch antenna [39], and the axial ratio of a circularly polarized antenna against variable design parameters [40]. In general, the SVR has advantage of mapping to convex quadratic optimization problems hence it does not suffer from local minima, but it might not be very efficient for highly non-linear multiple input problems. An improved approach combining the Gaussian process regression with the standard SVR was proposed in [41] and had been used to model the reflection coefficient of a square slot antenna against the frequency as well as some tunable geometry variables. This approach is more robust than the classic SVR against strong non-linearity.

Artificial Neural Networks (ANNs) also gains great consideration in antenna design and modeling problems [42]. For example, in [43] and [44] the resonant frequency, in [45] and [46] the input impedance, and in [47] the radiation pattern as well as the reflection coefficient of the considered antennas against variable design parameters were successfully modeled with ANNs. However, ANNs is a rather complicated method that is not straightforward to implement due to the lack of effective methods for determining the number of hidden layers and nodes. In addition, the “overfitting” problem – a model having too high degree of freedom to closely fit a particular set of observations may lose its ability for predicting future observations – is another drawback that should be paid careful attention when applying the ANNs.

Most recently, Stochastic Collocation Methods (SCM) based on the generalized Polynomial Chaos Expansion (gPCE) theory [48] have been investigated to characterize random effects on several classical FoMs, namely the resonant frequency, the input impedance, axial ratio and reflection coefficient (at a fixed operating frequency) of textile

antennas undergoing random uncertainties [49]-[51], where SCM shows its effectiveness in terms of good modeling accuracy and acceptable implementation complexity.

2.2.2 Trend of *complete* FF modeling

A *complete* knowledge of antennas' radiated FF rather than the FoMs, is mandatory for analyzing in a reliable way radio links in realistic complicated conditions. Moreover, once the FF is fully characterized, classical FoMs can be deduced from it straightforwardly.

Pioneering attempts of FF modeling were carried out in [52]-[54], where a canonical MC method combining the Vector Spherical Harmonics (VSH) expansion and the Singularity Expansion Methods (SEM) [55]-[57] was used to model the FF radiated by Ultra-Wideband (UWB) antennas whose design parameters are randomly varying.

Most recently, an attempt of quantitatively modeling the complete radiated field (in the Near-Field Fresnel region) of a textile antenna subject to uncertainties was presented in [58]. A "macromodel" was constructed by applying the gPCE to a VSH expansion of the radiated field. This work is an excellent example for demonstrating the interest and high efficiency of resorting to *complete* antenna models in radio links analysis, and the assessment of various performance indicators, such as the power transfer efficiency of the considered wireless power transfer system in this work.

Nevertheless, except these primary attempts mentioned above, the *complete* FF modeling of variable antennas has not yet been fully investigated to date.

2.3 Aims to be achieved by our work

In this thesis, we investigate efficient methodologies for quantitatively modeling the *overall* behavior of variable antennas. This includes the modeling of the antenna's *complete* radiated FF as well as the reflection coefficient $S_{11}(f)$. Particularly, we use the Antenna Transfer Function (ATF) [59], defined in (2.1), as the equivalent representation for the FF. The benefit is that ATF is independent of the input power, hence is a representation of the intrinsic properties of the considered antenna.

$$\mathcal{H}(f, \hat{\mathbf{r}}) \triangleq \frac{r e^{jkr}}{a_1(f)} \sqrt{\frac{4\pi}{\eta_0}} \mathbf{E}^\infty(f, \mathbf{r}) = \mathcal{H}_\theta(f, \hat{\mathbf{r}}) \hat{\boldsymbol{\theta}} + \mathcal{H}_\varphi(f, \hat{\mathbf{r}}) \hat{\boldsymbol{\phi}} \quad (2.1)$$

where a_1 is the incident wave at antenna port, η_0 the free space impedance, $\hat{\mathbf{r}} = (\theta, \varphi)$ the unit radial vector, k the scalar wave number, $j = \sqrt{-1}$ and \mathbf{E}^∞ the electric FF (see Figure 2.2).

Compared to existing works, the novel features or improvements that we are aiming to achieve in our proposed modeling methodology are:

- 1) Wide range of applications: suitable for various types of random uncertainties, particularly including the frequency behavior; and for relatively high dimensionality (i.e. large number of input parameters) and large range of variability.
- 2) Efficiency: minimized computational cost for constructing antenna models.
- 3) Versatility: scalable/adjustable according to required modeling accuracy.

And the antenna models constructed in such way should meet the properties of:

- 1) Explicitness: quantitative generation of the corresponding ATF & $S_{11}(f)$ for any new set of input parameters values.
- 2) Compactness: having a compact/parsimonious formulation.
- 3) Accuracy: meeting the application-dependent requirement on accuracy.
- 4) Efficiency: much faster than numerical full-wave simulators for ATF & $S_{11}(f)$ generation.

And they can be then incorporated into various types of higher level analysis, such as the joint antenna/channel modeling, antenna plugged-in asymptotic simulators (e.g. ray tracing), or used for a quick statistic study of some secondary observables, Figure 2.3.

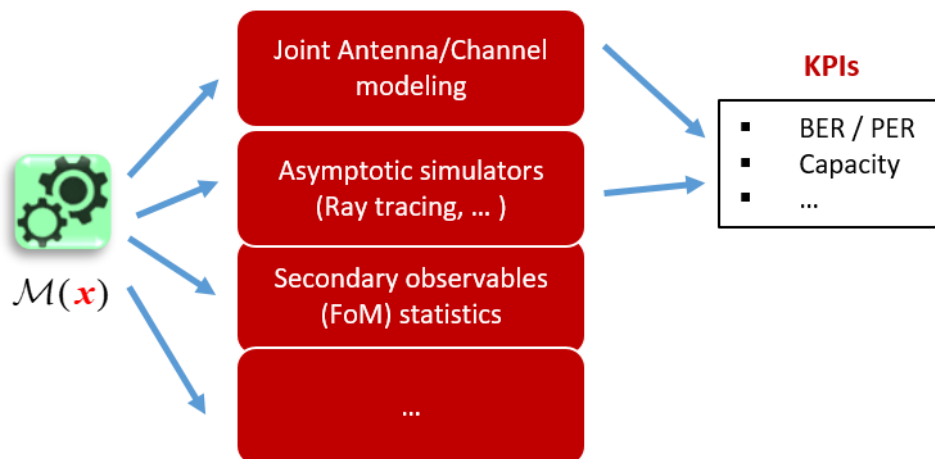


Figure 2.3: Antenna surrogate models for higher lever analysis.

Chapter	3
---------	---

3. Methodologies for modeling the ATF of variable antennas

3.1 Introduction

As discussed in the previous chapter, quantitatively characterizing the ATF is essential for knowing the *overall* behavior of antennas which are undergoing random uncertainties due to intrinsic deformations or external disturbances from the close (possibly fluctuating) environment.

Consider an antenna which is subject to the joint effects of M random uncertainties (e.g. those listed in § 2.1.3), denoted as a random vector $\mathbf{X} = (X_1, X_2, \dots, X_M)^T$. Then the variable antenna can be taken as a “*black box*” with \mathbf{X} being its input and the \mathbf{X} -dependent ATF $\mathcal{H}_{\mathbf{X}}(f, \hat{\mathbf{r}})$ being its output. Our objective is to represent the “*black box*” with explicit mathematical functions which permit, for any given values of \mathbf{X} , to generate the estimate of the corresponding output $\hat{\mathcal{H}}(\mathbf{X}, f, \hat{\mathbf{r}})$. In addition, the difference between the estimate $\hat{\mathcal{H}}(\mathbf{X}, f, \hat{\mathbf{r}})$ and the real observation $\mathcal{H}_{\mathbf{X}}(f, \hat{\mathbf{r}})$ must be minimized to a satisfactory level. For the purpose of convenience, we refer henceforth the aimed “explicit mathematical functions” or directly the estimate $\hat{\mathcal{H}}(\mathbf{X}, f, \hat{\mathbf{r}})$ as “*Surrogate model*” in the sense that it can serve as eminently suitable substitute for the real antenna (or cumbersome full-wave simulated antenna) in various types of analyses.

Constructing such surrogate models is not easy as long as we notice the cumbersome expression of the ATF, not to mention the complexity introduced by the vast sources of randomness. Indeed, from (2.1) we can see the ATF is not a simple scalar-valued parameter as any of the aforementioned FoMs, but a frequency-dependent, complex- *and* vector-valued function defined on the surface of a sphere. In other words, instead of having only one single observable (e.g. FoM) to monitor when the random uncertainties intervene, we are now having to oversee an infinity of observables – both the amplitude and the phase of both polarimetric components on the whole spherical surface will be impacted – an extremely complicated *multi-input/infinite-output* problem which is intractable by using conventional identification methods.

To deal with this daunting challenge we propose in this thesis a “*Two-Step*” modeling approach: “*field parsimony*” in the first step, followed by “*surrogate model extraction*” in the second step. The aim of the first step is to substitute the cumbersome ATF by a parsimonious/compact representation, for example, in the form of a limited number of discrete characteristic parameters. Thereby, the initial intractable *multi-input/infinite-output* problem can be downgraded to a *multi-input/multi-output* one, leading to the possibility for a quantitative characterization. In the second step, the relation between the random input and the parsimonious ATF will be interpreted via dedicated deterministic or statistical approaches, from where surrogate models will be derived. The principle of the “*Two-Step*” approach is illustrated in Figure 3.1, where the *field parsimony* operation is denoted \mathcal{F}_p .

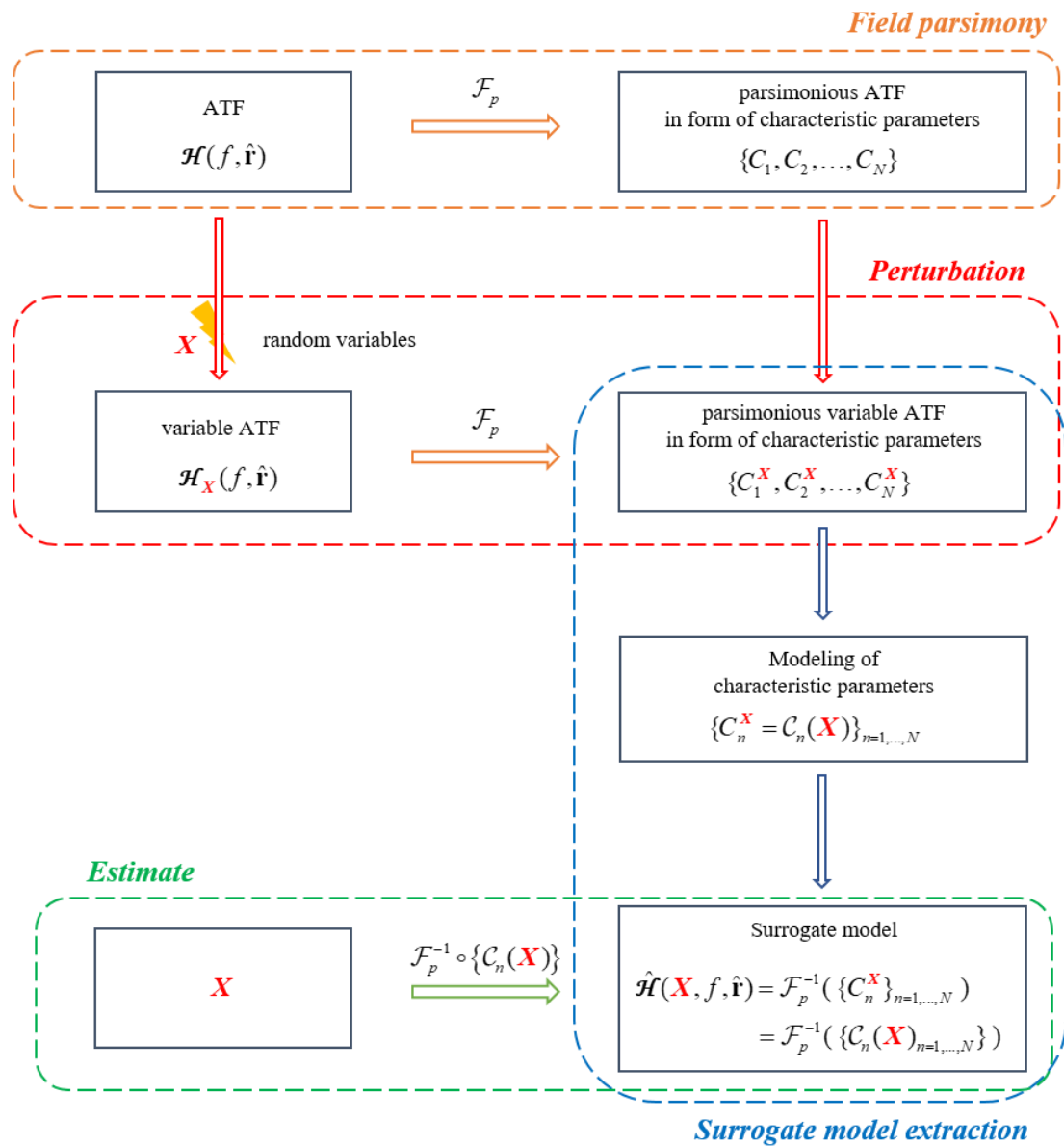


Figure 3.1: Principle of the “*Two-Step*” approach for modeling the ATF of variable antennas.

The organization of this chapter is that: first, the method for realizing the “*field parsimony*” will be presented; then, dedicated methods, both deterministic and statistical ones, for extracting antenna surrogate models will be introduced, and complete modeling procedure will be synthesized; for each proposed methodology, application examples will be given to justify its effectiveness as well as to bring to light its limitations.

3.2 Field parsimony

When the question of “*field parsimony*” is inevitably raised, the first solution we may think of intuitively is to discretize the ATF on the sphere, i.e. substitute the continuous function by a finite set of (spatial) samples considered as output observables. However, this proves not to be a good idea for two reasons. First, to guarantee perfect reconstruction of the original field the Shannon’s sampling theorem must be respected. That’s to say, the sampling rate should be at least twice higher than the highest spatial variation frequency contained in the field in both elevation and azimuth, i.e. for all look directions. Therefore, a good knowledge of the spectral distribution of the field under study is required prior to the sampling procedure. However, it is not easy or even impossible to have such kind of prerequisite for an antenna (except for those very simple types such as dipoles and monopoles), not to mention that when it is undergoing random uncertainties. Second, a sampling strategy suitable for one antenna configuration (corresponding to one state of deformation or environment) may not be suitable for other configurations (corresponding to other states of deformation or environment). In other words, the observables chosen are different from one configuration to another, leading in total to a prohibitive number of observables to be monitored, which is certainly not conducive to the aim of parsimony. Briefly, there is no universal principle to follow to obtain a satisfactory discretization solution suitable for all antenna configurations. In practice, we usually adopt a uniform and oversampling strategy for the purpose of conserving the information completeness as well as facilitating the data collection process. Therefore, more sophisticated methods should be investigated in order to efficiently represent the continuous ATF, or the oversampled sequence of the latter.

In the first part of § 3.2, two methods for parsimoniously representing those scalar functions defined on the surface of a sphere will be reviewed. These methods are latter applied separately to the two polarization components \mathcal{H}_θ and \mathcal{H}_ϕ (which are complex-valued scalar functions) of the ATF, and the limitations of these scalar methods will be discussed. In the second part, a parsimonious method of representation which is directly applicable onto those vector-valued functions, e.g. the ATFs, will be presented. The advantage of the latter will be demonstrated by comparing to the scalar methods.

3.2.1 Methods for parsimoniously representing scalar spherical functions

3.2.1.1 Double Fourier Series (DFS) expansion

Double Fourier Series (DFS) expansion is a simple and fast method for spectral analysis of scalar functions defined on the surface of a sphere. It is well-known that classical Fourier series permit to decompose a scalar function defined on the circle (or more generally, a periodic function) into a weighted sum of trigonometric (sine and cosine) functions. Analogically, DFS allows to expanding a scalar function $f(\theta, \varphi)$ defined on the surface of a sphere as a weighted sum of products of exponentials of separable spherical angular coordinates (θ, φ) :

$$f(\theta, \varphi) = \sum_{n=-\infty}^{\infty} \sum_{m=-\infty}^{\infty} a_{nm} e^{jn\theta} e^{jm\varphi} \quad (3.1)$$

On the viewpoint of duality, the Fourier coefficients $\{a_{nm}\}$ are the equivalent (in the dual space) of the continuous function $f(\theta, \varphi)$ (in its original space), hence the latter can be exactly recovered from the former. In practice, the expansion is always truncated according to the required tradeoff between accuracy and sparsity. In this way, a parsimonious while complete representation – in the form of a limited number of Fourier coefficients $\{a_{nm}\}$ – of the continuous function $f(\theta, \varphi)$ is obtained.

The DFS expansion was originally used for solving partial differential equations (elliptic or hyperbolic) which are defined on the surface of a sphere, such as the vorticity and shallow-water equations in the fluid mechanics domain [60]-[63]. Recently, newly emerging applications include the computation of gravitational fields (e.g. near black holes) [64] and some other space-time spectral analyses [65]. In the antenna-related domain, the DFS expansion could be useful for investigating some scalar-valued, spatially distributed performance indicators. For example, in [66] the DFS expansion was used to get a parsimonious representation for the radiation gain function $G(\theta, \varphi)$ before carrying out the statistical analysis of some uncertainty effects on $G(\theta, \varphi)$.

3.2.1.2 Scalar Spherical Harmonics (SSH) expansion

The Scalar Spherical Harmonics (SSH) expansion is the appropriate Fourier transform for scalar functions defined on the surface of a sphere. The basis functions adopted by the SSH are Laplace's scalar spherical harmonics, denoted $Y_{nm}(\theta, \varphi)$ as in (3.2), instead of simple sine/cosine waves by the DFS:

$$Y_{nm}(\theta, \varphi) = P_n^m(\cos\theta) e^{-jm\varphi} \quad (3.2)$$

where P_n^m is the associated Legendre function (1st kind) of degree n and order m [67].

Usually, the spherical harmonics are normalized as (3.3) with regard to the inner product (3.4), forming hence a complete orthonormal basis in the Hilbert space of square-integrable scalar-valued functions defined on the surface of a sphere. In this way, any function $f(\theta, \varphi)$ belonging to this Hilbert space can be expanded as a linear combination of “spherical modes” as (3.5), where the modal coefficients f_{nm} can be obtained by projection $f_{nm} = \langle f(\theta, \varphi), \hat{Y}_{nm}(\theta, \varphi) \rangle$.

$$\hat{Y}_{nm}(\theta, \varphi) = \sqrt{\frac{2n+1}{4\pi} \frac{(n-m)!}{(n+m)!}} Y_{nm}(\theta, \varphi) \quad (3.3)$$

$$\langle f, g \rangle = \int_0^\pi \int_0^{2\pi} f g^* \sin\theta d\theta d\varphi \quad (3.4)$$

$$f(\theta, \varphi) = \sum_{n=0}^N \sum_{m=-n}^n f_{nm} \hat{Y}_{nm}(\theta, \varphi) \quad (3.5)$$

The SSH expansion method has gained much more popularity than the DFS expansion method in physics since mathematically, the former offers more proper spectral representation for spherical functions. In the antenna-related domain, the SSH expansion method is also quite useful for spectral analysis of the radiation gain function $G(\theta, \varphi)$ or the realized gain function $G_r(\theta, \varphi)$.

However, both DFS and SSH expansion methods are unsuitable for representing vector-valued functions defined on a spherical surface, e.g. the ATF $\mathcal{H}(\hat{\mathbf{r}})$ encountered in our problem. This is because the two polarization components (\mathcal{H}_θ and \mathcal{H}_φ) of the ATF cannot be decomposed separately by using DFS or SSH method due to the uniqueness of vector-valued functions such as \mathcal{H} at the two poles ($\theta = 0$ and $\theta = \pi$). In fact, given that the zenith point ($\theta = 0, \varphi$) is associated with an infinity of φ -dependent local coordinates system $(\hat{\boldsymbol{\theta}}_{(0,\varphi)}, \hat{\boldsymbol{\phi}}_{(0,\varphi)})$, the unique vector $\mathcal{H}(\theta=0, \varphi)$ could have an infinity of possibilities of decomposition in \mathcal{H}_θ and \mathcal{H}_φ depending on the chosen local coordinates system:

$$\mathcal{H}(\theta=0, \varphi) = \mathcal{H}_\theta(0, \varphi) \hat{\boldsymbol{\theta}}_{(0,\varphi)} + \mathcal{H}_\varphi(0, \varphi) \hat{\boldsymbol{\phi}}_{(0,\varphi)} \quad (3.6)$$

As a result, an infinity of values of \mathcal{H}_θ and \mathcal{H}_φ are associated to this single point, which is evidently contradictory to a properly defined function. The same indetermination exists also at the nadir point ($\theta = \pi, \varphi$). As a result, because of the mathematical difficulty, significant errors can occur when the DFS or the SSH method is applied independently onto the two polarization components. Besides, the same problem occurs also if the partial (or “polarimetric”) gains $G_{\theta,\varphi}$ or $G_{r\theta,\varphi}$ instead of the total gains G or G_r are considered. Note that

the total gains G and G_r are proportional to $\|\mathcal{H}\|^2$, thence having unique values at the poles and are regularly defined on the whole sphere; by contrast, the polarization components which are proportional to $|\mathcal{H}_\theta|^2$ or $|\mathcal{H}_\phi|^2$ are not univocally defined at the poles.

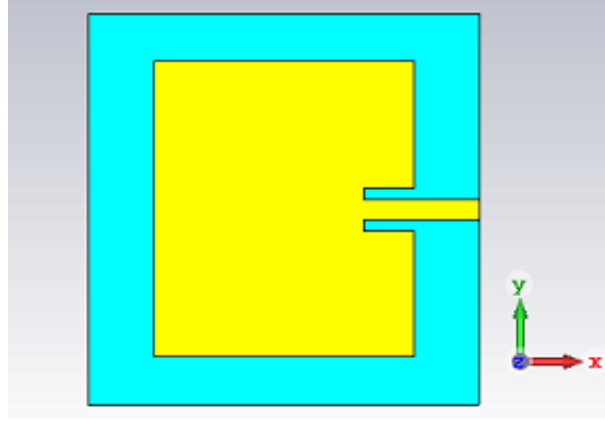


Figure 3.2: Patch antenna used for field parsimony test.

For the purpose of illustration, we applied the SSH expansion method to decompose the total realized gain function $G_r(\theta, \varphi)$ as well as its φ -component $G_{r\varphi}(\theta, \varphi)$ (of which the polar values are chosen at $(\theta=0/\pi, \varphi=0)$) of a classical patch antenna operating at 2.45 GHz (Figure 3.2). Results are shown in Figure 3.3 and 3.4. As expected, it can be seen that the SSH permits to represent the total G_r with excellent precision of reconstruction (the maximal difference of G_r in the -8 dB main radiation direction is only 0.07 dB), but is not able to recover the φ -component $G_{r\varphi}$ accurately especially in the vicinity of the two poles, even with a very high expansion degree $N_{SSH} = 30$. The failure of the SSH method for representing the polarimetric components of G (or G_r) has also been pointed out in other people's work, e.g. in [68].

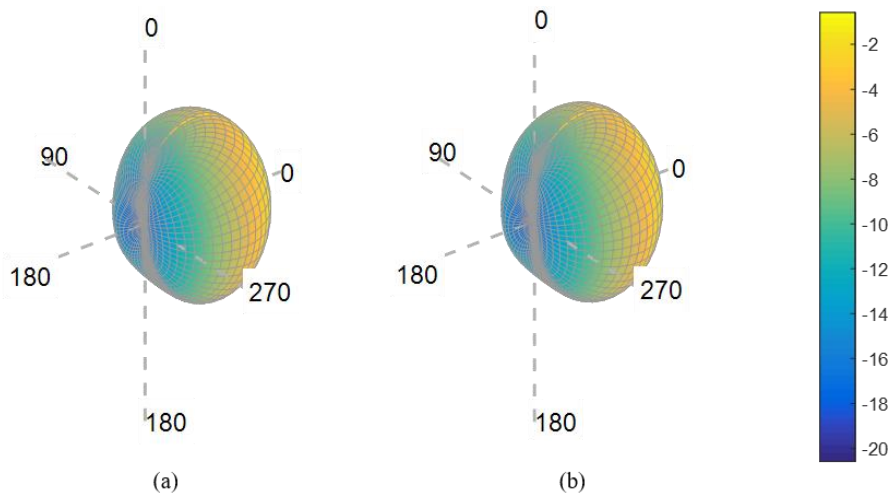


Figure 3.3: SSH expansion applied on the total realized gain $G_r(\theta, \varphi)$ of a patch antenna: (a) initial G_r ; (b) reconstructed G_r with the SSH modes ($N_{SSH} = 5$).

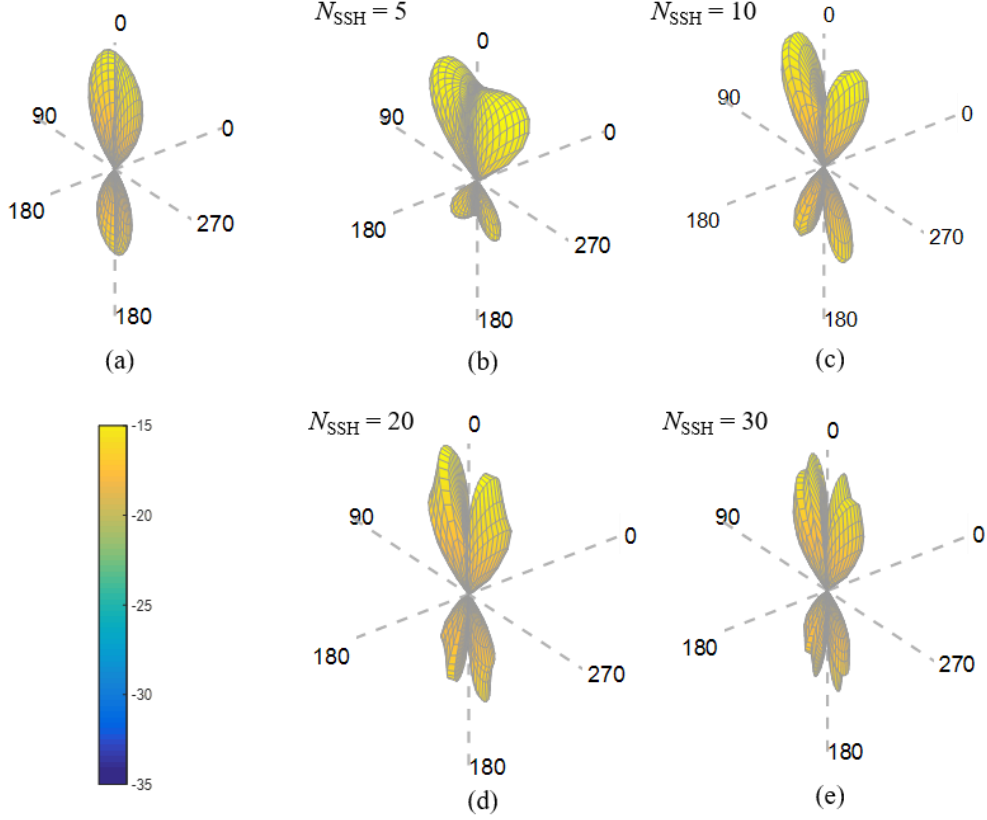


Figure 3.4: SSH expansion applied on the polarimetric realized gain $G_{r\varphi}(\theta, \varphi)$ of a patch antenna: (a) initial $G_{r\varphi}$; (b)-(e) reconstructed $G_{r\varphi}$ with the SSH modes ($N_{SSH} = 5, 10, 20$ and 30 respectively).

To summarize, although the DFS and the SSH expansion methods are efficient for parsimoniously representing the total gains G or G_r , they are insufficient for decomposing neither the polarimetric components nor the vector-valued ATF. We present in the following part a parsimony method which is directly applicable to vector-valued functions named Vector Spherical Harmonics (VSH) expansion method.

3.2.2 Vector Spherical Harmonics (VSH) expansion

3.2.2.1 Principle

The Vector Spherical Harmonics (VSH) expansion is the generalization of the SSH expansion for the Hilbert space consisting of square-integrable vector-valued functions defined in the 3D spherical coordinates system (r, θ, φ) . Hansen explained thoroughly in [70] the principle of using the VSH expansion as an efficient approach to represent the radiation source and to enable the near-field/far-field transformations of the EM waves in the context of antenna applications. In the framework of our problem we are interested in the far-field expression of the E -field, or the ATF $\mathcal{H}(f, \hat{\mathbf{r}})$, so we simplify the formulation proposed in [70] by excluding the r -dependence. Thereby, we are in the framework of vector-valued functions defined on the surface of a sphere, for which the appropriate orthonormal basis are the simplified VSHs [71] as:

$$\begin{cases} \hat{\Psi}_{nm}^{TM}(\hat{\mathbf{r}}) = v_{nm} \left[\partial_{\theta} Y_{nm} \hat{\boldsymbol{\theta}} + \frac{1}{\sin\theta} \partial_{\varphi} Y_{nm} \hat{\boldsymbol{\phi}} \right] \\ \hat{\Psi}_{nm}^{TE}(\hat{\mathbf{r}}) = v_{nm} \left[\frac{1}{\sin\theta} \partial_{\varphi} Y_{nm} \hat{\boldsymbol{\theta}} - \partial_{\theta} Y_{nm} \hat{\boldsymbol{\phi}} \right] \end{cases} \quad (3.7)$$

where TM and TE represent respectively the Transverse Magnetic and the Transverse Electric modes; Y_{nm} are the SSHs (3.2); v_{nm} are the normalization coefficients:

$$v_{nm} = \left[\frac{2n+1}{4\pi n(n+1)} \frac{(n-m)!}{(n+m)!} \right]^{1/2}$$

Then, the ATF $\mathcal{H}(f, \hat{\mathbf{r}})$ which is well-defined, regular and continuous on the whole spherical surface (including the two poles), can be expanded into a series of VSH modes as stated in (3.8).

$$\mathcal{H}(f, \hat{\mathbf{r}}) = \sum_{n=1}^{+\infty} \sum_{m=-n}^n \sum_{u=1}^2 H_{nm}^u(f) \hat{\Psi}_{nm}^u(\hat{\mathbf{r}}) \quad (3.8)$$

where

- $u=1, 2$ represents the TM or TE mode.
- n, m represent respectively the degree and the order of expansion. It is demonstrated that the power of the FF is mainly retained in VSH modes of lower degrees, and vanishes rapidly as n increases. The maximal degree (denoted as N_{VSH}) beyond which the power contribution can be neglected is related to the radius (r_0) of the minimal sphere circumscribing the antenna by an empirical rule: $N_{\text{VSH}} = kr_0 + O(\sqrt[3]{kr_0})$ [72]. Therefore, in general the VSH expansion is truncated at a proper N_{VSH} according to the required precision.
- $H_{nm}^u(f)$ are the complex-valued VSH coefficients which can be obtained by projection: $H_{nm}^u(f) = \langle \mathcal{H}(f, \hat{\mathbf{r}}), \hat{\Psi}_{nm}^u(\hat{\mathbf{r}}) \rangle$.

3.2.2.2 Test of the performance of VSH

To illustrate the superior advantage of the VSH method over the SSH method for sparsely representing vector-valued ATFs, we carried out a test on the same patch antenna used in § 3.2.1 as follows:

- 1) We applied the VSH expansion on the initial ATF \mathcal{H}^{init} at a truncated degree of $N_{\text{VSH}} = 5$.
- 2) We reconstructed the ATF from the VSH coefficients obtained in 1) by reversing the expansion procedure. Denote the reconstructed ATF as \mathcal{H}^{rcs} .

- 3) We calculated the total realized gain G_r , as well as the φ -component $G_{r\varphi}$ (of which the polar values are chosen at $(\theta = 0/\pi, \varphi = 0)$) respectively from \mathcal{H}^{init} and \mathcal{H}^{res} ; the comparison results are shown in Figure 3.5 and 3.6.

We see that both G_r and $G_{r\varphi}$ are accurately recovered from the VSH parsimony operation (the maximal difference in the -8 dB main radiation direction is 0.04 and 0.08 dB respectively). Particularly, the good recovery of the polarimetric components of G_r confirms the good recovery of the ATF components since we have $G_{r\varphi,\theta} = |\mathcal{H}_{\varphi,\theta}|^2$ [59]. Comparing to the unsatisfactory results when using the SSH expansion method (Figure 3.4 (b)-(e)), we see immediately the benefits of the VSH expansion method. In the subsequent modeling, we will adopt the VSH expansion method to achieve the purpose of “*field parsimony*”.

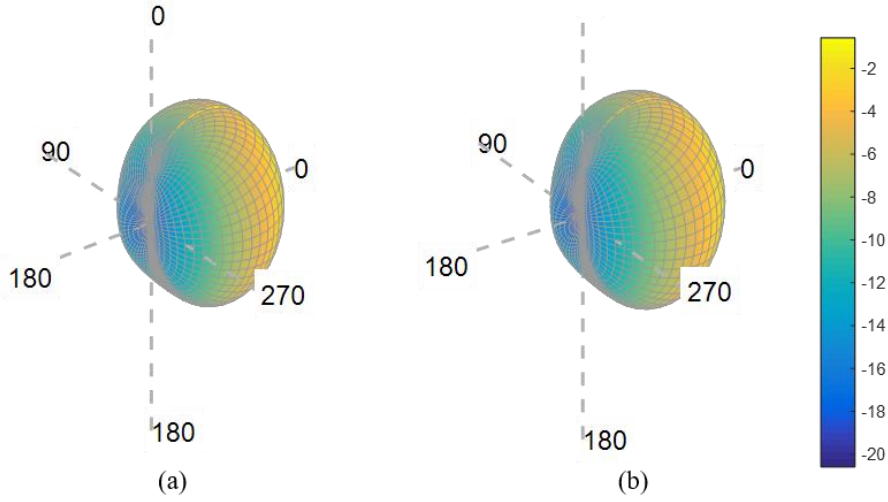


Figure 3.5: VSH expansion applied on the ATF of a patch antenna: (a) initial G_r ; (b) reconstructed G_r with the VSH modes ($N_{VSH} = 5$).

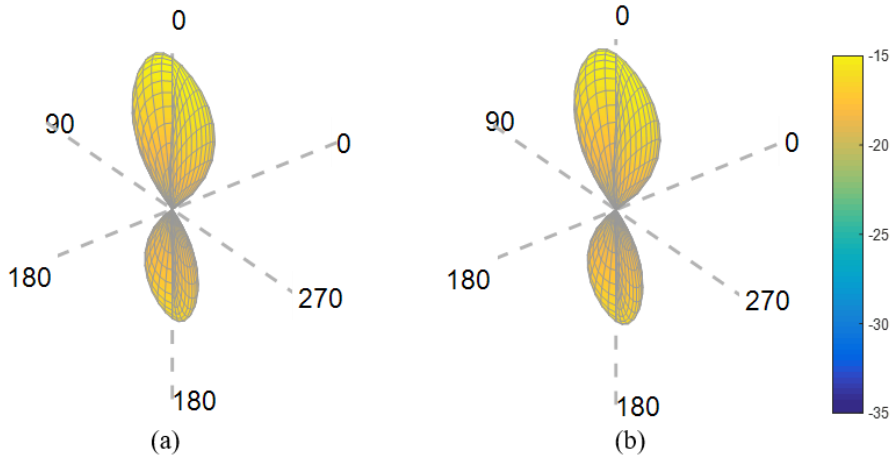


Figure 3.6: VSH expansion applied on the ATF of a patch antenna: (a) initial $G_{r\varphi}$; (b) reconstructed $G_{r\varphi}$ with the VSH modes ($N_{VSH} = 5$).

3.3 Deterministic modeling of ATF: PS

Once the cumbersome ATF is transformed into a parsimonious form, we can perform the second step of the “*Two-Step*” methodology, that’s to say, extract the surrogate model in order to explicitly interpret the relation between the random input variables and the parsimonious ATF (i.e. the selected VSH coefficients $H_{nm}^u(f)$) as illustrated in Figure 3.7.

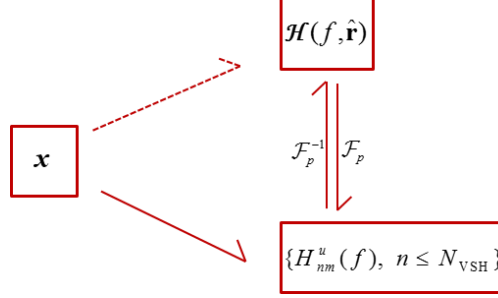


Figure 3.7: Surrogate model relating the random input variables and the parsimonious ATF.

We investigate first a deterministic modeling method named Parametric Study (PS). PS is an intuitive and canonical approach which provides non-intrusive, direct, and fast insights into the input-output relation of an unknown system. The underlying idea is simple – make varying only one parameter at a time while keeping the other parameters fixed, and observe how the FoMs of interest are evolving due to the single parameter effect. Because of its simplicity, PS has been widely used in many domains of applied physics and has been implemented in various types of commercially available Computer Aided Design (CAD) tools. In the domain of antenna design, PS can be used to analyze the sensitivity of the antenna on certain design parameters, and to hunt for the optimal parameter value. Some application examples can be found in [73]-[77]. Here, we adopt the PS to extract surrogate models to quantify the impact of some input variable x on the parsimonious ATF.

In order to evaluate the accuracy of the derived surrogate model, we define a performance indicator named the Relative Root Mean Square Error (*RRMSE*) of the realized gain G_r as:

$$RRMSE[G_r(f)] = \frac{RMSE[G_r(f)]}{\langle G_r^{init}(f, \hat{\mathbf{r}}) \rangle_{(\theta, \varphi)}} \quad (3.9)$$

with *RMSE* being the Root Mean Square Error of G_r :

$$RMSE[G_r(f)] = \sqrt{\frac{1}{4\pi} \iint_{\Omega} [G_r^{init}(f, \hat{\mathbf{r}}) - G_r^{rcs}(f, \hat{\mathbf{r}})]^2 d\Omega} \quad (3.10)$$

where G_r^{init} and G_r^{rcs} are respectively the realized gain of the initial field and that of the reconstructed field from the surrogate model; and $\langle G_r^{init}(f, \hat{\mathbf{r}}) \rangle_{(\theta, \varphi)}$ is the realized gain of the initial field averaged over the whole sphere ($\Omega=4\pi$ str) and is in fact the total radiation efficiency η of the antenna:

$$\eta(f) = \langle G_r^{init}(f, \hat{\mathbf{r}}) \rangle_{(\theta, \varphi)} = \frac{1}{4\pi} \iint_{\Omega} G_r^{init}(f, \hat{\mathbf{r}}) d\Omega$$

$d\Omega = \sin\theta d\theta d\varphi$ being the infinitesimal solid angle, and reminding $G_r(f, \hat{\mathbf{r}}) = \|\mathcal{H}(f, \hat{\mathbf{r}})\|^2$ [59].

Note that till now, the general expression of all physical quantities are frequency dependent, which means the antenna's frequency behavior has not been revealed yet in the surrogate model. However, from the open literatures we are aware that the frequency behavior is not an easy task to be addressed. To mitigate, some approaches were restricted to a single fixed frequency, e.g. in [49]-[51], [58], whereas other authors have chosen to investigate the FoMs of interest averaged over a range of frequencies, e.g. in [66], [68]. Here in our first attempt, we choose to temporarily bypass this thorny issue by simply fixing the frequency at a nominal value, e.g. the antenna's resonant frequency. An advanced modeling technique permitting to include the frequency behavior in the surrogate model will be presented in § 3.5.

3.3.1 Modeling procedures

An iterative modeling procedure combining the VSH expansion and the PS to extract surrogate model of an antenna undergoing a variable input parameter x is proposed hereby (Figure 3.8):

1. Generate a set of sampling points $\{x_k\}$ which cover the support of definition of the input parameter x . This set of points is also called the Experimental Design (ED).
2. For each value x_k reconfigure the antenna accordingly, carry out the EM simulation or measurement, and compute the ATF $\mathcal{H}_k(\hat{\mathbf{r}})$.
3. Apply the VSH expansion onto each ATF to get the VSH coefficients $\{H_{nm}^u, n \leq N_{\text{VSH}}\}_k$ up to the degree of truncation N_{VSH} depending on the required precision.
4. Reconstruct the ATFs from the VSH coefficients, and assess the *RRMSE* to verify the relevance of the choice of N_{VSH} . If the *RRMSE* is satisfactory then select the most energetically dominant VSHs; otherwise, restart from the Step 3 with a higher N_{VSH} .
5. Fit the evolution curve of those dominant VSH coefficients in terms of x with polynomial functions: $\{H(x) = \sum_{k=0}^P \beta_k(f) P_k(x)\}_{nm}^u$.
6. Reconstruct the ATFs from the whole set of polynomial coefficients $\{\beta_0, \beta_1, \beta_2, \dots\}_{nm}^u$, and assess the reconstruction error in terms of the *RRMSE*. If the model accuracy is satisfactory then stop; otherwise, return to Step 5 and increase the polynomial degree.

Eventually, a deterministic model relating quantitatively and explicitly the input parameter x and the output parameters $H_{nm}^u(x)$ via the whole set of polynomial coefficients

$\{\beta_0, \beta_1, \beta_2, \dots\}_{mm}^u$ is established, allowing the ATF prediction for any value of x , thanks to the inverse VSH transform.

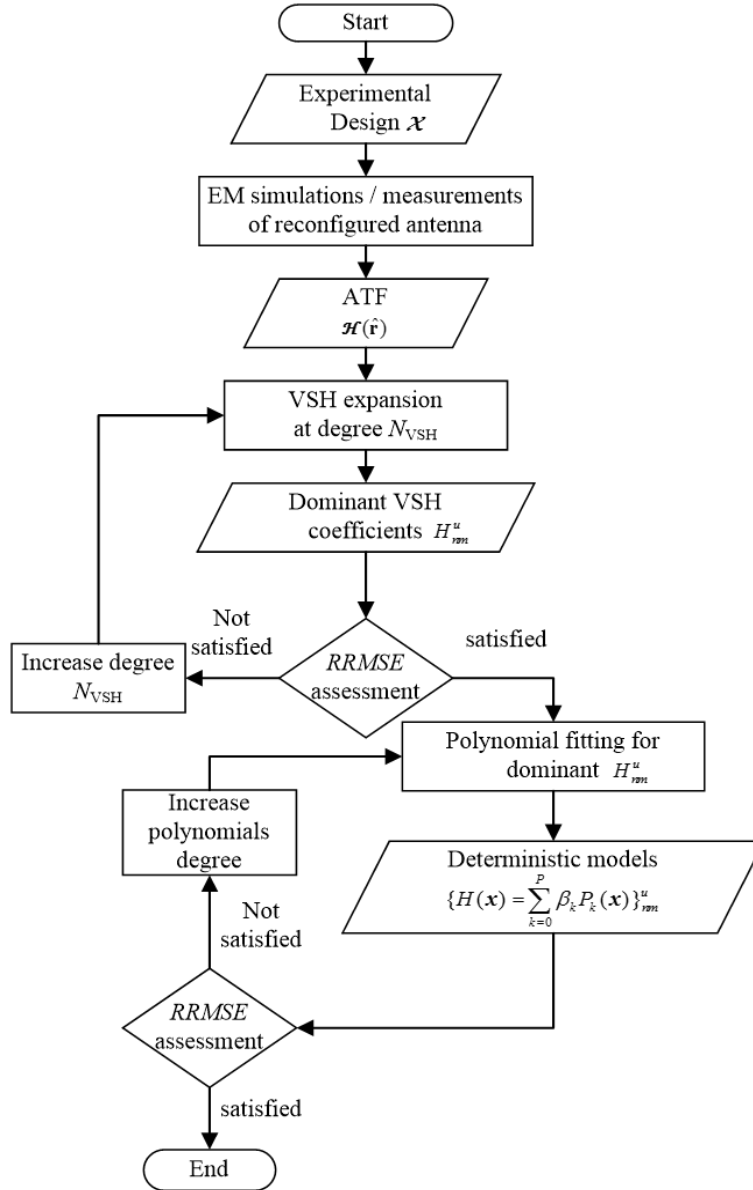


Figure 3.8: Algorithm flowchart of the parametric study procedure.

3.3.2 Application to a canonical dipole antenna - with one input variable

We are going to quantitatively validate the proposed PS approach in a rather academic framework. The procedure is applied to the half-wave dipole which is a simple and very well-known canonical antenna (so an ideal “test antenna”) to verify its relevance, and assess its accuracy and robustness [69].

3.3.2.1 Design of a deformable dipole

A dipole which is made of perfect electrical conductor (PEC) material, with length of $\ell_{dip} = 58.14$ mm and section radius of 1 mm is designed (Figure 3.9 (a)). In its straight state, the

dipole is well matched (i.e. $|S_{11}| < -10$ dB) over a frequency band of [2.1, 2.4] GHz. This dipole is assumed to be deformable and may undergo bending (Figure 3.9 (b)), torsion, or any combination of the two. In this example, only the bending effect is studied, i.e. the bending curvature κ (or the bending radius $R_b = 1/\kappa$) is considered as the only input variable. The frequency behavior will not be included and f is fixed at 2.3 GHz.

Electromagnetic simulations are undertaken in CST® MWS (with the Frequency domain solver and Tetrahedral adaptive mesh type) to obtain radiation fields which are sampled every 5° in both elevation ($\theta \in [0, 180^\circ]$) and azimuth ($\varphi \in [0, 360^\circ]$).

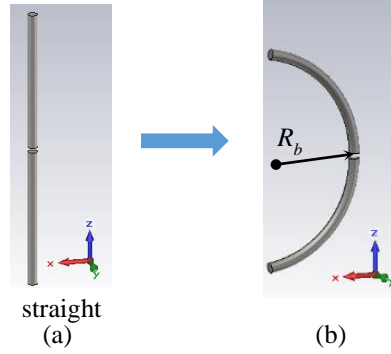


Figure 3.9: Illustration of the bending phenomenon of a dipole antenna.

Figure 3.10 shows the bending effect on the reflection coefficient S_{11} . The black line is the $|S_{11}|$ in straight state; the blue, red and purple lines correspond respectively to $R_b = 60$, 30 and 10 mm. Comparing to the straight state, the first two bending states present an upward shift of the resonant frequency, while the last one presents also a strong impedance mismatch. We are going to construct a surrogate model to quantitatively model the bending effect on the ATF of the dipole.

In the first stage, we choose to limit the bending effect in relatively moderate level. The sampling points of κ are taken such that the corresponding bending radius R_b takes values in the set $\{\infty\} \cup \{500:-50:200\} \cup \{150:-10:60\}$ (in mm). Note that $R_b = \infty$ (i.e. $\kappa = 0$) corresponds to the straight state.

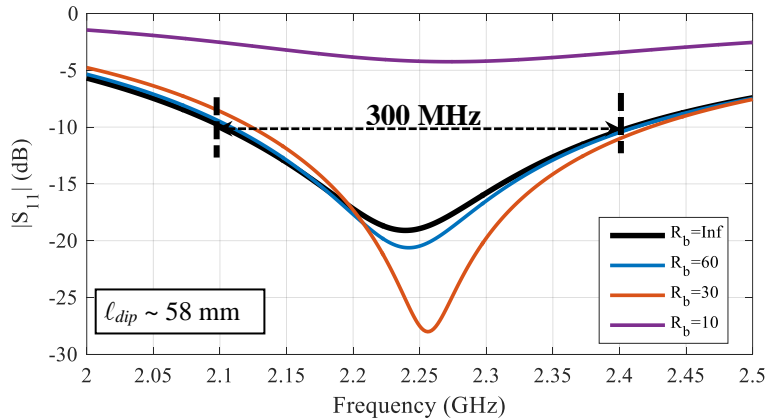


Figure 3.10: Reflection coefficient $|S_{11}|$ of the dipole in different bending states (R_b in mm).

3.3.2.2 Field parsimony with VSH expansion

The ATFs are computed from the FFs according to (2.1) and are expanded using the VSH method for degrees n up to $N_{\text{VSH}} = 3$ and thus in total 30 VSH modes ($1 \leq n \leq N_{\text{VSH}}$, $-n \leq m \leq n$ and $u = 1, 2$) are obtained. Then we notice that among these 30 VSH modes only 6, i.e. $(u, n, m) \in \{(1, 1, \pm 1), (2, 1, 0), (2, 2, \pm 1), (2, 3, 0)\}$ are dominant in terms of power, containing more than 99.9 % of the total power.

After that, the ATFs are reconstructed separately from the 30 VSH modes and from the 6 dominant modes. The bent dipole with $R_b = 60$ mm (which is the largest deformation in the current case) is taken for the illustration of results in the following context. The maximal difference in G_r between the reconstructed field from those 30 modes and the initial field is only about 0.03 dB, which justifies a very good accuracy with truncation to degree $N_{\text{VSH}} = 3$ in the expansion. Furthermore, the deviation in G_r of the reconstructed field from the 6 dominant modes is less than 0.1 dB compared to the initial field, which indicates that the approximation with only 6 dominant VSH modes is still very good. The *RRMSE* of the reconstructed fields are also computed, as shown in Figure 3.11. It is noted that the *RRMSE* of the reconstruction from 30 modes (the red dash line) is less than 0.2 %. This error is mainly due to the truncation of expansion ($N_{\text{max}} = 3$), a small part being related to the angular sampling inducing some approximations in the numerical quadrature performed in the VSH transform. The *RRMSE* of the reconstruction from 6 dominant modes (the blue dash line) is less than 0.4 %, confirming again the conservation of a high accuracy using only 6 dominant VSH modes instead of 30 ones.

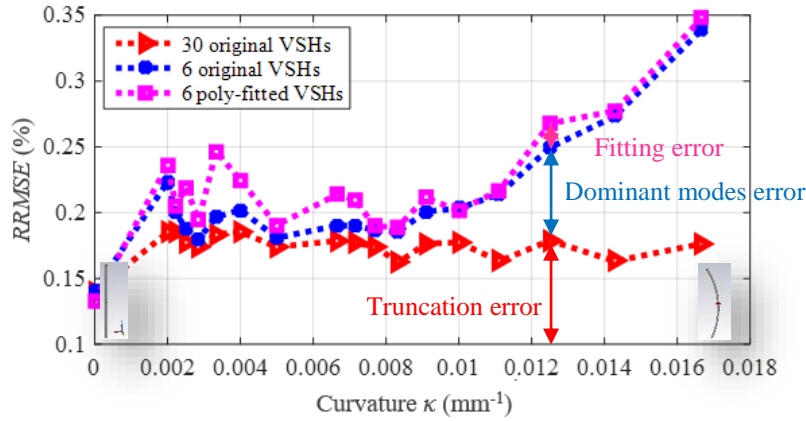


Figure 3.11: *RRMSE* of the reconstructed fields with different approaches.

Furthermore, as the dipole presents symmetries with respect to both the equatorial and meridian planes, the VSH coefficients verify relation:

$$\begin{cases} H_{n,-m}^u = (-1)^{m+u} H_{n,m}^u \\ H_{n,m}^u = 0 \quad \text{for } m+n+u \text{ even} \end{cases} \quad (3.11)$$

which implies simple relations:

$$H_{1,-1}^1 = H_{1,1}^1, \quad H_{2,-1}^2 = -H_{2,1}^2 \quad (3.12)$$

As a result, it remains only 4 VSH coefficients (i.e. $H_{1,1}^1$, $H_{1,0}^2$, $H_{1,1}^2$ and $H_{3,0}^2$) to be modeled.

3.3.2.3 Surrogate model extraction

In this step, the evolution of these 4 VSH coefficients as function of the curvature κ will be fitted with polynomials. As the VSH coefficients are complex values, their real and imaginary parts are fitted separately. This is done using the Matlab Curve Fitting Tool. Linear fits match well for all coefficients but one, which requires a quadratic fit. Finally we get a surrogate model with 17 polynomial coefficients. Figure 3.12 shows an example where the real and imaginary parts of the VSH coefficients $H_{1,1}^1$ and $H_{3,0}^2$ are fitted.

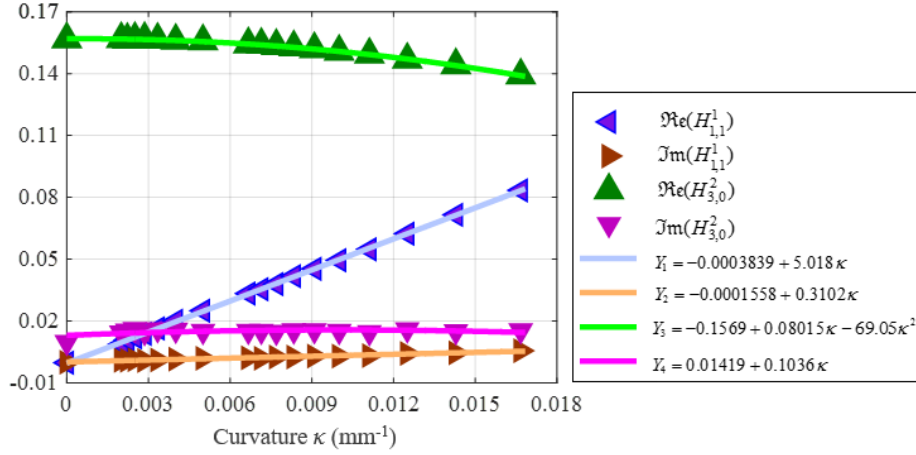


Figure 3.12: Polynomial fitting of the VSH coefficients $H_{1,1}^1$ and $H_{3,0}^2$.

3.3.2.4 Model accuracy assessment

To evaluate the model's accuracy, ATFs are reconstructed using the derived surrogate model: firstly the 6 dominant VSH coefficients are computed from the polynomial coefficients and the equations (3.12); then ATFs are computed by inverting the VSH expansion procedure. The difference in G_r between the reconstructed fields from the 6 dominant VSH coefficients with and without polynomial fitting is observed to be only 0.02 dB, which implies that the fitting is accurate enough. In Figure 3.11 the magenta dash line shows the $RRMSE$ of the model-reconstructed field. It can be seen that there isn't much difference when comparing to the case where the 6 original dominant VSHs are used for reconstruction, indeed, the $RRMSE$ remains inferior to 0.4 %, which indicates the good accuracy of the parametric modeling procedure.

The efficiency of parsimony of the surrogate model can be evaluated in terms of the data compression rate τ :

$$\tau = 1 - N_{rcs} / N_{init}$$

where N_{init} is the number of sampled data from the initial field, and N_{res} is the number of parameters of the surrogate model.

In one hand, the number of real sampled data representing the radiated FF is: $N_{init} = N_K \times N_\theta \times N_\varphi \times 2 \times 2$, where N_K , N_θ and N_φ represent the number of values of the input parameter, the number of sampling points in elevation and azimuth, and the last two factors “2” correspond to the two polarization components \mathcal{H}_θ and \mathcal{H}_φ which are complex quantities. This number must be divided by 4 to account for the two symmetries. In the other hand, the number of parameters of the final model N_{res} are the 17 polynomial coefficients. As a result, for an angular step of 5° both in elevation and azimuth, the data compression rate is 99.96 %.

3.3.2.5 Verification based on interpolation and extrapolation

It is necessary to verify if the proposed model is still valid for other range of values of the curvature κ . For this purpose, a verification based on both interpolation i.e. within the modeling interval ($\kappa \in [0, 1/60]$ mm^{-1}) and extrapolation i.e. outside the modeling interval ($\kappa \in [1/60, 1/30]$ mm^{-1}) has been carried out. More precisely, firstly 150 values of κ are generated randomly following the uniform distribution in the total interval $[0, 1/30]$ mm^{-1} . Secondly, the dipole’s FF for each value of κ is successively obtained by new CST® simulations, expanded over 30 VSH modes and reconstructed separately with 30 original VSH modes, with 6 original dominant VSH modes and with 6 polynomial-fitted dominant VSH modes. At last, reconstructed fields are compared to the simulated ones and the accuracy is assessed by means of *RRMSE* as shown in Figure 3.13.

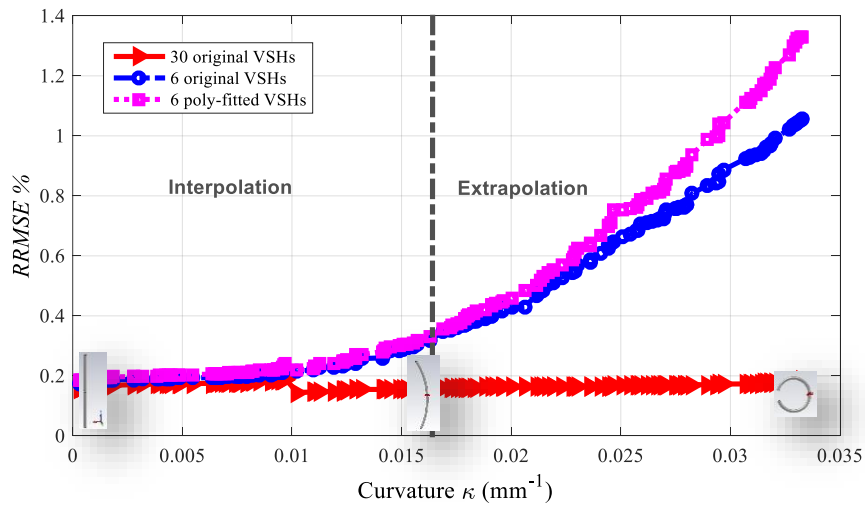


Figure 3.13: *RRMSE* of reconstructed fields with different approaches for 150 random values of the parameter $\kappa \in [0, 1/30]$ mm^{-1} .

It is noted that the *RRMSE* of reconstructed fields remains always less than 0.4 % for all interpolation values of κ and is still inferior to 1.4 % for all extrapolation values of κ despite that an average variation of G_r (relative to the straight dipole) of at most 6 % is caused due to the bending effect. In addition, the added error due to the polynomial fitting of the VSH coefficients (magenta curve in Figure 3.13) appears marginal compared to the error due to the modal truncation (blue curve). In other words, besides the 6 most dominant VSH modes, some less dominant ones are also needed if a better accuracy is required in the extrapolation interval. There is of course always a trade-off between the parsimony efficiency of the model and its accuracy, and the parametric model is fully adjustable according to the priority of criteria. In conclusion, the proposed model is both accurate and efficient for the whole bending range ($\kappa \in [0, 1/30]$ mm⁻¹), corresponding typically to “variational” deformations.

3.3.2.6 Modeling results for severer deformations

The moderate range of deformation chosen previously (for which the $|S_{11}|$ is slightly affected; see Figure 3.10) was intended to illustrate the principles of parametric modeling and its effectiveness. However, to verify the robustness of the proposed algorithm more severe deformations are now considered, with curvatures up to 1/10 mm⁻¹ (corresponding to $R_b \sim \ell_{dip}/6$). For the most curved dipole (with $R_b = 10$ mm) the $|S_{11}|$ is shown in Figure 3.10 (purple curve). In Figure 3.14 the brown lines show the corresponding changes of the radiation patterns. It can be seen from both figures that the effect of bending is now really significant. Actually, it corresponds to an average variation of G_r (relative to the straight dipole) of about 80 %.

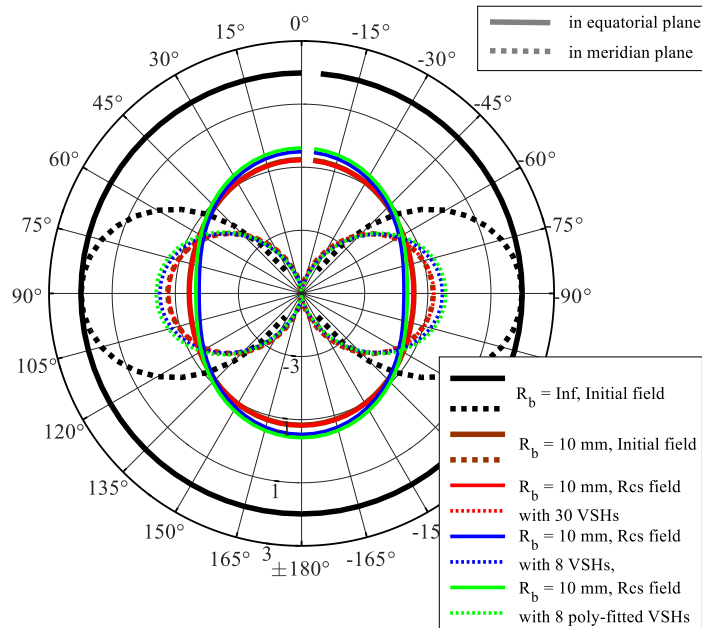


Figure 3.14: G_r patterns of the initial field (both for the straight and curved dipole with $R_b = 10$ mm) and the reconstructed fields with different approaches (only for the curved dipole with $R_b = 10$ mm).

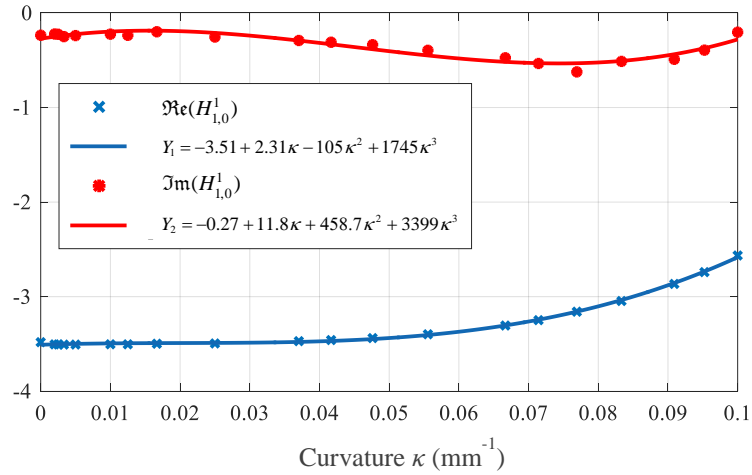


Figure 3.15: Polynomial fitting of the VSH coefficient $H_{1,0}^1$ (severe bendings: $\kappa \in [0, 1/10]$ mm^{-1}).

A new surrogate model is derived from 20 sampling points of the curvature for $\kappa \in [0, 1/10]$ mm^{-1} . The model consists of 8 dominant VSH coefficients, each of which is fitted with polynomials of order 3 (an example is shown in Figure 3.15). In Figure 3.14 the green lines show the radiation patterns for the field reconstructed with the proposed model. We can see that the deviation from of the initial field patterns (the brown lines) is very low (with a maximal difference of 0.2 dB). The *RRMSE* of fields reconstructed with the surrogate model is assessed, as shown in Figure 3.16. It is noted that the *RRMSE* remains below 4 %, whereas the average relative variation of G_r is as high as 80 %, demonstrating the robustness of the model. A similar verification process based on interpolation as in the previous example is carried out for the validation of the proposed model. In order to demonstrate the predictive capabilities of the model, two hundred random dipoles are generated with the proposed model and are compared to their simulated (with CST[®]) counterparts. This constitutes a sort of Monte Carlo test. It is noted that the *RRMSE* of G_r remains also always below 4 % for all values of κ (Figure 3.17). Finally the data compression rate of the constructed surrogate model is evaluated at 99.92 %.

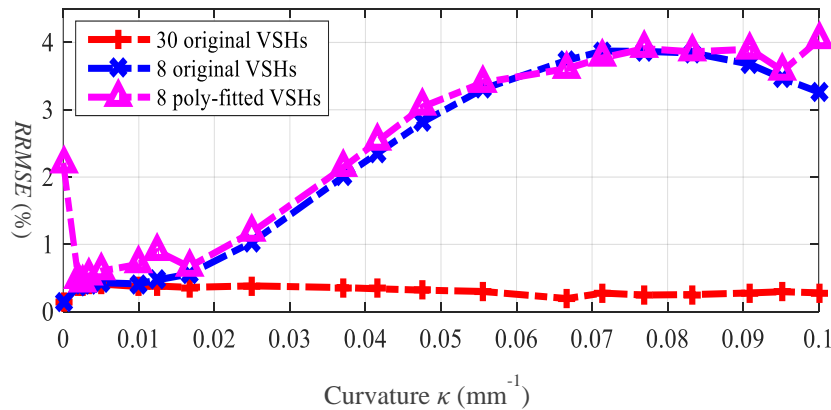


Figure 3.16: *RRMSE* of reconstructed fields with different approaches for the most severe bending state.

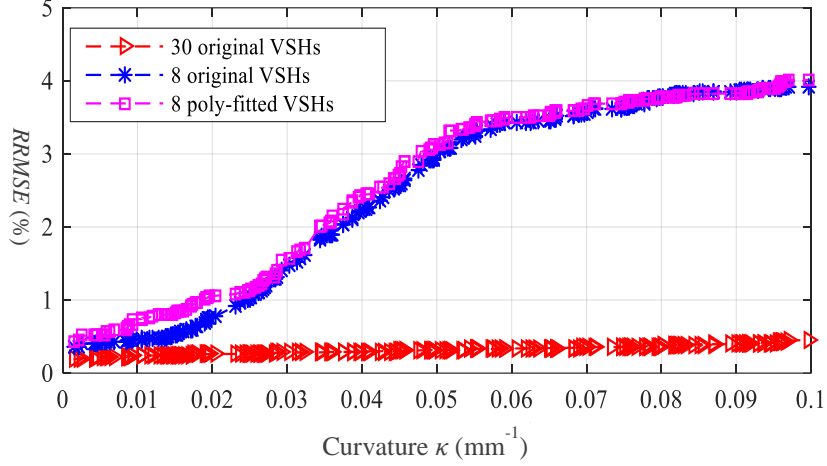


Figure 3.17: *RRMSE* of reconstructed fields with different approaches for 200 random values of the parameter $\kappa \in [0, 1/10] \text{ mm}^{-1}$.

3.3.3 Application to a canonical dipole antenna - with two input variables

In a second step, we investigate the joint effect of two input variables, namely bending and torsion (Figure 3.18), by using the PS approach. The torsion phenomenon is characterized by the torsion rate α , defined as:

$$\alpha = \frac{\theta}{|h|}$$

where θ is the rotation angle of the dipole around the vertical axis at height h along the $z'Oz$ axis.

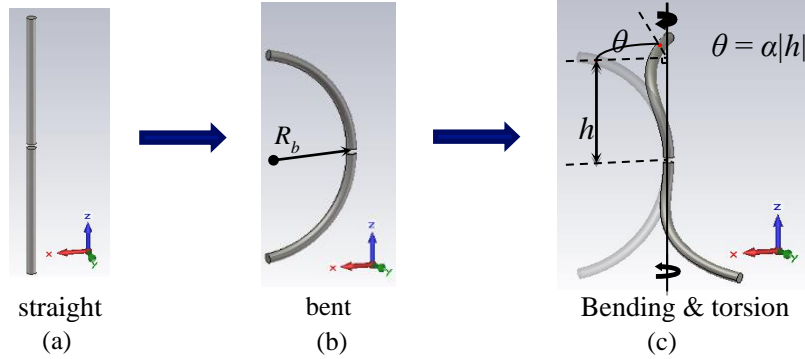


Figure 3.18: Illustration of the joint bending & torsion phenomenon of a dipole antenna.

In this case, 8 dominant VSH modes are finally chosen from the total 30 ones. The surrogate model is constructed by following the procedure presented in § 3.3.1 except that bivariate polynomials are used for fitting the sampled ATFs data. The performance of the final surrogate model is evaluated in terms of the metric *RRMSE*, as shown in Figure 3.19. The red surface shows the *RRMSE* of the fields reconstructed from 30 VSH modes, serving as the reference for comparison. The blue surface shows the *RRMSE* of the fields reconstructed from the 8 most dominant VSH modes, and the magenta surface shows the *RRMSE* of the fields predicted by the surrogate model. It can be seen that, on the one hand, the magenta

curve overlaps well with the blue one, which implies the satisfactory accuracy of the PS modeling; on the other hand, for both the magenta and blue cases, the *RRMSE* is quite low when the two input parameters are small, but increases significantly for larger values of the two input parameters, which implies the necessity of including more VSH modes in order to obtain better accuracy in the case of large variations. Other modeling results are summarized in Table II.

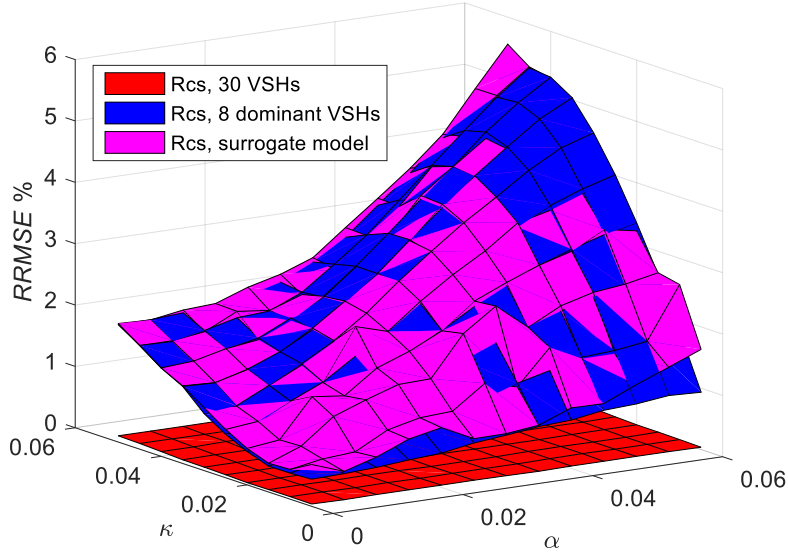


Figure 3.19: *RRMSE* of reconstructed fields with different approaches for bivariate case.

Table II: Parametric study of a deformable dipole: input parameters, modeling parameters and results.

PS study on a deformable dipole		Case 1	Case 2
Inputs	Input variable(s)	κ (mm^{-1})	(κ, α) ($\text{mm}^{-1} \times \text{rad} \cdot \text{mm}^{-1}$)
	Variability range	[0, 0.1]	[0, 0.05] \times [0, 0.06]
	Maximal field variation due to deformations (<i>RRMSE</i>)	80%	36.50%
Modeling parameters	Cardinal of the ED	20	$10 \times 13 = 130$
	Number of selected dominant VSH modes	8	8
	Maximal order for the polynomial fitting	3	3
	Number of polynomial coefficients in surrogate model	40	144
Modeling results	Model accuracy (<i>RRMSE</i>)	< 4 %	< 5.5 %
	Data compression rate, τ	1.33×10^3	9.62×10^3

3.3.4 Discussion

In this section, we combined the VSH expansion method with the PS to construct surrogate models to quantitatively characterize the ATF of antennas undergoing one or two types of deformations, corresponding to one or two input variables. The constructed surrogate

models have been tested on a canonical dipole antenna where the modeling results are relatively satisfactory in terms of accuracy, parsimony and efficiency. However, despite that PS is a fast and simple approach, it has two major methodological flaws: firstly, PS well suited for univariate or at most bivariate problems but cannot be generalized to multivariate cases especially when the number of input parameters is really large, because the number of required pre-evaluations would grow explosively; secondly, since there is no technique (such as cross-validation, early stopping, model comparison) adopted for ensuring the model's ability of generalization, i.e. for reliably predicting new set of observations, severe "overfitting" phenomenon risks to occur during the fitting. As a result, this simple deterministic methodology is rarely applicable for realistic complex problems where generally a large number of sources of uncertainties intervene. Nevertheless, this primary methodology justifies the relevance of the "Two-Step" modeling principle of "field parsimony" followed by "surrogate model extraction", thereby, has paved our way for further investigation of more sophisticate, efficient and robust modeling approaches, e.g. the statistical approaches.

3.4 Statistical modeling of the ATFs: PCE

3.4.1 Introduction

Conventional deterministic approaches which are suitable for designing or modeling those "classical" antennas e.g. rigid, or large-sized, or clearly isolated antennas, etc. are now inappropriate for variable antennas under uncertain conditions, especially when the number of random parameters is really large. Indeed, the combinatory of situations can be so explosive that only statistical methods can offer an efficient framework of analysis.

Some tentative researches on statistical modeling the FF or ATF are briefly reviewed in § 2.2.2. Particularly, the work of Rossi et al. [58] corroborated the feasibility for constructing quantitative antenna models by resorting to the combination of VSH expansion and gPCE methods. However, this method still has some limitations for treating much more complex problems of large dimensionality and high expansion degrees. A more detailed discussion will be given in § 3.4.2.3.

In this section, we propose a new statistical methodology for modeling the *complete* FF radiated by variable antennas. Our methodology has the similar principle of first applying the VSH expansion on the ATFs, then proceeding the PCE on the VSH coefficients. The novelty of our approach is that the unknown PCE coefficients will be solved in a more efficient way that permits to reduce drastically the pre-evaluation cost, notably in the situations where a significant number of random inputs are considered and high expansion degrees are required.

An adaptive modeling procedure is also proposed in order to control the convergence of the surrogate model.

The organization of this section is as follows: first, the principle of the PCE is briefly introduced; second, our proposed statistical methodology for modeling the ATF is detailed; finally, the application of the proposed methodology to a deformable dipole antenna is presented and the modeling results are analyzed.

3.4.2 Principle of the Polynomial Chaos Expansion (PCE)

PCE is an efficient method for characterizing the uncertainty propagation characteristics of an uncertain system. PCE was originally introduced by Norbert Wiener in the 1930s to model Gaussian processes with Hermite polynomials [78]. Here, “chaos” simply refers to “uncertainty”. According to the Cameron-Martin theorem [79], any stochastic process (not limited to Gaussian processes) with finite second-order moment can be represented by Hermite polynomials, but the convergence rate is optimal only for Gaussian processes. In the 1970s, Ogura found that Charlier polynomials are more appropriate for representing Poisson processes [80]. Then it was discovered that many of orthogonal polynomials belong to the so-called Askey-scheme [81]. In the 2000s, Xiu and Karniadakis generalized the scope of PCE to other types of stochastic process and proved numerically the optimal (exponential) convergence rate when using dedicated polynomial basis for a given stochastic process, known as the gPCE [48]. PCE has been verified to be more computational efficient than the “brute force” MC approach in a wide range of applications including e.g. vehicle dynamics [82]-[86], and electronics (circuits, interconnects, and multiport systems) [87]-[91]. In recent years, PCE has been adopted in electromagnetism to assess the human exposure to the EM field or the scattered field due to environmental uncertainties [92]-[95]. Some tentative researches on the flexible antennas are already briefly reviewed in § 2.2.

3.4.2.1 Formulation

Consider a physical system which undergoes random uncertainties. Denoted the input-output relation of the considered system as $Y = \mathcal{M}(\mathbf{X})$, where $\mathbf{X} = (X_1, X_2, \dots, X_M)$ is the random input variables which are defined in the input space $\mathcal{D}_X \subset \mathbb{R}^M$, and Y is a scalar output of interest of the system which is consequently also a random quantity. Suppose that the joint distribution, i.e. the Probability Density Function (PDF) f_X , of the input variables is known, and that the output Y has finite second-order moment, i.e. $\mathbb{E}[Y^2] = \int_{\mathcal{D}_X} \mathcal{M}^2(\mathbf{x}) f_X(\mathbf{x}) d\mathbf{x} < \infty$ (note that this applies to most physical systems), then Y belongs to the Hilbert space $L^2_{f_X}(\mathbb{R}^M, \mathbb{R})$ consisting of all the f_X -square-integrable real-

valued M -dimensional functions, associated with the inner product $\langle u, v \rangle = \int_{\mathcal{D}_X} u(\mathbf{x})v(\mathbf{x})f_X(\mathbf{x})d\mathbf{x}$. By appropriately defining the orthonormal multivariate polynomial basis $\{\Phi_\alpha(\mathbf{X})\}$ with respect to the inner product:

$$\langle \Phi_\alpha(\mathbf{x}), \Phi_\beta(\mathbf{x}) \rangle = \int_{\mathcal{D}_X} \Phi_\alpha(\mathbf{x})\Phi_\beta(\mathbf{x})f_X(\mathbf{x})d\mathbf{x} = \delta_{\alpha\beta} \quad (3.13)$$

with δ being the Kronecker delta function, Y can be expanded in terms of this basis as:

$$Y = \mathcal{M}(\mathbf{X}) \approx \sum_{\alpha \in \mathcal{A}^{M, N_{\text{PCE}}}} y_\alpha \Phi_\alpha(\mathbf{X}) \quad (3.14)$$

where $\alpha = (\alpha_1, \alpha_2, \dots, \alpha_M) \in \mathbb{N}^M$ is the multi-indices that indicate the degree α_i of the i -th variable X_i in the basis Φ_α ; for computational purpose, the expansion is often truncated up to a maximal total degree, denoted as N_{PCE} ; $\mathcal{A}^{M, N_{\text{PCE}}} = \{\alpha \in \mathbb{N}^M \mid \|\alpha\|_1 \leq N_{\text{PCE}}\}$ is the set of multi-indices of all basis with total degree less than N_{PCE} ($\|\alpha\|_1 = \alpha_1 + \alpha_2 + \dots + \alpha_M$ being the ℓ_1 -norm); and $y_\alpha \in \mathbb{R}$ are the expansion coefficients to be determined.

It is clear that the formulation of a PCE modeling problem consists of three main steps:

- 1) Choose the random input variables \mathbf{X} and determine their joint PDF (i.e. the variability range and the distribution); choose the output of interest Y .
- 2) Construct the appropriate orthonormal multivariate polynomial basis $\{\Phi_\alpha(\mathbf{X})\}$.
- 3) Compute the unknown PCE coefficients y_α .

The first step is obviously application-dependent. The selection of input/output depends on what uncertainty phenomenon is actually of interest. The estimation of the joint PDF of \mathbf{X} can be made upon one's work experience, literature review and experimental measurements, and is usually a trade-off after taking comprehensive consideration of the complexity and the feasibility. Note that, "modeling" is always of the sense to interpret the complex real world in a simplified way with some unavoidable loss of accuracy. The steps 2) and 3) are detailed in the following.

3.4.2.2 Construction of the orthonormal polynomial basis

The direct construction of orthonormal polynomial basis according to the definition in (3.13) is difficult and even infeasible for most of arbitrary probability distributions. It can only be made for some basic well-known distributions such as uniform, Gaussian, Gamma, Beta, etc., or "quasi-arbitrary" distributions defined by a finite number of mutually dependent basic random variables, see Soize's work [96]. Therefore, for a general uncertain system having random input variables with an arbitrary joint distribution, an appropriate solution is to transform the input variables into basic variables prior to the building of polynomial basis.

For univariate problems: the Askey-scheme and its extension [81], [48] summarize the appropriate basis for several basic random distributions, for example, Hermite polynomials are appropriate basis for the Gaussian distribution, whereas Legendre polynomials are appropriate basis for the uniform distribution. In the situation of other types of distribution of X , if the Cumulative Density Function (CDF) $F_X(x)$ is known, then X can be transformed into a uniform variable by using the inverse CDF transform as in (3.15):

$$X = F_X^{-1}(U) \quad (3.15)$$

where $U \sim \mathcal{U}(0,1)$ is a uniform random variable on $[0, 1]$; or into a standard Gaussian distribution by using a conventional normal translation as in (3.16):

$$X = F_X^{-1} \circ \Phi(Y) \quad (3.16)$$

where $Y \sim \mathcal{N}(0,1)$ is a standard normal variable, and Φ is the CDF of Y . Thereby, an arbitrary distribution can be easily handled after being transformed to a more “friendly” basic distribution.

For multivariate problems: if the input variables are independent each other, then the basis is simply the tensor product of the univariate basis $\phi_{\alpha_i}^{(i)}(X_i)$ which are constructed beforehand based on the marginal probability density function of each variable $f_{X_i}(x_i)$:

$$\Phi_{\alpha}(\mathbf{X}) \equiv \prod_{i=1}^M \phi_{\alpha_i}^{(i)}(X_i) \quad (3.17)$$

$$\left\langle \phi_{\alpha_j}^{(i)}(x_j), \phi_{\alpha_k}^{(i)}(x_k) \right\rangle \equiv \int_{\mathcal{D}_{X_i}} \phi_{\alpha_j}^{(i)}(x_j) \phi_{\alpha_k}^{(i)}(x_k) f_{X_i}(x_i) dx_i = \delta_{jk} \quad (3.18)$$

In the context of dependent variables, some iso-probabilistic transformation techniques can be applied under appropriate conditions to transform the correlated variables from the initial physical space (\mathbf{X}) to uncorrelated variables in the standardized space (\mathbf{U}). For example, in the situations where the copula (a function which relates the joint distribution function $F_{\mathbf{X}}(x_1, \dots, x_M)$ to the marginal distribution functions $\{F_{X_1}(x_1), \dots, F_{X_M}(x_M)\}$ [97]) is supposed to be Gaussian or more generally elliptical, the Nataf’s transform can be applied [98], [99]; while in the situations where the conditional distributions are known, the Rosenblatt’s [100] can be applied. Note however that in practice, for realistic problems such as those we are considering, the assessment of the empirical copula can be a challenging task, in particular if it must be performed experimentally.

3.4.2.3 Computation of the PCE coefficients

There exist several approaches for computing the PCE coefficients. Depending on whether the solving process relies on prerequisite knowledge on the system under study, these

approaches are classified into two categories – intrusive approaches and non-intrusive approaches. The intrusive approaches, typically the Galerkin’s scheme, require prior knowledge on the explicit equation for $\mathcal{M}(\mathbf{x})$ to assess the PCE coefficients. Obviously, this is not practical because for the great majority of situations we cannot have such kind of explicit form for $\mathcal{M}(\mathbf{x})$ due to its complexity. Besides, in Galerkin’s scheme all the unknown coefficients are obtained simultaneously by solving a coupled deterministic equation by modifying an existing deterministic solver [101]. In other words, a new program is required for the solution, and this is rather like developing an adjoint for a computer code. In contrast, the non-intrusive approaches consider the system under study as a *black-box* hence no prior knowledge is required, and the PCE coefficients are the result of the post-processing of model evaluation (over the ED) – a set of decoupled equations are solved by repeatedly calling an existing deterministic solver. It is consequently not necessary to modify underlying codes or to implement new codes. Hereafter, we will review some popular non-intrusive approaches, namely, the projection approaches which are based on the Monte-Carlo (MC) estimation or the Gaussian Quadrature (GQ) estimation, and the least square regression approaches which are based on the Ordinary Least Square (OLS) algorithm or the Least Angle Regression Sampling (LARS) algorithm.

◆ Projection

✧ Monte-Carlo (MC) estimation

Thanks to the orthonormality of the polynomial basis, the PCE coefficients y_α can be obtained by projecting $\mathcal{M}(\mathbf{x})$ onto the basis $\Phi_\alpha(\mathbf{x})$:

$$\langle \mathcal{M}(\mathbf{x}), \Phi_\alpha(\mathbf{x}) \rangle = \left\langle \sum_{\beta \in \mathcal{A}^{M, N_{\text{PCE}}}} y_\beta \Phi_\beta(\mathbf{x}), \Phi_\alpha(\mathbf{x}) \right\rangle = y_\alpha \quad (3.19)$$

Thereby, we only have to estimate the following integration:

$$\langle \mathcal{M}(\mathbf{x}), \Phi_\alpha(\mathbf{x}) \rangle \triangleq \int_{\mathcal{D}_X} \mathcal{M}(\mathbf{x}) \Phi_\alpha(\mathbf{x}) f_X(\mathbf{x}) d\mathbf{x} \quad (3.20)$$

This can be done via the MC method which considers the integration as the expectation of the random function $\mathcal{M}(\mathbf{X})\Phi_\alpha(\mathbf{X})$: $\mathbb{E}[\mathcal{M}(\mathbf{X})\Phi_\alpha(\mathbf{X})] \triangleq \int_{\mathcal{D}_X} \mathcal{M}(\mathbf{x})\Phi_\alpha(\mathbf{x})f_X(\mathbf{x})d\mathbf{x}$.

Numerically, the estimation of this expectation can be obtained by averaging $\mathcal{M}(\mathbf{X})\Phi_\alpha(\mathbf{X})$ over a substantial number of realizations sampled according to the joint PDF of \mathbf{X} :

$$y_\alpha = \mathbb{E}[\mathcal{M}(\mathbf{X})\Phi_\alpha(\mathbf{X})] \approx \frac{1}{N} \sum_{s=1}^N \mathcal{M}(\mathbf{x}^{(s)})\Phi_\alpha(\mathbf{x}^{(s)}) \quad (3.21)$$

Simplicity is the major advantage of the MC method. However, the great drawback of its slow convergence ($\mathcal{O}(1/\sqrt{N})$) limits its practical application.

✧ **Gaussian Quadrature (GQ) estimation**

A more efficient method for estimating the integration (3.20) is to resort to the GQ method (applicable because orthonormal polynomial families are involved), which approximates the integration by a weighted sum of integrand values at specified points, named Gaussian nodes, within the domain of integration [102]:

$$y_{\alpha} = \int_{\mathcal{D}_x} \mathcal{M}(x) \Phi_{\alpha}(x) f_x(x) dx \approx \sum_{k_1=1}^{n_1} \dots \sum_{k_M=1}^{n_M} w_1^{k_1} \dots w_M^{k_M} \mathcal{M}(x_1^{k_1}, \dots, x_M^{k_M}) \Phi_{\alpha}(x_1^{k_1}, \dots, x_M^{k_M}) \quad (3.22)$$

where $x_i^{k_i}$ is the k_i -th Gaussian node for the i -th input variable x_i and $w_i^{k_i}$ its corresponding weight. They are determined uniquely by the marginal probability density function $f_{x_i}(x_i)$.

It is proven theoretically that for a 1-dimensional integrand which is approximately polynomial of total degree n or less, a GQ scheme with $(n+1)/2$ nodes can provide exact estimation result. Suppose that a 1-dimensional system $\mathcal{M}(x)$ is polynomial of degree N_{PCE} and consider applying the PCE of degree N_{PCE} , then the integrand in (3.22) is polynomial of degree less or equal than $2N_{\text{PCE}}$. As a result, a GQ scheme of $(N_{\text{PCE}} + 1)$ nodes is required for exact estimation in (3.22).

In the situation of a M -dimensional system, the GQ scheme can be constructed as the tensor product of each 1-dimensional GQ scheme:

$$\mathbf{Q}_M^{N_{\text{PCE}}} \triangleq \mathbf{Q}_1^{n_1} \otimes \mathbf{Q}_2^{n_2} \otimes \dots \otimes \mathbf{Q}_M^{n_M} \quad (3.23)$$

with $\mathbf{Q}_k^{n_k}$ ($k=1, \dots, M$) being the 1-dimensional GQ scheme for approximating the polynomial (of the variable x_k) of degree n_k , and $(n_1 + n_2 + \dots + n_M) = N_{\text{PCE}}$. Thereby the total number of required nodes is:

$$N_{\text{GQ-nodes}} = \prod_{i=1}^M (n_i + 1) \quad (3.24)$$

If we assume $n_i \equiv N_{\text{PCE}}$ constant for all input variables, then $N_{\text{GQ-nodes}} = (N_{\text{PCE}} + 1)^M$ which grows too fast (exponentially) with respect to the dimensionality M , causing unaffordable computational cost. This problem is known as the ‘‘curse of dimensionality’’. As a result, the full tensor product grids are rarely applicable but only for low dimensions, e.g. $M \leq 5$. Actually, the full tensor product grids are able to exactly approximate the integration for an integrand of degree less or equal to $M \cdot N_{\text{PCE}}$, which is far greater than $2N_{\text{PCE}}$ for $M \gg 2$, thence necessarily leading to high overhead computational cost.

In order to mitigate this ‘‘curse of dimensionality’’, Smolyak first proposed sparse grids scheme [103] in which only a subset of the full tensor product grids are chosen:

$$\mathbf{Q}_{M,N_{\text{PCE}}}^S = \sum_{N_{\text{PCE}}-M+1 \leq n \leq N_{\text{PCE}}} (-1)^{N_{\text{PCE}}-n} C_{M-1}^{N_{\text{PCE}}-n} \mathbf{Q}_M^n \quad (3.25)$$

where $\mathbf{Q}_{M,N_{\text{PCE}}}^S$ denotes the sparse grids scheme for constructing a M -dimensional PCE model with total degree of N_{PCE} ; \mathbf{Q}_M^n denotes the full tensor product grids for constructing a M -dimensional PCE model with total degree of n ; $C_n^k = n!/(k!(n-k)!)$ is the binomial coefficient. The total number of required nodes in a Smolyak’s sparse scheme is estimated by $\approx (2M)^{N_{\text{PCE}}}/N_{\text{PCE}}!$ [104], which has a polynomial (instead of exponential) dependence on the dimensionality M . The Smolyak’s sparse scheme has been used in applications e.g. [105]-[108] and have been demonstrated to be more computationally efficient than full tensor product scheme for high degrees of expansion.

Quite recently, Zhang proposed another type of sparse grids scheme called Stochastic Testing (ST) [101] where only $K = C_{M+N_{\text{PCE}}}^{N_{\text{PCE}}}$ nodes, i.e. as the same number of the unknown PCE coefficients, are selected from the full tensor product grids. The selection logic prioritizes those nodes with large weight values and try to make the following matrix as well-conditioned as possible:

$$\Phi(\mathcal{X}) \triangleq [\Phi_{\alpha_1}(\mathcal{X}), \Phi_{\alpha_2}(\mathcal{X}), \dots, \Phi_{\alpha_K}(\mathcal{X})]$$

where $\mathcal{X} = \{\mathbf{x}^{(1)}, \mathbf{x}^{(2)}, \dots, \mathbf{x}^{(N_{\text{ED}})}\}^T$ is a set of points spanning the input variables space \mathcal{D}_X , conventionally referred as the Experimental Design (ED). It is easy to verify that this number of required nodes also has a polynomial dependence on M . The ST algorithm have been implanted in some stochastic collocation (SC) modeling such as in [58] where 3 random input parameters with relatively limited ranges of variability are considered. In such case a relatively low expansion degree ($N_{\text{PCE}} = 6$) is sufficient and the SC/ST was demonstrated to be a very efficient method. However, if additional random input parameters and/or larger variability ranges were to be considered, a higher expansion degree would be necessary. Under such situations, the SC approach would be less efficient than the least-squares based solutions that we will present in the next section.

To summarize, the GQ-based algorithms have the superiority over others in terms of the modeling exactness. The main drawbacks of GQ are: first, the ‘‘curse of dimensionality’’ limits their application to small to moderate dimensionalities, and also for relatively low polynomial expansion degrees (otherwise, a similar ‘‘curse of expansion degree’’ would occur). Second, the GQ scheme (i.e. nodes and weights) is so closely linked to the expansion degree N_{PCE} that, if a higher N_{PCE} is required, the GQ scheme

would be totally different, hence completely new pre-evaluations are required. Third, relating to the second one, the pre-evaluations should be made exactly at those pre-determined GQ nodes; however, it may happen in practice that, it is difficult (or even impossible) to build up the exact conditions corresponding to those nodes, in which situation the modeling would be completely blocked. Fourth, relating to the third one, in the situation where we already have some evaluation results at some points other than the GQ nodes, these results could be barely taken advantage of to save some computational cost. All these above-mentioned drawbacks reduce the efficiency of the GQ-based projection approaches in realistic applications.

◆ Least square regression

◇ Ordinary Least Square (OLS) regression

The equation (3.14) rewrites as the sum of a truncated series and a residual error:

$$Y = \mathcal{M}(\mathbf{X}) = \sum_{i=0}^{N_b-1} y_{\alpha_i} \Phi_{\alpha_i}(\mathbf{X}) + \varepsilon_{\text{PCE}} \quad (3.26)$$

with $N_b = C_{M+N_{\text{PCE}}}^{N_{\text{PCE}}}$ being the number of polynomial basis for a PCE of degree N_{PCE} ; and ε_{PCE} is the residual error of the approximation.

The PCE coefficients can be investigated upon the knowledge of the system responses over an ED $\mathcal{X} = \{\mathbf{x}^{(1)}, \mathbf{x}^{(2)}, \dots, \mathbf{x}^{(N_{\text{ED}})}\}^T$. Denote the corresponding system responses as $\mathcal{Y} = \{Y^{(1)}, Y^{(2)}, \dots, Y^{(N_{\text{ED}})}\}^T$. Thereby, we get a system of linear equations:

$$\mathcal{Y} = \Phi(\mathcal{X})\mathbf{y} + \boldsymbol{\varepsilon}_{\text{PCE}} \quad (3.27)$$

where $\Phi(\mathcal{X})$ is the $N_{\text{ED}} \times N_b$ matrix of which the i -th column is the evaluation of the basis $\Phi_{\alpha_{i-1}}$ over the ED \mathcal{X} , i.e. $\Phi_{\alpha_{i-1}}(\mathcal{X})$; $\mathbf{y} = [y_{\alpha_0}, y_{\alpha_1}, \dots, y_{\alpha_{N_b-1}}]^T$ is the vector consisting of the unknown PCE coefficients to be determined; $\boldsymbol{\varepsilon}_{\text{PCE}}$ is the vector consisting of the N_{ED} residual errors. Then, the initial problem of solving the PCE coefficients can be transformed into an optimization problem stated as: find $\hat{\mathbf{y}} \in \mathbb{R}^{N_b}$ to minimize the mean square error $\mathbb{E}[\boldsymbol{\varepsilon}_{\text{PCE}}^2]$:

$$\hat{\mathbf{y}} = \arg \min_{\mathbf{y} \in \mathbb{R}^{N_b}} \mathbb{E}[\boldsymbol{\varepsilon}_{\text{PCE}}^2] = \arg \min_{\mathbf{y} \in \mathbb{R}^{N_b}} \mathbb{E}[(\mathcal{Y} - \Phi(\mathcal{X})\mathbf{y})^2] \quad (3.28)$$

The OLS algorithm solves the optimization problem by:

$$\hat{\mathbf{y}} = (\Phi^T \Phi)^{-1} \Phi^T \mathcal{Y} \quad (3.29)$$

where $(\Phi^T \Phi)^{-1} \Phi^T$ is the Moore-Penrose pseudoinverse of $\Phi(\mathcal{X})$.

To ensure the good-conditioning of the least square regression problem, a minimum number of pre-evaluations are required for “training” the model. As a rule of thumb, the number of realizations is often chosen to be 2~3 times larger than N_b . We can see that the concern of high computational cost occurs again: in the situation where the input variables are numerous (i.e. high dimensionality) and/or where a high expansion degree N_{PCE} is indispensable for achieving satisfactory precision, the number of pre-evaluations becomes very large.

To circumvent this limitation, a possible way is to use a truncation basis scheme during the expansion. For example, Blatman and Sudret proposed “hyperbolic truncation scheme” (also named “ q -norm scheme”) [110] where only a subset of the full basis scheme $\mathcal{A}^{M, N_{\text{PCE}}}$ are retained. The set of multi-indices of the retained basis is defined as:

$$\mathcal{A}^{M, N_{\text{PCE}}, q} = \{ \boldsymbol{\alpha} \in \mathbb{N}^M \mid \|\boldsymbol{\alpha}\|_q \leq N_{\text{PCE}} \} \quad (3.30)$$

with $\|\boldsymbol{\alpha}\|_q = \left(\sum_{i=1}^M (\alpha_i)^q \right)^{1/q}$, $0 < q < 1$ being the q -quasi-norm. It can be seen that $q = 1$ corresponds to the full scheme $\mathcal{A}^{M, N_{\text{PCE}}}$ whereas a lower value of q would exclude high order interaction terms from the basis set (i.e. penalize the high-rank indices), thereby, the number of unknown PCE coefficients are reduced and then the required number of pre-evaluations can be reduced accordingly.

Furthermore, in [111] Blatman proposed a similar solution named “low-rank scheme” where only those basis of which the multi-indices $\boldsymbol{\alpha}$ has at most r ($\leq M$) non-zero elements are retained:

$$\mathcal{A}^{M, N_{\text{PCE}}, r} = \{ \boldsymbol{\alpha} \in \mathcal{A}^{M, N_{\text{PCE}}} \mid \|\boldsymbol{\alpha}\|_0 \leq r \} \quad (3.31)$$

with $\|\boldsymbol{\alpha}\|_0 = \sum_{i=1}^M 1_{\{\alpha_i > 0\}}$ being the rank of the multi-indices $\boldsymbol{\alpha}$. This scheme has the same objective as the hyperbolic one of excluding (more or less) high order interaction terms, i.e. to favor the main effects which are more probably significantly represented by low order interactions [111]. However, such selection techniques are based on the assumption that “the system response usually has less projection weight on those interaction terms”. This assumption cannot be always guaranteed for all realistic applications but is only a rule of thumb. In the situation that strong interaction intervenes, such sparse truncation schemes would be less efficient or even worse than a full scheme.

◇ Least Angle Regression Sampling (LARS)

With the previous discussions in mind, we are aware that on the one hand, sparse basis truncation schemes are essential for circumventing the prohibitive barrier of “curse of dimensionality”; on the other hand, crudely exclude those interaction terms which “seem to be” unimportant is not a credible strategy since their real significance i.e. their actual influence on the system response, can be determined only after a thorough investigation. Therefore, more “intelligent” strategies which permit to take into account the real influence of each basis element while constructing the truncation scheme are urgently needed. In 2004, Efron et al. proposed a less greedy selection strategy named Least Angle Regression Sampling (LARS) [112]. LARS selects iteratively those *regressors* (i.e. basis elements) that have the greatest impact factor on the system response. The impact factor is evaluated in terms of their correlation with the residue after subtracting the current model prediction from the initial response. Precisely, LARS algorithm consists of the following steps:

1. Initialization:
 - a) Choose a starting scheme $\mathcal{A}^{M, N_{\text{PCE}}}$ (e.g. full scheme, hyperbolic, low-rank);
 - b) Generate an initial ED $\mathcal{X} = \{\mathbf{x}^{(1)}, \mathbf{x}^{(2)}, \dots, \mathbf{x}^{(N_{\text{ED}})}\}^T$;
 - c) Evaluate the corresponding system responses $\mathcal{Y} = \{Y^{(1)}, Y^{(2)}, \dots, Y^{(N_{\text{ED}})}\}^T$, subtract the empirical mean response $\hat{\mu}_Y$ from \mathcal{Y} and obtain zero-mean responses $\underline{\mathcal{Y}}$;
 - d) Set the initial LARS scheme as $\mathcal{A}_0^{\text{LARS}} = \{\emptyset\}$, the initial PCE model as $\hat{\mathcal{M}}_0(\mathbf{X}) = \mathbf{0}$, and the initial residue as $\mathbf{R}_0 = \underline{\mathcal{Y}} - \hat{\mathcal{M}}_0(\mathbf{X}) = \underline{\mathcal{Y}}$.
2. Find the *regressor* in $\{\Phi_{\alpha} \mid \alpha \in \mathcal{A}\}$ which has the most correlation with the residue \mathbf{R}_0 ; denote this *regressor* as Φ_{α_1} and the 1st LARS scheme as $\mathcal{A}_1^{\text{LARS}} = \{\alpha_1\}$.
3. For $1 \leq k \leq m = \min\{\text{card}(\mathcal{A}), N_{\text{ED}}\} - 1$, construct the $(k+1)$ -th LARS scheme $\mathcal{A}_{k+1}^{\text{LARS}}$ as follows:
 - a) Construct the k -th PCE model in such way: $\hat{\mathcal{M}}_k(\mathbf{X}) = \hat{\mathcal{M}}_{k-1}(\mathbf{X}) + \gamma_k u_k(\mathbf{X})$ where $u_k(\mathbf{X})$ is the so-called “equiangular vector” of length N_{ED} and of unit norm ($\|u_k(\mathbf{X})\|^2 = 1$), and γ_k is the smallest step such that we can find in the rest candidate set $\{\Phi_{\alpha} \mid \alpha \in \mathcal{A} \setminus \mathcal{A}_k^{\text{LARS}}\}$ another regressor which has as much correlation with the k -th residue $\mathbf{R}_k = \underline{\mathcal{Y}} - \hat{\mathcal{M}}_k(\mathbf{X})$ as all selected *regressors* $\{\Phi_{\alpha} \mid \alpha \in \mathcal{A}_k^{\text{LARS}}\}$ do; denote the new selected regressor as $\Phi_{\alpha_{k+1}}$.

- b) The $(k+1)$ -th LARS scheme is set as $\mathcal{A}_{k+1}^{LARS} = \mathcal{A}_k^{LARS} \cup \{\alpha_{k+1}\}$.
4. Continue this way until \mathcal{A}_m^{LARS} . Meanwhile, we obtain a series of PCE models $\{\hat{\mathcal{M}}_k(\mathbf{X}) + \hat{\mu}_\gamma, k = 1, \dots, m\}$.

Figure 3.20 illustrates the principle of LARS in the case of $M = 2$ covariates.

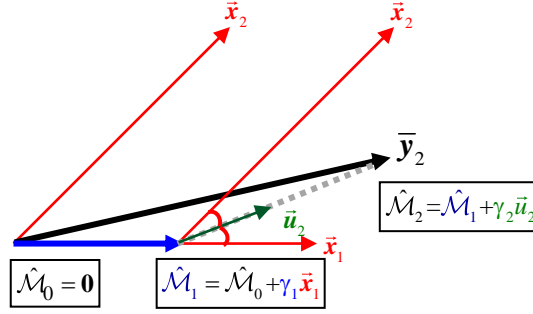


Figure 3.20: The LARS algorithm in the case of $M = 2$ covariates. $\bar{\mathbf{y}}_2$ is the projection of \mathbf{y} into $\mathcal{L}(\bar{\mathbf{x}}_1, \bar{\mathbf{x}}_2)$. Beginning at $\hat{\mathcal{M}}_0 = \mathbf{0}$, the residual vector $\bar{\mathbf{y}}_2 - \hat{\mathcal{M}}_0$ has greater correlation with $\bar{\mathbf{x}}_1$ than $\bar{\mathbf{x}}_2$; the next LARS estimate is $\hat{\mathcal{M}}_1 = \hat{\mathcal{M}}_0 + \gamma_1 \bar{\mathbf{x}}_1$, where γ_1 is chosen such that $\bar{\mathbf{y}}_2 - \hat{\mathcal{M}}_1$ bisects the angle between $\bar{\mathbf{x}}_1$ and $\bar{\mathbf{x}}_2$; then $\hat{\mathcal{M}}_2 = \hat{\mathcal{M}}_1 + \gamma_2 \bar{\mathbf{u}}_2$, where $\bar{\mathbf{u}}_2$ is the unit bisector; $\hat{\mathcal{M}}_2 = \bar{\mathbf{y}}_2$ in the case of $M = 2$, but not for higher dimensional case (i.e. $M > 2$).

◇ Hybrid LARS (HLARS) and adaptive HLARS

Based on Efron's LARS logic, Blatman and Sudret proposed a Hybrid LARS (HLARS) algorithm [113] in which LARS serves only to select the sparse truncation scheme and the PCE models are reconstructed using OLS method, instead of directly adopting the models obtained alongside in LARS. The first 4 steps of the HLARS are the same as in the LARS algorithm, and the 3 additional steps are briefly recalled herein:

5. For $k = 1, \dots, m$, extract the PCE model $\hat{\mathcal{M}}_k(\mathbf{X})$ based on the truncation scheme \mathcal{A}_k^{LARS} by applying OLS over $\{\mathcal{X}, \mathcal{Y}\}$. Then, estimate the model accuracy in terms of the Leave-One-Out Error (LOOE) e_{LOO} (refer to § 3.4.2.4 for definition).
6. Choose the truncation scheme $\mathcal{A}_{k_{\min}}^{LARS}$ which has the smallest e_{LOO} value.
7. Set the HLARS scheme as: $\mathcal{A}^{HLARS} = \mathcal{A}_{k_{\min}}^{LARS} \cup \{\alpha_0\}$ where α_0 is the index of the constant regressor $\Phi_{\alpha_0} = 1$. Note that Φ_{α_0} has never been selected in any truncation scheme \mathcal{A}_k^{LARS} since a constant vector has zero correlation with any residue \mathbf{R}_k . Then, extract the final PCE model based on \mathcal{A}^{HLARS} by applying OLS on $\{\mathcal{X}, \mathcal{Y}\}$.

It is worth mentioning that the choice of the departure scheme has great influence on the efficiency of the HLARS method. A small departure scheme (i.e. low N_{PCE} ,

and/or small q/r values) may be not sufficient for an accurate approximation; a large departure scheme (i.e. high N_{PCE} , and high q or r values) may increase the ensuing computational cost for searching the most important regressors. To mitigate this trouble, Blatman and Sudret proposed furthermore an adaptive HLARS method. The principle is to begin with a starting scheme of small size, extract the PCE model using the HLARS method; then repeat this process for gradually enriched starting schemes until the model accuracy cannot be further improved. Precisely, the whole process of an adaptive HLARS is:

1. Choose a series of nested starting schemes: $\{\mathcal{A}^{M,d_i}, i=1, \dots, i_{\text{Max}}\}$ (usually, this can be done by choosing a series of increasing expansion degrees N_{PCE}).
2. For the smallest starting scheme \mathcal{A}^{M,d_1} , construct the PCE model using the HLARS method. Denote its LOOE as e_{LOO}^1 (refer to § 3.4.2.4 for definition), and also denote the current smallest LOOE as $e_{\text{LOO_min}} = e_{\text{LOO}}^1$.
3. Then, for $i=2, \dots, i_{\text{Max}}$:
 - a) Construct the PCE model with \mathcal{A}^{M,d_i} as departure scheme using the HLARS method. Denote its LOOE as e_{LOO}^i .
 - b) If $e_{\text{LOO}}^i < e_{\text{LOO_min}}$, set the current smallest LOOE as $e_{\text{LOO_min}} = e_{\text{LOO}}^i$; otherwise, stop the iterative process.
4. Choose the PCE model corresponding to $e_{\text{LOO_min}}$ as the final model.

Comparing to the projection methods and the OLS method, the LARS-based methods can provide much better sparsity in basis scheme, which makes them more computationally efficient for treating complex realistic applications with higher dimensionality and higher expansion degree. Particularly, the adaptive HLARS achieves good performance both in terms of computational cost and model accuracy. Hereafter, we will adopt this method to build up our methodology for extracting surrogate models for variable antennas.

3.4.2.4 Error indicator for assessing the model accuracy

The accuracy of a PCE model $\hat{\mathcal{M}}(\mathbf{X})$ can be characterized by the expectation of the square residual error $e_{\text{MSR}} \triangleq \mathbb{E}[\varepsilon_{\text{PCE}}^2(\mathbf{X})]$. In practice, an intuitive way for estimating e_{MSR} is by means of the empirical error e_{EMP} :

$$e_{\text{EMP}} = \frac{1}{N_{\text{ED}}} \sum_{n=1}^{N_{\text{ED}}} [\mathcal{M}(\mathbf{x}^{(n)}) - \hat{\mathcal{M}}(\mathbf{x}^{(n)})]^2 \quad (3.32)$$

However, despite its simplicity, e_{EMP} risks to encounter severe “overfitting” problem – e_{EMP} can be systematically reduced by increasing the complexity (or the degree of freedom) of the PC approximation (i.e. the number of *regressors*) whereas e_{MSR} may increase. Indeed, a model of too high complexity to exhaustively fit a particular set of observations may lose its ability for predicting future observations. Figure 3.21 illustrates this phenomenon on a simple quadratic population with noise pollution, where polynomial fittings of order $N = 2$ and 10 are applied separately on a sample of 10 realizations (red diamond points) driven from the population (black round points). We can see that the high-order fitting curve (blue line) passes exactly through all those sample points (hence e_{EMP} almost equals to zero), but obviously it is not the appropriate approximation to the theoretical curve (black line) seeing that it predicts so badly in other zones (i.e. with a high e_{MSR}). In contrast, the low-order fitting curve (cyan line) which does not exactly pass through all the sample points (i.e with a higher e_{EMP}) but predicts averagely well over all the domain of definition (i.e. with a lower e_{MSR}) should be chosen as the appropriate approximation.

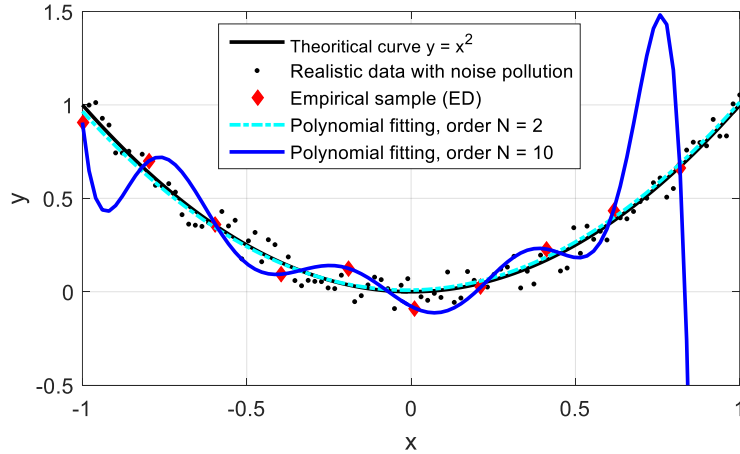


Figure 3.21: An example showing the overfitting problem when approximating an empirical sample with high order polynomials.

A more robust indicator against overfitting is the so-called Leave-One-Out Error (LOOE) e_{LOO} [114], which cross-validates the model’s prediction capability for new input values. Its definition is recalled herein:

$$e_{\text{LOO}} = \frac{N_{\text{ED}} - 1}{N_{\text{ED}}} \frac{\sum_{n=1}^{N_{\text{ED}}} [\mathcal{M}(\mathbf{x}^{(n)}) - \hat{\mathcal{M}}^{(n)}(\mathbf{x}^{(n)})]^2}{\sum_{n=1}^{N_{\text{ED}}} (Y^{(n)} - \hat{\mu}_Y)^2} \quad (3.33)$$

where $\mathcal{X} = \{\mathbf{x}^{(1)}, \dots, \mathbf{x}^{(N_{\text{ED}})}\}^T$ and $\mathcal{Y} = \{Y^{(1)}, Y^{(2)}, \dots, Y^{(N_{\text{ED}})}\}^T$ are respectively the ED and the corresponding system responses; $\hat{\mathcal{M}}^{(n)}$ is the PCE model derived from the whole set $\{\mathcal{X}, \mathcal{Y}\}$

except the n -th realization $\{\mathbf{x}^{(n)}, Y^{(n)}\}$; and $\hat{\mu}_Y = \sum_{n=1}^{N_{\text{ED}}} Y^{(n)} / N_{\text{ED}}$ is the empirical mean response. It is proven that in the context of linear regression, the LOOE can be calculated in a much more efficient way [115]:

$$e_{\text{LOO}} = \frac{1}{N_{\text{ED}}} \sum_{n=1}^{N_{\text{ED}}} \left[\frac{\mathcal{M}(\mathbf{x}^{(n)}) - \hat{\mathcal{M}}(\mathbf{x}^{(n)})}{1 - h_n} \right]^2 \quad (3.34)$$

where h_n is the n -th diagonal element of the matrix $\Phi(\Phi^T \Phi)^{-1} \Phi^T$. Consequently, the construction of N_{ED} PCE models $\hat{\mathcal{M}}^{(n)}$ can be avoided.

3.4.2.5 Post-processing with PCE model

Once the PCE model is extracted, it can serve as an efficient surrogated model for various types of statistical analysis and sensitivity analysis. Particularly, the first and second moments of the system response have analytical expression in terms of the PC coefficients as:

$$\hat{\mu}_{Y, N_{\text{PCE}}} = y_{\alpha_0} \quad (3.35)$$

$$\hat{\sigma}_{Y, N_{\text{PCE}}}^2 = \sum_{\alpha \in \{\mathcal{A}^{M, N_{\text{PCE}}} \setminus \alpha_0\}} y_{\alpha}^2 \quad (3.36)$$

The sensitivity of the system response to the input variables can be investigated by means of the distribution of the total variance of the response, in other words, which amount of the total variance is due to the uncertainty in which input variables. Among others, the Sobol's indices are commonly adopted indicators to assess the sensitivity. The total Sobol's indices of the input variable X_i can be quickly calculated from the PCE coefficients [116]:

$$S_T^{X_i} = \frac{1}{\hat{\sigma}_Y^2} \sum_{\alpha \in \mathcal{I}_i^\dagger} y_{\alpha}^2 \quad (3.37)$$

where $\mathcal{I}_i^\dagger = \{\alpha \in \mathcal{A}^{M, N_{\text{PCE}}} \mid \alpha_i \neq 0\}$ contains all the multi-indices with a non-zero i -th component.

3.4.2.6 Experimental design (ED)

◆ Typical space-filling techniques

All the least-square-regression based algorithms resolve the unknown PCE coefficients by investigating the system responses over a specific set of points in the input variables space \mathcal{D}_X , referred as the Experimental Design (ED). Therefore, the strategy for building up the ED has great impact on the performance of the derived PCE model, in terms of both convergence rate and model accuracy. Given that our objective is to model the variation of the system response caused by uncertainties in input variables, it is crucial that the ED reflects well the

uncertainty characteristics of the input variables. In other words, the ED points should follow as well as possible the distribution of the input variables.

Now take the situation where the input variables are independent and are uniformly distributed in the space $\mathcal{D}_X \triangleq [0, 1]^M$ for example, then the hypercube $[0, 1]^M$ should be sampled as uniformly as possible (remind that in the situation of other types of distribution, they can be mapped to uniform distribution using iso-probabilistic transforms as explained in § 3.4.2.2, hence there is no loss of generality within this example). Various types of space-filling techniques can be adopted in such context. Without trying to be exhaustive, we can mention the crude Monte Carlo sampling (MCS), the quasi MCS techniques e.g. Halton's [117], Faure's [118], and Sobol's sequences [119], or the Latin Hypercube sampling (LHS) [120], etc. Among all these sampling techniques, MCS is the simplest one for implementation, e.g. using a random number generator (available in many mathematical tools and programming languages e.g. Matlab, Excel, Python, C, etc.). However, the problem of "clustering" arises in case of small-sized samples. That's to say, some zones of \mathcal{D}_X are more densely covered than the other zones. Therefore, to guarantee a good uniformity in the entire \mathcal{D}_X , a substantial amount of points are often needed, hence inducing high computational cost especially when the pre-evaluation is time-consuming (such as EM simulations). The quasi MCS techniques aim at placing points at deterministic positions in order to uniformly cover the \mathcal{D}_X , hence mitigate the "clustering" problem for small sized samples. LHS is a widely used technique which retains both benefits of uniformity and "random ability" (hence the "uncertainty" characteristics of the inputs). Precisely, to select N_{ED} points from the input variables space \mathcal{D}_X four steps are to be followed:

- i. the definition domain of each input variable X_j ($j = 1, 2, \dots, M$) is divided into N_{ED} segments of equal probability, thereby, the entire space \mathcal{D}_X is divided into $(N_{ED})^M$ sub-hypercubes;
- ii. N_{ED} random permutations of the sequence $\{1, 2, \dots, N_{ED}\}$ are carried out, denote the i -th element of the j -th permutation reordered sequence as $\pi_{i,j}$;
- iii. N_{ED} sub-hypercubes are selected in the way that the i -th sub-hypercube ($i = 1, 2, \dots, N_{ED}$) is framed by the $\pi_{i,j}$ -th segment of the interval of X_j ($j = 1, 2, \dots, M$);
- iv. In each selected sub-hypercube, one point is randomly drawn with respect to the uniform distribution. Thereby, an ED of N_{ED} points is built up.

Mathematically, this reads as:

$$\mathcal{X}_{LHS} = \{x_j^{(i)} = \frac{\pi_{ij} - 1 + u_{ij}}{N_{ED}}, i = 1, \dots, N_{ED}; j = 1, \dots, M\} \quad (3.38)$$

where $[\pi_{ij}]$ is a $N_{ED} \times M$ matrix where each column is a random permutation of the sequence $\{1, 2, \dots, N_{ED}\}$, and where u_{ij} is a realization of a uniform random variable $U \sim \mathcal{U}(0,1)$.

In practice, we usually generate a large number of independent LHS designs for a desired size, then choose the one which best satisfies a favorable space-filling criterion, such as the ‘‘Maximin distance’’ [121] which aims at maximizing the smallest Euclidean distance between ED points. Thereby, the uniformity over the \mathcal{D}_x can be optimized.

◆ **Enrichment of the ED**

Abundant experience of researchers in computational engineering shows that instead of directly taking a large sized ED, it is more efficient to begin with an initial ED of small size, construct the surrogate model, assess the model performance, and then if necessary, enrich iteratively the ED until reaching a satisfactory precision. The enrichment of an existing ED can be achieved by adding new points with respect to some favorable space-filling criterion. The aforementioned ‘‘Maximin distance’’ is a popular criterion suitable for this context, and has been shown to be particularly efficient in the situations where the boundary zones have to be properly covered [122]. In practice, we usually generate a huge number (e.g. 10^5) of random points, and choose the one which has the ‘‘maximin distance’’ for the enrichment. Besides, other criteria include e.g. the so-called ‘‘ D -optimality’’ [123] and ‘‘ S -optimality’’ [124]. The underlying principle is to maximize the ‘‘good-conditioning’’ of the information matrix $\Phi^T \Phi$ in terms of: i) maximized determinant of $\Phi^T \Phi$; ii) maximized column orthogonality of $\Phi^T \Phi$ (hence minimized correlation between the ED points).

Furthermore, the feedback from accuracy assessment of the currently constructed model can also provide useful guidelines on the selection of new points for the next iteration. For example, regions where the current model predicts poorly should be sampled more densely.

3.4.3 Methodology based on VSH expansion and PCE

We propose an adaptive statistical methodology to extract surrogate models for variable antennas. The basic idea is to apply the HLARS-based PCE onto the VSH coefficients of the ATFs. For sake of simplicity, we adopt the notation of single condensed index $p = 2\{n(n+1) + m - 1\} + u$ as proposed in [70], and then (3.8) rewrites as:

$$\mathcal{H}(f, \hat{\mathbf{r}}) = \sum_{p=1}^P H_p(f) \hat{\Psi}_p(\hat{\mathbf{r}}) \quad (3.39)$$

with $P = 2N_{VSH}(N_{VSH} + 2)$.

Assume that there are M random variables, denoted as a random vector $\mathbf{X} = (X_1, X_2, \dots, X_M)^T$ with known joint PDF $f_{\mathbf{X}}$, the variable ATF as well as the complex-valued VSH coefficients H_p become random functions of \mathbf{X} :

$$\mathcal{H}(\mathbf{X}, f, \hat{\mathbf{r}}) = \sum_{p=1}^P H_p(\mathbf{X}, f) \hat{\Psi}_p(\hat{\mathbf{r}}) \quad (3.40)$$

To exploit the quantitative dependence of the ATF on \mathbf{X} , we apply the HLARS-based PCE on the real and imaginary part of the random functions $H_p(\mathbf{X}, f)$ separately:

$$H_p^{\text{Re/Im}}(\mathbf{X}, f) = \sum_{\alpha \in \mathcal{A}_p^{\text{HLARS}}}^{|\alpha| \leq N_{\text{PCE}}} y_{\alpha}^{p, \text{Re/Im}}(f) \Phi_{\alpha}(\mathbf{X}) \quad (3.41)$$

where $\mathcal{A}_p^{\text{HLARS}}$ is the sparse basis scheme built up with the HLARS method (cf. § 3.4.2.3).

Thereby, we get a surrogate model $\hat{\mathcal{H}}(\mathbf{X}, f, \hat{\mathbf{r}})$ relating the ATF to the random input variables by a set of scalar coefficients $\{y_{\alpha}^{p, \text{Re/Im}}(f)\}$, as:

$$\hat{\mathcal{H}}(\mathbf{X}, f, \hat{\mathbf{r}}) = \sum_{p=1}^P \sum_{\alpha \in \mathcal{A}_p^{\text{HLARS}}}^{|\alpha| \leq N_{\text{PCE}}} (y_{\alpha}^{p, \text{Re}} + j y_{\alpha}^{p, \text{Im}})(f) \Phi_{\alpha}(\mathbf{X}) \hat{\Psi}_p(\hat{\mathbf{r}}) \quad (3.42)$$

At this moment, we still only consider the antenna's mono-frequency behavior, hence the parameter “ f ” can be omitted in equation (3.42).

3.4.3.1 Iterative procedure

The entire procedure for extracting the surrogate model $\hat{\mathcal{H}}(\mathbf{X}, \hat{\mathbf{r}})$ comprises steps of:

1. Initialization:
 - a. Initialize the ED \mathcal{X} of a desired size with the LHS design;
 - b. Determine the maximal degree N_{VSH} for VSH expansion;
 - c. Choose a LOOE threshold ($e_{\text{LOO_th}}$) for assessing the accuracy of PCE models.
2. Evaluate the ATFs over the ED. Precisely, for each input value $\mathbf{x}^{(n)}$, $n=1, \dots, N_{\text{ED}}$, configure the corresponding antenna, carry out the EM simulations or measurements, and compute the ATF $\mathcal{H}(\hat{\mathbf{r}}, \mathbf{x}^{(n)})$.
3. Apply the VSH expansion to each ATF and obtain the VSH coefficients $H_p(\mathcal{X})$, $p=1, \dots, P$.
4. Apply the HLARS-based PCE method separately to the real and imaginary part of each VSH coefficient $H_p(\mathcal{X})$ and finally get PCE models as in (3.41).
5. Assess the LOOE e_{LOO} of the PCE models. If $e_{\text{LOO}} \leq e_{\text{LOO_th}}$ is satisfied for all models, or if N_{ED} exceeds an acceptable value (i.e. too costly to continue) then stop the

modeling procedure; otherwise, enrich the ED (i.e. $\mathcal{X}=[\mathcal{X};\mathcal{X}_{\text{add}}]$) with respect to the “Maximin distance criterion”, and return to Step 2.

Eventually, a surrogate model relating quantitatively and explicitly the random variables \mathbf{X} and the ATF via the whole set of polynomial coefficients $\{y_{\alpha}^{p,\text{Re/Im}}|\alpha \in \mathcal{A}_p^{\text{HLARS}}, p=1,\dots,P\}$ is established, allowing the ATF generation for any value of \mathbf{X} (within the variation ranges).

3.4.3.2 Validation on a canonical dipole antenna

To demonstrate the feasibility of our proposed methodology, we first apply it to a lossless half-wave wire dipole, which is a simple and very well-known canonical antenna, hence an ideal “test antenna” to verify systematically the relevance, accuracy and robustness of the methodology. The same dipole design as was used in § 3.3.2.1 is re-used.

a. Random input parameters

The dipole is assumed to be deformable using 3 independent parameters, namely stretching (with stretch ratio ξ), bending (with curvature κ or bending radius $R_b = 1/\kappa$), and torsion (with torsion rate α), see Figure 3.22 (b)-(d). We suppose also that the input parameters (ξ, κ, α) are uniformly distributed over respectively $[1, 1.05]$, $[0, 0.1]$ mm^{-1} , and $[0, 0.1]$ $\text{rad}\cdot\text{mm}^{-1}$. Figure 3.23 shows the joint effects of deformations on the reflection coefficient $|S_{11}|$ and on the radiation patterns (at $f = 2.3$ GHz). Compared to the original dipole, variations of more than 15 dB in $|S_{11}|$ and 13.5 dB in G_r , i.e. 92.6 % in terms of *RRMSE* are observed. These large variations justify to resort to an accurate quantitative approach. At the first stage, we consider the relatively simple case where f is fixed at 2.3 GHz, thus the index “ f ” will be omitted in all physical quantities.

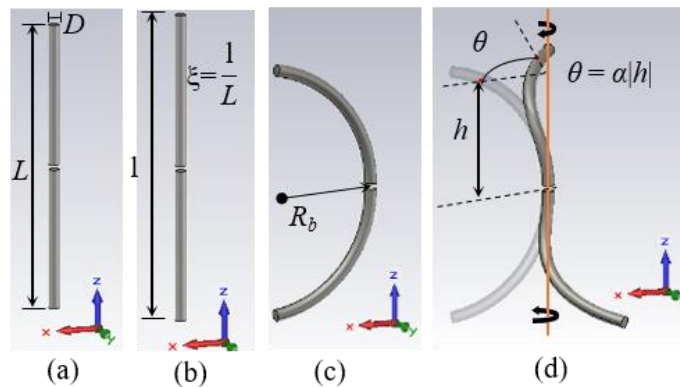


Figure 3.22: Illustration of a dipole undergoing different deformations: (a) original dipole; (b) stretched dipole; (c) curved dipole; (d) curved and twisted dipole.

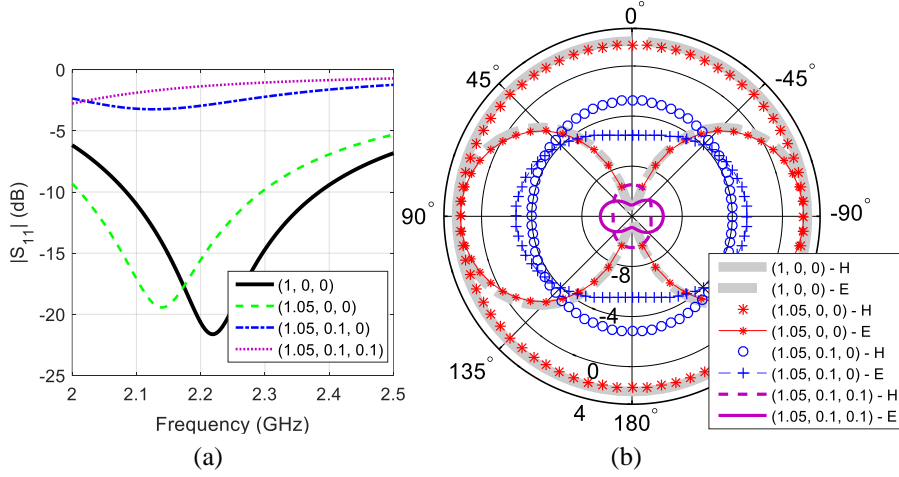


Figure 3.23: Joint effect of stretching, bending, and torsion (ξ , κ , α) on the dipole: (a) reflection coefficient $|S_{11}|$; (b) radiation patterns (in E/H plane) at $f = 2.3$ GHz.

b. Modeling description and results

The modeling approach described in § 3.4.3.1 is applied to the dipole. Firstly, the ED is initialized with a sample of 100 realizations using the LHS technique. The desired LOOE threshold $e_{\text{LOO_th}}$ is set to 4 %. Note that the choice of $e_{\text{LOO_th}}$ is subjective, depending on the required accuracy and the convergence rate. A typical value of < 5 % is popularly adopted in many publications e.g. [94]. Secondly, the evaluations of the ATFs are carried out in CST[®] MWS (with the FEM solver) to obtain radiation fields which are sampled every 5° in both elevation and azimuth. The full truncation degree of the VSH expansion is set to $N_{\text{VSH}} = 3$ (i.e. $P = 2N_{\text{VSH}}(N_{\text{VSH}} + 2) = 30$), for which the collected power is proved to be very close to the total power of the EMF in reality. The “Maximin distance” technique is used for iteratively enriching the initial ED. At last, we use the UQLab, a toolbox¹ for the uncertainty quantification developed by the team of B. Sudret [125], to implement the HLARS-based PCE algorithm.

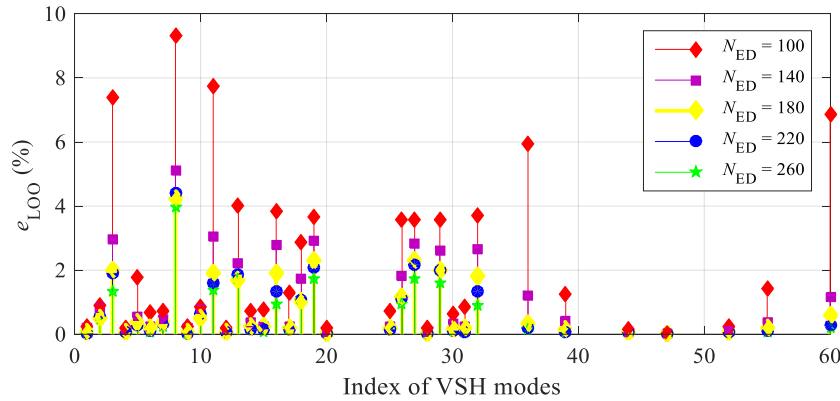


Figure 3.24: e_{LOO} of the PCE models derived from the iteratively enriched EDs.

¹ Available for free for academics. B. Sudret must be warmly thanked for offering this opportunity.

Figure 3.24 shows the evolution of the e_{LOO} of the PCE models. It can be seen that when N_{ED} increases the error decreases for all PCE models and the $e_{\text{LOO,th}}$ is satisfied for all models for $N_{\text{ED}} = 260$, for which we get a surrogate model with about 2000 polynomial coefficients.

In order to verify its accuracy and robustness, the constructed surrogate model has been used to generate the most deformed dipole, i.e. $(\xi, \kappa, \alpha) = (1.05, 0.1, 0.1)$, and a comparison of radiation patterns between the initial field, the reconstructed field with full ($P = 30$) VSH modes, and the generated field with the surrogate model is presented in Figure 3.25 (a). It is noted that the maximal difference in G_r is only 0.7 dB and the $RRMSE$ is less than 8 %.

Furthermore, the surrogate model has been used to generate dipoles for 500 random values of (ξ, κ, α) , which are compared to their simulated (with CST[®] MWS) counterparts, as shown in Figure 3.25 (b). This constitutes actually a test of Monte Carlo (MC). We see that the $RRMSE$ of the generated antennas remains below 2 % for 88 % of the cases and the extreme error is still less than 10 %, which confirms the accuracy and the robustness of the surrogate model. It is worth mentioning that there is always a trade-off between the model accuracy and the cost to achieve that precision – the higher the accuracy of the model, the higher the cost of the modeling procedure. One can choose the most appropriate trade-off according to each practical needs. Another conclusion we can draw is that the surrogate model also verifies high parsimony. Compared to the initial antennas representation by a huge amount of sampled EMF data ($\sim 10^6$), the surrogate model requires only a limited number of parameters (i.e. $\sim 10^3$), reaching a data compression rate of about 10^3 . It is actually much higher as input data (random input parameters or angle variables) can be interpolated as desired.

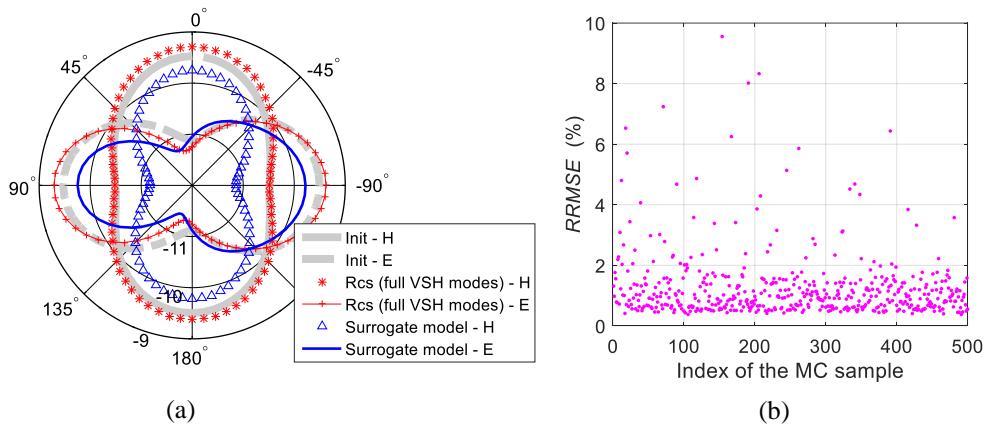


Figure 3.25: (a) Radiation patterns (in E/H plane) of the initial, reconstructed and generated fields for the most deformed case at $f = 2.3$ GHz; (b) $RRMSE$ of 500 generated dipoles for random values of (ξ, κ, α) .

c. Conclusion

The proposed methodology combining the VSH expansion and the HLARS-based PCE methods allows to develop compact and precise surrogate models of the ATF with a minimized cost. The feasibility, efficiency and high accuracy of this methodology have been preliminarily tested by means of modeling a canonical deformable dipole. The derived model is computationally costless for generating deformable dipole configurations, usable as surrogate models in various types of analyses where the *complete* field knowledge, including polarization and phase, are required.

However, although this methodology has been validated conceptually, there still remain some important issues that should be carefully solved before generalizing the methodology to much more complicated realistic applications, where robustness and efficiency are highly demanded. This aspect will be discussed in the next section.

3.5 Improvements of the statistical method

In this section, we further exploit the potential of our proposed method by: i) taking into account the frequency behavior; ii) enhancing the parsimony of the surrogate model; iii) more efficiently controlling the iterative modeling procedure with appropriate performance metrics. In particular, a more realistic application with larger number of input variables and more complicated random deformations will also be addressed.

3.5.1 Frequency behavior

Up to now the frequency-dependency of the ATF has not yet been modeled seeing that a single frequency (e.g. the nominal frequency) was considered in all previous examples. However, including the frequency behavior is fundamental to make the antenna model *complete*. To give an analogy, this is equivalent to switch from the modeling of a static to a dynamic problem, e.g. in mechanics (see e.g. [126]). For narrow-band (NB) antennas, taking into account the frequency allows to discriminate between mismatch/detuning effects (cf. Chapter 5) and directional effects due to the input variability in the FF behavior. A single frequency model is hence incomplete, and actually insufficient. For multi-band, wideband – and a fortiori for UWB – antennas, their frequency response is mandatory for obvious reasons. More generally, at least for moderate band (and beyond) or multi-band systems, if the model is used jointly with a stochastic frequency-dependent directional channel model in order to assess the radio links performance – e.g. for different PHY layer schemes – the antenna frequency response is mandatory (see e.g. [127]).

To address the frequency behavior, the simplest way is to consider the frequency as it is, a deterministic variable, i.e. to sample the frequency axis and built surrogate models separately for each frequency sample. Then, an interpolation technique can be used for covering the

entire frequency band. The cost is obviously a very significant reduction of the parsimony, and moreover, the interpolation may introduce additional errors.

Alternatively, the frequency can be considered somehow as a “random” input parameter for the problems for which the frequency behavior of the output quantity (represented by the vector-valued model $\mathbf{Y} = [y_{\alpha}^q(f)]$ in our case) is sufficiently regular with respect to the input parameters variability. Indeed, the final derived surrogate model is actually deterministic, because it allows to recover the exact ATF for any given values in the input space.

The “regularity” here refers to such situation, for which the frequency response (in the statistical sense) does not vary abruptly (*locally*) with respect to the random input variables. Note indeed that polynomials are rather “smooth” functions (compared to rational functions), thus, in some situations, the PCE is not the most appropriate technique (polynomials are not suitable bases) if the local variations of the output quantities with respect to some input parameters are too considerable. It should be pointed out that the assumption of “smoothness” does not necessarily lead to insignificant global sensitivities – which measure how the variance (i.e. range of variation) of the output quantities depends on the input variables (see Sobol’s indices in § 3.4.2.5). In practice, this “regularity” corresponds to antennas which are not too much resonant. If the considered antenna is resonant, the question whether the frequency can be treated as another random input variable or not must be specifically addressed. In other words, some preliminary tests must be driven. If the frequency behavior appears too difficult to model this way, alternative approaches must be envisaged. For resonant systems, at least an alternative method proposed by Sudret’s team exists, based on preliminary affine transformations of the frequency axis, applied prior to PCEs [128]. However, this technique is significantly more sophisticated, and requires the realization of two independent EDs, which means a significant computational cost.

After including the frequency parameter “ f ” in the random input vector \mathbf{X} , the *complete* surrogate model (3.42) is simplified into:

$$\hat{\mathcal{H}}(\mathbf{X}, \hat{\mathbf{r}}) = \sum_{p=1}^P \sum_{\alpha \in \mathcal{A}^{HLARS}}^{| \alpha |_1 \leq N_{\text{PCE}}} (y_{\alpha}^{p,\text{Re}} + j y_{\alpha}^{p,\text{Im}}) \Phi_{\alpha}(\mathbf{X}) \hat{\psi}_p(\hat{\mathbf{r}}) \quad (3.43)$$

where \mathbf{X} includes now the frequency “ f ” as an additional input variable, and $y_{\alpha}^{q,\text{Re/Im}}$ are purely constant real coefficients to be determined.

3.5.2 Enhanced parsimony

The benefit of a parsimonious surrogate model is twofold: first, the computational cost for constructing the model can be reduced, since the number of unknown parameters thereby the number of required pre-evaluations (which are often time-consuming) becomes smaller.

Second, the computational cost for generating ATFs with the surrogate model can be reduced, since there will be less algorithmic operations in a more compact model. Such type of saving could become impressive when a substantial amount of realizations are demanded, such as for a Monte Carlo analysis, in particular when multiple statistics must be combined, e.g. in joint antenna/channel statistical modeling. We discussed in § 3.4.2 that the HLARS algorithm helps to obtain a sparse PCE expression. In this section, we try to exploit the possibility of sparsity in the VSH expansion.

3.5.2.1 Sparse VSH expansion

We express the complex-valued VSH coefficient H_p in (3.39) explicitly by its real and imaginary parts in order to highlight their individual contribution.

$$\hat{\mathcal{H}}(\hat{\mathbf{r}}) = j \sum_{q=1}^Q (-j)^{\text{mod}(q,2)} H_q \hat{\Psi}_{\lceil q/2 \rceil}(\hat{\mathbf{r}}) \quad (3.44)$$

where $Q = 2P$; H_q are scalar coefficients representing either the real or imaginary part of H_p according to the following rule: $H_q = \Re\{H_p\}$ (or $\Im\{H_p\}$) for $t = 1$ (or 2) with $q = 2(p-1) + t$; “mod(a, n)” means “ a modulo n ”; “ $\lceil \cdot \rceil$ ” is the ceiling round function; and $j = \sqrt{-1}$.

We note that the radiated power P_{rad} (which is normalized to an incident power of 1 Watt) of the antenna can be calculated easily from (3.44), thanks to the orthonormality of the basis:

$$P_{\text{rad}}(\mathbf{X}) = \frac{1}{4\pi} \iint_{\Omega} \|\mathcal{H}(\mathbf{X}, \hat{\mathbf{r}})\|^2 d\Omega = \frac{1}{4\pi} \sum_{q=1}^Q H_q(\mathbf{X})^2 \quad (3.45)$$

By defining the modal power weight as:

$$W_q(\mathbf{X}) = \frac{1}{4\pi} \frac{H_q(\mathbf{X})^2}{P_{\text{rad}}(\mathbf{X})} \quad (3.46)$$

we can construct a sparse VSH expansion: all $H_q(\mathbf{X})$ are sorted in descending order according to their power weight, and then only the first dominant ones with their collected weights amounting to a predefined threshold, denoted as $E_{\text{c_th}}$ (e.g. 99.9 %), will be retained. This allows either to reduce the number of VSH coefficients for a given truncation degree N_{VSH} (affecting only marginally the accuracy), or to increase N_{VSH} for a given maximal number of coefficients (hence enabling to reduce the truncation error).

Denoting I_D the set of index for all selected dominant modes, and N_D the cardinal of I_D , equation (3.44) is simplified to:

$$\hat{\mathcal{H}}(\hat{\mathbf{r}}) = j \sum_{q \in I_D}^{q \leq Q} (-j)^{\text{mod}(q,2)} H_q \hat{\Psi}_{\lceil q/2 \rceil}(\hat{\mathbf{r}}) \quad (3.47)$$

3.5.2.2 Correlation analysis on the selected dominant VSH modes

The influence of input randomness may induce detuning, impedance mismatch, power loss, and variation of the radiation pattern shape. The first two effects change the antenna total efficiency, such that all dominant VSH modes are influenced in the same way, and the last effect may lead to power transfer among different modes. In other words, we think it is possible that the random effects may increase the modal energy of one VSH mode, and at the same time, decrease that of another mode. As a result, one can anticipate that evolutions of these VSH modes are not totally independent each other, and this can be efficiently exploited towards further parsimony. This can be for example observed in the parametric approach presented in §3.3.2.3: see e.g. the behavior of the modal coefficients $\Re\epsilon(H_{1,1}^1)$ and $\Re\epsilon(H_{3,0}^2)$ in Figure 3.12.

Only the strong linear correlations between modes have been exploited here in order to preserve quantitative explicitness and precision of the surrogate model. From the sparse VSH expansions of the N_{ED} ATFs we calculate the $N_{\text{D}} \times N_{\text{D}}$ correlation matrix $\boldsymbol{\rho} = [\rho_{m,n}]$ of which the element $\rho_{m,n}$ is the correlation coefficient of the m -th and the n -th column vector of the matrix \mathbf{H} (3.48). Then, the VSH modes having a correlation coefficient greater than a pre-defined threshold (e.g. 0.995) are considered as linearly dependent and arranged in disjoint subsets \mathcal{G}_l ($l = 1, \dots, N_{\text{G}}$), each containing at least one mode. Each \mathcal{G}_l forms an equivalent class represented by its “generator” (the lower order VSH coefficient), denoted $H_{q_{\mathcal{G}_l}}$. As a result, instead of N_{D} , only N_{G} ($N_{\text{G}} < N_{\text{D}}$) VSH coefficients have to be modeled with the PCE method; the other VSH coefficients of each class are represented by their linear regression parameters and can be simply computed from them once the generator is modeled. This correlation procedure reduces significantly the model complexity, i.e. the number of PCE coefficients and the computational cost, resulting in favorable compactness of the surrogate model.

$$\mathbf{H} = \begin{bmatrix} H_{q_1}(\mathbf{x}^{(1)}) & H_{q_2}(\mathbf{x}^{(1)}) & \dots & H_{q_{N_{\text{D}}}}(\mathbf{x}^{(1)}) \\ H_{q_1}(\mathbf{x}^{(2)}) & H_{q_2}(\mathbf{x}^{(2)}) & \dots & H_{q_{N_{\text{D}}}}(\mathbf{x}^{(2)}) \\ \vdots & \vdots & \vdots & \vdots \\ H_{q_1}(\mathbf{x}^{(N_{\text{ED}})}) & H_{q_2}(\mathbf{x}^{(N_{\text{ED}})}) & \dots & H_{q_{N_{\text{D}}}}(\mathbf{x}^{(N_{\text{ED}})}) \end{bmatrix} \quad (3.48)$$

After integrating all compaction techniques (i.e. frequency behavior modeling, sparse VSH expansion, and correlation analysis) the *complete* surrogate model (3.42) finally reduces to:

$$\left\{ \begin{array}{l} \hat{\mathcal{H}}(\mathbf{X}, \hat{\mathbf{r}}) = j \sum_{q \in I_D}^{q \leq Q} (-j)^{\text{mod}(q, 2)} H_q(\mathbf{X}) \hat{\Psi}_{\lfloor q/2 \rfloor}(\hat{\mathbf{r}}) \\ H_q(\mathbf{X}) = \begin{cases} \sum_{\alpha \in \mathcal{A}_q^{\text{HLARS}}}^{|\alpha| \leq N_{\text{PCE}}} y_\alpha^q \Phi_\alpha(\mathbf{X}), & \text{if } q \in I_G = \{q_{G_1}, \dots, q_{G_{N_G}}\} \\ \mathcal{L}_q[H_{q_{G_l}}(\mathbf{X})], & \text{if } H_q \in \mathcal{G}_l \text{ and } q \neq q_{G_l} \end{cases} \end{array} \right. \quad (3.49)$$

where \mathbf{X} is the random vector containing the input random parameters and the frequency “ f ” as an additional parameter; I_D is the subset containing the index of the selected dominant VSH modes; I_G is the subset containing the index of the N_G “generator” modes; $\mathcal{A}_q^{\text{HLARS}} \subset \mathbb{N}^M$ is the sparse HLARS scheme adopted for the $H_q(\mathbf{X})$ expansion; \mathcal{L}_q is the linear operator relating the mode H_q to the generator $H_{q_{G_l}}$ of the class \mathcal{G}_l it belongs to, which can be easily obtained by linear regression analysis.

3.5.3 Appropriate metrics

New metrics for controlling the algorithm convergence and evaluating the accuracy of such vector-valued surrogate models are defined: the Weighted Total Leave-One-Out error, denoted e_{WTLOO} , and the Supremum error, denoted e_{Sup} . These indicators play a major role for assessing the convergence of the iterative approach and ensuring the reliability and the robustness of the deduced surrogate model.

- 1) The e_{Sup} , defined in (3.50), assesses the absolute difference between the reconstructed and the initial ATFs in terms of the realized gain G_r over an appropriate solid angle.

$$e_{\text{Sup}}(\mathbf{x}) = \max_{(\theta, \varphi) \in \Omega_m(\mathbf{x})} \left\{ \left| G_r^{\text{init}}(\mathbf{x}, \theta, \varphi) - G_r^{\text{rcs}}(\mathbf{x}, \theta, \varphi) \right| \right\} \quad (3.50)$$

where G_r^{init} and G_r^{rcs} denote the G_r (in “dB”) of the initial and the reconstructed fields respectively; $\Omega_m(\mathbf{x}) \triangleq \{(\theta, \varphi) \mid G_r^{\text{init}}(\mathbf{x}, \theta, \varphi) \geq \max_{(\theta, \varphi) \in [0, \pi] \times [0, 2\pi]} [G_r^{\text{init}}(\mathbf{x}, \theta, \varphi)] - \Delta G_r\}$ is the so-called main radiation zones, with $\Delta G_r > 0$ an adjustable margin.

- 2) The e_{WTLOO} , an analogue of the LOOE when taking into consideration the modal weight, is defined for our multi-input/multi-output problem as:

$$e_{\text{WTLOO}} = \sum_{l=1}^{N_G} e_{\text{LOO}}^l W_l \quad (3.51)$$

where e_{LOO}^l is the e_{LOO} of the PCE model of the “generator” $H_{q_{G_l}}$ of the l -th group \mathcal{G}_l , and W_l is the total power weight of \mathcal{G}_l . This indicator takes into account the power proportion of each scalar PCE model. This “penalty” applied to modes with a lower

power contribution (but with a significant e_{LOO}) is aiming to avoid any artificial overestimation of the error.

3.5.4 Iterative modeling procedure

The improved algorithm for constructing antenna surrogate models is summarized below:

1. Initialization:
 - a. Build up the initial ED \mathcal{X}_0 of a desired size with the LHS design;
 - b. Determine the maximal degree N_{VSH} for VSH expansion;
 - c. Assign a WTLOOE threshold ($e_{\text{WTLOO_th}}$) for assessing the accuracy of derived PCE models;
 - d. Set an initial power threshold $E_{\text{c_th}}$ for sparse VSH expansion.
2. Construct the surrogate model $\hat{\mathcal{H}}^{(0)}$ by applying the VSH/HLARS-based PCE method:
 - a. Evaluate the ATFs over the ED: $\mathcal{H}(\mathbf{x}^{(n)}, \hat{\mathbf{r}})$, $n = 1, \dots, N_{\text{ED}}$;
 - b. Apply the sparse VSH expansion to each ATF under the power criterion $E_{\text{c_th}}$ according to (3.47) and obtain the index set of dominant modes $I_d^{(n)}$;
 - c. Define the aggregated index set as $I_D = \bigcup_{n=1}^{N_{\text{ED}}} I_d^{(n)}$;
 - d. Re-decompose all ATFs into modes $\{\hat{\Psi}_{\lceil q/2 \rceil}, q \in I_D\}$ and obtain the VSH coefficients $\{H_q(\mathcal{X}), q \in I_D\}$. Note that the purpose of Step 2.b – 2.d is to guarantee that all VSH expansions are based on the same set of modes, whereas the power criterion $E_{\text{c_th}}$ is also satisfied;
 - e. Reconstruct the ATFs from the selected dominant modes $\{(H_q(\mathcal{X}), \hat{\Psi}_{\lceil q/2 \rceil}), q \in I_D\}$ and assess the error of reconstruction: if e_{Sup} is satisfied then pass to Step 2.f; otherwise increase $E_{\text{c_th}}$ and go back to Step 2.b;
 - f. Group all the H_q into equivalent classes \mathcal{G}_l using correlation analyses;
 - g. Apply the HLARS-based PCE on the “generator” modes $H_{q_{\mathcal{G}_l}}$, and finally get the surrogate model $\hat{\mathcal{H}}^{(0)}$ as in (3.49).
3. Improve iteratively the model accuracy. For $i = 1 : I_{\text{max}}$
 - a. Enrich the ED using the “Maximin” technique: $\mathcal{X}_i = [\mathcal{X}_{i-1}; \mathcal{X}_{\text{add}}]$;
 - b. Repeat Step 2 to construct the new surrogate $\hat{\mathcal{H}}^{(i)}$;
 - c. Predict the ATFs over \mathcal{X}_i using the latest two successive surrogates, i.e. $\hat{\mathcal{H}}^{(i-1)}(\mathcal{X}_i)$ and $\hat{\mathcal{H}}^{(i)}(\mathcal{X}_i)$; and investigate the accuracy and convergence:

- ✓ is the e_{WTLOO} of the surrogate model $\hat{\mathcal{H}}^{(i)}$ sufficiently small, i.e. $e_{\text{WTLOO}} \leq e_{\text{WTLOO_th}}$?
- ✓ are the e_{Sup} of the predicted ATFs $\hat{\mathcal{H}}^{(i)}(\mathcal{X}_i)$ sufficiently small?
- ✓ is the e_{WTLOO} still decreasing (rapidly) when passing from $\hat{\mathcal{H}}^{(i-1)}$ to $\hat{\mathcal{H}}^{(i)}$?
- ✓ does the distribution of the e_{Sup} converge passing from $\hat{\mathcal{H}}^{(i-1)}(\mathcal{X}_i)$ to $\hat{\mathcal{H}}^{(i)}(\mathcal{X}_i)$?

If the e_{WTLOO} and e_{Sup} criteria are satisfied or the e_{Sup} converges, i.e. no remarkable improvement is achieved by further enrichment, we stop the algorithm and the actual model $\hat{\mathcal{H}}^{(i)}$ is chosen; if not, continue until reaching the maximum loop number I_{max} .

The final surrogate model, represented by a set of scalar coefficients $\{y_{\alpha}^q \mid \alpha \in \mathcal{A}_q^{\text{HLARS}}, q \in I_G\}$, allows to quantitatively predict the ATFs taking into account the random variabilities.

3.5.5 Application to a realistic deformable textile patch antenna

We test the performance of the improved methodology on a rather complex and realistic antenna other than the dipole antenna. Consider now a microstrip-fed rectangular textile patch antenna, as shown in Figure 3.26 (a). Its substrate is a thin layer of weakly compressible jeans tissue, and the patch and ground plane are made with a thin copper tape (thickness $\approx 25 \mu\text{m}$). This patch could be integrated into clothing, for example, on or into the sleeve of a jacket or coat, for transmitting to an access point vital signs data measured by sensors (such as body temperature, blood pressure, pulse rate, etc), in the context of *off-body* communications. The patch being deformable is subject to various sources of random variability such as crumpling, bending, etc. as shown in Figure 3.26 (b) which could seriously impact its radiation performance. Our proposed methodology is now applied to extract a surrogate model of this antenna example in order to quantitatively account for those statistical effects.

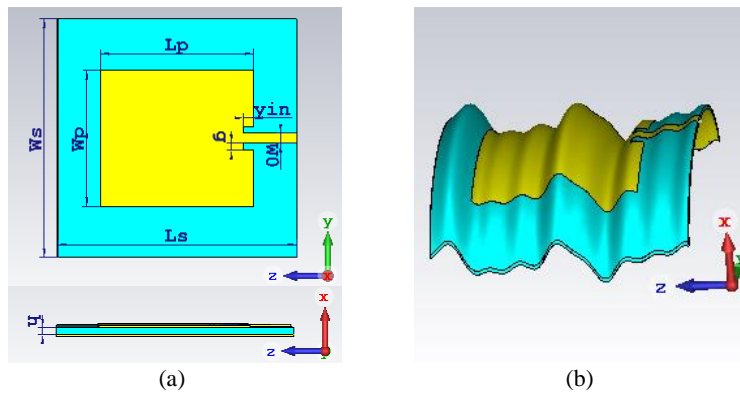


Figure 3.26: Wearable textile patch antenna: (a) un-deformed plane patch; (b) patch undergoing the joint effect of crumpling, bending and thickness variation.

3.5.5.1 Design of the textile patch antenna

The antenna dimensions are optimized for a good impedance matching over the Industrial Scientific Medical (ISM) frequency band of 2.4 – 2.5 GHz. The obtained design parameters are, $L_p = 44.96$ mm, $W_p = 40$ mm, $L_s = W_s = 70$ mm, $W_0 = 3$ mm, $g = 2$ mm, $y_{in} = 3$ mm, $h = 0.85$ mm, $\epsilon_r = 1.776$, $\tan\delta = 0.05$ (Figure 3.26 (a)). In order to illustrate the modeling principle with a problem of already high but tractable complexity, we choose to restrict the antenna random variability to classical deformations encountered in practice, namely bending, crumpling, and thickness change, and to material property variations. Precisely,

- The bending around the $z'Oz$ axis is quantified by its curvature κ (or its bending radius $R_b = 1/\kappa$).
- The crumpling along the $z'Oz$ axis is modeled in a very realistic way (instead of purely periodic variations used e.g. in [129]) with surfaces of revolution created by rotating a bandlimited Weierstrass function $W(z)$ (3.52) [130] around the $z'Oz$ axis. The *amplitude* C and the *spatial pseudo-frequency* s are used to adjust the crumpling. The other parameters are fixed to $N_2 = 3$, $b = 2e/3 \sim 1.8$, and the *dimension* D to 1 corresponding to rather smooth curves.

$$W(z) = C \sum_{n=1}^{N_2=3} b^{(D-2)n} \cos\left\{2\pi s b^n \left(\frac{L_s}{2} + z\right) + \frac{8}{5}\pi\right\}, z \in \left[-\frac{L_s}{2}, \frac{L_s}{2}\right] \quad (3.52)$$

- The thickness change is quantified by the variation of substrate height h .
 - The tissue property is characterized by the variation of its relative permittivity ϵ_r , the variation of its loss tangent $\tan\delta$ is not considered here, since the effect is only of second-order compared to that of the permittivity [51].
- Additionally, the frequency “ f ” is also considered as a “random variable” so as to account for the frequency behavior.

3.5.5.2 Joint distribution of the random input parameters

We assume that these 6 random parameters are independent each other and are uniformly distributed over their proper ranges listed in Table III.

Table III: Random input parameters of the textile patch.

Random parameter	Unit	Nominal value	Support
κ	mm ⁻¹	0	[0, 1/30]
C	mm	0	[0, 5]
s	-	1	[1, 1/0.6]
h	mm	0.85	[0.8, 0.9]
ϵ_r	-	1.776	[1.6, 1.9]
f	GHz	2.45	[2.4, 2.5]

This assumption is a simplification from the complex reality. In general, global geometric deformations, in particular complex ones such as the combination of bending and crumpling, induce intricate local mechanical stress over the substrate (compression – or even tension – often anisotropic, possible shear stress, etc.), causing various types of local and often anisotropic deformations such as thinning, stretching, and possibly thickening, inducing some variations of the substrate permittivity. As pointed out in Boeykens’ work [49], [131] and Locher’s work [132], bending tends to reduce the substrate thickness when the patch is not stretchable, causing an increase of the permittivity by densification. Therefore, the permittivity is correlated to the curvature, and for a given curvature, the thicker the substrate, the stronger the “compression effect”, and the stronger the correlation between ε_r and h . Indeed, the combination of bending and crumpling is significantly more complex than the bending alone, so that the induced influence on the permittivity is certainly more complicated than the possible “compression effect”. As a result, in general but in particular for fabrics of high thickness and high compressibility, the substrate permittivity is certainly more or less correlated with the global geometrical parameters. In the general case, correlations between the input parameters should of course be taken into account. This could be done either using classical decorrelation techniques based on appropriate isoprobabilistic transforms such as the one used e.g. in [51], before performing the PCE expansion, or using gPCE, as presented in [133]. However, one of the difficulties is of course to assess these possible correlations (i.e. the covariance matrix) for complex deformations such as the combination of bending and crumpling. To our knowledge, to date, no data are available in the literature, neither even a possible methodology, for this case (notably in the context of our crumpling modeling with surfaces based on Weierstrass curves, which is new). Nevertheless, this does not call into question the very principle of the proposed modeling (once the decorrelation is performed, if needed, or if these correlations can be neglected as a first approximation).

Indeed, we assume deliberately independency between the input parameters in order to simplify the modeling complexity. That is a reason why we have chosen, for the substrate material, a type of thin and weakly compressible jeans tissue. Various advantages of using these types of textile which have relatively “stable” mechanical and electrical properties under geometrical deformations, including “large” ones are e.g. reported in Osman’s work [24]. In this context, although the assumption of independency is an approximation, it can be considered as a reasonable simplification. The consistency of our assumption on the joint distribution (independency and uniform distribution) of the input parameters in our considered context is broadly justified by the following qualitative and quantitative arguments.

1. Justification of the assumption of independency of the input parameters

First, irrespective of any other potential physical effects, it is obvious that global geometrical deformations induce a variation of the current density distribution, affecting both the input impedance (hence the reflection coefficient S_{11} , the center frequency f_c , etc.) and the radiation characteristics. This effect on the f_c will be called here “geometric effect”. Second, the eventual effects induced by local stress (compression, etc.) on the substrate (variability of its thickness and permittivity) will be called the “substrate effect”. Our point of view is that the simplifying assumption neglecting the correlation between ϵ_r and (h, R_b) due to bending is a reasonable approximation if the two following conditions are met:

C1: The “geometrical effect” is dominant compared to the “substrate effect”;

C2: The “substrate effect” is sufficiently small compared to the considered variability range of ϵ_r .

In order to verify quantitatively (or semi-quantitatively) whether these two conditions are verified in our case, we carried out a set of experiments and simulations to bring out the impact of bending around the $z'Oz$ axis on the shift of the center frequency $f_c = \arg \min_f |S_{11}(f)|$.

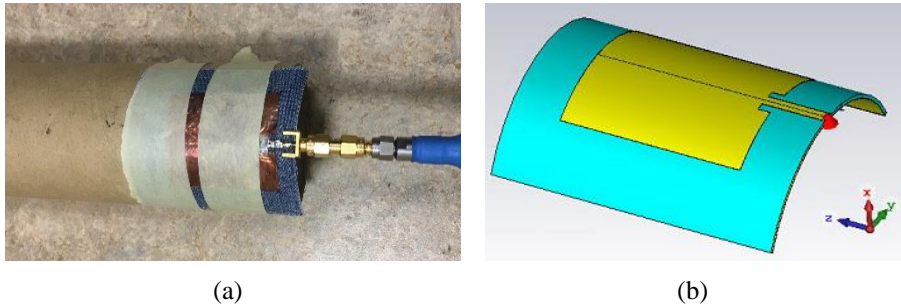


Figure 3.27: Experimental setup (a) and simulation design (b) for bending analysis.

1.1. Experimental measurements

A flat patch is bent around a hollow carton tube of 31.75 mm radius (close to the considered minimal value $R_{b,min} = 30$ mm) and 1.9 mm thickness (Figure 3.27 (a)). The resonance frequencies before and after bending were measured with a Vector Network Analyzer (VNA) ROHDE&SCHWARZ ZVA 40. Prior to the measurement, we had verified that the carton tube (placed directly under the ground plane) has no influence on the antenna behavior. This is due to the isolation effect of the large ground plane of the antenna, the low permittivity of the carton and the thinness of the tube. Three prototypes were fabricated and each one was measured 3 times following complete “flat-bent-flat” cycles in order to ensure the reliability of the measurements. The result found is that the maximal bending causes on average a relative f_c shift of $\delta f_{c,meas} = -0.54 \% \pm 0.06 \%$. Of course, as this shift value comes from measurements, it accounts for the combination of all possible effects.

1.2. Simulations using CST MWS (with adaptive meshing for good precision)

- The flat patch with nominal design parameters (W_{p0} , h_0 , ε_{r0}) is simulated. The center frequency is denoted f_{c0} .
- Only the pure “geometric effect” of bending is simulated, for which the parameters are assigned as: $W_p = W_{p0}$, $h = h_0$, $\varepsilon_r = \varepsilon_{r0}$, and the bending radius is $R_b = 31.75$ mm. The center frequency is denoted $f_{c,g}$. The obtained frequency shift $\Delta f_{c,g} = f_{c,g} - f_{c0}$ is of $\delta f_{c,g} = \Delta f_{c,g}/f_{c0} = -0.37$ % relative to f_{c0} .
- Both the “geometric effect” and the entire “substrate effect” of bending are included in simulation. To simulate this case, we need to assign reasonable values for the parameters W_p , h , and ε_r . For this, we followed Boeykens’ work [131] in which was proposed a phenomenological model relating the “compressed permittivity” $\varepsilon_{r,comp}$ to the “initial” ε_{r0} , the “initial” height h_0 and the bending radius R_b , for a textile patch antennas under bending:

$$\varepsilon_{r,comp} = \varepsilon_{r,0} \left(1 + \eta \frac{h_0(d-0.5)}{R_b} \right)$$

where d and η are empirical parameters; $d \in [0.5, 1]$ indicates the stretchability of the patch, and the factor η is dependent on the substrate material and can be derived from experimental measurements.

As our prototype is made of copper foil & jeans (> 99 % cotton) and is bent symmetrically with respect to the feeding point, we first considered the “most possible correlated” situation, for which $d = 1$, and $\eta = 0.654$ (which is the largest value among the three cotton-based prototypes presented in [131]), and $R_b = 31.75$ mm. Therefore, the “real” permittivity value is given by $\varepsilon_r = \varepsilon_0 \left(1 + 0.654 \frac{0.85(1-0.5)}{31.75} \right) = 1.792$ (corresponding to a relative variation of $\Delta \varepsilon_r / \varepsilon_{r0} = 0.88$ %). W_p is set to W_{p0} since our patch is considered perfectly non-stretchable. However, we do not have exact information about the value of h , except that we know it decreases more or less due to the local compression effect. Hence, we performed simulations with a set of values of h , decreasing from h_0 down to 50 % of h_0 , in order to compute the center frequency denoted $f_{c,g+\varepsilon}$. The blue line in Figure 3.28 shows the frequency shift of $f_{c,g+\varepsilon}$ with respect to f_{c0} . We see that the shift is typically constant at -0.81 % up to 33 % of compression. In addition, we carried out measurements of the substrate thickness, *under the patch*, of two antenna prototypes (appropriately cut for that purpose) bent around another (smaller height) cylinder of about 30.7 mm radius, with a microscope and a Neltec/Micro-control micrometric precision linear translation platform (of less than 10 μm resolution): on average, the measured thicknesses are about 0.71 mm,

i.e. a relative compression of $\sim 17\%$, that is about half the “threshold” of about 33% found in simulation. Thereby, the obtained f_c shift value of -0.81% represents well the case of “geometric effect” + entire “substrate effect” for the considered curvature (and for the considered value of η).

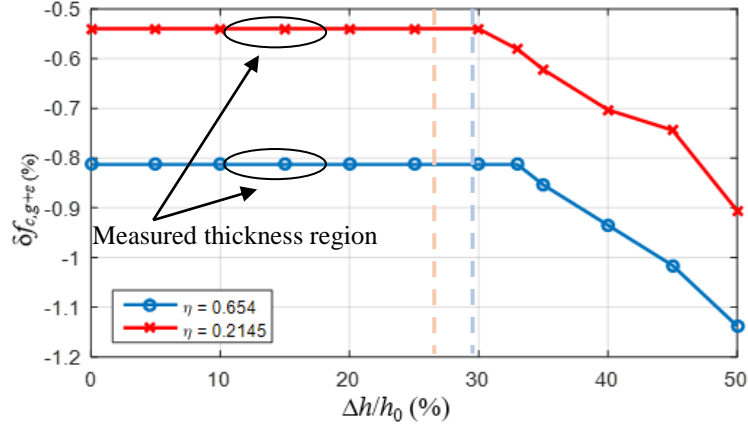


Figure 3.28: Center frequency shift under bending ($R_b = 31.75$ mm) for increasing substrate compression $\Delta h/h_0$ (by simulation).

- As the simulated frequency shift is clearly beyond the measured one ($\delta f_{c,meas} = -0.54\%$), new simulations were performed in order to seek for a more appropriate value of the empirical parameter η . The target ($\delta f_{c,g+\varepsilon} = \delta f_{c,meas}$) is reached for $\eta = 0.2145$ (corresponding to $\varepsilon_r = 1.781$, i.e. $\Delta\varepsilon_r/\varepsilon_{r0} = 0.28\%$). This value is significantly smaller than the previous one, when assuming a stronger correlation. As a result, in reality the correlation is indeed rather moderate. Note also that this value of η is very close to the smallest value obtained in [131] which gives some confirmation of the reliability of our combined measurements and simulations approach. New simulations were performed for $\eta = 0.2145$ and for the same set of decreasing values of h . The f_c shift with regard to h is shown by the red line in Figure 3.28. It can be seen that f_c shift is constant at -0.54% up to 30% (significantly larger than 17%) of compression.

1.3. Interpretation and conclusion

- The condition **C1** can be typically considered as verified, since:
 - ✓ The comparison between simulations and experiments show that the “geometric effect” (-0.37%) is the dominant “explicative contribution” to the measured shift (-0.54%), whereas the remainder (-0.17%) is due to rather complicate physical mechanisms including the “substrate effect”.

- ✓ These results show that the resulting “substrate effect” obtained assuming a rather significant correlation between ε_r and h (with $\eta = 0.654$), i.e. -0.44% ($-0.81 - (-0.37)$) % is 2.6 times larger than expected (-0.17%).
- The condition **C2** is verified, since:
 - ✓ Even if we took full consideration of the “most appropriate” correlation between ε_r and the global bending deformation, the variation of ε_r due to this deformation would be only of $\Delta\varepsilon_r/\varepsilon_{r0}(\eta = 0.2145) = +0.28\%$ (corresponding to the residual variation of -0.17% of f_c), and this for the “extreme” bending case. Comparing to the variability range of 17.1% assigned to ε_r , this amount is very small (about 1.6% of this range) and could be neglected to first order in a simplified statistical model.
- Conclusion:
 - ✓ The observed correlation is not as strong as “theoretically” predicted (following Boeykens’s model), as the “substrate effect” explicative contribution appears to correspond to an equivalent value of η smaller than expected (about 0.2145 instead of about 0.654). A possible interpretation is that the thin layer of copper tape glue between the patch and the substrate (which is probably stretchable) reduces to some extent the stress due to the copper tape during bending. This would correspond to a lower value of parameter d : if the empirical value $\eta \sim 0.654$ is a correct order of magnitude for the considered jean textile, this would correspond to a value of $d \sim 0.66$ ($= 0.5 + 0.2145 \times 0.5 / 0.654$).

We also performed a simulation corresponding to a perfectly stretchable patch (for which W increases from 40 mm to 40.53 mm for $R_b = 31.75\text{ mm}$, i.e. by 1.3%), all other parameters remaining constant ($d = 0.5$ in this case). The obtained simulated frequency shift is -0.41% (in between $\delta f_{c,g} = -0.37\%$ and $\delta f_{c,meas} = -0.54\%$).

- ✓ The result that the influence of h on ε_r under bending is typically marginal is due to the fact that the type of jean fabrics considered in the model (and used in practice for prototyping) is: (i) really thin, (ii) moderately compressible, and (iii) the variation range of h (although significant in relative scale; about 11.8%) is rather small (0.1 mm).
- ✓ For the same reasons, there is no particular argument to think that the crumpling could have a noticeable influence on ε_r , in the considered context. Indeed, crumpling is mainly due to a global constraint exerted “laterally”, i.e. along the antenna plane. The resulting local stresses can thus induce as well

local thickening than local thinning. Although local curvatures larger than the largest bending curvature considered above can be encountered, local curvatures far lower are necessarily present as well. It is consequently difficult to anticipate – and even more difficult to quantitatively assess – the crumpling influence *on average*, over ε_r . However, all the preceding arguments, in particular the substrate thinness, suggest that the overall effect should be weak.

- ✓ As a conclusion, we consider that the assumption of independency between the input parameters, notably between ε_r and the geometric parameters (h on the one hand, and the deformation parameters R_b , C and s , on the other hand) is a reasonable approximation, simplifying the modeling process without significant loss of accuracy.

2. Justification of the choice of the uniform distribution

We have chosen to address a *set* (or *category*) of thin jeans-based patch antennas, with some common substrate features (typically “dense” woven jeans) but with variable *nominal* permittivities, rather than simply considering the variability of ε_r due to fabrication tolerances. In such context, it is more appropriate to assume a uniform distribution for ε_r (rather than a normal one for example) since there is no particular reason that one value of ε_r be privileged from another. The above mentioned “common features” are notably their mechanical properties (weakly “compressible” or stretchable, compared to other fabrics), the type of fiber used (mainly cotton-based, in particular without elastane), and the type of fabrication process (mainly woven, rather than e.g. embroidered, knitted, etc.). The chosen range is based on a survey of the open literature [129], [134], [135]: typically, ε_r takes values between 1.4 and 2 for jeans or denim tissues, and commonly used values are around 1.7 – 1.8. After considering the trade-off between a large enough representative “population” and a moderate enough variation for limiting the model complexity (maximal degree of the PCE and required ED size), we choose to limit ε_r in the range [1.6, 1.9].

Regarding the other parameters:

- The frequency f is a deterministic parameter which would be evenly sampled if it were not considered as an input “random” parameter. The uniform distribution choice is hence obvious.
- For the reasons already discussed, the nominal thickness of the chosen substrate ($h = 0.85$ mm), as well as its absolute variability range ([0.8, 0.9] mm), are small. Hence, although its relative range of variability is noticeable (~ 11.8 %), it was pointed out above that its overall influence is limited (if not marginal), so that its

distribution appears not really critical. It is why we chose a uniform distribution for sake of simplicity. For example, we think that a possible alternative choice of a truncated Gaussian (in particular with a significant σ) would only marginally affect the results.

- Regarding the crumpling deformation (controlled by parameters C and s) an amplitude of 5 mm is chosen for the “Weierstrass-based” surfaces. This corresponds to a maximal “vertical” variation of $2 \times 5 = 10$ mm of crumpling corresponding to a ratio of $1/7$ with respect to the overall antenna side length. Parameter s is set between 1 and $1/0.6$. These ranges seem to represent well the real crumples. Considering that, (i) to our knowledge there are no available data in the open literature with regards to the crumpling statistics (in particular in the context of our crumpling model based on Weierstrass curves), (ii) the experimental assessment of such statistics is far from obvious and would require a significant dedicated work, and (iii) the relation between the “overall crumpling shape” (modeled by the Weierstrass curves) and the parameter s is not simple (actually nonlinear), we chose a uniform distribution for these two parameters for sake of simplicity as well.
- The bending is actually a particularly “application-dependent” deformation. Even in the context of wearable devices, the bending statistics (distribution and variability range) depends in practice on “usages”. First, these statistics depend on the considered *location(s)* of the antenna on the body (arm, wrist, thigh, ankle, chest, etc.). Second, the *way* the device/antenna is placed on the body – e.g. directly on the skin or in garments – plays as well a role in the choice of the statistics (in particular the variation ranges). For a specific “scenario” (e.g. an antenna embedded in a garment at the arm level), one could resort to some public anthropometric statistical databases. However, even for such specific scenario we observed that the bending deformation does not necessarily follow exactly the anthropometric parameters. In addition, these statistics depend on the considered population. For example, if we refer to the arm circumference database 2015-2016 provided by the US National Center for Health Statistics (from which the “medium” arm radius can be deduced; note that this is already an approximation), and if the entire population is considered, it appears that the radius statistics is not normal, but bimodal (close to a Gaussian mixture), as shown in Figure 3.29.

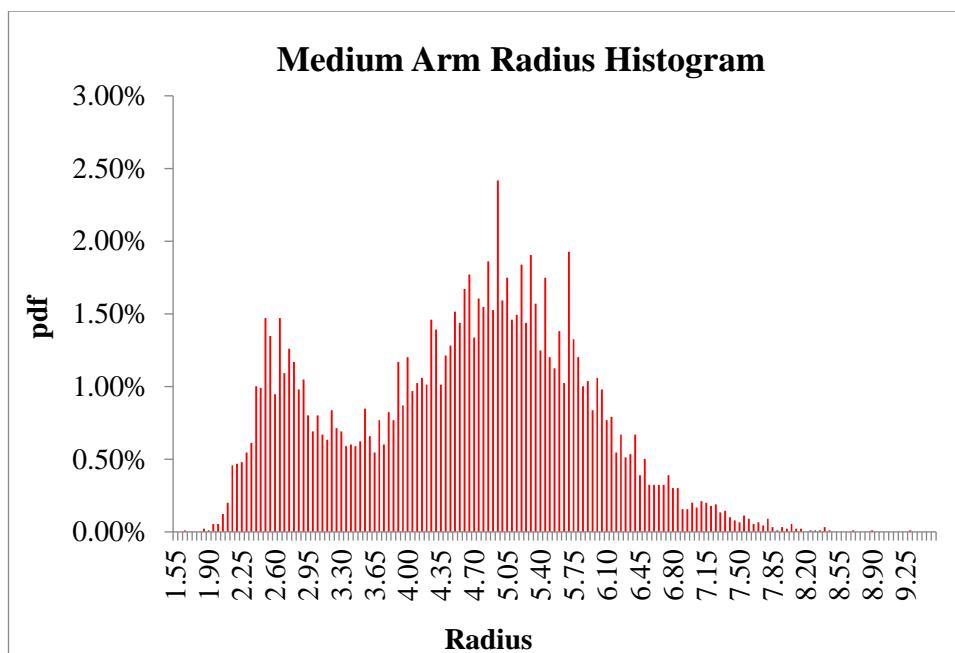


Figure 3.29: Statistic of the medium human arm radius, derived from the database 2015-2016 provided by the US National Center for Health Statistics.

Moreover, since we consider only the “symmetrical” bending (whose effect is less than that of the bending along the patch length), its overall impact is moderate, at least over the reflection coefficient. All these elements suggest that the choice of the bending distribution must have a moderate influence on the output statistics. We decided also for sake of simplicity to assume a uniform distribution for the curvature κ . Note that this assumption leads to the fact that the bending radius R_b follows random distribution of PDF as $1/R_b^2$, which favors the smallest radii, hence, e.g. a part of adults wrist statistics is somehow represented, and extend the radius range to infinity with a lower probability, hence e.g. suited for a location on the chest, or for some loose clothes whose deformations don’t necessarily follow precisely the morphology.

3. Conclusion regarding the assumption about the joint distribution of the input parameters

Our simplifying assumption of a uniform and independent joint distribution has been broadly justified as reasonable in first approximation for the considered thin and weakly compressible jean fabrics. The advantage of assuming the same distribution for all the parameters is of course to simplify the process – Legendre polynomials are appropriate for all parameters for the PCE; otherwise, hybrid of different categories of polynomials (e.g. Legendre or Hermite) would be necessary which would complicate the solution

process without bringing too much added value for illustrating the principle of our methodology.

Nevertheless, it is clear that our simplifying assumption is an approximation that cannot be generalized to other types of fabrics which can be far more compressible or stretchable. In that case, a dedicated work should be done to quantify the actual joint distribution of the input parameters (and their potential correlations) in advance. Then, it is generally possible to resort to decorrelation techniques based on appropriate isoprobabilistic transformations prior to building the PCE expansion, in order to go back to independent parameters following the same type of distribution (uniform, normal, for which the PCE bases are known – respectively Legendre or Hermit polynomials according to the Wiener-Askey scheme [48]) before applying our methodology. For example, if one wishes to address some specific scenario, one can drive dedicated analyses of the input statistics (distributions, interdependencies) if the operational conditions are clearly defined. In the context of wearables e.g., the antenna positioning – on the arm or wrist, etc., directly placed on the skin or into garments, etc. – would be a key information allowing to assess the bending or crumpling statistics.

3.5.5.3 Pre-evaluation of the ATFs

We use the full-wave simulator CST[®] MWS which is controlled by a Matlab routine for the automatic evaluation of ATFs over the ED. First, a parametrical patch antenna is designed and optimized at nominal parameters values; second, for each ED sample the patch is reconfigured accordingly and the transient solver with adaptive meshing is run to compute the FF. Once we get the evaluations a process of data quality check procedure is applied before further exploitation.

The reliability of the pre-evaluations depends on the quality of each operation during the automatic routine, notably: i) the precision of the geometric model of the antenna, i.e. the ability to transform the input parameters values to the corresponding geometrical dimension; ii) the accuracy of the solver; iii) eventual unexpected and abnormal software behavior (e.g. w.r.t the importation, exportation, etc.). Therefore, some preliminary tests (such as, parametric study in case of only one variable, see e.g. [69]) should be carried out in order to: i) find a robust automatic shaping process (analytical curve, lofting, extrusion, layer discretization, conforming...) for generating accurate antenna models (note that in CST, crumples of “Weierstrass” form & bending curves are not so easy to realize on a patch antenna composed of three thin layers, not to mention that we need to repeat the process a large number of times for different input parameters values); ii) adjust the control parameters of the adaptive meshing technique in order to obtain a good balance between the

stability/accuracy and the computational cost; iii) overcome possible software unexpected and non-physical behaviors.

3.5.5.4 Prototyping and control measurements

The comparison between the simulated and measured results (i.e. S_{11} and G_r) for three representative patch configurations was achieved (Figure 3.31). The 3 prototypes were all made of jeans tissue ($h = 0.85$ mm, $\epsilon_r = 1.776$, characterized using the Resonant-Patch method proposed in [136]) and 0.025 mm thick copper tape. Patch #1 is the un-deformed patch, considered as the reference; Patch #2 corresponds to a “severely bent & moderately crumpled” configuration, with $C = 5$ mm, $s = 1$, $\kappa = 1/30$ mm⁻¹; Patch #3 corresponds to a “severely bent & crumpled” configuration, with $C = 5$ mm, $s = 1/0.6$, $\kappa = 1/30$ mm⁻¹. The crumpling and bending were realized with two complementary extruded polystyrene matrices.

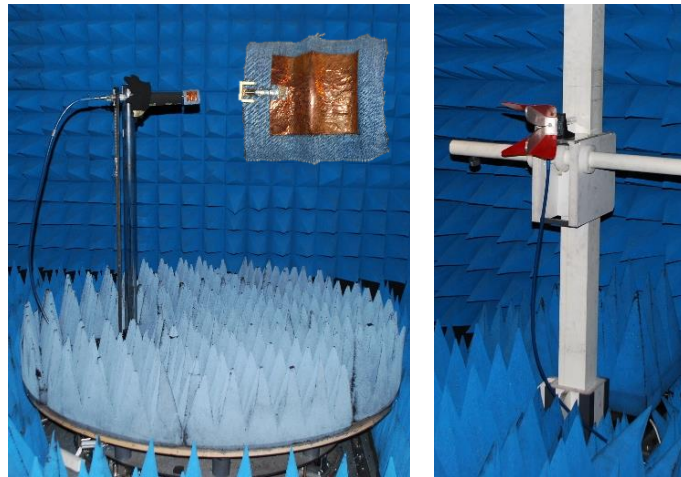


Figure 3.30: Experimental setup for measuring the ATFs.

Measurements of the ATFs (along two principal plane cuts) were carried out in a Siepel anechoic chamber (see the setup in Figure 3.30) equipped with an ETS-Lindgren two-axis Positioning System (controlled by a PC through a dedicated driver), and a Double-Ridged Waveguide Horn Lindgren-3117 (BW of 1 – 18 GHz) as reference antenna (positioned on a fix mast). The Antenna Under Test (AUT) and the reference antenna were placed 3.5 m away, and aligned using a multi-beam Laser system. The deformed prototypes #2 and #3 were measured without the foam matrices as the ground plane and patch copper tape used rigidifies the antennas sufficiently to avoid any deformation during rotations of the positioner. The transmission coefficient S_{21} was measured with the R&S ZVA40 VNA. The ATF is computed using the deconvolution procedure described in [57] based on the “complex Friis equation” [59]. The reflection coefficients S_{11} were measured with the same VNA.

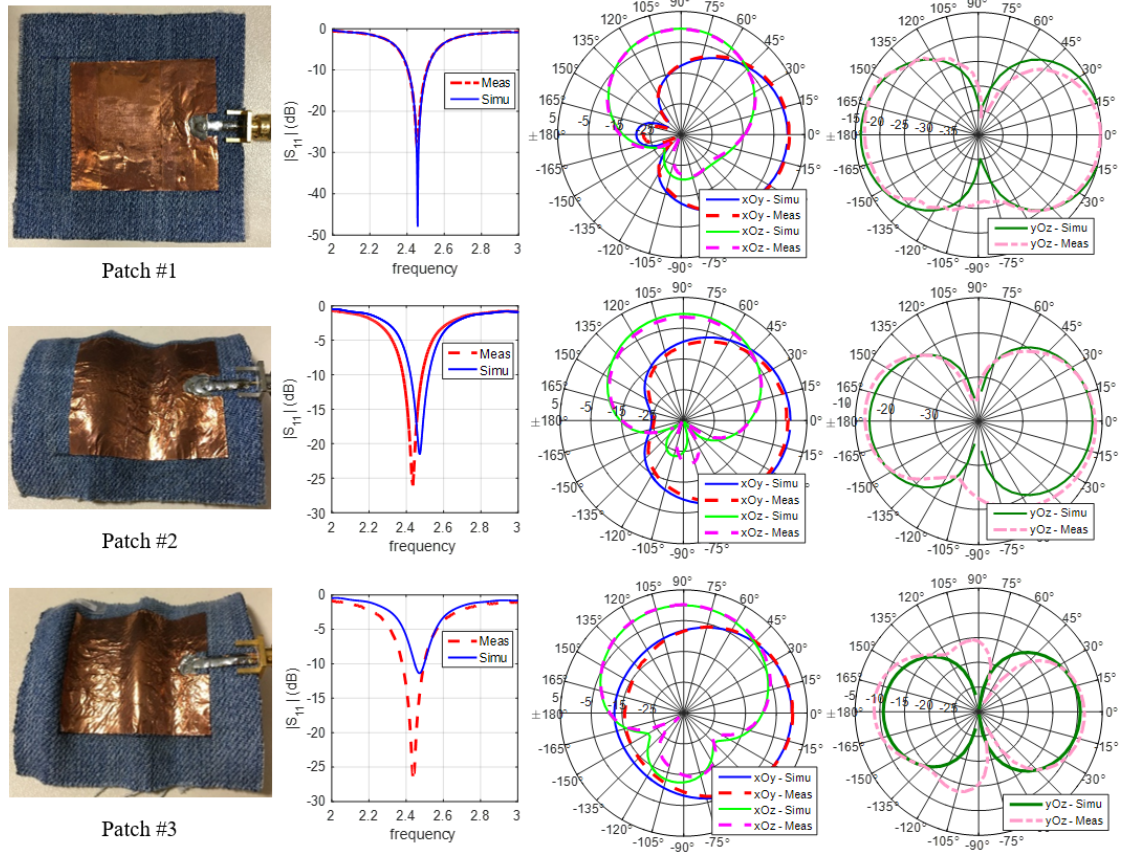


Figure 3.31: Three representative patches for which: the prototypes, the simulated/measured reflection coefficient $|S_{11}|$, and the simulated/measured G_r at 2.45 GHz in principal cut-planes for the co-polarization and cross-polarization components are presented in columns.

Figure 3.31 depicts for each patch: the picture of the prototype; the simulated and measured reflection coefficient ($|S_{11}|$); the simulated and measured realized gain patterns G_r at 2.45 GHz for the co-polarization (CP) in two principle cut-planes (xOy and xOz planes) and for the cross-polarization (XP) in one principle cut-plane (yOz plane). We see that for Patch #1 the simulations are fully consistent with the measurements for both the $|S_{11}|$ and the G_r . For Patch #2 and #3, some deviations of the center frequency are observed (resp. ~ 37 and 34 MHz) but globally the measured and simulated $|S_{11}|$ remain consistent. Regarding G_r , a good agreement within the measurement error margins (typically ± 0.5 dB) is observed for the CP, and also for the XP in the main radiation directions; the discrepancies observed in the XP patterns around the zeros ($\pm 90^\circ$) are due to the perturbation of the turntable mast. In addition, since the XP component is significantly lower than the CP component, this error can be tolerated. Briefly, the full-wave simulator is reliable for ATF evaluations.

3.5.5.5 Preliminary study: sensitivity analysis

We first investigated roughly the sensitivity of the ATF to the random parameters. The parameters of least influence can be discarded so as to reduce the model complexity (and modeling process) without weakening its representativeness. Based on the total Sobol's

indices (TSI) in (3.37), we define the weighted TSI, a more appropriate indicator to quantify the influence of each input parameter on our multi-output system:

$$S_{WT}^{(m)} = \sum_{l=1}^{N_G} S_T^{(m,l)} W_l \quad (3.53)$$

where $S_{WT}^{(m)}$ is the weighted TSI of the m -th input parameter for the whole antenna system; $S_T^{(m,l)}$ is the TSI of the m -th input parameter for the “generator” H_{q_l} of the l -th class \mathcal{G}_l ; and the weight W_l is the total power contribution of the class \mathcal{G}_l .

As shown by (3.37) for a PCE-modeled system the TSI of its input parameters can be obtained directly from the polynomial coefficients of the model. For this purpose, we constructed a preliminary model for the six-input system using our proposed statistical methodology. Then, the S_{WT} of all the 6 random parameters were calculated, as shown in Figure 3.32.

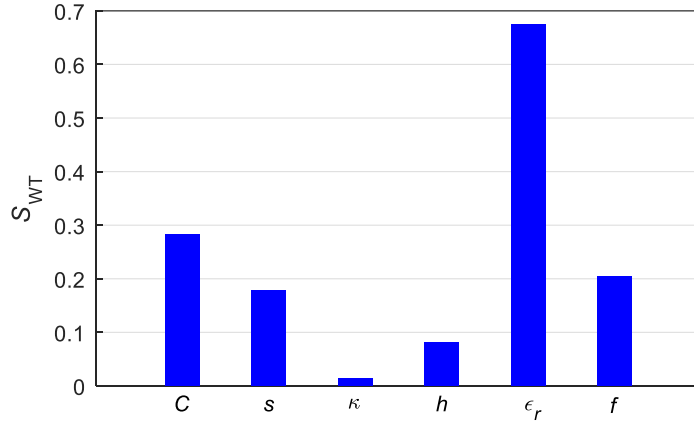


Figure 3.32: S_{WT} of the 6 random input parameters.

It can be seen that the curvature κ and the thickness h have the lowest impact on the ATF. Therefore, one reasonable choice is to ignore these two parameters and to concentrate on the remaining dominant factors for a fast analysis. However, bending is by essence a common random phenomenon for wearable devices and should have some effect on the beamwidth in azimuth, thence is useful to be included in the surrogate model. In contrast, the thickness h is not a so timely varying factor. Having this in mind, we decided to discard only the parameter h and to keep the 5 remaining input parameters in our model.

3.5.5.6 Modeling procedure and results

The algorithm in § 3.5.4 was adopted to extract the surrogate model for the actual five-input system. First, the ED was initialized with 200 points using the LHS design. Second, the ATFs were evaluated over the ED and then decomposed into full VSH modes with a maximal degree of $N_{VSH} = 5$, from which the most dominant modes were selected. The error of

reconstruction e_{Sup} (taking $\Delta G_r = 10$ dB as the main radiation zones margin) for different power thresholds E_{c_th} is shown in Figure 3.33. The blue (+) curve corresponds to the “full decomposition” ($N_{\text{VSH}} = 5$), used as reference; the black (\diamond), magenta (\square) and green (\times) curves correspond to E_{c_th} values of 99 %, 99.5 % and 99.9 % respectively. We see that the e_{Sup} decreases progressively as E_{c_th} is growing, but at the cost of an increase of the number of dominant modes (from 27 to 44), which degrades the model compactness. We finally chose the value of 99.9 % for E_{c_th} , since it offers a good compromise between accuracy and compactness ($e_{\text{Sup}} < 0.2$ dB for all dominant modes).

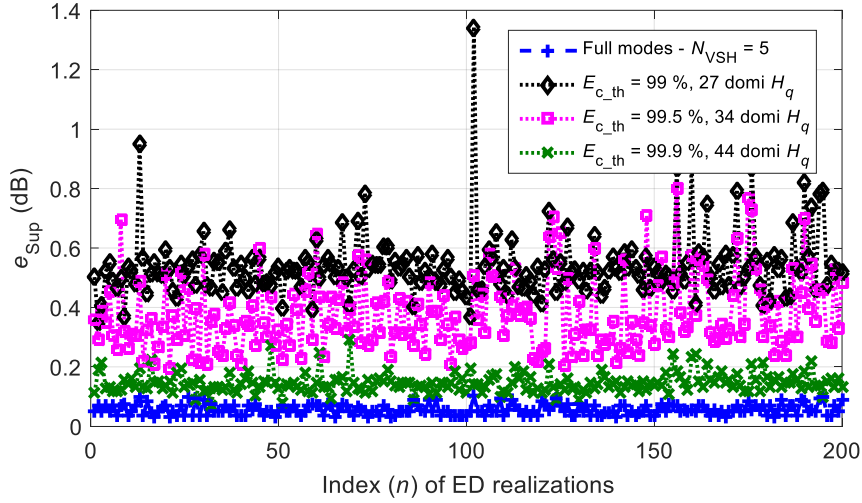


Figure 3.33: ATF reconstruction errors for different power threshold E_{c_th} .

The coefficients of the selected dominant VSH modes were then expanded onto polynomials where a maximal degree $N_{\text{PCE}} = 10$ was adopted. Finally a first surrogate model $\hat{\mathcal{H}}^{(0)}$ was constructed. The model accuracy was then progressively improved following Step 3, in which the “Maximin” technique is used to enrich iteratively the ED (by 100 new points each time). It is worth mentioning that the “Maximin” technique enriches preferentially the regions near boundaries. This property is suitable in our considered context since the boundaries correspond to more severe deformations thence must be sampled densely.

The convergence of the algorithm is analyzed as follows. As shown in Figure 3.34, by enriching the ED from 200 to 694 effective points, the prediction error e_{WTLOO} is reduced from 10.9 % to 4.9 %. Furthermore, we take a deeper look at the distribution of the estimation errors by classifying them into three categories: A – “very satisfactory” ($e_{\text{Sup}} < 1$ dB), B – “satisfactory” ($1 < e_{\text{Sup}} < 1.5$ dB), and C – “poor” ($1.5 < e_{\text{Sup}} < 2.5$ dB), as shown in Figure 3.35. For the i -th ED, the left and right color bars are respectively the e_{Sup} distribution for the predicted ATFs using the $(i-1)$ -th and the i -th surrogate model $\hat{\mathcal{H}}^{(i-1)}(\mathcal{X}_i)$, $\hat{\mathcal{H}}^{(i)}(\mathcal{X}_i)$. We can see that at the beginning, the error distribution of $\hat{\mathcal{H}}^{(0)}(\mathcal{X}_1)$ is quite different from that of $\hat{\mathcal{H}}^{(1)}(\mathcal{X}_1)$, which implies that the 1st surrogate model $\hat{\mathcal{H}}^{(0)}$ is not reliable enough as predictor

for new sets of random input values. This difference decreases gradually as the ED is enriched, and finally stabilizes when passing from $\hat{\mathcal{H}}^{(4)}$ to $\hat{\mathcal{H}}^{(5)}$. For $\hat{\mathcal{H}}^{(5)}(\mathcal{X}_5)$, the e_{Sup} is below 1.5 dB for 98.41 % of the cases, and the average and maximal value of e_{Sup} are respectively 0.52 dB and 1.96 dB, which can be considered relatively satisfactory as it meets almost the precision level of usual FF measurements in anechoic chamber. As a result, we first stopped the algorithm and chose $\hat{\mathcal{H}}^{(5)}$ as a “final” surrogate model offering a reasonable compromise between cost and accuracy. It comprises 3217 scalar coefficients, resulting from a 1st data compression rate of 65.71 % by sparse VSH expansion (i.e. 48 dominant modes among 140 full modes), followed by an “ultra-compression” of 43.75 % by correlation analysis (i.e. 48 dominant modes sorted into 27 equivalent classes).

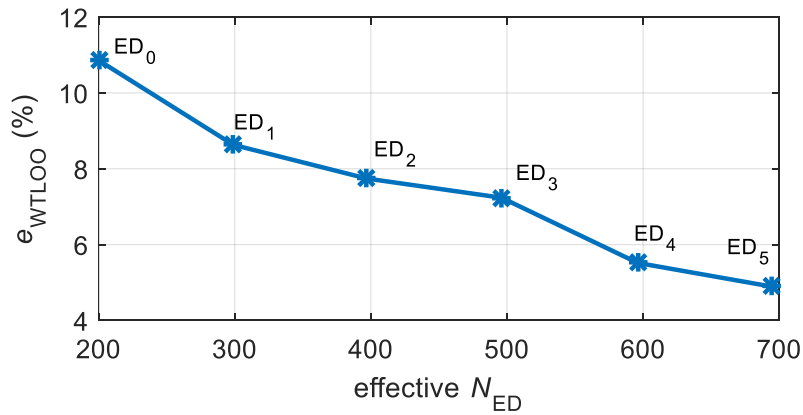


Figure 3.34: Prediction error e_{WTLOO} of surrogate models iteratively constructed by enriching the ED.

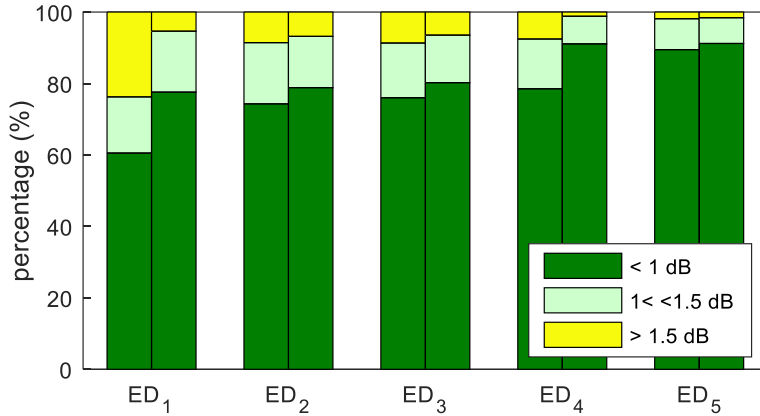


Figure 3.35: Comparison between the errors of two successive surrogate models for different EDs.

3.5.5.7 Validation of the surrogate model

Note first that the criteria chosen in § 3.5.4 regarding the algorithm convergence and the trade-off between the model accuracy and complexity ($E_{\text{c_th}}$, N_{PCE} , and the stop criterion of the enrichment of the ED) presents some arbitrariness, but they must be put into perspective with the other sources of uncertainty and/or errors in practical usages. In particular, in a real

radio communication system, a stochastic antenna model with an excessive precision would be actually useless in comparison with the added noise, channel variability, interferences, etc.

In any case, in order to verify the prediction performance of the extracted models, a MC analysis with a new statistical sample of 2000 realizations (i.e. 2000 new EM simulations) was realized. The ATFs computed with the models from the MC sample were compared with those directly obtained from the EM simulations, used as reference. Note that the MC sample was limited to 2000 realizations for practical reasons (e.g. the simulation cost of 10 000 realizations would have been prohibitive, about 104 days!).

The e_{Sup} for the generated ATFs are shown in Figure 3.36. The average and maximal value are respectively 0.53 and 2.2 dB; the proportions of category A, B and C are respectively 89.32 %, 8.16 %, and 2.52 %, which coincides with the accuracy level reached by our final surrogate model $\hat{\mathcal{H}}^{(5)}$. Figure 3.37 and 3.38 show the 3D G_r patterns for representative average-error (0.53 dB) and maximal-error (2.2 dB) configurations. We see that for the former, the generated patterns, both in CP and XP, are close to the simulated ones; for the latter, the generated patterns still have very similar appearance as the simulated, except for a moderate attenuation of ~ 2 dB in amplitude. Nevertheless, the accuracy and robustness of the derived surrogate model can be considered satisfactory.

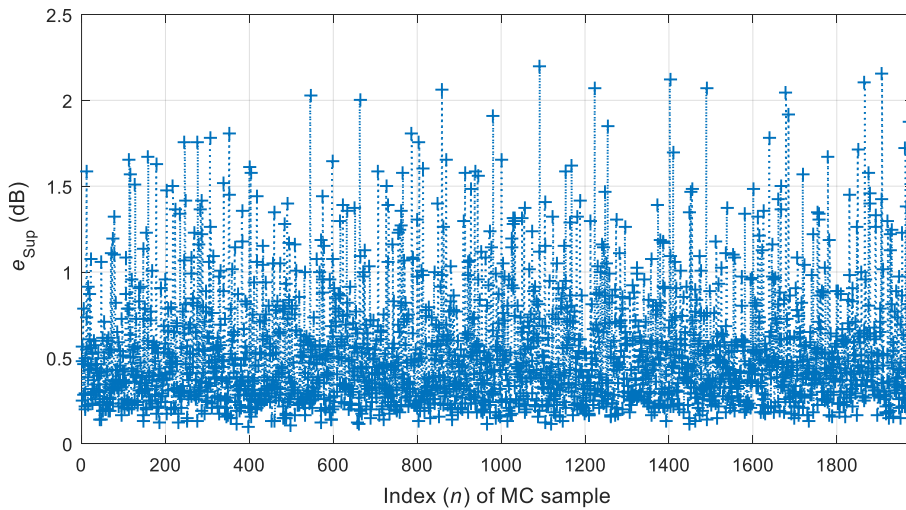


Figure 3.36: Error of the model-generated ATFs w.r.t. the reference MC sample.

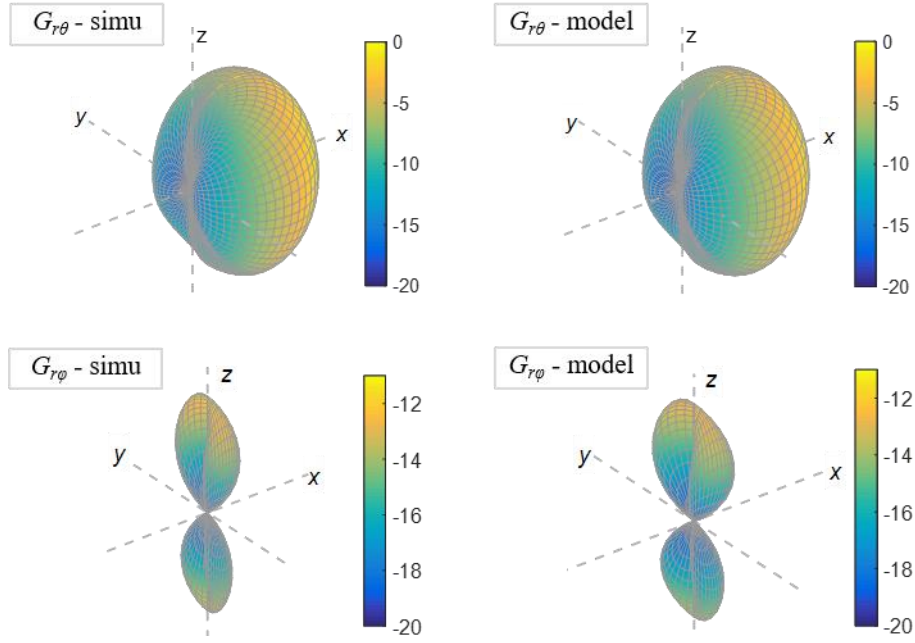


Figure 3.37: EM-simulated (left column) and model-generated (right column) G_r patterns for a representative average-error configuration.

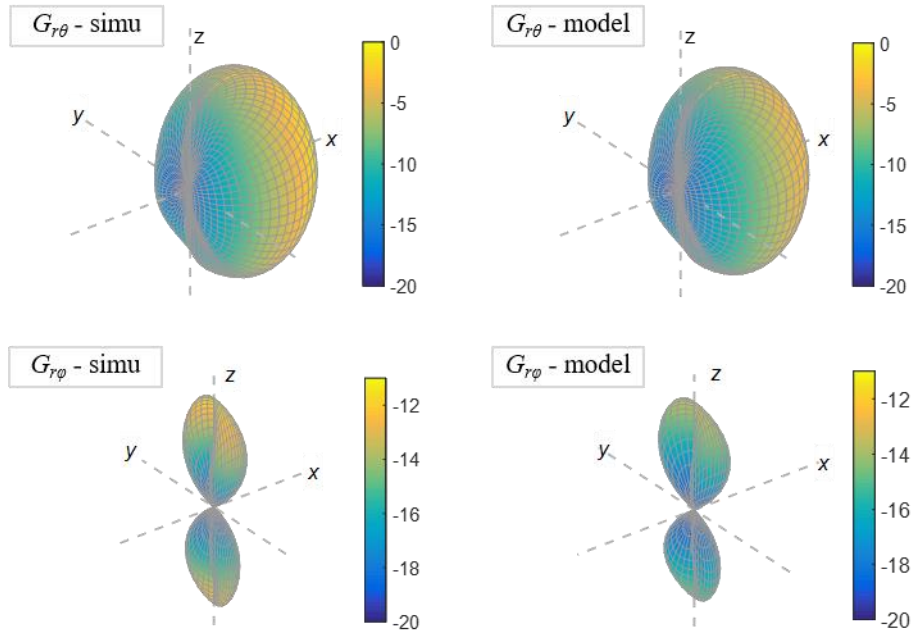


Figure 3.38: EM-simulated (left column) and model-generated (right column) G_r patterns for a representative maximal-error configuration.

3.5.5.8 Application examples of the surrogate model

Once the surrogate model of the radiated FF is built up, any “secondary observable” can be easily computed, and the computational cost of the statistical analysis of such “secondary observable” is low, even if slow convergence techniques such as the MC method are used.

For example purpose, we consider here, first, the -10 dB beamwidth of the principal cut-planes (xOy and xOz) for the CP component, and second, the maximal G_r of the CP

component. Their statistics, computed from the EM simulations and from the surrogate model (from the MC sample), are compared in Figure 3.39 using the CDF. It can be seen that for the beamwidths, the CDFs deviations are within 2.2 degrees, whereas the deviations of the maximal $G_{r\theta}$ are within 0.25 dB, in agreement with the e_{Sup} values shown in Figure 3.35 and 3.36.

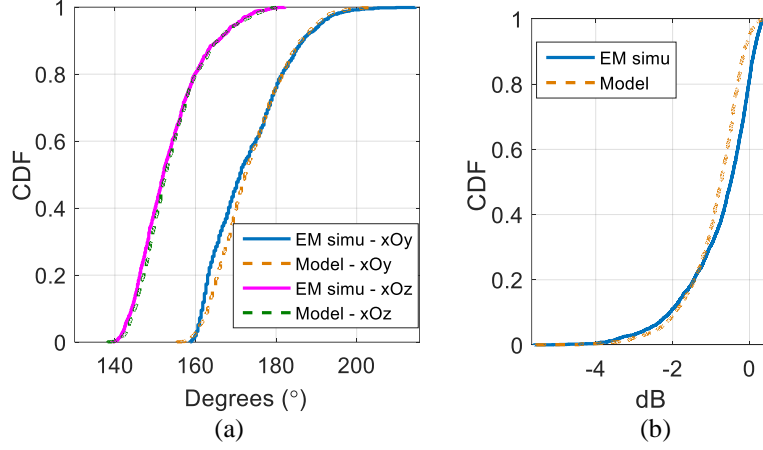


Figure 3.39: Comparison between the CDFs of: (a) -10 dB beamwidth, (b) maximal $G_{r\theta}$ computed from the model and EM-simulations from the MC sample.

3.5.5.9 Discussion about the model accuracy

Certainly, the accuracy of the surrogate model could be further improved in case of necessity. That could be achieved by including more VSH modes in the model (i.e. increasing the power threshold E_{c_th}), and by offering more information to train the surrogate model (i.e. enriching the ED). For example, if we enrich the ED up to 1470 realizations (denoted ED_{13}) and adopt a higher PCE degree of $N_{PCE} = 13$, the prediction error e_{WTLOO} of the derived model $\hat{\mathcal{H}}^{(13)}$ falls to 2.7 % (Figure 3.40). In Figure 3.41, the CDFs of those dominant VSH coefficients computed with the model $\hat{\mathcal{H}}^{(13)}$ from the MC sample were compared with those directly obtained from the EM simulations. The Kolmogorov-Smirnov (K-S) test was performed to quantitatively verify the consistency between the model-generated and the EM-simulated CDFs. The maximum distances D between the two are shown in TABLE II. We see that the K-S test is satisfied with a significance level $\alpha = 0.01$ (i.e. $D \leq D_{\alpha=0.01} = 0.0515$) for all VSH coefficients, and is still satisfied with $\alpha = 0.05$ (i.e. $D \leq D_{\alpha=0.05} = 0.043$) for the vast majority of these VSH modes (except the mode 1, 6, 17; note that the distance D is however close to the threshold for mode 1, which is often the most energetic).

However, the cost for a more accurate model is obviously a high computation time and a degradation in model compactness. In brief, there is always a trade-off between the cost/compactness and the accuracy, and our proposed modeling methodology is versatily scalable according to application-specific requirements.

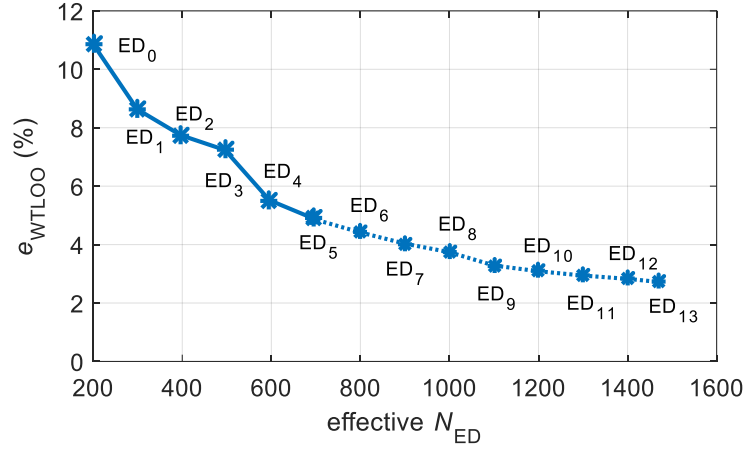


Figure 3.40: Prediction error e_{WTLOO} of surrogate models iteratively constructed by enriching the ED till large cardinal.

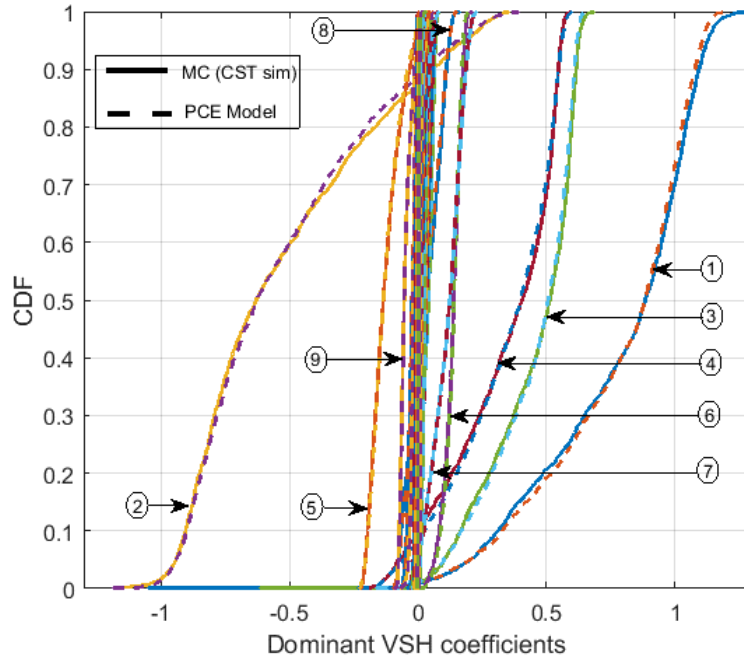


Figure 3.41: Comparison between the CDFs of the model-generated and the EM-simulated dominant VSH coefficients from the MC sample.

Table IV: K-S test on the 27 dominant VSH coefficients.

VSH Coeff	1	2	3	4	5	6	7	8	9
D	0.0439	0.0216	0.043	0.0309	0.0222	0.0513	0.0175	0.0284	0.0286
VSH Coeff	10	11	12	13	14	15	16	17	18
D	0.0279	0.0172	0.0357	0.0255	0.0252	0.022	0.0284	0.0515	0.0219
VSH Coeff	19	20	21	22	23	24	25	26	27
D	0.0323	0.0244	0.0288	0.0206	0.0198	0.0399	0.0354	0.0192	0.0222

3.5.5.10 Discussion about the computational cost

A high performance computing server equipped with a dual-core CPU (Intel Xeon @ 2.6 GHz, 256 GB RAM) and 2 GPU (Graphical Processor Unit) accelerators (NVIDIA Tesla K80)

was used to perform the EM simulations with CST. It takes averagely 15 minutes for a single ATF computation. Therefore, a total elapsed time of about 175 hours is necessary for computing the 700 pre-evaluations of ED_5 , and 367.5 hours for ED_{13} . It should be emphasized that such rather high simulation cost is the result of the demanding constraints imposed to the EM solver so as to guarantee a sufficient precision, because of the complexity of the considered geometries, involving in particular thin layers. The computation time of the surrogate models (including Step 2.b-2.g in § 3.5.4) varies from 25 seconds (for model $\hat{\mathcal{H}}^{(0)}$) to 153 seconds (for model $\hat{\mathcal{H}}^{(5)}$) and 17 minutes (for model $\hat{\mathcal{H}}^{(13)}$). The computation of the ATF with the model $\hat{\mathcal{H}}^{(5)}$ or $\hat{\mathcal{H}}^{(13)}$ for any values of the input parameters takes only 7 milliseconds corresponding to a speedup factor of $(15 \times 60)/(7 \times 10^{-3}) = 1.3 \times 10^5$ with respect to using EM simulations.

3.6 Conclusion

In this chapter, we presented methodologies for quantitatively characterizing the *complete* ATF of antennas undergoing random uncertainties due to deformations or disturbances from fluctuating environments. To mitigate the prohibitive complexity of a direct modeling, we proposed to split the modeling procedure into two steps, i.e. a first step of “*field parsimony*” followed with a second step of “*surrogate model extraction*”. The first step aims to get a sparse/compact expression of the ATF, and is effectively achieved by means of the VSH expansion method which transforms the spatial 3-dimensional complex vector-valued ATF into a finite set of scalar parameters. The second step aims to quantitatively and explicitly interpret the dependency of the sparse ATF on those random input parameters. Both conventional deterministic and advanced statistical approaches have been investigated.

At the first stage, a deterministic approach based on the conventional parametric study was proposed. This approach was applied to a canonical bendable dipole for the purpose of modeling the single effect of bending, or the joint effect of bending & torsion, on the dipole’s ATF. The modeling results justified the relevance of this simple approach. However, this approach is suited only for relatively simple univariate or bivariate systems, and cannot be generalized to complex systems subject simultaneously to a higher number of random uncertainties. Nevertheless, this preliminary study has demonstrated the feasibility of our “*Two-Step*” idea and thence paved the way for the exploration of more sophisticated modeling approaches.

At the second stage, we presented a statistical methodology based on the HLARS-PCE method. Comparing to the deterministic approach, the statistical methodology is much more computationally efficient, flexible and robust for treating multivariate problems. This

approach was firstly applied to a canonical deformable dipole (with 3 input parameters, i.e. stretching, bending and torsion) to demonstrate its effectiveness. Then, the methodology was improved/enhanced, in particular by taking into account the frequency behavior and by further exploiting the parsimony. The improved approach was tested on a more realistic complex wearable textile patch antenna (with 4 geometrical random parameters and the frequency as an additional “random” parameter) for which accurate and robust surrogate models were successfully derived.

In the following chapter, we will present the utility of such accurate *complete* antenna surrogate models in the performance evaluation of radio links where they are implemented jointly with propagation channel models.

Chapter 4

4. Antenna surrogate models in radio links analysis

4.1 Introduction

The quality of service (QoS) provided by a wireless communication system is notably determined by the real-time and *in situ* performance of the radio link, which is a combination of the base station (or access point), the propagation channel and the user end terminal antenna (see Figure 4.1). In practice, various sources of uncertainties may randomly arise in each of the three parts (notably the last two parts) and drastically degrade the radio link quality. Today, with the increasing demands on reliability and robustness in many application scenarios, accurately assess the radio link performance while taking into account those randomness becomes crucially important. In recent years, a lot of efforts have been made to develop empirical models to account for random effects (mainly the large-scale fading effect due to reflection, diffraction, scattering, etc., and medium-scale fading or *shadowing*) on the propagation channel. Conversely, the random characteristics of the terminal antenna have not been fully incorporated in such kind of radio link analysis. The main reasons are, firstly, the large-scale fading effect of the propagation channel is most often decisively dominant in front of the variabilities of the terminal antenna; secondly, the “effective” performance of the terminal antenna which suffers from both inherent uncertainties (especially true for variable antennas, e.g. deformable ones) and external uncertainties from its complex local environment, is not easy or straightforward to model efficiently. Consequently, those random effects on the terminal antenna side are often roughly taken into account or even ignored in a traditional radio link analysis, where a simplistic and fixed antenna model (e.g. “isotropic” antenna of 0 dBi gain) is used, to which an ad hoc margin is added in order to roughly account for those randomness that may be encountered in real environments [53]. However, resorting to finer modeling approaches in place of such kind of rough approximation can be profitable for many application contexts, notably in the wake of emerging networks, standards and usages (5G, IoT, femtocells, etc.), which require more precise performance analyses.

This problem could not be effectively tackled only if we can efficiently model on the one side, the effect of inherent uncertainties of the terminal antenna itself, and on the other side, the effect of external uncertainties from the propagation environment. The first goal can be

achieved by using our proposed ATF modeling methodology; and the second aspect could be described by some existing advanced channel models, such as the well-known WINNER2/+ model [137], [138]. In this chapter we will present a preliminary approach to show the advantage of using accurate antenna surrogate models instead of a simplistic fixed antenna for radio links analysis.

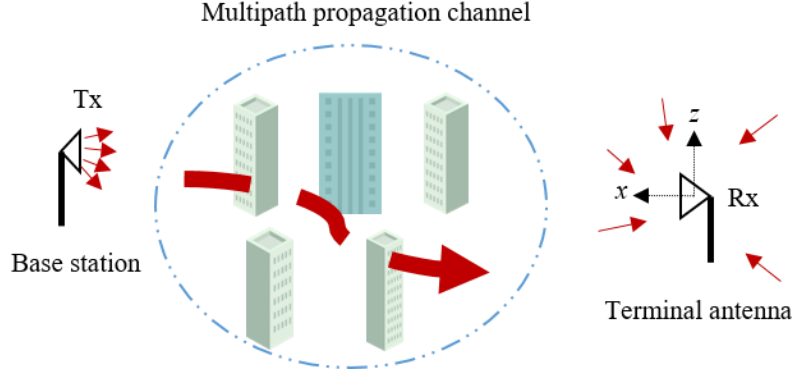


Figure 4.1: Illustration of the radio link of a wireless communication system.

4.2 Effective performance of terminal antenna

In practical usage, the “effective” performance of the terminal antenna depends on both the radio-electric properties of the antenna itself – ATF or radiation pattern, and its local propagation environment – the spatial and polar distribution of the incoming waves. The Mean Effective Gain (MEG) is a popular parameter for quantifying such “effective” performance of an *in situ* antenna. It is defined as the ratio of the average power received by the antenna under study and the sum of the average power that would be received by two isotropic antennas which are respectively vertically and horizontally polarized [139], given by:

$$G_{MEG} = \frac{P_{rec}}{P_V + P_H} = \oint \left(\frac{P_V G_\theta(\theta, \varphi) P_\theta(\theta, \varphi) + P_H G_\varphi(\theta, \varphi) P_\varphi(\theta, \varphi)}{P_V + P_H} \right) d\Omega \quad (4.1)$$

$$= \oint \left(\frac{\chi G_\theta(\theta, \varphi) P_\theta(\theta, \varphi) + G_\varphi(\theta, \varphi) P_\varphi(\theta, \varphi)}{\chi + 1} \right) d\Omega$$

where,

- $\chi = P_V/P_H$ is called the cross-polarization power ratio (XPR), defined as the ratio of the average power available in the vertical polarization P_V to the average power available in the horizontal polarization P_H . This parameter characterizes the depolarization effect of the propagation channel on the transmitted waves.
- $P_\theta(\theta, \varphi)$ ($P_\varphi(\theta, \varphi)$) is the angular power distribution density of the vertical (horizontal) polarization component. These two parameters characterize the spatial distribution of the incoming waves in the vicinity of the terminal antenna.

- $G_\theta(\theta, \varphi)$ and $G_\varphi(\theta, \varphi)$ are the polarimetric gain (or realized gain) of the terminal antenna.

For sake of simplicity, we adopt herein a normalized form of the MEG for evaluating the effective performance of a terminal antenna when it is combined with a discrete multipath channel model – the Effective Gain (EG) [140] as defined:

$$\begin{aligned} G_{EG} &= \sum_n |A_{nH}|^2 G_{nH} + |A_{nV}|^2 G_{nV} \\ &= \sum_n |A_{nH}|^2 (G_{nH} + \chi_n G_{nV}) \end{aligned} \quad (4.2)$$

where $|A_{nH}|$ ($|A_{nV}|$) is the normalized amplitude of the horizontal (vertical) polarization component of the n -th path satisfying the normalization relation: $\sum_n |A_{nH}|^2 + |A_{nV}|^2 = 1$; χ_n is the cross-polarization ration (XPR) for the n -th path: $\chi_n = |A_{nV}|^2 / |A_{nH}|^2$. Note that for an ideal lossless isotropic antenna with equal polarization components (i.e. $G_\theta(\theta, \varphi) = G_\varphi(\theta, \varphi) \equiv 0.5$), its EG is constantly equal to -3 dB regardless of the variability of the propagation environment. It should also be noted that the interference between multipath, i.e. the fast fading (or small scale fading) effect is neglected in the computation of the EG, seeing that the phases of multipath do not appear in (4.2).

Clearly, for a terminal antenna which is subject to inherent random uncertainties \mathbf{X} (a common case by essence for wearable textile antennas and other types of deformable antennas), its gain patterns G_{nH} and G_{nV} change randomly, and so do the G_{EG} as well as the final radio link budget. It is in such situations that an accurate antenna surrogate model $\hat{\mathcal{H}}(\mathbf{X}, f, \hat{\mathbf{r}})$ taking into account those inherent random effects plays a beneficial role for precise performance evaluation.

In the following we will implement the derived antenna surrogate model for the wearable textile patch antenna (cf. § 3.5.5) in some classical local propagation environments to show its influence with regards to only considering the “nominal” flat antenna. We use a simplified version of the WINNER2/+ model to consider different types of propagation environments.

4.3 Local propagation environments

The WINNER2/+ is a cluster-based channel model which describes a propagation environment consisting of multiple Non-Line-Of-Sight (NLOS) paths by Rayleigh distribution, and a propagation environment consisting of several NLOS paths plus a LOS path by Rice distribution. We adopted a simplified version of WINNER2/+ [36] by assuming: i) a vertically-polarized base station; ii) only one path per cluster; and iii) ignored phase for all paths (since they are not used for computing the EG). Precisely, the random generation of

the directions of arrival (DoAs) and amplitudes of multipath is carried out with respect to the following rules [141]:

For NLOS paths:

- The number of clusters (i.e. paths) obeys a Gaussian distribution, and at least one cluster (path) is required:

$$N = \text{Max}[1, \text{Int}(\mathcal{N}(\mu_c, \sigma_c))]$$

with (μ_c, σ_c) being the mean and standard deviation of the number of clusters for the considered propagation environment.

- The DoAs (θ_n, φ_n) of the paths are defined such that the elevation angles obey Laplacian distribution and the azimuth angles obey Gaussian distribution:

$$\begin{cases} \theta_n \sim \mathcal{L}(\mu_\theta, b_\theta) \\ \varphi_n \sim \mathcal{N}(\mu_\varphi, \sigma_\varphi) \end{cases}$$

where μ_θ is the mean position in elevation; b_θ is the spread in elevation, which obeys a Log-normal distribution of mean and standard deviation (μ_b, σ_b) ; μ_φ is the mean position in azimuth, assumed to be uniformly distributed in a specified angular range; σ_φ is the spread in azimuth, which obeys a Gaussian distribution of mean and standard deviation $(\mu_{\sigma_\varphi}, \sigma_{\sigma_\varphi})$.

- The vertical polarization amplitudes are assumed to obey Rayleigh distribution:

$$|A_{nV}| \sim \mathcal{R}(\sigma_{nV})$$

where the variance σ_{nV}^2 of the Rayleigh distribution is a Laplacian function of the azimuth angle of the n -th path φ_n , and the stochastic parameters of the azimuth distribution $(\mu_\varphi, \sigma_\varphi)$:

$$\sigma_{nV}^2 = C \cdot \exp(-\sqrt{2} |\varphi_n - \mu_\varphi| / \sigma_\varphi)$$

- The horizontal polarization amplitudes are related to the vertical one through the cross polarization ration XPR: $|A_{nH}| = |A_{nV}| / \chi_n$, where χ_n is assumed to be lognormally distributed with mean and standard deviation (μ_χ, σ_χ) , and C is a normalization constant satisfying $\sum_n |A_{nH}|^2 + |A_{nV}|^2 = 1$.

For LOS paths: The DOA of the LOS path is taken as the closest one to the mean direction $(\mu_\theta, \mu_\varphi)$, and its power relative to the total power of all NLOS paths is defined by the K factor, which is assumed to be lognormally distributed, with mean and standard deviation (μ_K, σ_K) .

In our case, we chose four types of WINNER2/+ propagation environment, namely:

- Env. 1: Indoor (small office/ residential), NLOS
- Env. 2: Indoor (small office/ residential), LOS
- Env. 3: Typical Urban (hot spot), NLOS from base station
- Env. 4: Typical Urban Macro-cell, NLOS from base station

The standard stochastic characteristics of these environments are summarized in Table V.

Table V: Characteristics of 4 WINNER2/+ propagation environments.

Env.	K factor (dB) μ_K / σ_K	XPR (dB) μ_χ / σ_χ	Azimuth		Elevation*		# Paths μ_c / σ_c
			Mean (°) μ_ϕ	Spread (°) $\mu_{\sigma_\phi} / \sigma_{\sigma_\phi}$	Mean (°) μ_θ	Spread ($\log_{10}([\text{°}])$) μ_b / σ_b	
1	-	10/4	$\mathcal{U}([0, 360^\circ])$	49/7	91.6	1.10/0.17	16/4.5
2	7/6	11/4		45/9	91.6	0.94/0.26	12/6
3	-	8/3		35.5/35	92	0.88/0.16	16/3
4	-	7/3		52.5/20.5	100	1.26/0.16	20/4

* $\theta_n \sim \mathcal{L}(\mu_\theta, b_\theta)$, $b_\theta = 10^{N(\mu_b, \sigma_b)}$.

4.4 Effective performance and discussion

4.4.1 Relative Effective Gain (REG)

We can anticipate that taking into account or not of those inherent randomness of the terminal antenna will result in more or less difference in antenna's effective performance. The more the antenna patterns change dramatically with the inherent randomness, the more significant this difference will be, and the more justifiable it is to use a precise antenna model for the radio links analysis. To visualize the dispersion of G_{EG} , we resort to the quantity "relative Effective Gain (REG)" which is the ratio between the G_{EG} of a specified antenna realization and that of the fixed reference antenna, i.e. the original non-deformed flat patch operating at the nominal frequency ($C = 0, s = 1, \kappa = 0, \varepsilon_r = 1.75, f = 2.45$ GHz):

$$G_{REG} \triangleq G_{EG} / G_{EG}^{ref} \quad (4.3)$$

Note that the choice to use the nominal flat patch as the reference antenna is to highlight the antenna variability in the channel context. Another possible choice would have been to resort, e.g., to an "ideal" isotropic radiator as was done in [36]. However, this would have over-represent the directive character of the patch antenna, which is not the main objective of these analyses.

We generated 1000 antenna realizations using our surrogate model for 1000 random values of $(C, s, \kappa, \varepsilon_r, f)$. For each considered propagation environment (Env. 1-4), we generated randomly 100 channel realizations using the simplified WINNER2/+ model and:

- i. For each of these 100 channel realizations, we combined it with the 1000 random antennas and computed the 1000 REGs. Then we drew the corresponding CDF curve, referred to as “partial CDF” (color thin lines in Figure 4.2) and exhibited its variability range and standard deviation. The average value of variability ranges and standard deviations for the 100 channels were summarized in Table VI.
- ii. We combined all these 100 channel realizations with the 1000 random antennas and computed the $100 \times 1000 = 10^5$ REGs. Then we drew the CDF curve, referred to as “global CDF” (red thick line in Figure 4.2) and exhibited its variability range and standard deviation, see Table VI.

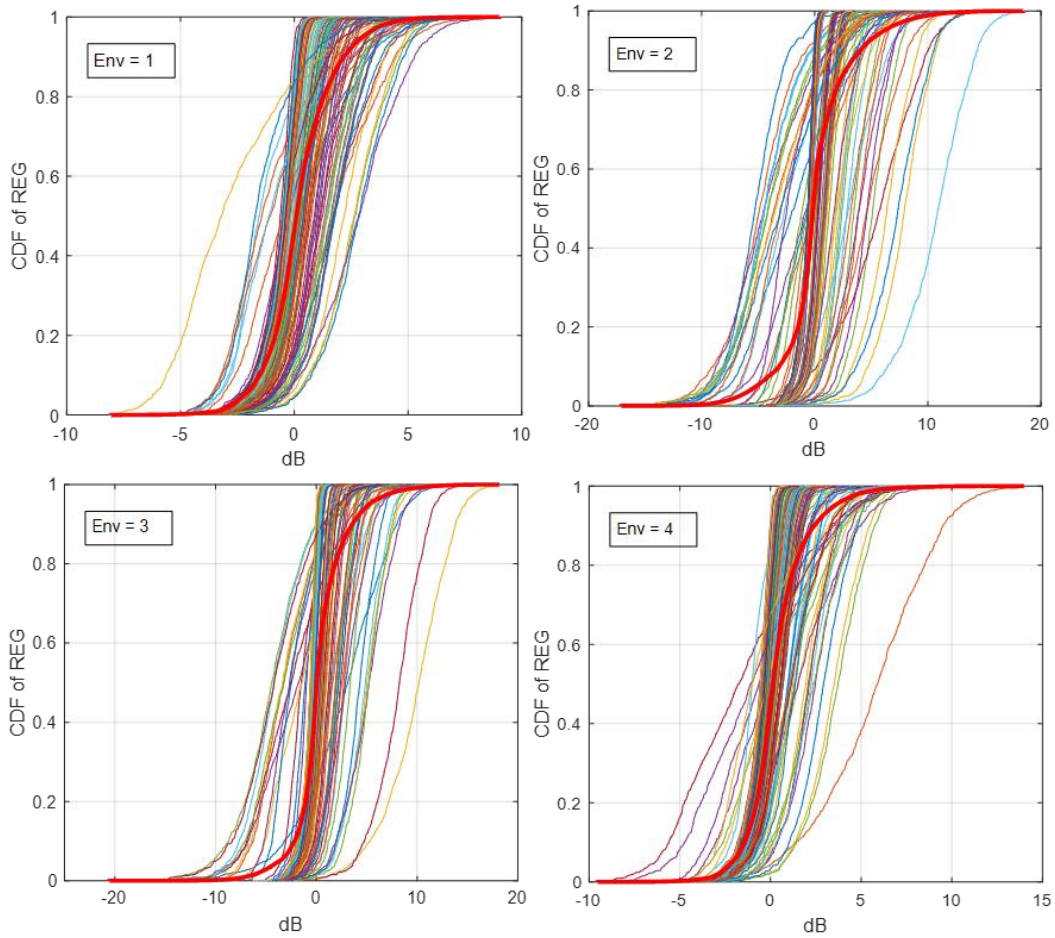


Figure 4.2: CDFs of the relative effective gain of the textile patch antenna in different propagation environments: color thin lines – partial CDFs; red thick line – global CDF.

Table VI: Statistics of the relative effective gains.

REG Env.	Partial CDFs		Global CDF	
	Average Variability range (dB)	Average Std (dB)	Variability range (dB)	Std (dB)
1	7.57	1.12	17	1.54
2	10.24	1.61	35.6	3.23
3	9.27	1.43	38.8	2.76
4	8.1	1.21	23.6	1.73

Observations and discussions are given herein:

1. The “partial CDFs” (see color thin lines in Figure 4.2 and Table VI) show that for whichever considered channel in whichever Env., the REG always retains a wide dispersion – the average variability range is between 7.57 ~ 10.24 dB and the average standard deviation is larger than 1.1 dB. This dispersion is a direct reflection of the inherent randomness (caused by \mathbf{X}) of the terminal antenna. In other words, the effective performance of a randomly deformed antenna could dramatically differ from that of the nominal flat design. Therefore, in the application contexts where precise performance analyses are required, those random effects must not be ignored and accurate antenna models in place of a fixed (original) antenna must be used.
2. Env. 1 and 2 are of similar “Indoor” type, except that the former only has NLOS paths while the latter has both NLOS paths and a LOS path. From their “global CDF” (see red thick line in Figure 4.2 and Table VI) we note that the latter has wider variability range – 35.6 dB vs. 17 dB, and more significant standard deviation – 3.23 dB vs. 1.54 dB. Our explanation is that: a channel containing only NLOS paths is not quite “directional” because the NLOS paths are of statistically equal mean power weight and their DoAs are more or less “ubiquitous” in the space. In such situation, the EG is determined by the average “matching degree” between the antenna’s gain pattern and all the NLOS paths, thereby, the effect of the antenna’s inherent randomness is weakened (or “randomized”) to some extent by this global averaging aggregation. In contrast, a channel containing both LOS and NLOS paths is somewhat more “directional” because the LOS path is energetically dominant in front of all NLOS paths. In such situation, the antenna’s effective performance will be mainly determined by the “matching degree” between its gain pattern and the single LOS path (e.g. DoA and polarization). Therefore, if the randomness causes significant variation in the LOS direction, this would be immediately reflected (in an obvious manner) on the statistics of the REG.
3. Env.3 and 4 have similar NLOS parameters, except that the former has narrower spreads in DoAs – 35.5° vs. 52.5° in azimuth, and 0.88 vs. 1.22 (in $\log_{10}([\cdot])$) in elevation. Comparing their “global CDF” (see red thick lines in Figure 4.2 and Table VI), we note that the former has wider variability range – 38.8 dB vs. 23.6 dB, and more significant standard deviation – 2.76 dB vs. 1.73 dB. It is not difficult to figure out the reason since narrower spreads in DoAs imply indeed higher “directionality” of the propagation channel, where the variation in terminal antenna can be more evidently captured.

4.4.2 Relative Average EG (RAEG) in sub-bands

In the previous example, we have considered the frequency “ f ” as an ordinary random input variable. However, in practical applications, a terminal antenna never operates at discrete frequencies but over an allowable sub-band. For example, in the 2.4 – 2.5 GHz range for the WiFi standard there are 14 sub-bands designated, as shown in Figure 4.3. Therefore, it is indeed its “equivalent” effective performance over a considered operating sub-band that determines the final performance of the terminal antenna. Having this in mind, we choose to consider hereby the EG averaged over a considered sub-band (\bar{G}_{EG}) as in (4.4):

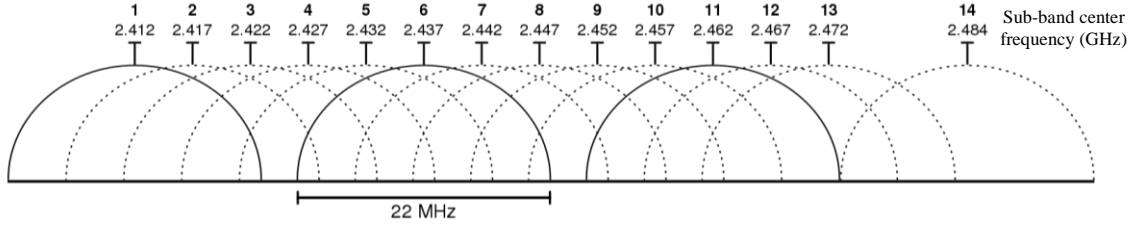


Figure 4.3: Allowable sub-bands for WiFi standard in the 2.4 – 2.5 GHz range.

$$\begin{aligned}\bar{G}_{EG} &= \sum_n |A_{nH}|^2 \bar{G}_{nH} + |A_{nV}|^2 \bar{G}_{nV} \\ &= \sum_n |A_{nH}|^2 (\bar{G}_{nH} + \chi_n \bar{G}_{nV})\end{aligned}\quad (4.4)$$

where \bar{G}_{nV} and \bar{G}_{nH} are the polarimetric realized gain averaged over the considered sub-band:

$$\bar{G}_{nV,H} = \frac{1}{N_f} \sum_{i=1}^{N_f} G_{nV,H}(f_i) \quad (4.5)$$

The relative average Effective Gain (RAEG) is defined as the ratio between the \bar{G}_{EG} of a specified antenna realization and that of the fixed reference antenna, i.e. the original non-deformed flat antenna operating over the same sub-band ($C = 0, s = 1, \kappa = 0, \varepsilon_r = 1.75$):

$$G_{RAEG} \triangleq \bar{G}_{EG} / \bar{G}_{EG}^{ref} \quad (4.6)$$

We generated randomly 1000 antenna realizations. For each realization:

- 1) A value of $(C, s, \kappa, \varepsilon_r)$ was randomly drawn according to their joint distribution.
- 2) One of the 14 sub-bands (see Figure 4.3) was randomly chosen, in which a series of frequencies (spaced by 1 MHz) spanning the sub-band were chosen. For instance, if the sub-band #1 is chosen, the frequency samples are $F_{sub} = [2401:1:2423]$ MHz.
- 3) The ATFs were generated for the input parameters $(C, s, \kappa, \varepsilon_r, F_{sub})$.
- 4) The average realized gain patterns \bar{G}_{nV} and \bar{G}_{nH} of this specified antenna realization as well as those of the reference antenna were computed according to (4.5).

For each Env., we generated randomly 100 channel realizations using the simplified WINNER2/+ model. Finally, we computed the RAEG of each channel-antenna combination according to (4.4) and (4.6), and derived the “partial CDFs” and “global CDFs” of the RAEGs in the same manner as for the REGs in § 4.4.1. The CDFs are shown in Figure 4.4 and the variability ranges and the standard deviations are summarized in Table VII.

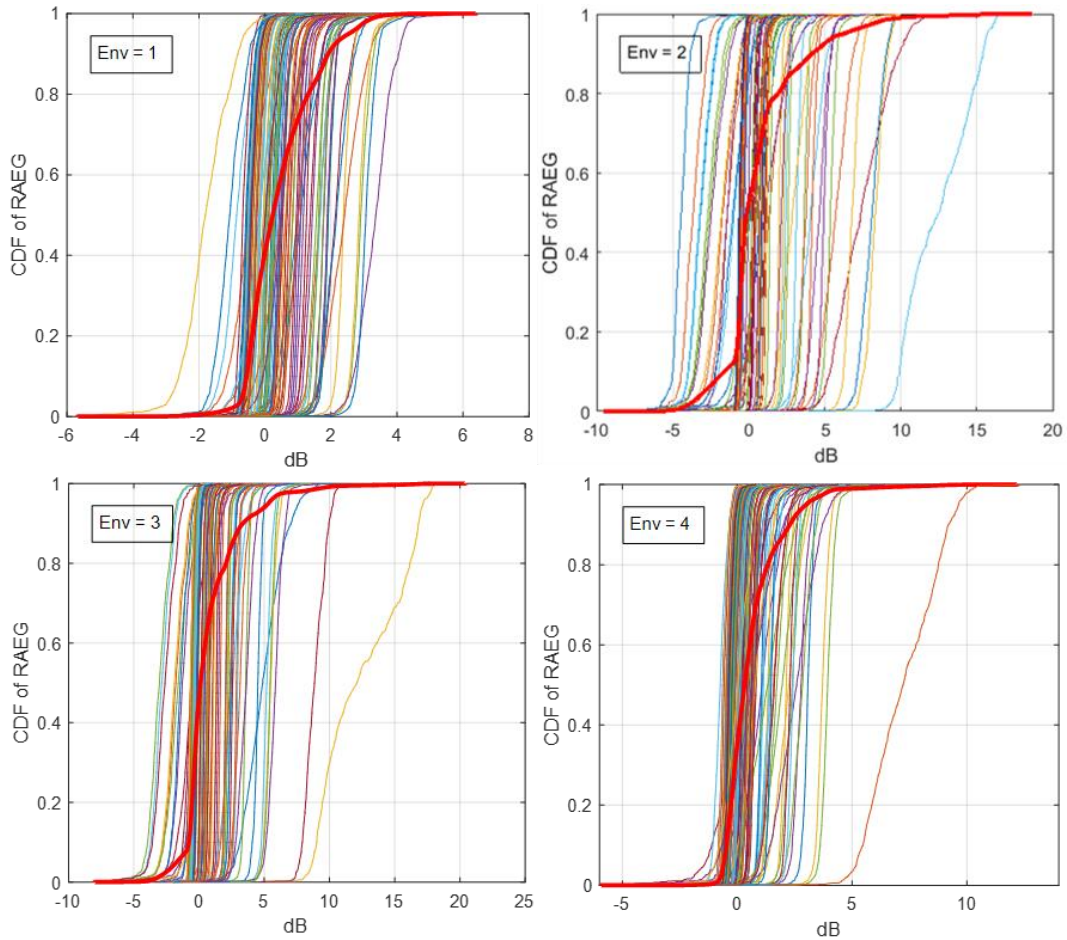


Figure 4.4: CDFs of the relative average effective gain of the textile patch antenna in different propagation environments: color thin lines – partial CDFs; red thick line – global CDF.

Table VII: Statistics of the relative average effective gains.

RAEG Env.	Partial CDFs		Global CDF	
	Average variability range (dB)	Average std (dB)	Variability range (dB)	Std (dB)
1	3.74	0.28	12.1	1.03
2	4.99	0.45	28.27	2.68
3	4.53	0.39	28.45	2.32
4	4.1	0.32	18.15	1.26

Remarks and discussions are given herein.

If we look at the “global CDF” which aggregates all channel-antenna combinations, we draw some conclusions similar to those drawn for the REGs, e.g. concerning the directional

effect of the considered propagation environment. Effectively, more “directional” channels lead to wider dispersion in RAEG: larger variability ranges – 28.27 (Env. 2) vs. 12.1 dB (Env. 1), and 28.45 (Env. 3) vs. 18.15 dB (Env. 4); and larger standard deviations – 2.68 (Env. 2) vs. 1.03 dB (Env. 1), and 2.32 (Env. 3) vs. 1.26 dB (Env. 4).

Moreover, when we take a deeper look at those “partial CDFs”, we note some significant difference comparing to those of the REGs:

1. The “partial CDFs” of RAEGs have much smaller dispersions: average variability range between 3.74 ~ 5 dB (vs. 7.57 ~ 10.24 dB for REGs), and average standard deviation between 0.28 ~ 0.45 dB (vs. > 1.1 dB for REGs).
2. The “partial CDFs” seem to be somehow “parallel” spaced one to another, each occupies a small range of variability, and together contribute to a wide “global” variability range.

This phenomenon implies the fact that the random effect on the terminal antenna side is small in front of that on the propagation channel side – the latter determines the first-order moment and the former describes the second-order moment of the partial distributions. Therefore, using the REG in § 4.4.1 which evaluates the performance of the terminal antenna operating at discrete frequencies is actually inappropriate since it exaggerates the dispersion of the antenna’s effective gain, as well as the random effect of antenna’s inherent randomness. On the contrary, the RAEG appear as a more appropriate and relevant indicator for exhibiting the random effects.

4.4.3 RAEG for restricted azimuthal DoAs

However, even if we resort to the RAEG indicator, the quantitative conclusions drawn in the above section should still be taken with caution. In the previous examples, the WINNER2/+ model suggests that the azimuthal mean angle μ_ϕ obeys uniform distribution in $[0, 360^\circ]$. This assumption would be reasonable when considering more or less omnidirectional terminal antennas or an application context where the 360° fully free azimuth rotation of the terminal antenna is required. Yet, for directional antennas that are dedicated for directional usages, such as our patch antenna, it seems more appropriate to evaluate its effective performance in “realistic scenarios” more consistent with the practical antenna usage², i.e. with DoAs restricted in only the broadside hemisphere. Here, by assuming that $\mu_\phi \sim \mathcal{U}([-90^\circ, 90^\circ])$ we re-computed the statistics of the RAEGs. The CDFs are shown in Figure 4.5 and the variability ranges and the standard deviations are summarized in Table VIII.

² For example, downloading a file more or less in front of a hotspot terminal in a shopping mall.

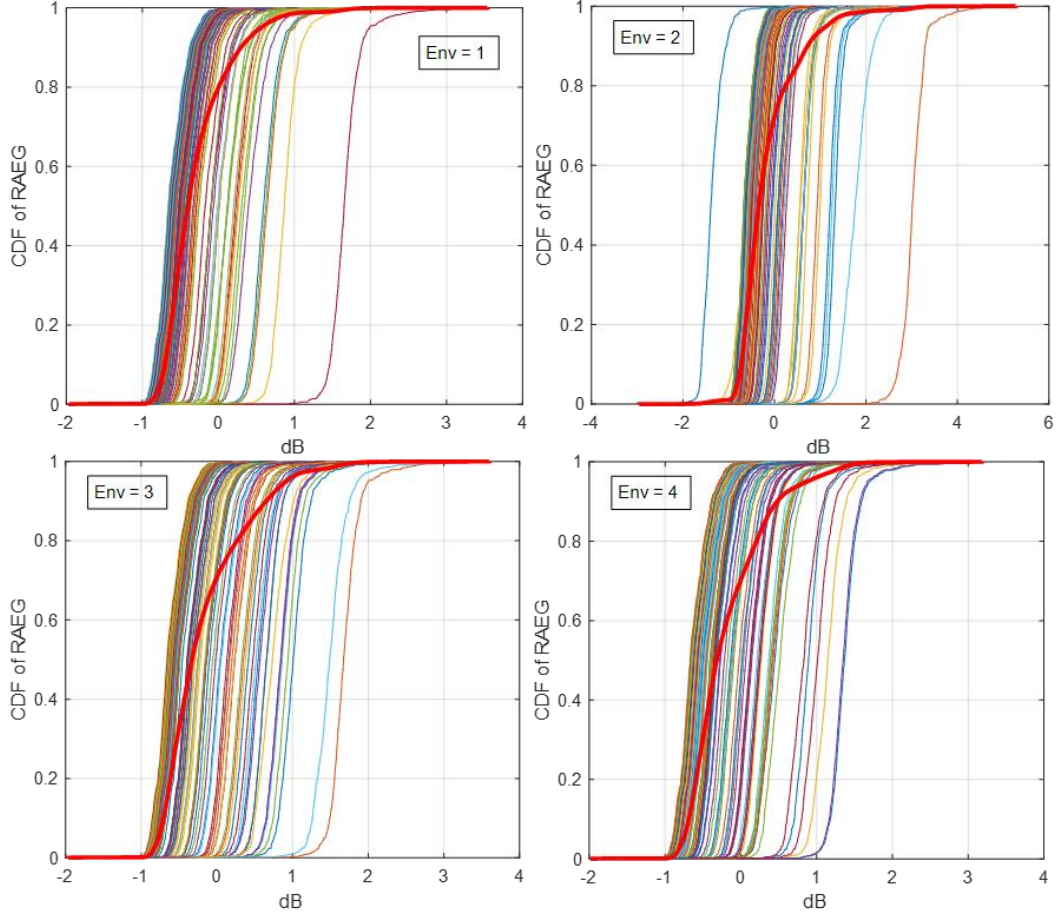


Figure 4.5: CDFs of the relative average effective gain of the textile patch antenna ($\mu_\varphi \sim \mathcal{U}([-90^\circ, 90^\circ])$) in different propagation environments: color thin lines – partial CDFs; red thick line – global CDF.

Table VIII: Statistics of the relative average effective gains ($\mu_\varphi \sim \mathcal{U}([-90^\circ, 90^\circ])$).

RAEG Env.	Partial CDFs		Global CDF	
	Average variability range (dB)	Average std (dB)	Variability range (dB)	Std (dB)
1	2.65	0.2	5.52	0.66
2	2.84	0.21	8.26	0.68
3	2.73	0.2	5.58	0.55
4	2.75	0.2	5.17	0.51

Remarks and discussions are given herein.

1. The “global CDFs” now have much narrower dispersions than in § 4.4.2 – smaller variability ranges and smaller standard deviations. Therefore, the assumption of identical possibility of the mean azimuth angle in the whole range of $[0, 360^\circ]$ will overestimate the dispersion of the RAEG of our textile patch antenna.
2. The variability ranges are of comparable level (~ 5 dB) for the 3 NLOS propagation environments Env. 1, 3, 4, and they are all smaller than that of the LOS channel Env. 2 (~ 8 dB). This is because the LOS path plays a decisive role in the channel

directionality while the effect due to azimuthal spreads is not very significant, since the DoAs have been largely restricted, i.e. in the broadside hemisphere.

3. Generally, such large variability (> 5 dB) must not be neglected for precise radio links analysis, and the adoption of accurate antenna models in place of fixed reference antenna is highly required.

4.5 Conclusion

In this chapter, we showed the utility of antenna surrogate models for evaluating radio links performance. The latter depends strongly, among others, on the effective performance of the terminal antenna. In practical usage, the terminal antenna generally suffers from inherent random uncertainties as well as external random uncertainties from its surrounding environment (especially true for e.g. wearable textile antennas), which may drastically perturb the performance of the terminal antenna, hence the radio links performance. In such context, antenna surrogate models which account for antenna inherent randomness are highly advantageous over either a conventional simplistic “isotropic model” or a practical but fixed reference model (whether simulated or measured).

To show the benefit of antenna surrogate models, we resorted to some performance indicators (i.e. REG and RAEG) based on the MEG – a commonly used indicator e.g. in mobile radio communications. We computed firstly the variability of the REG, and then that of the RAEG of our textile patch antenna in some classical propagation environments. A significant variability in REG and RAEG was observed in all propagation environments, which justifies the necessity for adopting antenna surrogate models if one requires accurate radio links analysis. This is particularly demanding when both the terminal antenna and the propagation environment are more “directional”. In such context, we can construct accurate surrogate models for the terminal antenna (by using our proposed modeling methodology) in the first step, and then implement the antenna surrogate model in appropriate propagation environments to carry out accurate radio links analysis in the second step.

This approach of joint antenna/channel modeling can be further refined to be able to address e.g. the received signal as shown in [142]. In particular, if the phase is taken into account (which was not the case here – see a discussion about this matter e.g. in [36]), it is possible to perform simulations at some system level, including e.g. the physical layer so as to test various modulation schemes (see e.g. [127]) and assess system performance indicators such as the Bit Error Rate. This kind of approach, more elaborate and finer, which would highlight the interest of developing surrogate models of the complete radiated field (vector and phased), is left as future development.

Chapter **5**

5. Statistical modeling of the reflection coefficient of variable antennas

5.1 Introduction

As introduced in Chapter 2, the *overall* FF behavior of a transmitting antenna (or of a receiving antenna because of the reciprocity theorem) can be completely described by two complex quantities: the *complete* radiated FF or equivalently, the ATF $\mathcal{H}(f, \hat{\mathbf{r}})$, and the reflection coefficient $S_{11}(f)$, which describe respectively the transmission and the reflection properties of the considered antenna. In the previous chapters we presented effective methodologies for modeling the ATF; and in this chapter we will concentrate on the modeling of the $S_{11}(f)$, thereby to complete the *overall* modeling scheme for variable antennas.

In general, $S_{11}(f)$ is a quantity quite sensitive to random uncertainties – notably for NB antennas – since any type of deformations, material properties change, or environmental perturbation could easily induce impedance mismatches, hence causing variations in $S_{11}(f)$. In recent years, the problem of modeling the $S_{11}(f)$ or its equivalent – the input impedance $Z_{in}(f)$ due to tunable design parameters has been widely addressed by means of relatively sophisticated methods such as ANNs [45], [46], Gaussian Process Regression (GPR) [143], Support Vector Regression (SVR) [39], [41], and gPCE [50], etc. In [39], [45], [46] and [50], the Z_{in} of the considered antennas were modeled only at the resonant frequency; in [41] and [143], the $S_{11}(f)$ were modeled over a wide frequency band by means of taking the frequency “ f ” as one of the random input parameters. These methods have been proved to be effective for handling highly non-linear problems. However, on the one hand, some of these methods are not always straightforward for implementation; on the other hand, taking the frequency as an additional random input parameter would weaken the space-filling property of the other input parameters, hence larger-sized ED might be required inducing higher computational cost. Hereby, we propose a simpler alternative approach for modeling the $S_{11}(f)$ of NB antennas. Instead of directly considering the frequency as a random parameter in the input space, we split the modeling procedure into two steps: first, we use an

identification technique to convert the frequency-dependent $S_{11}(f)$ to a finite set of frequency-independent characteristic parameters. This is analogue to the “separation of variables” for solving partial differential equations. Second, we extract surrogate models by using the HLARS-based PCE method to quantify the impact of random variables on those frequency-independent characteristic parameters derived in the 1st step.

5.2 Identification

The identification of a system represented by its transfer function has been widely addressed since the 1950s. The objective is to approximate the transfer function with a rational function either in the Laplace, frequency or Z domain. Numerous algorithms have been proposed for identifying the corresponding polynomial coefficients, among which some ones are directly applicable in the frequency domain, and some others are applicable in the time domain (i.e. on the impulse response), which requires a prior inverse Fourier transform if the data are available in the frequency domain. Without being exhaustive, we can mention the Cauchy’s method [144], the Levy’s complex curve fitting method [145], and the Kumaresan’s Frequency-domain Prony’s method [146] for the former category; and the famous Prony’s method [147], the Steiglitz–McBride’s method [148], and the Matric-Pencil method [149] for the latter category. Hereby, we investigate two identification techniques as a first attempt for verifying the *Two-Step* modeling methodology. The first technique is the classical polynomial fitting method, which relies on the continuity of the real and imaginary parts of $S_{11}(f)$ and approximates them separately with polynomial functions. This rather simple method has shown good accuracy and robustness while applied to NB antennas. Besides, the Levy’s algorithm has also been tested, in the purpose of verifying the relevance of the rational interpolation.

5.2.1 Technique 1: Polynomial fitting

The real and imaginary parts of the $S_{11}(f)$, respectively denoted $S_R(f)$ and $S_I(f)$, are both continuous functions of the frequency. They can be fitted with polynomial functions as:

$$S_R(f) = \sum_{m=0}^{M_R} R_m f^m + \varepsilon_R(f), \quad S_I(f) = \sum_{n=0}^{N_I} I_n f^n + \varepsilon_I(f) \quad (5.1)$$

where $M_R(N_I)$, $\varepsilon_R(\varepsilon_I)$ are respectively the maximal polynomial degree and the residual error for the real (imaginary) part function. For NB antennas, usually the $S_{11}(f)$ is only considered over a very limited band around the resonant frequency. In such cases the variability of the S_R and S_I is rather smooth, which implies that low or moderate fitting order could be sufficient for a good precision. Once the polynomial degrees are determined, the unknown polynomial coefficients can be calculated by solving linear equations while minimizing the square error

$\sum_{k=1}^{N_f} |\varepsilon_{R,1}(f_k)|^2$. Therefore we get a parsimonious representation for $S_{11}(f)$, i.e. a finite set of frequency-independent characteristic parameters $P = \{R_0, R_1, \dots, R_{M_R}, I_0, I_1, \dots, I_{N_I}\}$.

5.2.2 Technique 2: Levy's complex curve fitting with rational functions

Denoting $S_{11}(z)$ the discrete transfer function of the reflection coefficient, where $z = \exp(j2\pi f/F_s)$, F_s being the sampling frequency, $S_{11}(z)$ can be approximated by a rational function as:

$$S_{11}(z) = \sum_{m=0}^{M_b} b_m z^{-m} / (1 + \sum_{n=1}^{N_a} a_n z^{-n}) + \varepsilon(z) \quad (5.2)$$

where M_b and N_a are respectively the order of the numerator and the denominator functions, and ε is the residue. Again for NB and resonant antennas, the order could not be too high. The Levy's algorithm combined with the damped Gauss-Newton method [150] allow to calculate the unknown coefficients while minimizing the square error $\sum_{k=1}^{N_f} |\varepsilon(z_k)|^2$. Therefore, $S_{11}(z)$ is compacted to a set of frequency-independent characteristic parameters $P = \{b_0, \dots, b_{M_b}, a_1, \dots, a_{N_a}\}$.

5.3 Surrogate model extraction

We apply the HLARS-based PCE method for mapping between the random uncertainties and the parsimonious $S_{11}(f)$. Assume the input variables are represented by $\mathbf{X} = (X_1, X_2, \dots, X_M)^T$ of which the joint PDF is known, then the modeling of the S_{11} comprises the following steps:

1. Initialize the ED $\mathcal{X} = \{\mathbf{x}^{(1)}, \mathbf{x}^{(2)}, \dots, \mathbf{x}^{(N_{ED})}\}^T$, and set the LOOE threshold (e_{LOO_th}) for the HLARS-based PCE algorithm.
2. Pre-evaluate the frequency responses over the ED set. Precisely, for each value $\mathbf{x}^{(n)}$, $n = 1, \dots, N_{ED}$, design the corresponding antenna configuration, carry out the EM simulations or measurements to get the frequency data $S_{11}(f, \mathbf{x}^{(n)})$.
3. Apply an identification technique to obtain the characteristic parameters $P = \{P_1, P_2, \dots, P_{N_p}\}$ for each $S_{11}(f)$ function.
4. Apply the HLARS-based PCE method to each characteristic parameter, and finally get surrogate models $P_i = \sum_{\alpha \in \mathcal{A}_i^{HLARS}} y_{\alpha}^i \Phi_{\alpha}(\mathbf{X})$, $\{i = 1, \dots, N_p\}$.
5. Assess the e_{LOO} . If $e_{LOO} \leq e_{LOO_th}$ for all models, or if N_{ED} exceeds an acceptable value then stop the procedure; otherwise enrich the ED and return to Step 2.

Eventually, a surrogate model mapping quantitatively the input-output relation between these random variables \mathbf{X} and $S_{11}(f)$ via a set of polynomial coefficients $\{y_{\alpha}^i | \alpha \in \mathcal{A}_i^{HLARS}, i=1, \dots, N_p\}$ is established, allowing the reproduction of $S_{11}(f)$ for any value of \mathbf{X} .

5.4 Applications

We applied the proposed modeling methodology on two NB antennas to verify its performance. Firstly, the same deformable dipole (undergoing three independent deformations) used in § 3.4.3.2 was reconsidered; secondly, a wearable textile patch subject to four sources of uncertainties was considered.

To evaluate the accuracy of the derived surrogate model, we chose the maximal difference between the model-evaluated and the original frequency responses as the error indicator:

$$err = \underset{k=1, \dots, N_f}{Max} \{ |dB[\hat{S}_{11}(f_k)] - dB[S_{11}(f_k)]| \} \quad (5.3)$$

Note that when both the initial and the model-evaluated values are less than -15 dB, the difference is considered as negligible and will not be accounted for when calculating the *err*.

5.4.1 Application to a canonical dipole

Recall that the dipole was assumed to be deformable considering three independent sources of deformation: stretching (with stretch ratio ξ), bending (with curvature κ or bending radius $R_b = 1/\kappa$), and torsion (with torsion rate α); and the input variables (ξ , κ , α) are uniformly distributed over respectively $[1, 1.05]$, $[0, 0.1] \text{ mm}^{-1}$, and $[0, 0.1] \text{ rad} \cdot \text{mm}^{-1}$. It was shown in Figure 3.23 that the joint effect of deformation on the dipole is significant: variations of $|S_{11}|$ up to more than 15 dB are possible, which justifies the necessity of an accurate quantitative model.

We applied the iterative procedure in § 5.3 with the LOOE threshold $e_{\text{LOOE}_{\text{th}}}$ being chosen as 4 %, and the polynomial degrees for the two identification techniques set as $M_R = N_I = 3$, and $M_b = 2$, $N_a = 3$ respectively. We took advantage of the already obtained pre-evaluations in § 3.4.3.2 for training the surrogate model in the current framework. The modeling results are summarized below. Figure 5.1 and 5.2 show the results for the Approach I: “Technique 1 + PCE”. In Figure 5.1 (a), it is noted that the model error decreases for all characteristic parameters when enriching progressively the ED. The predefined LOOE threshold is finally satisfied for $N_{\text{ED}} = 260$, for which a statistical model with about 570 polynomial coefficients is derived. To illustrate visually the performance of the constructed model, we compared the initial, the identified (with polynomial fitting), and the model-generated frequency responses

for two cases: the worst case (i.e. with the maximal value of err) and the median case (with the median value of err), as in Figure 5.2. We see that the responses overlap well for the median case, and remain satisfactory for the worst case, which justify the accuracy and the robustness of this approach.

Similar results are shown in Figure 5.3 and 5.4 for the Approach II: “Technique 2 + PCE”. It is noted that this approach requires fewer pre-evaluations (only 120 compared to 260 in Approach I), without degrading the accuracy of the model. As a result, it is more computationally efficient.

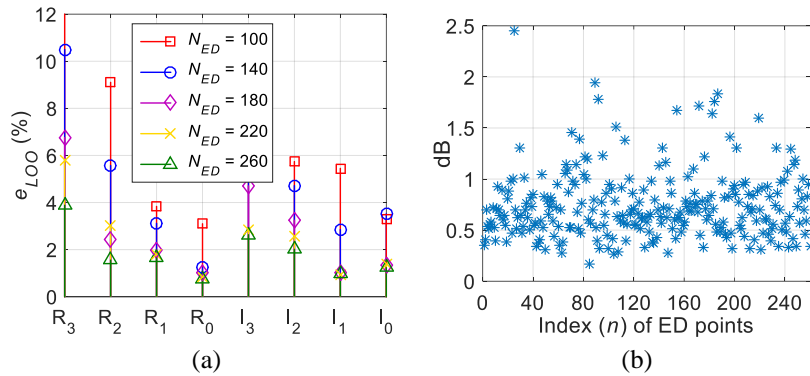


Figure 5.1: Dipole – Approach I: (a) e_{LOO} of the PCE models of characteristic parameters for different ED; (b) err of reconstruction in case of $N_{ED} = 260$.

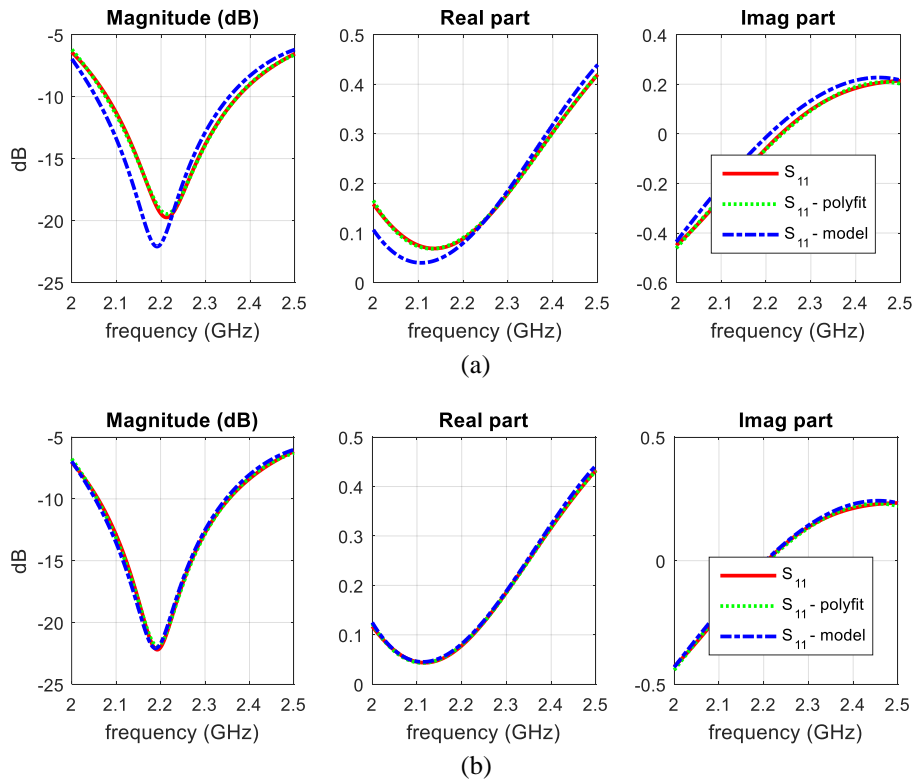


Figure 5.2: Dipole – Approach I: comparison of the frequency responses of the initial, the identified (with polynomial fitting), and the final surrogate model for: (a) the worst case (i.e. with maximal err); (b) the median case (i.e. with median err).

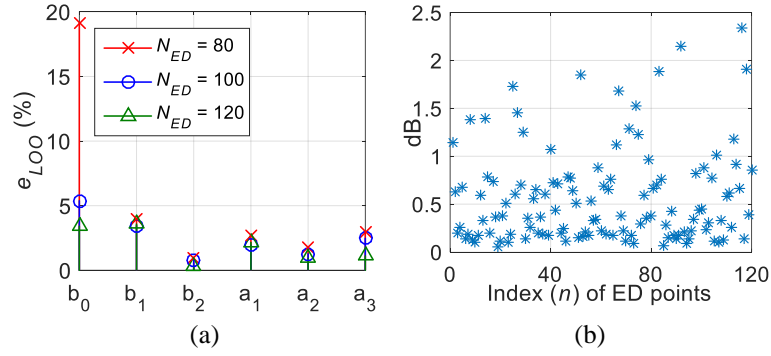


Figure 5.3: Dipole – Approach II: (a) e_{LOO} of the PCE models of characteristic parameters for different ED; (b) err of reconstruction in case of $N_{ED} = 120$.

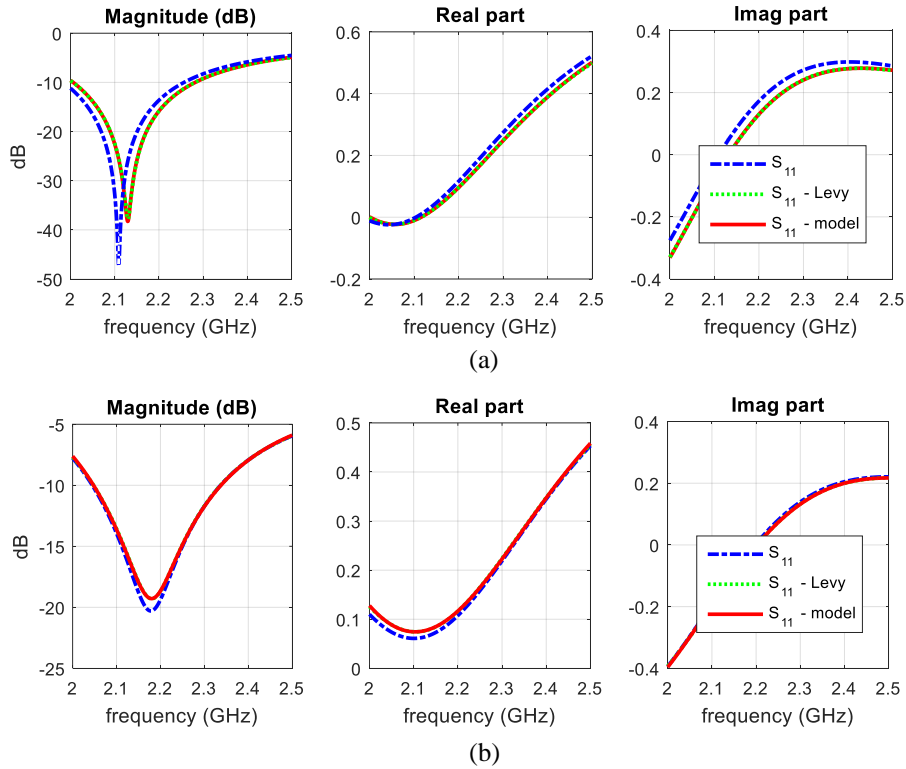


Figure 5.4: Dipole – Approach II: comparison of the frequency responses of the initial, the identified (with Levy's), and the final surrogate model for: (a) the worst case (i.e. with maximal err); (b) the median case (i.e. with median err).

5.4.2 Application to a textile patch

A wearable textile patch antenna designed for the ISM band was chosen as the second application example. The antenna was assumed to be subject to variations in length, bending curvature, substrate thickness and relative permittivity when attached around a human arm or leg, as shown in Figure 5.5. For sake of simplicity, we made simplifying assumption of independent uniform distribution of the four random variables. Their nominal values and variation ranges are listed in Table IX.

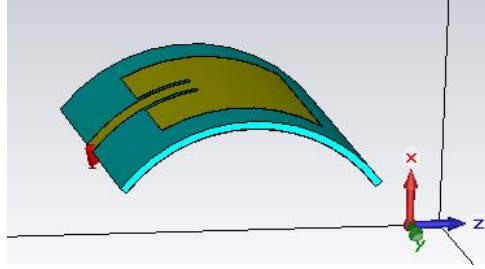


Figure 5.5: Textile patch undergoing random variations in length, bending radius, substrate height and permittivity.

Table IX: Design parameters and variability range for the textile patch.

Patch parameter	Nominal value	Variability range
Length, l	46.7 mm	$\pm 1\%$
Bending curvature, κ	0	$[0, 1/40] \text{ mm}^{-1}$
Substrate thickness, h	2 mm	$\pm 20\%$
Permittivity, ϵ_r	1.67	$[1.5, 1.9]$

The proposed modeling methodology was applied to characterize the combined effect of deformations on the reflection coefficient. The ED was initialized with 120 points, and the LOOE threshold $e_{\text{LOOE_th}}$ is chosen as 4%. The polynomial orders for the two identification techniques were chosen as $M_R = N_I = 5$, and $M_b = N_a = 5$ respectively. Figure 5.6 and 5.8 show the results for the Approach I and Figure 5.7 and 5.9 show those for the Approach II.

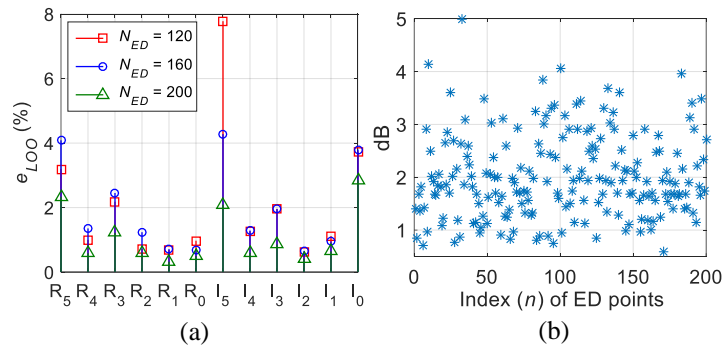


Figure 5.6: Patch – Approach I: (a) e_{LOOE} of the PCE models of characteristic parameters for different ED; (b) err of reconstruction in case of $N_{ED} = 200$.

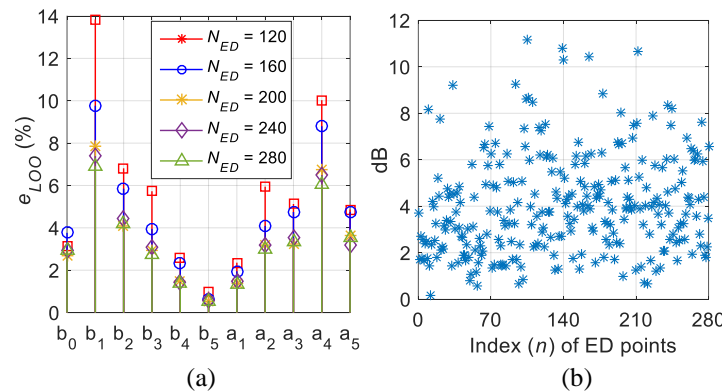


Figure 5.7: Patch – Approach II: (a) e_{LOOE} of the PCE models of characteristic parameters for different ED; (b) err of reconstruction in case of $N_{ED} = 280$.

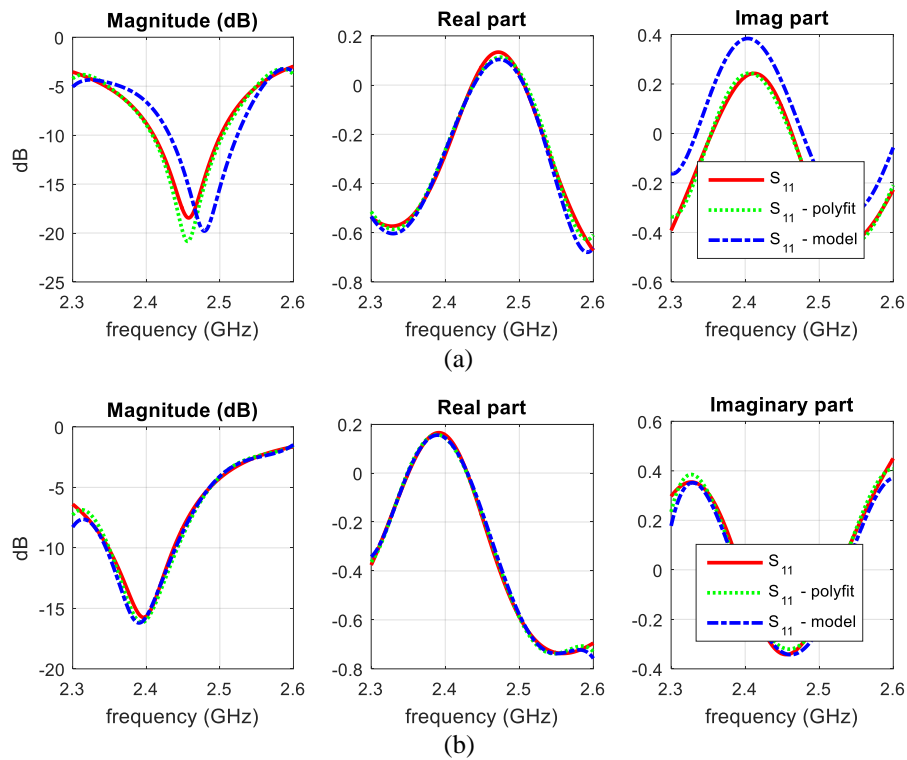


Figure 5.8: Patch – Approach I: comparison of the frequency responses of the initial, the identified (with polynomial fitting), and the final surrogate model for: (a) the worst case (i.e. with maximal *err*); (b) the median case (i.e. with median *err*).

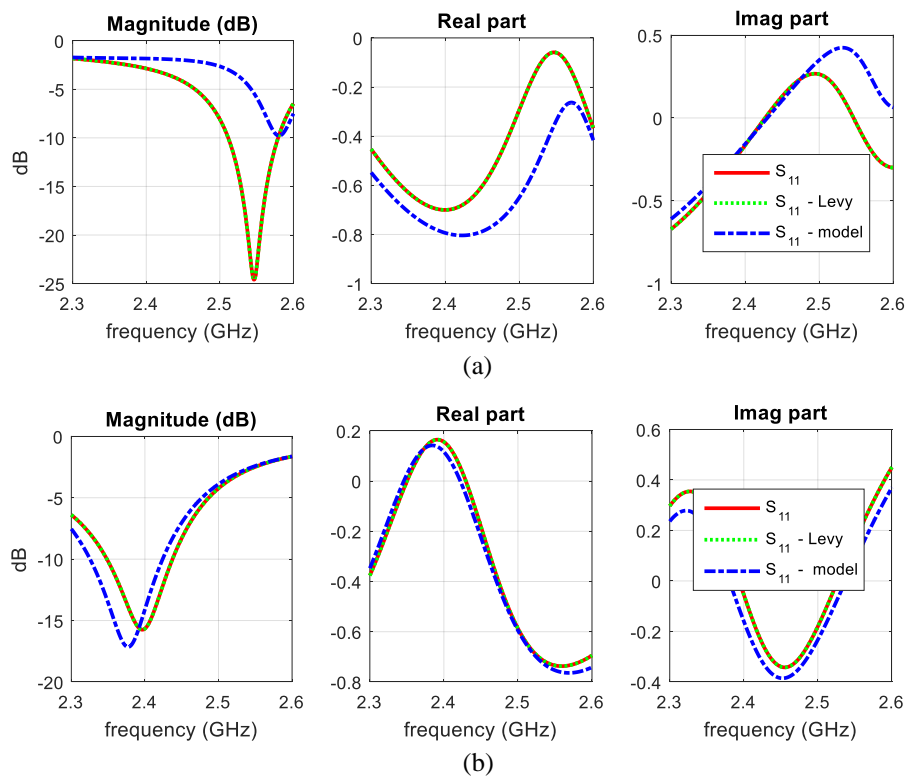


Figure 5.9: Patch – Approach II: comparison of the frequency responses of the initial, the identified (with Levy's), and the final surrogate model for: (a) the worst case (i.e. with maximal *err*); (b) the median case (i.e. with median *err*).

It is noted that the former approach outmatches the latter in this application example: in Approach I, only 200 pre-evaluations are used to satisfy the PCE model precision (Figure 5.6 (a)), while in Approach II, 280 pre-evaluations are even not sufficient to obtain a correct accuracy (the computational cost is considered too high beyond). As a result, the final model obtained in Approach II is much less accurate than that in Approach I, see Figure 5.6 (b) and 5.7 (b). From Figure 5.8 and 5.9 we can see that the green lines coincide quite well with the red lines for all cases, which implies that the characteristic parameters derived with both identification techniques offer a very accurate parsimonious representation of the $S_{11}(f)$. The observed inaccuracy (mainly for the worst case) occurs during the PCE step. A possible reason is that the rational function is very sensitive to the accuracy of the poles. Therefore, if the PCE modeling procedure is not able to recover the poles with “perfect” accuracy, then the whole rational function also cannot be recovered within good accuracy. More generally, it is known that many transfer function identification methods in the frequency domain are prone to be more or less important sensitive to noise [71].

Briefly, the 1st approach works well for both the dipole and the textile patch, while the 2nd works well for the dipole but is not fully satisfactory for the patch. The advantages of Approach I are its robustness and its simplicity, but it is not necessarily the most efficient approach in terms of parsimony and computational cost. Moreover, the causality, i.e. the relations of Bayard-Bode or Kramers-Kronig are not guaranteed. The Approach II provides a deeper insight into the inherent resonance modes of the antennas – thanks to the zeros/poles derived from the rational functions, which is a natural and efficient way to characterize a linear time invariant (LTI) system, notably for resonant devices in NB as in our examples. In general, the *Two-Step* modeling methodology has been justified through the two application examples.

5.5 Conclusion

In this chapter, we proposed a relatively simple and fast statistical method to model the frequency-dependent reflection coefficient $S_{11}(f)$ of NB variable antennas. The main idea of this method is to realize a separation of the variable “ f ” of $S_{11}(f)$ by means of identification techniques, prior to the extraction of statistical models with the HLARS-base PCE approach in a second stage. Two identification techniques were tested, each having its own advantages and draw-backs. Once the surrogate model has been constructed, we can reproduce the reflection coefficient over the whole frequency band of interest for any values of the random input parameters, producing considerable computational savings compared to full-wave EM simulations.

In the future work, we will take into account the causality of the antenna system. Some existing methods which permit to impose the causality should be studied, for example the algorithm based on the Hilbert transform that was proposed by F. M. Tesche [151]. This algorithm was already used in the lab previously to improve UWB antenna measurements in the frequency domain. This actually results somehow in “noise filtering” by imposing causality to the noise contribution, which is not necessarily causal in this case.

Chapter 6

6. Conclusions and Perspectives

6.1 Conclusions

This thesis is dedicated to the exploration of effective methodologies for quantitatively modeling random effects on soft or flexible antennas in fluctuating conditions (referred to as “variable antennas”). The work mainly covers three parts: parsimonious modeling of the *complete* FF radiated by the antenna under study; deterministic and statistical modeling of those random effects on the antenna’s *complete* FF; statistical modeling of those random effects on the antenna’s reflection coefficient $S_{11}(f)$.

Starting from the state of the art, we have reviewed the development of soft or flexible antennas and their promising applications in the context of IoT and WBANs. Soft or flexible antennas have prominent advantages such as flexibility, low-profile, low-cost, etc. over traditional rigid antennas, but they generally suffer from severe disturbances due to enormous intrinsic and/or external random uncertainties. This complex context of randomness leads to the widespread awareness of the urgency to quantitatively characterize their effects on variable antennas. Most of the existing work have focused on the modeling of certain FoMs which are only a partial description of the antenna’s behavior. Yet, to our knowledge, not too much effort has been made to model the antenna’s *complete* radiated field. A first attempt was recently presented in Rossi’s work [58] where the field modeling was carried out in a rather different context (in Near-Field instead of FF). However, this method is not necessarily always computationally efficient for some complex conditions. This fact motivates us to explore more appropriate methodologies for quantitatively and efficiently modeling the *overall* behavior of variable antennas.

Regarding the FF parsimony, we reviewed the principles of two scalar transform methods, i.e. the DFS and SSH, and a vector transform method, i.e. the VSH. We have compared their performance for representing scalar and vector-valued spherical functions, and are finally convinced that to accurately and parsimoniously represent vector-valued spherical functions such as the FF or its equivalent, the ATF, it is more appropriate to resort to the VSH method.

Then, the relation between the random variables (representing those random uncertainties) and the parsimonious ATF has been investigated explicitly. A canonical deterministic

approach based on the principle of parametric study has been firstly proposed. This simple approach proves to be suited for univariate or at most bivariate systems, but suffers from limited expressiveness for more complicated problems where higher number of random inputs and larger range of variability are considered.

After that, we have investigated an advanced statistical methodology based on the HLARS-PCE, which is more robust and computationally efficient for dealing with multivariate and higher variability range problems. This approach has been applied to a canonical deformable dipole (with 3 input parameters, i.e. stretching, bending and torsion) to demonstrate its effectiveness. Then, the methodology has been further improved/enhanced, in particular by taking into account the frequency behavior and by exploiting extreme parsimony. The improved approach has been tested on a realistic wearable textile patch antenna (with 4 geometrical random parameters and the frequency as an additional “random” parameter) for which accurate and robust surrogate models have been derived, which confirms its effectiveness in terms of efficiency, robustness and scalability. The surrogate models derived in such way have been implemented in several classical local propagation environments (realized with WINNER2/+ model) to demonstrate their practical utility for joint channel/antenna modeling and accurate radio links analysis.

A statistical methodology has also been proposed in order to model the frequency-dependent reflection coefficient $S_{11}(f)$ of variable antennas. This approach aims to parsimoniously represent the reflection coefficient by means of some identification techniques (e.g. polynomial fitting, rational functions), prior to statistical modeling through the HLARS-PCE. This approach has shown good effectiveness for NB antennas.

We believe that our proposed methodology can be beneficial for various types of analyses, notably when the *complete* knowledge (including polarization, amplitude and phase of the field, as well as the reflection coefficient) is mandatory for the antenna under study. Such application contexts comprise for example, joint antenna & directional channel modeling, antenna plugged-in asymptotic simulators (e.g. ray tracing), end-to-end radio links analysis, MIMO systems characterization, or beamforming designs, etc.

6.2 Perspectives

The methodologies that we have proposed in this thesis open the way for an *overall* modeling of variable antennas. However, there are still some aspects that should be further improved, both from a methodological and an applicative point of view.

1. *Improvements of the modeling methodology*

To model the frequency behavior of the ATF, we have chosen to consider the frequency “ f ” as an ordinary “random” input variable. However, as we have already pointed out in §

3.5.1, this wise and flexible choice is viable only for antennas whose frequency behavior is not too sensitive to the other input variables, for example, non-resonant antennas. Obviously, for resonant antennas, alternative solutions must be envisaged. The idea of “separation of variables” that we adopted for modeling the reflection coefficient can be quite instructive in such context. For example, we may firstly apply the Singularity Expansions Method (SEM) to expand the ATF onto a sum of rational functions which are characterized by their poles and frequency-independent residues; then, those residues as a function of the input variables (except the frequency) can be modeled efficiently with the HLARS-PCE method.

Regarding the ED, we have adopted the LHS algorithm for the initialization, and the “Maximin” technique for the iterative enrichment. However, there is no guarantee that the “Maximin” technique enriches the ED always in the most efficient way. More “intelligent” or “educated” strategies which take into account feedback from the performance evaluation of the currently constructed model should be further developed. For example, regions where the current model predicts poorly should be sampled more densely in the next iteration.

2. *Generalization to more realistic applications*

The implementation of our proposed methodologies can be generalized to more realistic and complex context. This would include e.g. considering other types of antennas (e.g. IFA), materials (e.g. conductive fabrics which are more flexible than copper foil) as well as fluctuating environments e.g. the human body. This work is planned to be realized in the near future. A preliminary study has already been carried out. The purpose is to work out a low-profile, compact and highly flexible UWB integrated IFA (IIFA) antenna that is an alternative candidate to other antenna types, notably suitable for on-body communications, hence paving the way for the ensuing statistical modeling of the *in situ* antenna in the vicinity of human bodies. The detailed description of this work can be found in the Annex.

References

- [1] <https://www.statista.com/statistics/471264/iot-number-of-connected-devices-worldwide/>
- [2] <https://lessemf.com/fabric.html>
- [3] A. Kiourti, and J. L. Volakis, "Stretchable and flexible e-fiber antennas with high geometrical accuracy," in *EuCAP*, Lisbon, Portugal, 2015.
- [4] Z. Wang, L. Zhang, Y. Bayram, and J. L. Volakis, "Embroidered conductive fibers on polymer composite for conformal antennas," *IEEE Transactions on Antennas and Propagation*, vol. 60, n° 9, pp. 4141-4147, 2012.
- [5] A. Rida, L. Yang, R. Vyas, and M. M. Tentzeris, "Conductive inkjet-printed antennas on flexible low-cost paper-based substrates for RFID and WSN applications," *IEEE Antennas and Propagation Magazine*, vol. 51, n° 3, 2009.
- [6] I. Llatser, C. Kremers, A. Cabellos-Aparicio, J.M. Jornet, E. Alarco, and D.N. Chigrin, "Graphene-based nano-patch antenna for terahertz radiation," *Photonic Nanostruct*, vol. 10, pp. 353-358, 2012.
- [7] M. Dragoman, D. Neculoiu, A.C. Bunea, and M. Modreanu, "A tunable microwave slot antenna based on graphene," *Appl Phys Lett*, vol. 106, n° 15, 2015.
- [8] R. Salvado, C. Loss, R. Gonçalves, and P. Pinho, "Textile materials for the design of wearable antennas: A survey," *Sensors*, vol. 12, n° 11, pp. 15841-15857, 2012.
- [9] G. DeJean, R. Bairavasubramanian, D. Thompson, G. E. Ponchak, M. M. Tentzeris, and J. Papapolymerou, "Liquid crystal polymer (LCP): A new organic material for the development of multilayer dual-frequency/dual-polarization flexible antenna arrays," *IEEE Antennas and Wireless Propagation Letters*, vol. 4, n° 1, pp. 22-26, 2005.
- [10] C.P. Lin, C.H. Chang, Y.T. Cheng, and C.F. Jou, "Development of a flexible SU-8/PDMS-based antenna," *IEEE Antenn Wireless Propag*, vol. 10, pp. 1108-1111, 2011.
- [11] Q. Liu, A. P. Robinson, K. L. Ford, R. J. Langley, and S. P. Lacour, "Elastic dipole antenna prepared with thin metal films on elastomeric substrate," *Electronics letters*, vol. 48, n° 2, pp. 65-66, 2012.
- [12] X. Guo, Y. Hang, Z. Xie, C. Wu, L. Gao, and C. Liu, "Flexible and wearable 2.45 GHz CPW-fed antenna using inkjet-printing of silver nanoparticles on pet substrate," *Microwave and Optical Technology Letters*, vol. 59, n° 1, pp. 204-208, 2017.
- [13] H. Liu, S. Zhu, P. Wen, X. Xiao, W. Che, and X. Guan, "Flexible CPW-fed fishtail-shaped antenna for dual-band applications," *IEEE Antennas and Wireless Propagation Letters*, vol. 13, pp. 770-773, 2014.

- [14] Y. Li, Z. Zhang, Z. Feng, and H. R. Khaleel, "Fabrication and measurement techniques of wearable and flexible antennas," *WIT Transactions on State of the Art in Science and Engineering*, vol. 82, 2014.
- [15] H. R. Khaleel, H. M. Al-Rizzo, and A. I. Abbosh, "Design, fabrication, and testing of flexible antennas," *Advancement in Microstrip Antennas With Recent Applications*, InTech, 2013.
- [16] S. Cheng, A. Rydberg, K. Hjort, and Z. Wu, "Liquid metal stretchable unbalanced loop antenna," *Applied Physics Letters*, vol. 94, n° 14, 144103, 2009.
- [17] M. Kubo, X. Li, C. Kim, M. Hashimoto, B. J. Wiley, D. Ham, and G. M. Whitesides, "Stretchable microfluidic radiofrequency antennas," *Advanced materials*, vol. 22, n° 25, pp. 2749-2752, 2010.
- [18] G. J. Hayes, J. H. So, A. Qusba, M. D. Dickey, and G. Lazzi, "Flexible liquid metal alloy (EGaIn) microstrip patch antenna," *IEEE Transactions on Antennas and Propagation*, vol. 60, n° 5, pp. 2151-2156, 2012.
- [19] A. Vorobyov, C. Henemann, and P. Dallemagne, "Liquid Metal based antenna for wearable electronic," in *EuCAP*, Davos, Switzerland, 2016.
- [20] V. K. Varadan, K. A. Jose, and V. V. Varadan, "Design and development of electronically tunable microstrip antennas," *Smart materials and structures*, vol. 8, n° 2, 1999.
- [21] D. F. Sievenpiper, J. H. Schaffner, H. J. Song, R. Y. Loo, and G. Tangonan, "Two-dimensional beam steering using an electrically tunable impedance surface," *IEEE Transactions on antennas and propagation*, vol. 51, n° 10, pp. 2713-2722, 2003.
- [22] S. V. Hum, M. Okoniewski, and R. J. Davies, "Realizing an electronically tunable reflectarray using varactor diode-tuned elements," *IEEE Microwave and Wireless Components Letters*, vol. 15, n° 6, pp. 422-424, 2005.
- [23] B. R. Holland, R. Ramadoss, S. Pandey, and P. Agrawal, "Tunable coplanar patch antenna using varactor," *Electronics Letters*, VOL. 42, n° 6, pp. 319-321, 2006.
- [24] M. A. R. Osman, M. K. A. Rahim, M. A. N. A. Samsuri, F. Zubir, and K. Kamardin, "Design, implementation and performance of ultra-wideband textile antenna," *Progress In Electromagnetics Research B*, vol. 27, pp. 307-325, 2011.
- [25] L. Yang, R. Zhang, D. Staiculescu, C. P. Wong, and M. M. Tentzeris, "A novel conformal RFID-enabled module utilizing inkjet-printed antennas and carbon nanotubes for gas-detection applications," *IEEE Antennas and Wireless Propagation Letters*, vol. 8, pp. 653-656, 2009.

- [26] H. A. Rahman, S. K. A. Rahim, M. Abedian, and N. Najib, "Design of a flexible antenna using printed silver loaded epoxy on PDMS/plastic substrate for wearable applications," in *EuCAP*, Davos, Switzerland, 2016.
- [27] P. J. Soh, G. A. Vandenbosch, and J. Higuera-Oro, "Design and evaluation of flexible CPW-fed ultra wideband (UWB) textile antennas," in *IEEE International RF and Microwave Conference (RFM)*, 2011.
- [28] J. G. Santas, A. Alomainy, and Y. Hao, "Textile antennas for on-body communications: Techniques and properties," in *EuCAP*, Edinburgh, UK, 2007.
- [29] <http://www.marketwired.com/press-release/under-armour-powers-nfl-scouting-combine-with-zephyr-technology-1401804.html>
- [30] D. Curone, E. L. Secco, A. Tognetti, G. Loriga, G. Dudnik, M. Risatti, and G. Magenes, "Smart garments for emergency operators: the ProeTEX project", *IEEE Transactions on Information Technology in Biomedicine*, vol. 14, n° 3, pp. 694-701, 2010.
- [31] <http://www.cyberglovesystems.com/cyberglove-iii/>.
- [32] Z. N. Chen, A. Cai, T. S. See, X. Qing, and M. Y. W. Chia, "Small planar UWB antennas in proximity of the human head," *IEEE Transactions on Microwave Theory and Techniques*, vol. 54, n° 4, pp. 1846-1857, 2006.
- [33] M. Pelosi, O. Franek, M. B. Knudsen, G. F. Pedersen, and J. B. Andersen, "Antenna proximity effects for talk and data modes in mobile phones," *IEEE Antennas and Propagation Magazine*, vol. 52, n° 3, pp. 15-27, 2010.
- [34] Y.S. Shifrin, *Statistical antenna theory*, Boulder, Colorado, The Golem Press, 1971.
- [35] T. Olsson, and A. Koptioug, "Statistical analysis of antenna robustness," *IEEE Transactions on Antennas and Propagation*, vol. 53, n° 1, pp. 1253-1260, 2005.
- [36] A. Sibille, "Statistical modeling of the radio-electric properties of wireless terminals in their environment," *IEEE Antennas and Propagation Magazine*, vol. 54, n° 6, pp. 117-129, 2012.
- [37] E. Sundarsingh, M. Kanagasabai, and V. Ramalingam, "Statistical analysis on the bandwidth of a dual frequency textile antenna," *IET Microwaves, Antennas & Propagation*, vol. 9, n° 15, pp. 1683-1690, 2015.
- [38] A. Sibille, "A small signal analysis of statistical antenna modelling," in *EuCAP*, Berlin, Germany, 2009.
- [39] G. Angiulli, M. Cacciola, and M. Versaci, "Microwave devices and antennas modelling by support vector regression machines," *IEEE Trans. Magn.*, vol. 43, pp. 1589-1592, 2007.

- [40] N. Chauhan, A. Mittal, and M. V. Kartikeyan, "Support vector driven genetic algorithm for the design of circular polarized microstrip antenna," *Int J Infrared Millim. Waves*, vol. 29, pp. 558-569, 2008.
- [41] J. P. Jacobs, "Bayesian support vector regression with automatic relevance determination kernel for modeling of antenna input characteristics," *IEEE Transactions on Antennas and Propagation*, vol. 60, n° 4, pp. 2114-2118, 2012.
- [42] A. Patnaik, D. E. Anagnostou, R. K. Mishra, and J. C. Lyke, "Applications of neural networks in wireless communications," *IEEE Antennas and Propagation Magazine*, vol. 46, n° 3, pp. 130-137, 2004.
- [43] K. Guney, S. Sagiroglu, and M. Erler, "Generalized Neural Method to Determine Resonant Frequencies of Various Microstrip Antennas," *International Journal of Wand Microwave Computer-Aided Engineering*, vol. 12, pp. 131-139, 2002.
- [44] R. K. Mishra, and A. Patuaik, "Neurospectral Computation for Complex Resonant Frequency of Microstrip Resonators," *IEEE Microwave and Guided Wave Letters*, vol. 9, n° 9, pp. 351-353, 1999.
- [45] K. Guney, and N. Sarikaya, "Artificial Neural Networks for Calculating the Input Resistance of Circular Microstrip Antennas," *Microwave and Optical Technology Letters*, vol. 37, n° 2, pp. 107-111, 2003.
- [46] R. K. Mishra, and A. Patnaik, "Neurospectral Computation for Input Impedance of Rectangular Microstrip Antenna," *Electronics Letters*, vol. 35, n° 20, pp. 1691-1693, 1999.
- [47] Q. Q. He, Q. Wang, and B. Z. Wang, "Conformal array based on pattern reconfigurable antenna and its artificial neural model," *Journal of Electromagnetic Waves and Applications*, vol. 22, n° 1, pp. 99-110, 2008.
- [48] D. Xiu, and G. E. Karniadakis, "The Wiener–Askey polynomial chaos for stochastic differential equations," *SIAM J. Sci. Comput.*, vol. 24, n° 2, pp. 619-644, 2002.
- [49] F. Boeykens, H. Rogier, and L. Vallozzi, "An Efficient Technique Based on Polynomial Chaos to Model the Uncertainty in the Resonance Frequency of Textile Antennas Due to Bending," *IEEE Transactions on Antennas and Propagation*, vol. 62, n° 3, pp. 1253-1260, 2014.
- [50] M. Rossi, A. Dierck, H. Rogier, and D. Vande Ginste, "A Stochastic Framework for the Variability Analysis of Textile Antennas," *IEEE Transactions on Antennas and Propagation*, vol. 62, n° 12, pp. 6510-6514, 2014.

- [51] M. Rossi, S. Agneessens, H. Rogier, and D. Ginste, "Stochastic Analysis of the Impact of Substrate Compression on the Performance of Textile Antennas," *IEEE Transactions on Antennas and Propagation*, vol. 64, n° 6, pp. 2507-2512, 2016.
- [52] C. Roblin, and R. D'Errico, "Statistical analysis of a parametric model of a "population" of UWB antennas," in *EuCAP*, Berlin, Germany, 2009.
- [53] A. Sibille, and C. Roblin, "Analysis and modelling of the randomness in terminals antennas," *WAVES Magazine*, pp. 39-48, 2010. (available from <http://www.iteam.upv.es/>)
- [54] C. Roblin, and M. A. Yousuf, "Statistical models of wideband and UWB omnidirectional antennas based on a parametric modelling," in *EuCAP*, Barcelona, Spain, April 2010.
- [55] C. E. Baum, "On the singularity expansion method for the solution of electromagnetic interaction problems", *Interaction Notes, Note 88*, 1971.
- [56] C. Roblin, "Ultra compressed parametric modelling of UWB antenna measurements," in *EuCAP*, Nice, France, Nov. 2006.
- [57] C. Roblin, "Representation, characterization, and modelling of Ultra Wide Band antennas," in X. Begaud (Ed.) et al, *Ultra Wide Band Antennas*, WILEY/ISTE, 2011.
- [58] M. Rossi, G. J. Stockman, H. Rogier, and D. Vande Ginste, "Stochastic analysis of the efficiency of a wireless power transfer system subject to antenna variability and position uncertainties," *Sensors*, vol. 16, n° 7, 2016.
- [59] C. Roblin, S. Bories, and A. Sibille, "Characterization tools of antennas in the Time Domain," in *IWUWBS*, Oulu, June 2003.
- [60] P.E. Merilees, "The pseudospectral approximation applied to the shallow water equations on a sphere," *Atmosphere*, vol.11, no.1, pp. 13-20, 1973.
- [61] S. A. Orszag, "Fourier series on spheres," *Monthly Weather Review*, vol. 102, n° 1, pp. 56-75, 1974.
- [62] H. B. Cheong, "Double Fourier series on a sphere: Applications to elliptic and vorticity equations," *Journal of Computational Physics*, vol. 157, n° 1, pp. 327-349, 2000.
- [63] H. B. Cheong, "Application of double Fourier series to the shallow-water equations on a sphere," *Journal of Computational Physics*, vol. 165, n° 1, pp. 261-287, 2000.
- [64] R. Bartnik, and A. H. Norton, "Numerical methods for the Einstein equations in null quasi-spherical coordinates," *SIAM Journal on Scientific Computing*, vol. 22, n° 3, pp. 917-950, 2000.
- [65] C. Sun, J. Li, F. Jin, and F. Xie, "Contrasting meridional structures of stratospheric and tropospheric planetary wave variability in the Northern Hemisphere," *Tellus A: Dynamic Meteorology and Oceanography*, vol. 66, n° 1, 2014.

- [66] Z. Mhanna, and A. Sibille, "Statistical modeling of the power gain pattern of a random set of parameterized planar dipoles," in *COST IC1004*, Lund, Sweden, 2011.
- [67] G. Arfken, *Mathematical Methods for Physicists*, 3rd ed. Orlando, Florida: Academic Press, 1985.
- [68] Z. Mhanna, A. Sibille, M. A. Yousuf, and C. Roblin, "Parametric statistical modeling of power gain patterns for RFID backscattering channels," in *EuCAP*, Prague, Czech Republic, 2012.
- [69] J. Du, and C. Roblin, "Parametric modeling of deformable antennas based on the spherical modes expansion method," in *EuCAP*, Davos, Switzerland, April 2016.
- [70] J. E. Hansen (Ed.), *Spherical near-field antenna measurements*, IEEE Electromagnetic waves series 26, London, UK: Peter Peregrinus, 1988.
- [71] C. Roblin, "Ultra compressed parametric modelling of UWB antenna measurements," in *EuCAP*, Nice, France, 2006.
- [72] F. Jensen, and A. Frandsen, "On the number of modes in spherical wave expansion," in *Proc. 26th AMTA*, Stone Mountain Park, GA, pp. 489-94, Oct. 2004.
- [73] S. K. Padhi, and M. E. Bialkowski, "Parametric study of a microstrip Yagi antenna," in *Microwave Conference, 2000 Asia-Pacific. IEEE*, 2000.
- [74] Y-F. Lin, H-M. Chen, and K-L. Wong, "Parametric study of dual-band operation in a microstrip-fed uniplanar monopole antenna," *IEE Proceedings-Microwaves, Antennas and Propagation*, vol. 150, n° 6, pp. 411-414, 2003.
- [75] H-M. Chen, Y-F. Lin, P-S. Cheng, H-H. Lin, C. T. P. Song, and P. S. Hall, "Parametric study on the characteristics of planar inverted-F antenna," *IEE Proceedings-Microwaves, Antennas and Propagation*, vol. 152, no.6, pp. 534-538, 2005.
- [76] Aaron. Kerkhoff, and Hao Ling, "A parametric study of band-notched UWB planar monopole antennas," *Antennas and Propagation Society International Symposium, IEEE*, vol. 2, 2004.
- [77] A. Alomainy, Y. Hao, and D. M. Davenport, "Parametric study of wearable antennas with varying distances from the body and different on-body positions," *IET Seminar on Antennas and Propagation for Body-Centric Wireless Communications*, pp. 84-89, 2007.
- [78] N. Wiener, "The homogeneous chaos," *American Journal of Mathematics*, vol. 60, n° 4, pp. 897-936, 1938.
- [79] R. Cameron, and W. Martin, "The orthogonal development of nonlinear functionals in series of Fourier-Hermite functionals," *Annals of Mathematics*, pp. 385-392, 1947.
- [80] H. Ogura, "Orthogonal functionals of the Poisson process," *IEEE Transactions on Information Theory*, vol. 18, n° 4, pp. 473-481, 1972.

- [81] R. Askey, and J. Wilson, "Some basic hypergeometric polynomials that generalize Jacobi polynomials," *Memoirs Amer. Math. Soc., AMS, Providence RI*, 319 (1985).
- [82] G. Kewlani, J. Crawford, and K. Iagnemma, "A polynomial chaos approach to the analysis of vehicle dynamics under uncertainty," *Vehicle system dynamics*, vol. 50, n° 5, pp. 749-774, 2012.
- [83] L. Li, and C. Sandu, "On the impact of cargo weight, vehicle parameters, and terrain characteristics on the prediction of traction for off-road vehicles," *J. Terramech.*, vol. 44, n° 3, pp. 221-238, 2003.
- [84] A. Sandu, C. Sandu, and M. Ahmadian, "Modeling multi body dynamic systems with uncertainties. Part I:Theoretical and computational aspects," *Multibody Syst. Dyn.*, vol. 15, n° 4, pp. 1-23, 2006.
- [85] C. Sandu, A. Sandu, and M. Ahmadian, "Modeling multi body dynamic systems with uncertainties. Part II:Numerical applications," *Multibody Syst. Dyn.*, vol. 15, n° 3, pp. 241-262, 2006.
- [86] X. Wan, and G. E. Karniadakis, "An adaptive multi-element generalized polynomial chaos method for stochastic differential equations," *J. Comput. Phys.*, vol. 209, n° 2, pp. 617-642, 2005.
- [87] J. Wang, P. Ghanta, and S. Vrudhula, "Stochastic analysis of interconnect performance in the presence of process variations," in *Proc. IEEE/ACM Int. Conf. Comput. Aided Des. (ICCAD'04)*, San Jose, CA, USA, 2004.
- [88] D. Vande Ginste, D. De Zutter, D. Deschrijver, T. Dhaene, P. Manfredi, and F. Canavero, "Stochastic modeling-based variability analysis of onchip interconnects," *IEEE Trans. Compon. Packag. Manuf. Technol.*, vol. 2, n° 7, pp. 1182-1192, 2012.
- [89] P. Sumant, H. Wu, A. Cangellaris, and N. Aluru, "Reduced-order models of finite element approximations of electromagnetic devices exhibiting statistical variability," *IEEE Trans. Antennas Propag.*, vol. 60, n° 1, pp. 301-309, 2012.
- [90] D. Spina, F. Ferranti, T. Dhaene, L. Knockaert, G. Antonini, and D. Vande Ginste, "Variability analysis of multiport systems via polynomial-chaos expansion," *IEEE Trans. Microw. Theory Techn.*, vol. 60, n° 8, pp. 2329-2338, 2012.
- [91] P. Li, and L. J. Jiang, "Uncertainty quantification for electromagnetic systems using ASGC and DGTD method," *IEEE Trans. Electromagn. Compat.*, vol. 57, n° 4, pp. 754-763, 2015.
- [92] J. Wiart, E. Conil, A. Hadjem, M. Jala, , P. Kersaudy, and N. Varsier, "Handle variability in numerical exposure assessment: the challenge of the stochastic dosimetry," in *EuCAP*, Gothenburg, Sweden, 2013.

- [93] J. Wiart, P. Kersaudy, A. Ghanmi, N. Varsier, A. Hadhem, P. Odile, and R. Mittra, "Stochastic dosimetry to manage uncertainty in numerical EMF exposure assessment," in *Forum for Electromagnetic Research Methods and Application Technologies (FERMAT)*, vol. 12, 2015.
- [94] P. Kersaudy, S. Mostarshedi, B. Sudret, O. Picon, and J. Wiart, "Stochastic analysis of scattered field by building facades using polynomial chaos," *IEEE Transactions on Antennas and Propagation*, vol. 62, n° 12, pp. 6382-6393, 2014.
- [95] P. Kersaudy, B. Sudret, N. Varsier, O. Picon, and J. Wiart, "A new surrogate modeling technique combining Kriging and polynomial chaos expansions—Application to uncertainty analysis in computational dosimetry," *Journal of Computational Physics*, vol. 286, pp. 103-117, 2015.
- [96] C. Soize, and R. Ghanem, "Physical systems with random uncertainties: chaos representations with arbitrary probability measure," *SIAM Journal on Scientific Computing*, vol. 26, n° 2, pp. 395-410, 2004.
- [97] A. Sklar, "Random variables, joint distribution functions, and copulas," *Kybernetika*, vol. 9, n° 6, pp. 449-460, 1973.
- [98] A. Nataf, "Statistique mathematique-determination des distributions de probabilites dont les marges sont donnees," *Comptes Rendus Hebdomadaires des Seances de l'Academie des Sciences*, vol. 255, 1962.
- [99] R. Lebrun, and A. Dutfoy, "A generalization of the Nataf transformation to distributions with elliptical copula," *Probabilistic Engineering Mechanics*, vol. 24, n° 2, pp. 172-178, 2009.
- [100] M. Rosenblatt, "Remarks on a multivariate transformation," *The annals of mathematical statistics*, vol. 23, n° 3, pp. 470-472, 1952.
- [101] Z. Zhang, T.A. El-Moselhy, I.M. Elfadel, and L. Daniel, "Stochastic testing method for transistor-level uncertainty quantification based on generalized polynomial chaos," *IEEE Trans. Comput. Aided Des. Integr. Circ. Syst.* vol. 32, pp. 1533-1545, 2013.
- [102] G. Golub, and J. Welsch, "Calculation of gauss quadrature rules," *Math. Comput.*, vol. 23, pp. 221-230, 1969.
- [103] S. Smolyak, "Quadrature and interpolation formulas for tensor products of certain classes of functions," *Soviet Math. Dokl*, vol. 4, 1963.
- [104] A. Geletu, "Integration methods for multidimensional probability integrals", IFAC2011, Pre-conference tutorial, August 27-28, 2011, Milano, Italy. Available on line: <https://www.tu->

ilmenau.de/fileadmin/media/simulation/Lehre/Vorlesungsskripte/Lecture_materials_Abebe/Abebe_IFACTut-2011.ppt

- [105] O. P. Le Maître, O. M. Knio, H. N. Najm, and R. G. Ghanem, “Uncertainty propagation using Wiener–Haar expansions,” *Journal of computational Physics*, vol. 197, n° 1, pp. 28-57, 2004.
- [106] D. Xiu, and J. S. Hesthaven, “High-order collocation methods for differential equations with random inputs,” *SIAM Journal on Scientific Computing*, vol. 27, n° 3, pp. 1118-1139, 2005.
- [107] D. Xiu, “Efficient collocation approach for parametric uncertainty analysis,” *Commun. Comput. Phys*, vol. 2, n° 2, pp. 293-309, 2007.
- [108] I. Babuška, F. Nobile, and R. Tempone, “A stochastic collocation method for elliptic partial differential equations with random input data,” *SIAM Journal on Numerical Analysis*, vol. 45, n° 3, pp. 1005-1034, 2007.
- [109] P. Manfredi, D. V. Ginste, D. De-Zutter, and F. G. Canavero, “Generalized decoupled polynomial chaos for nonlinear circuits with many random parameters,” *IEEE Microwave and Wireless Components Letters*, vol. 25, n° 8, pp. 505-507, 2015.
- [110] G. Blatman, and B. Sudret, “An adaptive algorithm to build up sparse polynomial chaos expansions for stochastic finite element analysis,” *Probabilistic Engineering Mechanics*, vol. 25, n° 2, pp. 183-197, 2010.
- [111] G. Blatman, *Adaptive sparse polynomial chaos expansions for uncertainty propagation and sensitivity analysis*, Ph.D. Thesis, Université Blaise Pascal, Clermont-Ferrand, 2009.
- [112] B. Efron, T. Hastie, I. Johnstone, and R. Tibshirani, “Least angle regression,” *The Annals of statistics*, vol. 32, n° 2, pp. 407-499, 2004.
- [113] G. Blatman, and B. Sudret, “Adaptive sparse polynomial chaos expansion based on least angle regression,” *Journal of Computational Physics*, vol. 230, n° 6, pp. 2345-2367, 2011.
- [114] A. M. Molinaro, R. Simon, and R. M. Pfeiffer, “Prediction error estimation: A comparison of resampling methods,” *Bioinformatics*, vol. 21, n° 15, pp. 3301-3307, 2005.
- [115] G. Saporta, *Probabilités, analyse des données et statistique*. Editions Technip, 2006.
- [116] B. Sudret, “Global sensitivity analysis using polynomial chaos expansions,” *Reliability Engineering & System Safety*, vol. 93, n° 7, pp. 964-979, 2008.
- [117] J. H. Halton, “On the efficiency of certain quasi-random sequences of points in evaluating multi-dimensional integrals,” *Numerische Mathematik*, vol. 2, n° 1, pp. 84-90, 1960.

- [118] H. Faure, “Discr pance de suites associ es   un syst me de num ration (en dimension s),” *Acta Arithmetica*, vol. 41, n  4, pp. 337-351, 1982.
- [119] I.M. Sobol, “On the distribution of points in a cube and the approximate evaluation of integrals,” *USSR Comput. Math. Phys.*, vol. 7, pp. 86-112, 1967.
- [120] M. D. McKay, R. J. Beckman, and W. J. Conover, “Comparison of three methods for selecting values of input variables in the analysis of output from a computer code,” *Technometrics*, vol. 21, n  2, pp. 239-245, 1979.
- [121] M. E. Johnson, L. M. Moore, and D. Ylvisaker, “Minimax and maximin distance designs,” *Journal of Statistical Planning and Inference*, vol. 26, n  2, pp. 131-148, 1990.
- [122] P. Kersaudy, *Mod lisation statistique de l’exposition humaine aux ondes radiofr quences*, PhD thesis, Universit  Paris-Est, 2015.
- [123] S. Zein, B. Colson, and F. Glineur, “An efficient sampling method for regression-based polynomial chaos expansion,” *Communications in computational physics*, vol. 13, n  4, pp. 1173-1188, 2013.
- [124] Y. Shin, and D. Xiu, “Nonadaptive quasi-optimal points selection for least squares linear regression,” *SIAM Journal on Scientific Computing*, vol. 38, n  1, pp. A385-A411, 2016.
- [125] S. Marelli, and B. Sudret, UQLab user manual – Polynomial Chaos Expansions, Report UQLab-V0.9-104, Chair of Risk, Safety & Uncertainty Quantification, ETH Zurich, 2015.
- [126] C. V. Mai, and Bruno Sudret, “Surrogate models for oscillatory systems using sparse polynomial chaos expansions and stochastic time warping,” *SIAM/ASA Journal on Uncertainty Quantification*, vol. 5, n  1, pp. 540-571, 2017.
- [127] A. Sibille, C. Roblin, S. Bories, and A. C. Lepage, “A channel-based statistical approach to antenna performance in UWB communications,” *IEEE Transactions on Antennas and Propagation*, vol. 54, n  11, pp. 3207-3215, 2006.
- [128] V. Yaghoubi, S. Marelli, B. Sudret, and T. Abrahamsson, “Sparse polynomial chaos expansions of frequency response functions using stochastic frequency transformation,” *Probabilistic Engineering Mechanics*, vol. 48, pp. 39-58, 2017.
- [129] Q. Bai, and R. Langley, “Crumpling of PIFA Textile Antenna,” *IEEE Transactions on Antennas and Propagation*, vol. 60, n  1, pp. 63-70, 2012.
- [130] D. H. Werner, and R. Mittra (Ed.), *Frontiers in Electromagnetics*, D L. Jaggard, A D. Jaggard, and P. Frangos, Ch. 1 “Fractal electrodynamics: Surfaces and Superlattices,” *IEEE Press Series on RF and Microwave Technology*, 2000.

- [131] F. Boeykens, L. Vallozzi, and H. Rogier, "Cylindrical bending of deformable textile rectangular patch antennas," *International Journal of Antennas and Propagation*, 2012.
- [132] I. Locher, M. Klemm, T. Kirstein, and G. Trster, "Design and characterization of purely textile patch antennas," *IEEE Transactions on advanced packaging*, vol. 29, n° 4, pp. 777-788, 2006.
- [133] C. Soize, and R. Ghanem, "Physical systems with random uncertainties: chaos representations with arbitrary probability measure," *SIAM Journal on Scientific Computing*, vol. 26, n° 2, pp. 395-410, 2004.
- [134] W. El Hajj, C. Person, and J. Wiart, "A Novel Investigation of a Broadband Integrated Inverted-F Antenna Design; Application for Wearable Antenna," *IEEE Transactions on Antennas and Propagation*, vol. 62, n° 7, pp. 3843-3846, 2014.
- [135] A. Tsolis, W. Whittow, A. Alexandridis, and J. Vardaxoglou, "Embroidery and Related Manufacturing Techniques for Wearable Antennas: Challenges and Opportunities", *Electronics*, vol. 3, n° 2, pp. 314-338, 2014.
- [136] S. Sankaralingam, and B. Gupta, "Determination of Dielectric Constant of Fabric Materials and Their Use as Substrates for Design and Development of Antennas for Wearable Applications," *IEEE Transactions on Instrumentation and Measurement*, vol. 59, n° 12, pp. 3122-3130, 2010.
- [137] J. Meinilä, P. Kyösti, T. Jämsä, and L. Hentilä, "WINNER II channel models," *Radio Technologies and Concepts for IMT-Advanced*, pp. 39-92, 2009.
- [138] IST-4-027756 WINNER II, D1.1.2, *WINNER II Channel Models*, v1.2, April 2008.
- [139] Tokio Taga, "Analysis for mean effective gain of mobile antennas in land mobile radio environments", *IEEE Transactions on Vehicular Technology*, vol. 39, no.2, pp. 117-131, 1990.
- [140] A. Sibille, "Statistical modeling of the radio-electric properties of wireless terminals in their environment," *IEEE Antennas and Propagation Magazine*, vol. 54, n° 6, pp. 117-129, 2012.
- [141] A. Sibille, and M. A. Mellah, "A frequency wise statistical model of the effective gain incorporating terminals and local propagation variability," *TD (09)*, 735, pp. 16-18, 2009.
- [142] C. Roblin, "A statistical assessment of ambient electromagnetic field using body-worn multi-axial sensors," *Comptes Rendus Physique*, vol. 16, n° 9, pp. 802-818, 2015.
- [143] J. P. De Villiers, and J. P. Jacobs, "Gaussian process modeling of CPW-fed slot antennas," *Progress In Electromagnetics Research*, vol. 98, pp. 233-249, 2009.

- [144] S. Narayana, T. K. Sarkar, R. Adve, M. Wicks, and V. Vannicola, "A comparison of Two techniques for the interpolation/extrapolation of frequency domain responses," *Digital Signal Processing*, vol. 6, n° 1, pp. 51-67, 1996.
- [145] E. C. Levy, "Complex-curve fitting," *IRE Transactions on Automatic Control*, vol. AC-4, n° 1, pp. 37-43, 1959.
- [146] R. Kumaresan, "On a frequency domain analog of Prony's method," *IEEE Transactions on Acoustics, Speech, and Signal Processing*, vol. 38, n° 1, pp. 168-170, 1990.
- [147] R. Kumaresan, D. W. Tufts, and L. L. Scharf, "A Prony method for noisy data: Choosing the signal components and selecting the order in exponential signal models," *Proceedings of the IEEE*, vol. 72, n° 2, pp. 230-233, 1984.
- [148] K. Steiglitz, and L. McBride, "A technique for the identification of linear systems," *IEEE Transactions on Automatic Control*, vol. 10, n° 4, pp. 461-464, 1965.
- [149] T. K. Sarkar, and O. Pereira, "Using the matrix pencil method to estimate the parameters of a sum of complex exponentials," *IEEE Antennas and Propagation Magazine*, vol. 37, n° 1, pp. 48-55, 1995.
- [150] J. E. Dennis, and R. B. Schnabel, *Numerical methods for unconstrained optimization and nonlinear equations*. Englewood Cliffs, NJ, United States: Prentice-Hall, 1983.
- [151] F. M. Tesche, "On the use of the Hilbert transform for processing measured CW data", *IEEE Transactions on Electromagnetic Compatibility*, vol. 34, n° 3, pp. 259-266, 1992.

Publications

Journal papers:

- [1] J. Du and C. Roblin, "Stochastic surrogate models of deformable antennas based on vector spherical harmonics and polynomial chaos expansions : application to textile antennas," *IEEE Transactions on Antennas and Propagation*, vol. 66, n° 7, 2018.
- [2] J. Du and C. Roblin, "Statistical modeling of disturbed antennas based on the polynomial chaos expansion," *IEEE Antennas and Wireless Propagation Letters*, (online Sept. 2016), vol. 16, pp. 1843-1846, 2017.

International conference papers:

- [1] J. Du and C. Roblin, "An UWB Coplanar Waveguide Fed Integrated IFA Design for Wearable Communications," in *EuCAP*, London, England, April 2018.
- [2] J. Du and C. Roblin, "Statistical Modeling of the Reflection Coefficient of Deformable Antennas," in *EuCAP*, Paris, France, March 2017.
- [3] J. Du and C. Roblin, "Parametric modeling of deformable antennas based on the spherical modes expansion method," in *EuCAP*, Davos, Switzerland, April 2016.

Annex

Abstract — An UWB CPW-fed Integrated “IFA-like” design is proposed. This design has a much longer short-ended arm and a much narrower gap between the radiating arms and the coplanar ground plane. The bandwidth increase is achieved thanks to the superposition of multi-resonances induced by the joint effects of a strong coupling between the radiating arms and the ground plane and the excitation of both even and odd modes in the feedline. The design has been tested for two types of substrate, FR4 and denim, for which -10 dB bandwidths of more than 60 % and 87 % are achieved respectively. Body proximity effects are analysed for the denim IIFA by simulation. It shows that the antenna remains working well in the presence of human body thanks to its UWB feature. This extremely simple, low-profile and easily integrable UWB IIFA-like design can be potentially used for wearable communications (on-body/off-body), supporting multi-standards.

I. Introduction

Since recent years, wearable antennas are gaining exceptional research attention due to their vital roles in wearable communications such as the Wireless Body Area Network, WBAN. Appropriate wearable antennas should verify good properties such as low-profile, light weight, easy integration, etc. and particularly, should be robust to body proximity effects such as detuning, impedance mismatch, losses, etc. which are well known since long ago.

For minimizing the body influence, a simple and intuitive idea is to isolate the antennas from the human body by introducing a shielding layer. Large-size backing ground planes are the most commonly used for this purpose, for example, in patch antennas [A-1]. These antennas usually achieve excellent isolation, however, they have disadvantages such as either narrow bandwidth (≈ 6 %), or moderate [A-2] to large size, reduced flexibility and are mostly suitable for off-body (rather than on-body) radio links. Other solutions include metamaterial based, Artificial Magnetic Conductor (AMC) based or ferrite based screening layers [A-3]-[A-6]. They usually allow to have a good isolation while keeping a satisfactory to a relatively large bandwidth, but their thickness is generally significant and the overall size is large, which is quite inconvenient for integration into clothes. An alternative approach to improve the *resilience* of antennas to body proximity effects (notably the detuning effect) is to increase their bandwidth (BW) significantly – instead of resorting to isolation techniques (which often increase their complexity – design, size, cost, etc.). Of course, this approach does not prevent antenna/body Near-Field (NF) coupling effects, inducing extra losses and noticeable modifications of both NF and Far-Field (FF) patterns. In this context, one of the design objectives – considering as early as possible the body proximity effects – is notably to

“monitor” losses (trying to maximize the total efficiency as much as possible), in order to achieve an interesting compromise between performance and complexity suitable for some applications. Thereby, planar ultra-wideband (UWB) antennas are interesting candidates for wearable communications. The above-mentioned body proximity effects still exist for UWB antennas, but their bandwidth is so wide that the possible detuning effects appear somehow more “globally” regarding the matching over the BW of interest (although for multi-resonant antennas each resonance can be affected). Therefore, possible abrupt radio link outage due to the collapse of the total efficiency which often occurs for narrow band antennas in the vicinity of a human body (when the detuning is such that the mismatch becomes extremely severe) is generally avoided for UWB antennas [A-7].

Among various antenna types, Coplanar Waveguide fed integrated Inverted-F Antennas (CPW-fed IIFAs) present interesting features such as large bandwidth as well as easy integrability; therefore, it is a quite suitable candidate for wearable communications. In [A-8], a folded CPW-fed IIFA printed on FR4 substrate ($\epsilon_r = 4.4$, $\tan\delta = 0.025$, $h = 1.6$ mm) is proposed. The radiating element of the antenna measures 25×8 mm², for an overall size including the ground plane as large as 50×60 mm². This antenna achieves a -10 dB bandwidth of about 20 % around 2.045 GHz. In [A-9], a general design of a wideband CPW-fed IIFA, based on a design proposed in [A-7], is presented. The shorted end and open end horizontal strips being close enough to the CPW ground plane “patches”, their coupling is strong and they can be viewed as asymmetrical coplanar strip (ACPS) [A-10]. In addition, the IIFA is asymmetrically fed by the CPW which induces an additional resonance of the ground plane (explicable by the theory of characteristic modes). This resonance is close enough to the classical IFA resonance so that the bandwidth is increased to more than 40 % for a FR4 based IIFA and to about 25 % for a denim ($\epsilon_r = 1.7$, $\tan\delta = 0.05$, $h = 0.76$ mm) based IIFA.

Herein, we propose a new UWB small size CPW-fed “IIFA-like” design, as shown in Fig. 1. The design has quite similar form as classical IIFAs except that the short-ended arm is much longer and the gap between the radiating element and the coplanar ground plane is much narrower than conventionally. This special choice of the geometry leads to different mechanisms of radiation compared to classical IIFAs (hence the terminology “IIFA-like”). Indeed, it allows to create strong coupling between the radiating arms and the coplanar ground plane, and also to excite both the even mode (i.e. the CPW fundamental mode) and the odd mode (i.e. the asymmetrical slot-line mode) within the feedline. The combination of these factors results in close multi-resonances leading to a very significant increase of the bandwidth. We applied the new design with both FR4 and denim substrates. Full-wave simulations are performed for both antennas, and measurements are also carried out for the FR4 based IIFA. Results are presented and analysed below. It shows that the proposed design allows to achieve ultra-wide band for both antennas. Even in the presence of human body, the

denim based IIFA can maintain quite good performance: the reflection coefficient $|S_{11}|$ is below -6.5 dB over a bandwidth of about 3 GHz, which remains a completely acceptable matching level, avoiding any dramatic radio link outage, as pointed out in the above paragraph. This compact UWB CPW-fed IIFA design can be suitable for wearable applications.

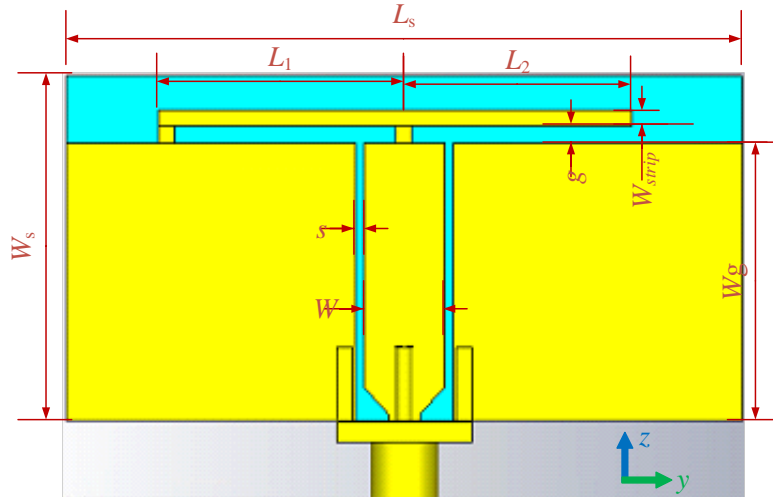


Fig. 1. Geometry of the proposed CPW-fed IIFA design.

II. CPW-Fed IIFA on FR4 Substrate

a. Design of the antenna

In the first stage, the proposed antenna (Fig. 1) was designed with a commonly used FR4 substrate (relative permittivity $\epsilon_r = 4.4$, loss tangent $\tan\delta = 0.025$ and thickness $h = 1.6$ mm). Dimensions are chosen for operation in the ISM band at 2.45 GHz. The radiating element is a horizontal strip which is fed at the middle by a 50Ω CPW feedline (linewidth $W = 6$ mm, slot width $s = 0.6$ mm, length $W_g = 21$ mm), short-ended to the left (arm length $L_1 = 19$ mm) and open-ended to the right (arm length $L_2 = 16$ mm). The width of the strip is $W_{\text{strip}} = 1$ mm and the gap between the horizontal strip and the CPW ground plane is very narrow: $g = 1$ mm. The CPW feedline is chamfered at the edge to facilitate the connection to a 50Ω SMA connector by welding. The overall size of the antenna is $L_s \times W_s = 50 \text{ mm} \times 26 \text{ mm}$.

b. Simulation and measurement results

The proposed antenna structure was firstly studied using the full-wave simulator CST[®] MWS. Note that the adaptive meshing functionality has been used for all simulations, so that they can be considered reliable and accurate. Then, a prototype was fabricated and measurements were carried out in a well-conditioned anechoic chamber. Fig. 2 shows the

reflection coefficient $|S_{11}|$ from simulation (blue solid line) and measurement (red dash line). We can see that the -10 dB impedance bandwidth is 61.3 % (1.835 GHz – 3.455 GHz) in simulation and 63.3 % (1.89 – 3.64 GHz) for the measurement – more than 10 % larger than that obtained in [A-9].

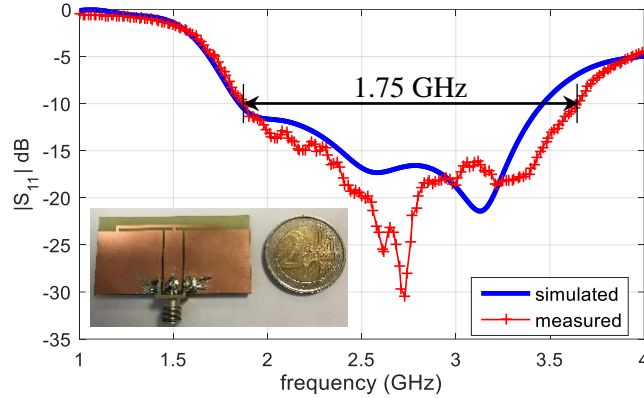


Fig. 2. Simulated and measured reflection coefficient $|S_{11}|$ of the proposed FR4 based CPW-fed IIFA.

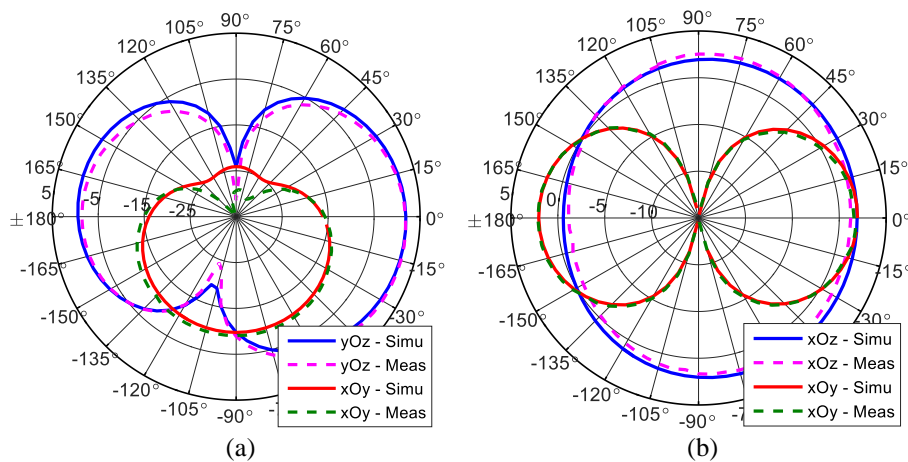


Fig. 3. Simulated and measured realized gain G_r in principle cut-planes of the proposed FR4 based CPW-fed IIFA: (a) $G_{r\theta}$ in yOz and xOy planes; (b) $G_{r\phi}$ in xOz and xOy planes.

In Fig. 3 the simulated and measured realized gain patterns (G_r) in principal cut-planes for both θ and ϕ polarizations are compared. It can be seen that measurements and simulations are in relatively good agreement. Fig. 4 (a) shows the simulated 3D radiation pattern of the antenna at 2.45 GHz. A maximal G_r of 2.3 dBi is observed. We also point out that the antenna radiates significantly towards both the perpendicular broadside ($+x$) and the “end-fire” ($+z$) – i.e. in the antenna plane – directions, implying that both off-body and on-body communications can be supported. Fig. 4 (b) shows that the simulated total efficiency η_t ($\eta_t = \eta_e(1 - |S_{11}|^2)$ with η_e the radiation efficiency) is between 70 % and 93 % over the whole -10 dB band.

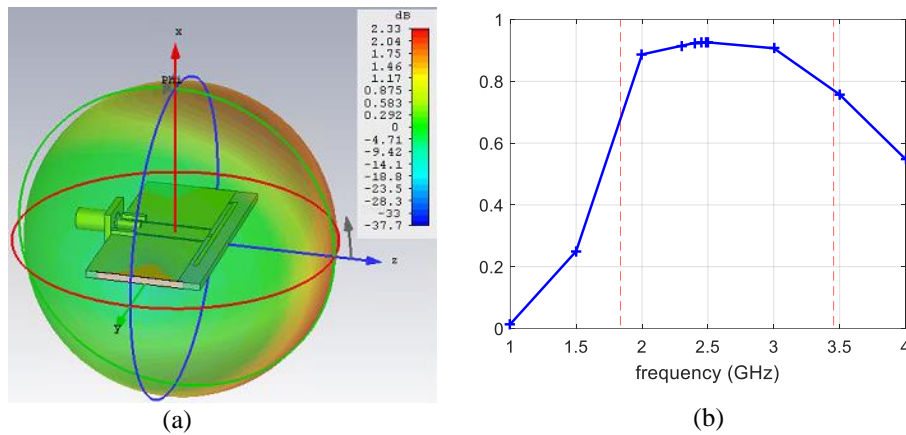


Fig. 4. (a) 3D radiation pattern at 2.45 GHz; (b) total efficiency, of the proposed FR4 based CPW-fed IIFA in free space.

The ultra-wide band is the result of superposition of multi-resonances close to each other. In fact, it can be seen from Fig. 5 that three resonances or anti-resonances (at which $Imag(Z_{in}) = 0$) are located within the -10 dB input BW (at 2.1, 3.05 and 3.36 GHz) and two others are very close (at 1.78 and 3.99 GHz). Conventional IIFA structures present generally only one resonance; in [A-9] an additional close resonance is created thanks to the technique already described, notably by coupling the CPW feedline and the ground plane. A thorough inspection of the current and E-field distributions allows to interpret the obtained multiple resonances as a multi-mode behaviour.

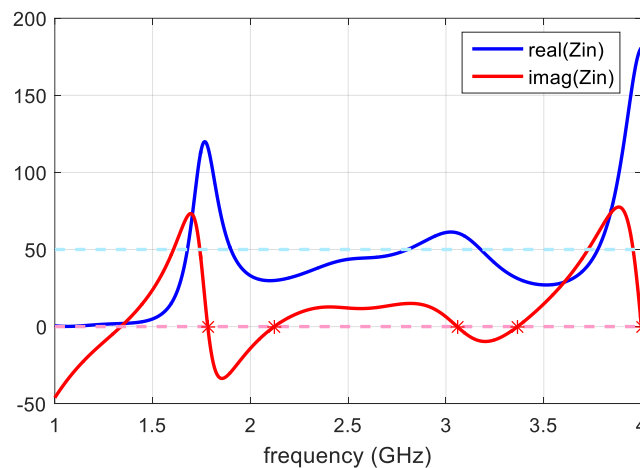


Fig. 5. Impedance (Z_{in}) of the FR4 based CPW-fed IIFA.

Fig. 6 (a) shows the surface current density at the resonance of 3.05 GHz. We can see that there exists a strong coupling between the radiating arms and the CPW ground plane due to the high length of the short-ended arm and the narrow inter-gap. Fig. 6 (b) shows the E-field distribution (for two different phase values) in the vertical cut-plane at the SMA pin point. It can be seen that both the even mode and the odd mode are excited “in parallel” within the feedline. The same phenomenon has also been observed for almost all other resonances, except the one at 2.1 GHz for which only the fundamental even mode is excited. The latter

can be considered as the “fundamental IIFA mode”. In other words, our proposed design seems to behave as a parallel combination of a classical CPW-fed IIFA and an asymmetrical coplanar slot-line-fed IIFA. However, as the antenna is fed symmetrically, contrary to the design proposed in [A-7] or [A-9], no characteristic mode of the ground plane is excited.

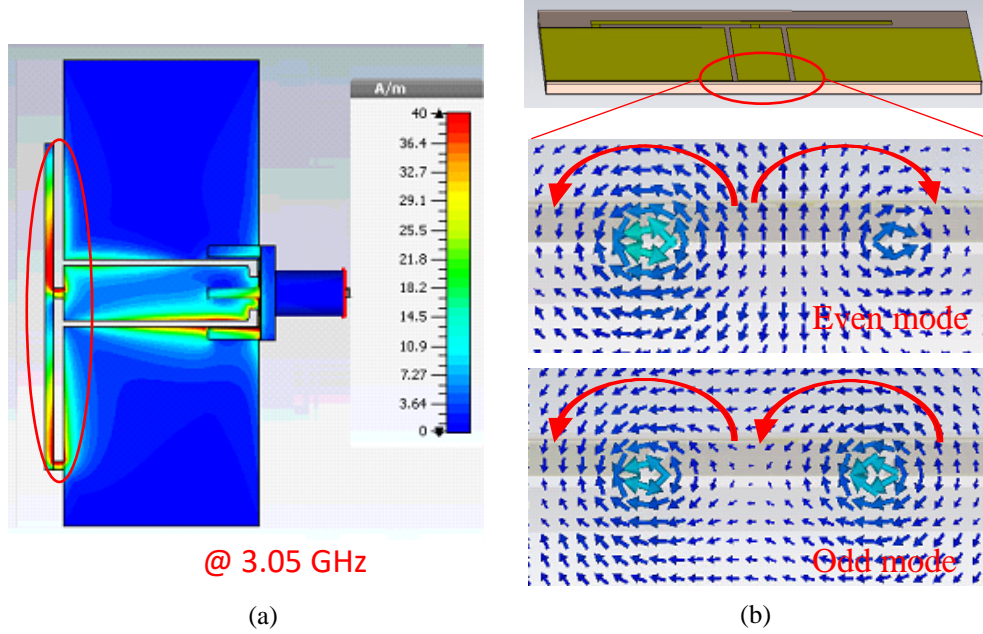


Fig. 6. (a) Surface current density distribution; (b) E-field distribution, in the vertical cut-plane at the SMA pin point for the FR4 based CPW-fed IIFA (at 3.05 GHz).

III. CPW-Fed IIFA on FR4 Substrate

a. Design of the antenna

In the second stage, we applied the same principle for designing an UWB CPW-fed IIFA on denim ($\epsilon_r = 1.7$, $\tan\delta = 0.05$, $h = 0.85$ mm). The dimensions taken are comparable to previous values: $L_s = 50$ mm, $W_s = 25.5$ mm, $W_g = 20.5$ mm, $L_1 = 19.4$ mm, $L_2 = 15.6$ mm, $W_{\text{strip}} = 1.2$ mm, $g = 1.3$ mm, $W = 6$ mm, $s = 0.6$ mm. In particular, we took exactly the same dimensions for the CPW feedline after analysing the trade-off between the impedance matching and the antenna size. Actually, the design of a 50Ω CPW feedline on denim would require a very high ratio of W/s , corresponding to either an excessively large strip or very narrow slots. However, none of them would be favourable for the practical fabrication and integration. Keeping the same dimensions increases the characteristic impedance to about $Z_{\text{cpw}} \sim 67 \Omega$ for the Denim version. Nevertheless, we’ll see next that this value of Z_{cpw} operates an impedance transformation favourable to the overall performance of the proposed antenna.

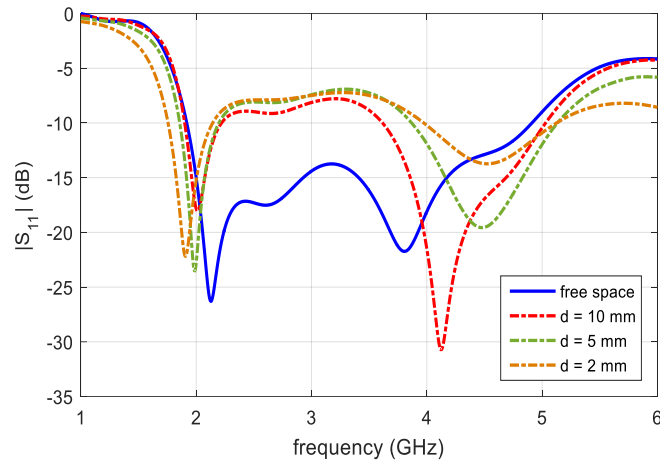


Fig. 7. Simulated reflection coefficient $|S_{11}|$ of the proposed denim based CPW-fed IIFA in free space and on the phantom arm at different distances.

b. Simulation results

In Fig. 7 the blue solid line shows the simulated reflection coefficient $|S_{11}|$ of the denim based IIFA in free space. It can be seen that the -10 dB input bandwidth is 2.99 GHz (1.92 GHz – 4.91 GHz), i.e. a relative BW of 87.6 %, which is very high for such kind of antenna, as far as we know. Fig. 8 (a) shows the simulated 3D radiation pattern at 2.45 GHz. A maximal G_r of 2.24 dBi is obtained. The radiation pattern is comparable to the previous one so that the same comments still hold with regards to on and off body usage. Fig. 8 (b) shows that the simulated total efficiency is between 70 % and 93 % over the whole operating band.

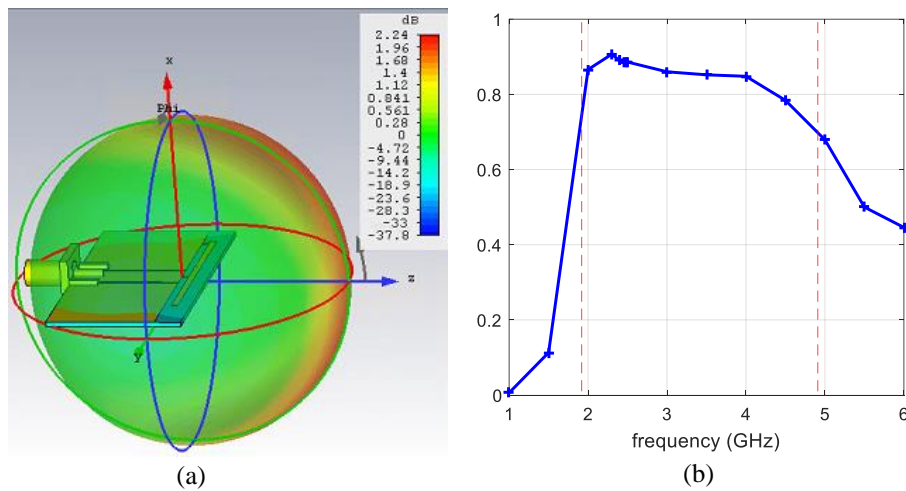


Fig. 8. (a) 3D radiation pattern at 2.45 GHz; (b) total efficiency, of the proposed denim based CPW-fed IIFA in free space.

Fig. 9 illustrates the multi-resonances phenomenon: four resonances are located in the passband (at 2.15, 2.29, 2.855 and 4.39 GHz) and two other ones in the vicinity (at 1.75 and 5.05 GHz), consequently resulting in a widely enhanced bandwidth. Similarly to the FR4 substrate case, analyses on the current and E-field distributions reveal the reason for the induced multi-resonances: a combined effect of, 1) a strong coupling between the radiating

arms and the ground plane, and 2) the excitation of both even mode (for all the 6 resonances) and odd mode (for the resonances at 2.15, 2.29 and 4.39 GHz) within the feedline.

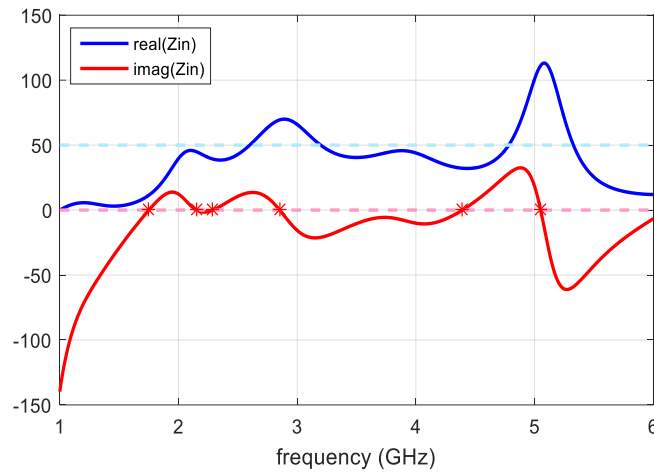


Fig. 9. Impedance (Z_{in}) of the denim based CPW-fed IIFA.

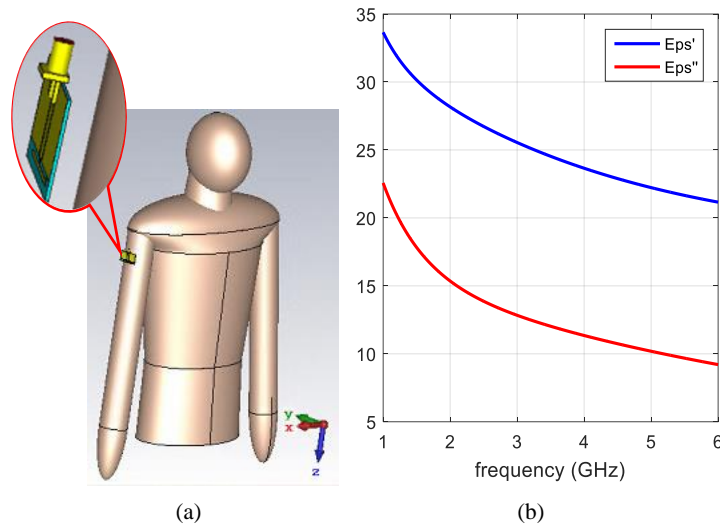


Fig. 10. Homogeneous phantom: (a) “IIFA – phantom” view; (b) dispersion law of the effective medium of the phantom.

c. Test on a body phantom

The proposed denim based IIFA can be easily integrated into clothes for WBAN communications. To verify its *in situ* performance in the presence of human body, we carried out simulation tests with a canonical homogeneous phantom, as shown in Fig. 10 (a). The dispersion law (Fig. 10 (b)) of its effective medium is chosen to follow the measured values of a real body phantom used for experiments at our laboratory [A-11] (it is demonstrated in this article – amid others – that such simplified homogeneous phantom models designed with canonical geometries can be used satisfactorily in place of heterogeneous anthropomorphic phantoms for *external* electromagnetic problems). The antenna was placed on the phantom arm, near the shoulder, at a distance d of 10 mm, 5 mm and 2 mm.

In Fig. 7, the dash lines illustrate the evolution of the reflection coefficient as the distance decreases, which calls for the following comments. First, the low cut-off frequency decreases because the phantom behaves as an “additional substrate layer” for the antenna. Given that the phantom has a much higher effective permittivity than denim, the antenna equivalent electrical size becomes larger. Second, the input impedance is affected by the antenna-body coupling, inducing a degradation of the reflection coefficient $|S_{11}|$ over a part of the band. However, the matching remains acceptable (the $|S_{11}|$ remaining below -6.5 dB for the worst case), avoiding any dramatic radio link outage as pointed out in the introduction. Third, the BW is enlarged because the phantom operates as a dissipative load lowering the antenna quality factor. Meanwhile, the total efficiency of the antenna is decreased to values over the input band between 30 % and 55 %, 18 % and 35 %, 9 % and 17 % respectively for the 10, 5, 2 mm cases. These preliminary tests with a body phantom justify globally the applicability of the proposed CPW-fed IIFA for wearable communications.

Note finally that this antenna can be used for multi-standard/multi-band applications as it covers, when used on the body, the GSM 1800, UMTS, WiFi (2.45 GHz and possibly “5 GHz”), LTE/LTE-A 2100 and 2600, and WiMAX (2.5 GHz, 3.5 GHz and possibly 5.8 GHz) bands.

IV. Conclusion

An extremely simple, compact, and small UWB CPW-fed IIFA design is investigated. A -10 dB bandwidth of more than 61 % and 87 % is achieved for FR4 and denim based realizations respectively. Tests with a phantom show that the body proximity effects are relatively moderate for the denim based IIFA. This antenna design can be suitable for wearable applications, including on-body and off-body communications and/or can support multi-standard applications. At the present time, the optimisation of the in-situ denim based IIFA (in order to improve the input matching and total efficiency) is still ongoing.

Reference

- [A-1] S. Sankaralingam, and B. Gupta, “Development of textile antennas for body wearable applications and investigations on their performance under bent conditions,” *Progress In Electromagnetics Research B*, vol. 22, pp. 53-71, 2010.
- [A-2] Y. F. Wei, and C. Roblin, “Multislot Antenna with a Screening Backplane for UWB WBAN Applications,” *International Journal of Antennas and Propagation*, Hindawi Publishing Corporation, 2012.

- [A-3] S. Zhu, and R. Langley, "Dual-Band Wearable Textile Antenna on an EBG Substrate," *IEEE Transactions on antennas and propagation*, vol. 57, n° 4, pp. 926-934, 2009.
- [A-4] C. T. Islam, M. Faruque, and N. Misran, "Reduction of specific absorption rate (SAR) in the human head with ferrite material and metamaterial," *Prog. Electromagn. Res. C*, vol. 9, n° 4758, 2009.
- [A-5] H. R. Raad, A. I. Abbosh, H. M. Al-Rizzo, and D. G. Rucker, "Flexible and compact AMC based antenna for telemedicine applications," *IEEE Transactions on antennas and propagation*, vol. 61, n° 2, pp. 524-531, 2013.
- [A-6] R. Augustine, T. Alves, T. Sarrebourg, B. Poussot, K. T. Mathew, and J. M. Laheurte, "Polymeric ferrite sheets for SAR reduction of wearable antennas," *Electronics letters*, vol. 46, n° 3, pp. 197-198, 2010.
- [A-7] C. Roblin *et al*, "Antenna design and channel modeling in the BAN context—part I: antennas," *Annals of Telecommunications*, Springer, vol. 66, n° 3-4, pp. 139-155, 2011.
- [A-8] Y. L. Kuo, and K. L. Wong, "Coplanar waveguide-fed folded inverted-F antenna for UMTS application," *Microwave and optical technology letters*, vol. 32, n° 5, pp. 364-366, 2002.
- [A-9] W. El Hajj, C. Person, and J. Wiart, "A novel investigation of a broadband integrated inverted-F antenna design; application for wearable antenna," *IEEE Transactions on Antennas and Propagation*, vol. 62, n° 7, pp. 3843-3846, 2014.
- [A-10] P. Hui, "Design of integrated inverted F antennas made of asymmetrical coplanar striplines," *Appl. Microw. Wireless*, vol. 14, n° 1, pp. 28-37, 2002.
- [A-11] C. Roblin, "A statistical assessment of ambient electromagnetic field using body-worn multi-axial sensors", *Compte Rendus Physique (Académie des Sciences)*, Elsevier publisher., vol. 16, n° 9, pp. 802-818, 2015.

Résumé français

Condensé du manuscrit en français

Analyse et modélisation statistique d'antennes souples ou flexibles dans des conditions fluctuantes

Jinxin DU

Soutenu : le 03/07/2018

Superviseur : Prof. Christophe ROBLIN

Département Communications et Electronique (COMEELEC)

Télécom ParisTech (Institut Mines-Télécom and LTCI), Université Paris-Saclay

46 rue Barrault, Paris CEDEX 13, 75634, France

Introduction

Depuis la publication de la norme de communication mobile de première génération (1G) (Système de Téléphonie Mobile Avancée, développé par Bell Laboratoire), les technologies de communication sans fil ont connu une croissance fulgurante et ont considérablement facilité la vie des gens. Aujourd'hui, les gens sont fortement dépendants de tous les types de services sans fil tels que les réseaux cellulaires (2G/3G/4G), les systèmes mondiaux de navigation par satellite, les réseaux locaux sans fil, et les réseaux corporels sans fil (par exemple, Wi-Fi, Bluetooth, ZigBee). Le rythme de la révolution n'a jamais cessé et est encore plus rapide que jamais. Nous sommes maintenant presque prêts à accueillir la technologie 5G grâce à laquelle non seulement des personnes mais aussi de nombreuses "choses" (par exemple des machines, des véhicules, des capteurs ...) seront connectées, formant un immense « Internet of Things (IoT) ». L'IoT est censé contribuer à un monde "intelligent" (par exemple, réseau intelligent, transport intelligent, soins de santé en temps réel, maison/ bureau/usine intelligentes, etc.) et améliorer la qualité de vie des personnes considérablement. Avec l'expansion généralisée des technologies sans fil, le besoin d'appareils électroniques sans fil connaîtra certainement une croissance explosive dans les années à venir.

Étant l'interface unique pour communiquer avec l'extérieur, l'antenne est un composant essentiel pour tous les appareils électroniques sans fil. Les succès dans l'industrie des communications sans fil n'auraient pas été atteints sans les progrès continus de la technologie des antennes. Ces dernières années, les antennes ont tendance à être hautement intégrées, miniaturisées et organisées pour répondre à la demande de déploiement massif, de cycle de R & D court, de faible coût et de haute performance. De plus, d'autres propriétés avantageuses sont également indispensables dans des scénarios d'application spécifiques. En particulier, dans le contexte des réseaux corporels sans fil où les antennes devraient être intégrées dans des vêtements ou collées directement sur le corps humain, la souplesse ou la flexibilité leur permettant de se conformer à diverses formes et tailles de corps serait vraiment utile.

Cependant, la souplesse ou la flexibilité implique une déformation géométrique (par exemple, flexion, torsion, froissement ...) qui peut perturber de façon drastique le comportement (par exemple, diagramme de rayonnement, impédance ...) des antennes. Les antennes perturbées ne sont plus fixes ou statiques, mais variables ou dynamiques car leur comportement varie de manière aléatoire au cours de l'opération. Outre les auto-déformations, le caractère aléatoire externe de l'environnement proche (éventuellement fluctuant) peut également perturber les antennes. Par exemple, la variation de la température et de l'humidité peut entraîner des modifications des propriétés du matériau des antennes, telles que la permittivité et la conductivité ; les environs proches, notamment le corps humain, pourraient

perturber la zone de proximité des antennes, entraînant une forte absorption, réflexion, diffusion ou l'effet conjoint de celles-ci. Cet effet devient remarquable lorsque les antennes deviennent miniaturisées.

De nos jours, avec l'utilisation répandue de l'électronique flexible (comme l'électronique textile) et la complexité croissante des environnements d'exploitation, la présence de aléas et d'incertitudes sur les antennes est plus réaliste que jamais dans presque tous les contextes d'application. Cela pose de sérieux problèmes dans la conception des antennes et dans l'analyse des liaisons radio. Comment caractériser la performance des antennes devient une préoccupation incontournable et attire de plus en plus l'attention. De plus, afin de garantir la fonctionnalité des antennes, la solution traditionnelle consiste à ajouter une marge de gain *ad hoc* pour rendre compte en gros des effets aléatoires pouvant être rencontrés dans le monde réel. Cependant, cela induit généralement un coût élevé et un gaspillage d'espace et/ou de ressources énergétiques précieux. Pour éviter des valeurs de marge excessives, il est indispensable de caractériser quantitativement et précisément le comportement *in situ* des antennes perturbées et d'attirer de plus en plus l'attention des ingénieurs des antennes.

Traditionnellement, la caractérisation d'une antenne déterministe classique (par exemple, antennes rigides ou de grande taille, ou clairement isolées, etc.) peut être réalisée au moyen de mesures ou de simulations. Cependant, cette approche devient inappropriée pour les problèmes d'antenne dans des conditions incertaines où un grand nombre de sources aléatoires interviennent. En effet, la combinatoire des situations peut être si explosive que l'exécution de mesures ou de simulations une par une serait trop longue et même physiquement impossible pour nous en ce moment. Dans telles circonstances, des approches de caractérisation plus efficaces seront requises de toute urgence.

Cette thèse vise à étudier des méthodologies efficaces pour analyser et modéliser quantitativement les effets aléatoires sur le comportement "global" des antennes souples ou flexibles dans des conditions fluctuantes. Ici le terme "global" signifie que le champ lointain rayonné (Far-Field en Anglais, FF) ainsi que le coefficient de réflexion des antennes considérées seront étudiés. Notamment, des méthodologies statistiques qui fournissent de la bonne précision tout en minimisant les coûts de modélisation sont présentées.

Le principe est d'essayer de ne réaliser qu'un nombre très limité de pré-évaluations (par mesure ou simulation) et d'en tirer pleinement parti pour extraire des modèles de substitution efficaces (aussi appelé Métamodèles) qui ensuite permettent de prédire le comportement des antennes considérées dans d'autres situations éventuelles. Les perspectives applicatives de tels metamodèles consistent à substituer des antennes réelles ou des simulations encombrantes lourdes dans différents types d'analyses de niveaux supérieurs, notamment lorsque la connaissance complète (y compris la polarisation, l'amplitude et la phase du champ) de l'antenne étudiée est obligatoire. Tels contextes d'application comprennent, par exemple, la

modélisation conjointe antenne/canal, puis celle du lien radio, l'intégration des antennes dans les simulateurs asymptotiques (lancé ou tracé de rayons), la caractérisation des systèmes Multi-Entrée & Multi-Sortie, ou la formation de faisceaux (illustré par Figure 10).

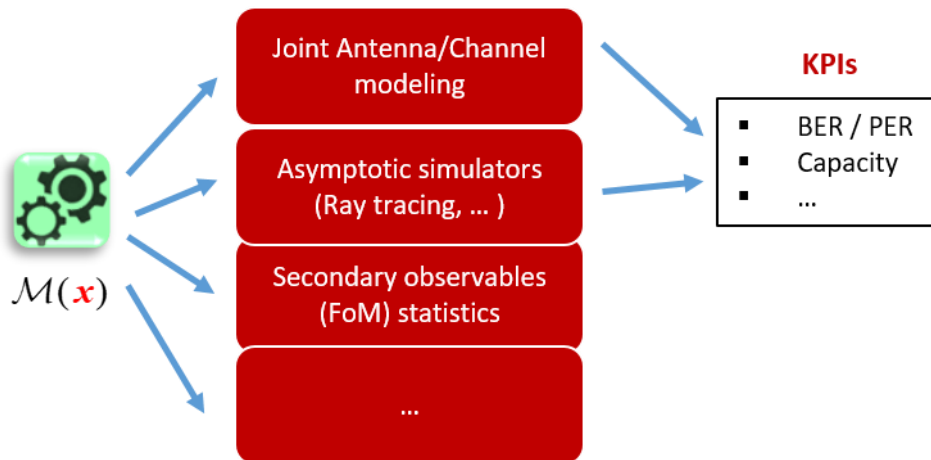


Figure 10: Modèles de substitution (Métamodèles) d'antenne pour l'analyse de niveau supérieur.

Organisation de la thèse

L'organisation de cette thèse est la suivante :

Le *Chapitre 2* présente l'état de l'art des antennes souples ou rigides. Dans la première partie, les technologies de conception, les avantages et les grandes perspectives d'application, ainsi que les problèmes liés aux antennes souples ou rigides, sont brièvement présentés. Dans la seconde partie, l'état de la technique de la modélisation des antennes est passé en revue et les objectifs que nous souhaitons atteindre dans cette thèse sont décrits.

Le *Chapitre 3* propose des méthodologies pour modéliser les FF ou ATF (Antenna Transfer Function) rayonnés par l'antenne. En premier lieu, la technique de parcimonie du champ basée sur l'expansion des harmoniques sphériques vectoriels (Vector Spherical Harmonics, VSH, en Anglais) est introduite. Ensuite, des méthodologies de modélisation déterministes ainsi que stochastiques sont proposées. Toutes les méthodologies ont un processus en deux étapes, c'est-à-dire la parcimonie suivie de l'extraction du métamodèle. La méthodologie déterministe est la combinaison de l'expansion VSH et de l'étude paramétrique conventionnelle ; en revanche, la méthodologie statistique est la combinaison de l'expansion VSH et de la méthode avancée d'expansion du chaos polynomial (Polynomial Chaos Expansion, PCE, en Anglais).

Le *Chapitre 4* étudie l'utilité des métamodèles d'antenne pour l'analyse des liaisons radio, où les performances effectives de l'antenne sont quantifiées en tenant compte des incertitudes inhérentes à l'antenne elle-même et à celles des environnements de propagation locaux stochastiques.

Le *Chapitre 5* présente une méthodologie statistique pour la modélisation du coefficient de réflexion complexe des antennes à bande étroite. Cette approche est divisée en deux étapes : identification et extraction du métamodèle en utilisant la méthode PCE.

Le *Chapitre 6* résume le travail réalisé au cours de cette thèse et présente quelques perspectives pour de futures recherches.

Chapitre 2 : Etat de l'art

Ce chapitre présente le contexte de recherche de cette thèse. Premièrement, la technologie des antennes souples ou flexibles et leurs larges perspectives d'application sont brièvement présentées. Les problèmes liés aux caractéristiques stochastiques des antennes flexibles/souples sont également expliqués. Ensuite, la demande croissante de méthodes de modélisation efficaces est discutée. Enfin, l'état de la technique de la modélisation des antennes est passé en revue et les objectifs que nous souhaitons atteindre dans cette thèse sont décrits.

L'état de l'art est présenté en deux parties, l'une relative aux antennes flexibles et l'autre relative au traitement des fluctuations des paramètres d'entrée concourant à l'analyse des performances de telles antennes. La description d'antennes flexibles et de leurs caractéristiques (matériaux diélectriques et conducteurs) ainsi que leur utilisation dans un contexte des réseaux corporels (par exemple, Figure 11) permet de réaliser rapidement et concrètement où on souhaite en venir.

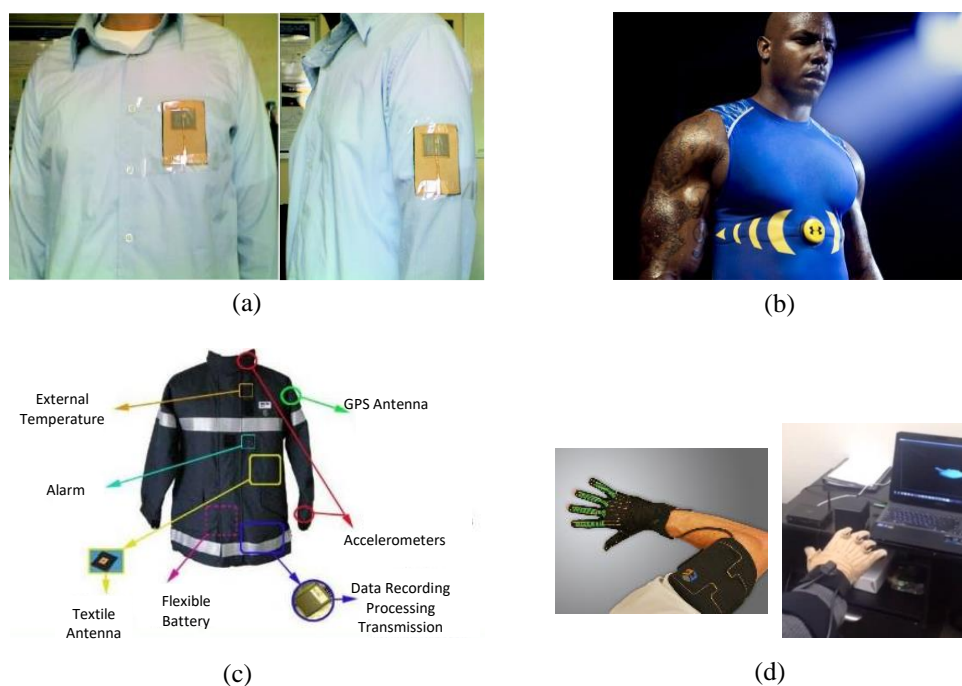


Figure 11: Antennes portables : (a) surveillance de la santé ; b) T-shirt intelligent pour les athlètes ; c) vêtements intelligents pour les pompiers ; d) des gants intelligents pour le contrôle à distance.

En effet, les avantages liés à ces antennes (légèreté, flexibilité, procédures de fabrication, ...) sont associés à leur contrepartie : des aléas relatifs aux propriétés des matériaux inhomogènes employés, aux modifications géométriques, aux tolérances de fabrication, et enfin à la proximité du corps humain. Ces antennes sont donc significativement variables dans leur comportement pour justifier le caractère quasi-obligatoire d'une analyse stochastique.

Dans la seconde partie de ce chapitre, on évoque les méthodes habituelles de mise au point d'antennes par la simulation numérique. Cette dernière permet de réaliser une analyse paramétrique en vue de rechercher la configuration optimale au sens de certains facteurs de mérite (efficacité, bande passante, coefficient de réflexion, ...). Cependant, dans le contexte évoqué plus haut la combinaison de (trop) nombreux paramètres fluctuants rendent l'analyse paramétrique inaccessible. Le recours aux méthodes statistiques s'impose. Les différentes méthodes statistiques possibles ont été énumérés en partant de l'approche classique de Monte-Carlo. Les méthodes successivement évoquées sont ANOVA, analyse petits signaux et développement en série de Taylor associé, « Support vector machine », processus gaussiens (Kriging), réseaux de neurones et collocation stochastique notamment basée sur le chaos polynomial généralisé.

Des références sont données ayant pour application le domaine des antennes. Quelques arguments sont utilisés en vue de privilégier l'approche du chaos polynomial. Il est toujours difficile de comparer ces méthodes entre elles, aucune d'entre elles ne pouvant prétendre à être universelle. L'approche du chaos polynomial possède aussi ses limites.

Chapitre 3 : Méthodologies de modélisation de l'ATF d'antennes variables

Ce chapitre volumineux comporte les principales contributions scientifiques de la thèse et décrit en particulier l'approche méthodologique innovante pour traiter de la question soulevée au chapitre précédent.

Le problème posé consiste à déterminer une estimation de la fonction de transfert d'une antenne qui dépend non seulement de la fréquence et des coordonnées du point d'observation mais d'un vecteur constitué d'un nombre plus ou moins important de variables aléatoires. Cependant, le champ électromagnétique (en se plaçant dans un système de coordonnées sphériques) s'écrit sous la forme d'une expansion de fonctions vectorielles de type harmoniques sphériques. Sa description est alors compacte ou parcimonieuse au moyen d'un nombre limité de coefficients complexes de pondération de cette base de fonctions (Figure

12). L'idée formulée consiste alors à extraire cette représentation parcimonieuse à partir de la simulation électromagnétique effectuée pour une réalisation particulière des variables aléatoires.

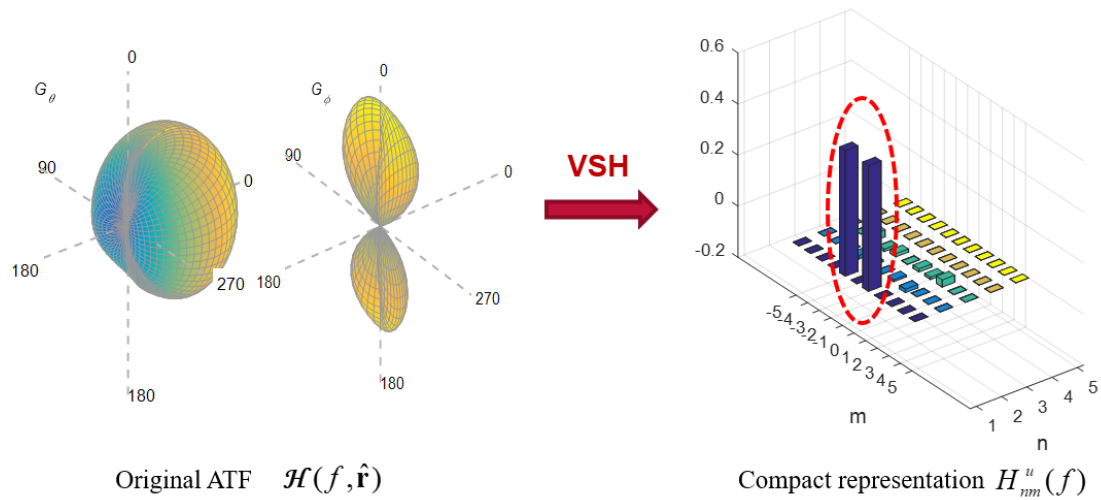


Figure 12: Principe de l'expansion VSH.

Dans un second temps, les coefficients d'harmoniques sphériques sont eux-mêmes projetés sur une base de polynômes des variables aléatoire d'entrée. Ce sont donc ces coefficients de pondération d'harmoniques sphériques qui porteront l'information sur la propagation d'incertitude (Figure 13).

C'est ici l'idée phare de cette thèse dont la pertinence sera évaluée tout au long de ce chapitre. Ce principe de modélisation en deux étapes est illustré par Figure 14.

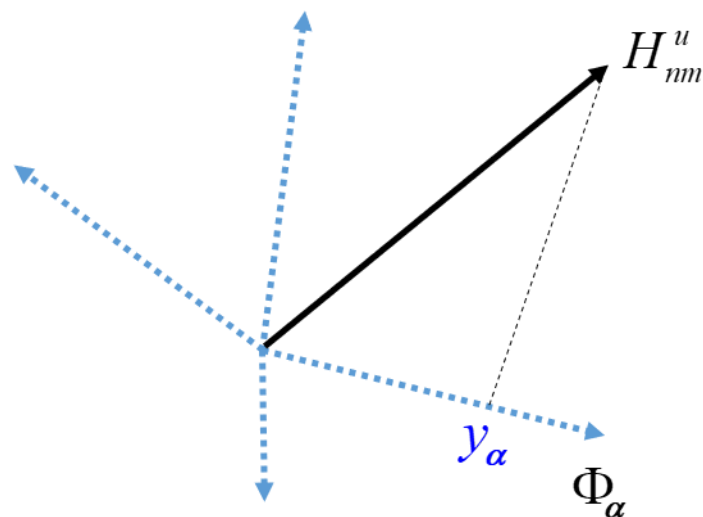


Figure 13: Projection des VSH modes sur des bases chaos polynomial.

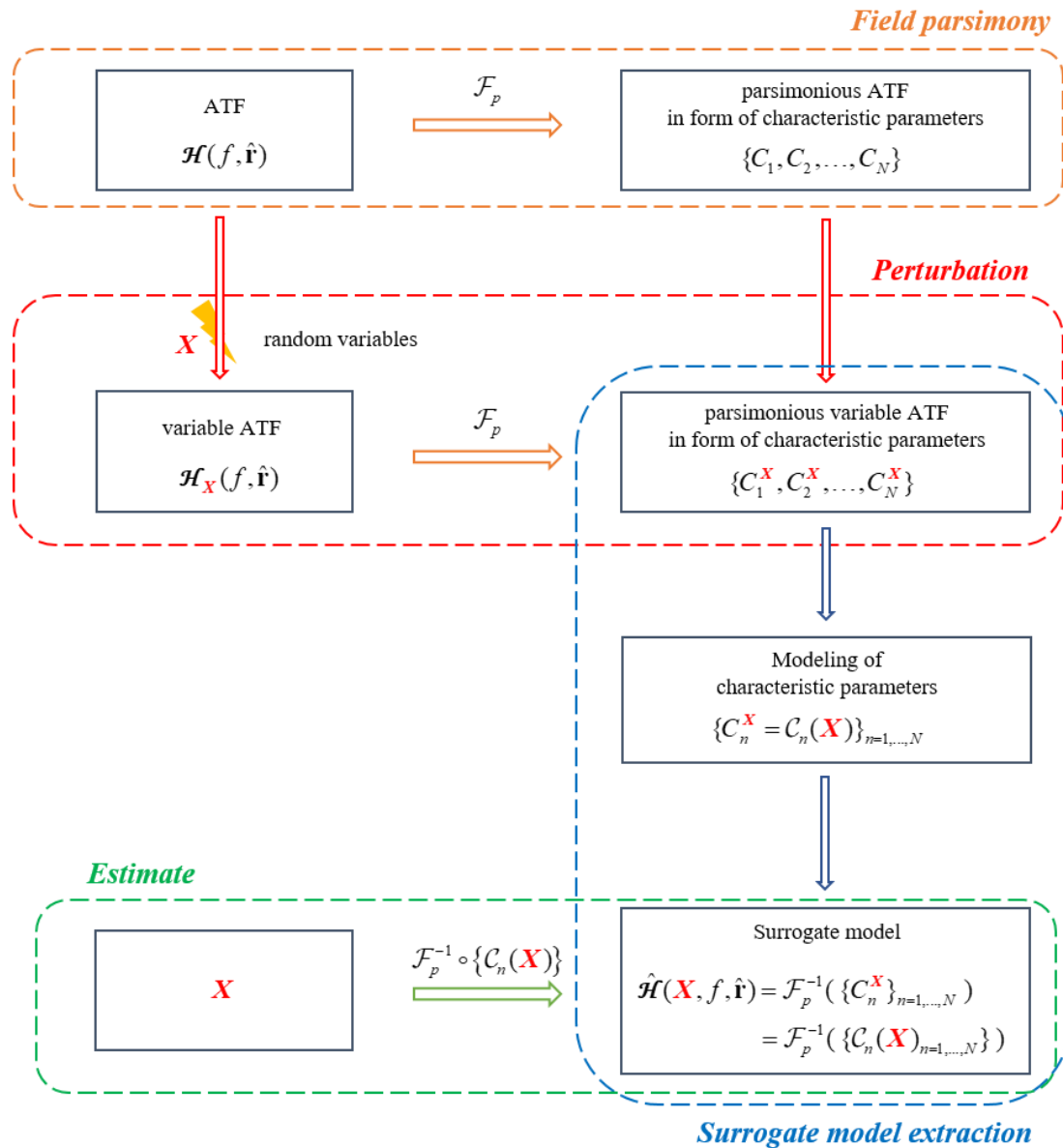


Figure 14: Construction des métamodèles en deux étapes.

On distingue ensuite deux méthodes permettant de parvenir à cette représentation polynomiale des variables aléatoires d'entrée. Si le nombre de variables aléatoires est faible, une étude paramétrique menée sur chacune de ces variables permet d'adapter les coefficients et l'ordre d'un polynôme pour chacune de ces variables de manière déterministe. Lorsque la réponse d'intérêt est fonction d'un plus grand nombre de variables aléatoires, cette méthode n'est plus réaliste et c'est alors une représentation sous la forme d'une base de polynômes du chaos qui est proposée.

On expose dans le détail l'approche statistique qui forme le cœur de cette thèse. L'historique du chaos polynomial ainsi que son principe est tout d'abord rappelé. Il s'agit de décomposer la réponse d'intérêt sous la forme d'une somme pondérée de coefficients de projection sur une base de polynômes orthonormés des variables d'entrée. Cette base est

orthogonale au sens d'un produit scalaire impliquant la loi de distribution des paramètres d'entrée. Ainsi, selon la nature de la distribution des variables aléatoires concernées, la famille de polynômes peut être choisie de manière optimale (exemple : polynômes de l'Hermite pour des processus gaussiens) selon le schéma d'Askey. On rappelle également qu'en cas de corrélations entre les variables aléatoires dont les distributions diffèrent, des transformations en des variables aléatoires équivalentes de distribution identiques peuvent être réalisées, ce qui rend l'application de la méthode très générale. Le calcul des coefficients peut être réalisé de différentes manières. Le processus retenu pour cette thèse est non intrusif et basé une approche de régression. Cette technique, appliquée sous sa forme classique est cependant limitée à l'analyse de quelques variables aléatoires. En effet, malgré la troncature opérée sur l'ordre des polynômes (troncature hyperbolique qui limite l'ordre total à un degré maximal P), le nombre de coefficients à estimer devient prodigieusement élevé et la méthode inexploitable car moins efficace qu'une simulation directe de type Monte Carlo. Pour contourner ce problème, différents auteurs ont proposé des solutions afin de sélectionner de manière itérative un nombre très limité de polynômes après troncature en privilégiant des degrés de polynômes peu élevés. C'est en particulier ce que permet la méthode LARS ou ses évolutions Hybrid-LARS, adaptative Hybrid LARS. C'est cette dernière option qui sera utilisée par la suite dans cette thèse. Elle aboutit à la sélection du meilleur ensemble de polynômes au sens du « leave-one-out error (LOOE) ».

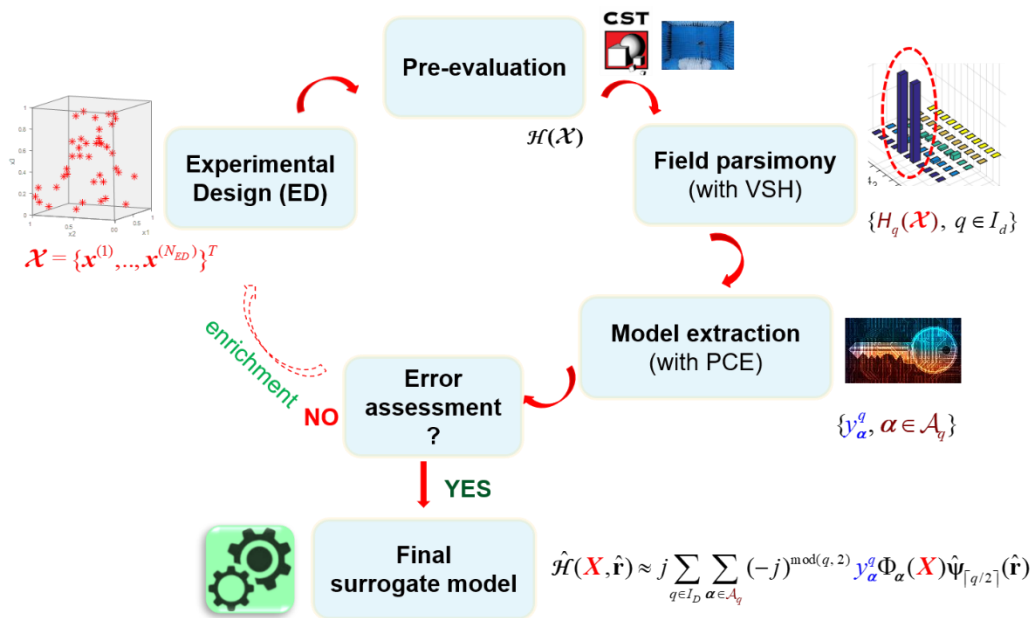


Figure 15: Approche itérative pour la construction des métamodèles.

On a proposé une approche itérative (Figure 15) pour extraire du métamodèle en minimisant au maximum le coût computationnel. Le métamodèle est ajusté au moyen d'un plan d'expérience dont l'objectif est d'obtenir une évaluation du modèle initial en certains

points. Ce plan d'expérience peut lui-même être enrichi après une première estimation du métamodèle.

Les performances des méthodes déterministes et stochastiques sont illustrées par un exemple canonique d'un dipôle à géométrie variable (Figure 16). En particulier, la méthode stochastique est évaluée pour 3 variables aléatoires. Après enrichissement du plan d'expérience à $N_{ED} = 260$ réalisations selon un tirage de type LHS (Latin Hypercube Sampling), l'ensemble des 30 métamodèles associés aux 30 modes (degré des harmoniques sphériques limité à $N_{VSH} = 3$) est alors estimé. Le métamodèle complet comporte environ 2000 coefficients polynomiaux pour une erreur de type LOOE de 4%.

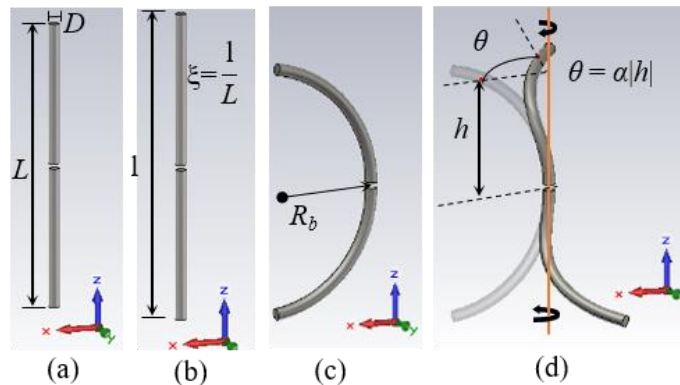


Figure 16: Illustration d'un dipôle subissant différentes déformations : (a) dipôle d'origine ; (b) dipôle étiré ; (c) dipôle courbé ; (d) dipôle courbé et torsadé.

A la suite de ce premier résultat, bien que positif, on ait cherché des améliorations potentielles. Plusieurs axes sont proposés et peuvent être employés simultanément. La fréquence peut être incorporée comme variable aléatoire si la réponse d'intérêt est suffisamment régulière vis-à-vis de ce paramètre. Une description plus parcimonieuse des modes sphériques peut être également adoptée, en ne retenant que les modes dominants (contribution significative à la puissance totale rayonnée). Plus encore, certains de ces modes dominants sont corrélés au sens de la corrélation de leur pondération. Dès lors l'examen préalable de la matrice de corrélation, permet de regrouper certains modes et donc de diminuer le nombre de métamodèles élémentaires.

La méthode stochastique initiale ainsi enrichie est appliquée au cas d'une antenne patch sur textile dans la bande 2.4 à 2.5 GHz pour un problème à 6 variables aléatoires uniformes (courbure, repliement, épaisseur du substrat, permittivité, fréquence), Figure 17. Il faut préciser qu'il s'agit ici d'une approximation de la réalité puisque, notamment, ces variables sont supposées indépendantes les unes des autres. On suit une discussion concernant cette hypothèse ainsi qu'une analyse numérique permettant de conforter cette hypothèse d'indépendance. C'est évidemment une étape très délicate du processus et on comprend ici qu'il n'est pas aisé de détecter et quantifier d'éventuelles corrélations.

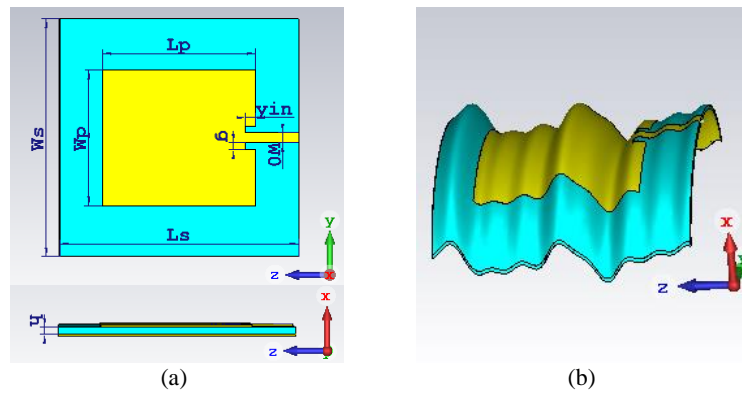


Figure 17: Antenne patch textile portable : (a) patch plan non déformé ; (b) patch subissant l'effet conjoint du froissement, de la flexion et de la variation d'épaisseur.

Une analyse préliminaire conduit à ne plus considérer la hauteur comme variable aléatoire. Finalement, le métamodèle est ajusté pour 5 variables aléatoires. Le modèle final, résultat d'un bon compromis précision/complexité comporte 3217 coefficients scalaires, et est ensuite comparé à 2000 réalisations. L'erreur moyenne et maximale en terme du gain réalisé sont 0,53 et 2,2 dB (Figure 18 - 19). Le temps consommé par notre métamodèle est considérablement plus faible que celui quand on utilise simulation classique (150s vs 15 mins).

Les résultats reportés dans ce manuscrit confortent totalement la méthodologie en deux étapes (représentation parcimonieuse du rayonnement électromagnétique et chaos polynomial) qui permet d'aboutir à une représentation particulièrement compacte de la fonction de transfert de l'antenne. Les limites de la méthode sont également judicieusement mentionnées. La question de la connaissance a priori de la loi support est effectivement centrale et constitue à elle seule une voie de recherche future.

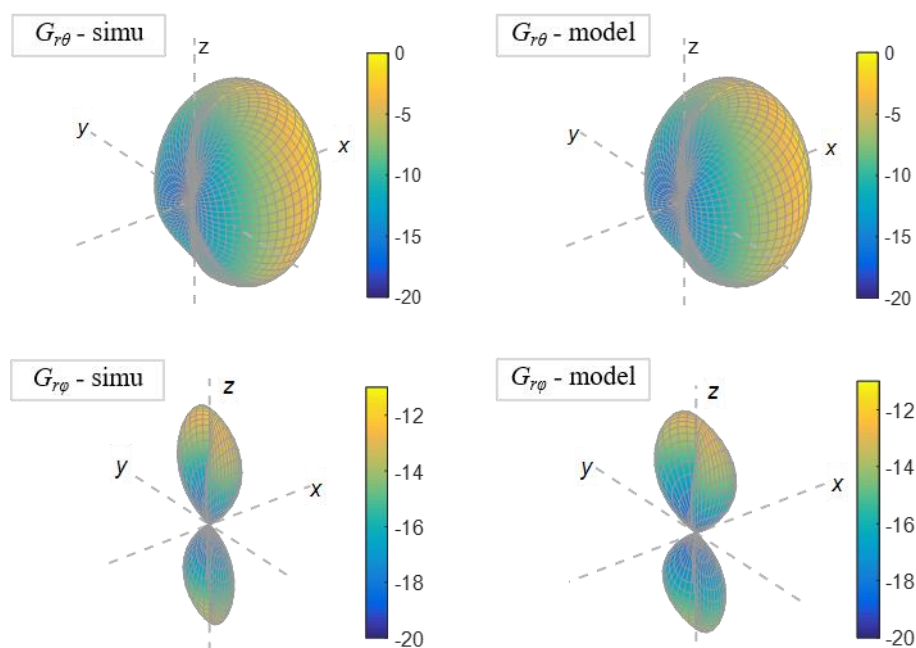


Figure 18: Gr simulés par EM (colonne de gauche) et générés par modèle (colonne de droite) pour une configuration d'erreur moyenne représentative.

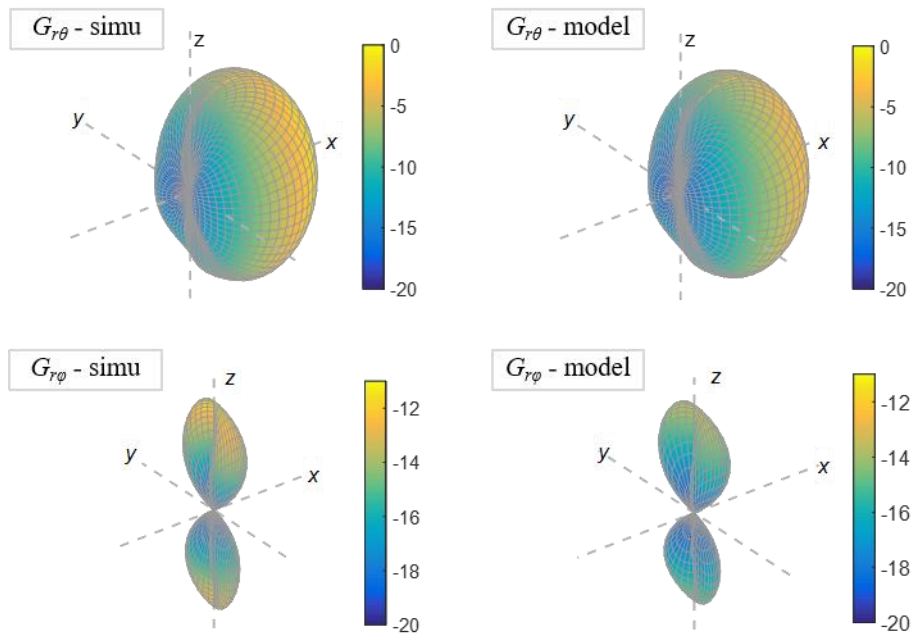


Figure 19: Gr simulés par EM (colonne de gauche) et générés par modèle (colonne de droite) pour une configuration d'erreur maximale représentative.

Chapitre 4 : Métamodèles pour des analyses des liaisons radio

Dans ce chapitre, On rend compte d'une application originale du métamodèle développé au cours de cette thèse. Il s'agit d'évaluer le bilan de réception radio englobant la statistique du canal de propagation et son interaction avec le diagramme de rayonnement de l'antenne, Figure 20.

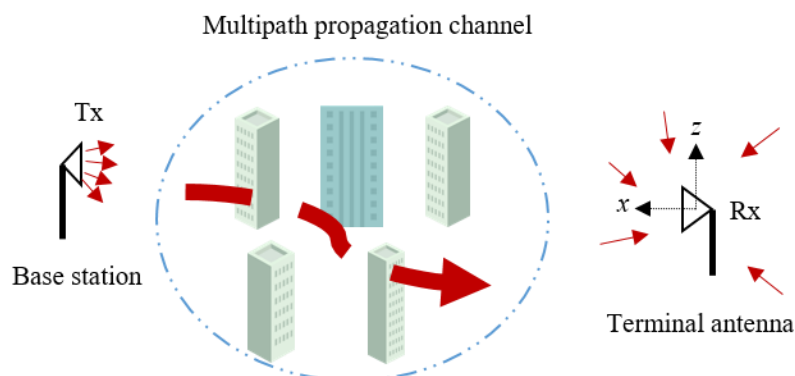


Figure 20: Illustration de la liaison radio d'un système de communication sans fil.

Ce bilan de réception s'évalue classiquement selon le critère de gain effectif moyen. Ce gain est défini par la puissance reçue par l'antenne de réception sous test rapportée à la

somme des puissances qui auraient été collectées par deux antennes isotropes en polarisation horizontale et verticale. Cette grandeur intègre le gain de l'antenne physique mais également le canal de propagation décrit sous sa forme statistique éventuellement standardisée. Le modèle de canal exploité est de type multi-trajets avec station de base en polarisation verticale Winner 2/+.

Dans le contexte des antennes flexibles, significativement variables, l'introduction du comportement aléatoire des antennes semble justifiée. Afin de le démontrer dans le cas précis de l'antenne textile étudiée au chapitre précédent, on combine le métamodèle de cette antenne avec le calcul du gain effectif moyen. Concrètement, 1000 réalisations d'antennes sont produites à partir du métamodèle. Chacune de ces antennes est alors combinée avec 100 réalisations de canal différentes.

La statistique du gain effectif moyen peut alors être établie pour chaque réalisation d'antenne. Les résultats produits montrent qu'il existe une forte dispersion d'une réalisation d'antenne à l'autre par rapport à une antenne non déformée, comme montré par Figure 21. Ceci s'explique par la nature même de l'environnement traité. L'analyse est ensuite raffinée par sous-bandes de fréquence ou en restreignant le secteur angulaire azimutal des angles d'arrivée. Les dispersions observées initialement sont alors réduites.

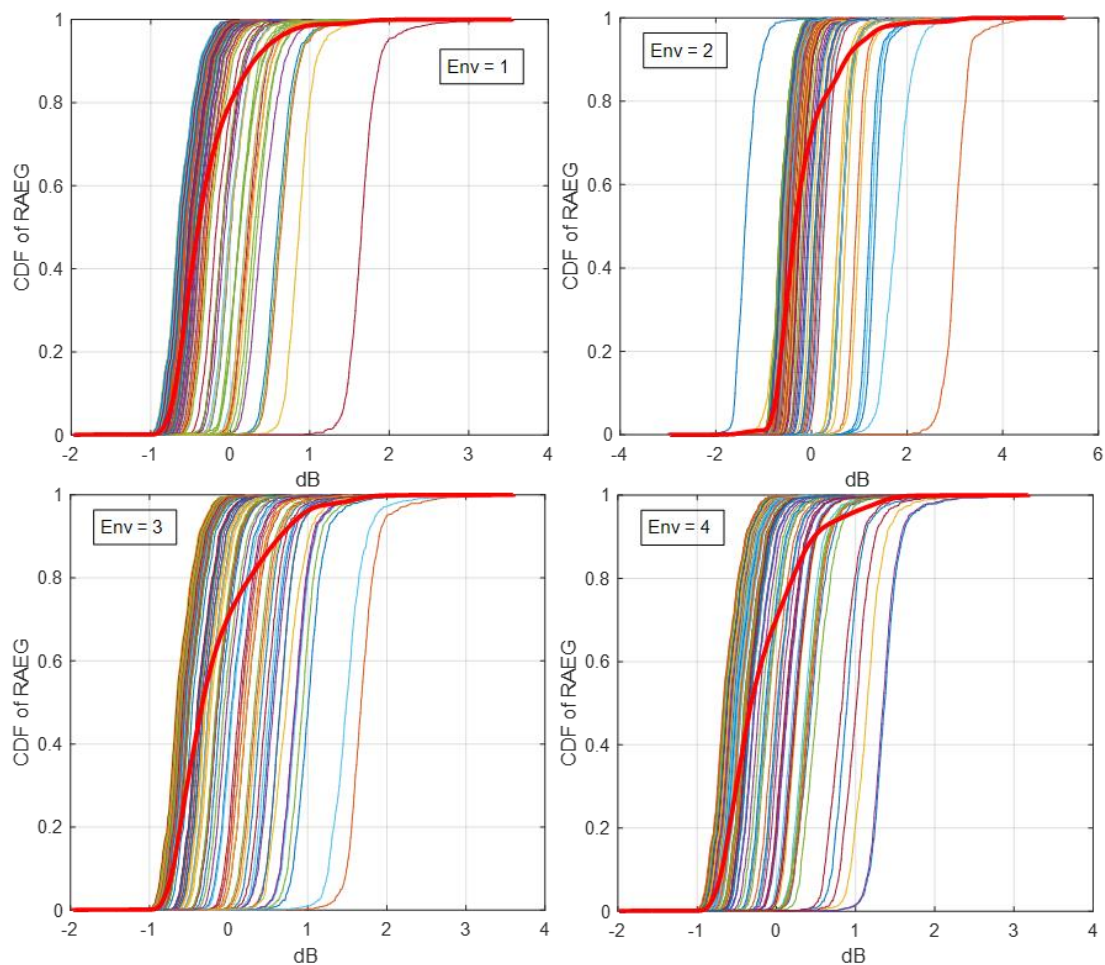


Figure 21: CDF du gain effectif moyen relatif de l'antenne textile patch dans différents environnements de propagation : lignes fines en couleur - CDF partielles ; ligne épaisse rouge - CDF global.

Pour conclure sur ce chapitre, la démonstration de l'utilité d'un tel modèle est claire et justifiée au regard des dispersions enregistrées lorsque le modèle de la liaison radio intègre la variabilité des antennes. Cette approche de modélisation conjointe antenne/canal peut être encore affinée pour pouvoir, par exemple, traiter le signal reçu. En particulier, si la phase est prise en compte, il est possible d'effectuer des simulations au niveau de certains systèmes, par ex. la couche physique de manière à tester différents schémas de modulation et à évaluer des indicateurs de performance du système tels que le taux d'erreur sur les bits. Ce type d'approche, plus élaboré et plus fin, qui mettrait en évidence l'intérêt de développer des modèles de substitution du champ rayonné complet (vecteur et phasé), reste un développement futur.

Chapitre 5 : Modélisation statistique du coefficient de réflexion des antennes variables

Dans ce dernier chapitre, on traite de l'estimation du coefficient de réflexion d'une antenne variable. Tout d'abord, on signale que ce type de problème a déjà été traité par différentes méthodes (réseaux de neurones, processus gaussiens, Support Vector Machine et également par le chaos polynomial) en intégrant la fréquence comme variable aléatoire. A cette occasion, on énonce que ces méthodes sont en capacité de reproduire la réponse d'intérêt lorsque celle-ci possède un comportement non-linéaire (forte sensibilité de la réponse aux variations des paramètres aléatoires) mais au prix d'une certaine complexité.

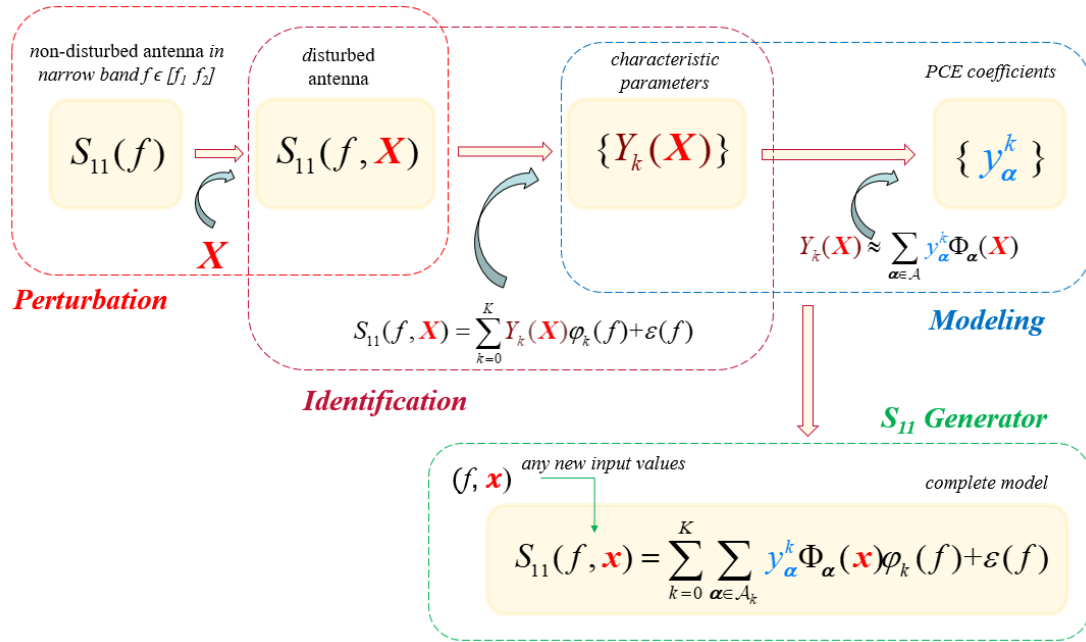


Figure 22: Modélisation du coefficient de réflexion en deux étapes.

On décide, compte tenu des difficultés, de ne pas considérer la fréquence comme variable aléatoire et de procéder de manière similaire à la description de la fonction de rayonnement d'antenne, en représentant dans le modèle la fréquence par une courbe de régression de type polynomiale ou rationnelle. Chacun des coefficients de régression fait alors l'objet d'une expansion de type chaos polynomial. Ce principe de modélisation en deux étapes est montré par Figure 22.

Deux approches sont appliquées pour l'antenne canonique et l'antenne textile. Il n'est pas possible de statuer sur l'avantage de l'une ou de l'autre mais les performances sont correctes au sens du seuil d'erreur toléré initialement. Il semble toutefois que pour l'antenne textile, il soit difficile de converger avec un modèle compact (notamment avec la seconde approche de Levy), les performances paraissent alors difficiles à garantir de manière systématique.

En bref, la première approche fonctionne bien tant pour le patch dipôle que pour le patch textile, tandis que la deuxième fonctionne bien pour le dipôle mais n'est pas totalement satisfaisante pour le patch. Les avantages de l'approche I sont sa robustesse et sa simplicité, mais ce n'est pas nécessairement l'approche la plus efficace en termes de parcimonie et de coût de calcul. De plus, la causalité, c'est-à-dire les relations de Bayard-Bode ou de Kramers-Kronig, n'est pas garantie. L'Approche II permet de mieux comprendre les modes de résonance inhérents aux antennes – grâce aux zéros/pôles dérivés des fonctions rationnelles, ce qui constitue un moyen naturel et efficace de caractériser un système invariant linéaire (LTI), notamment pour les dispositifs résonnants au NB comme dans nos exemples. En général, la méthodologie de modélisation en deux étapes a été justifiée par les deux exemples d'application.

Chapitre 6 : Conclusions et perspectives

Conclusions

En conclusion, cette thèse a été consacrée à l'exploration de méthodologies efficaces pour la modélisation quantitative des effets aléatoires sur les antennes souples ou flexibles dans des conditions fluctuantes. Les travaux couvrent principalement trois parties : la modélisation parcimonieuse du champ lointain (FF) rayonné par l'antenne considérée ; modélisation déterministe et statistique de ces effets aléatoires sur le FF de l'antenne ; modélisation statistique de ces effets aléatoires sur le coefficient de réflexion de l'antenne.

En partant de l'état de l'art, nous avons examiné le développement d'antennes souples ou souples et leurs applications prometteuses dans le contexte de l'IoT et des WBAN. Les antennes souples ou flexibles présentent des avantages notables tels que la flexibilité, le faible encombrement, le faible coût, etc., par rapport aux antennes rigides traditionnelles, mais elles souffrent généralement de perturbations graves dues à d'énormes incertitudes aléatoires intrinsèques et/ou externes. Ce contexte complexe d'aléa conduit à la conscience générale de l'urgence de caractériser quantitativement leurs effets sur les antennes variables. La plupart des travaux existants ont porté sur la modélisation de certaines caractéristiques qui ne sont qu'une description partielle du comportement de l'antenne. Cependant, à notre connaissance, peu d'efforts ont été faits pour modéliser le champ rayonné complet de l'antenne. Un premier essai a récemment été présenté dans les travaux de M. Rossi où la modélisation de champ a été réalisée dans un contexte assez différent (dans le champ proche au lieu de FF). Cependant, cette méthode n'est pas nécessairement toujours efficace pour certaines conditions complexes. Ce fait nous pousse à explorer des méthodologies plus appropriées pour modéliser quantitativement et efficacement le comportement global des antennes variables.

En ce qui concerne la parcimonie du FF, nous avons examiné les principes de deux méthodes de transformation scalaire, à savoir le DFS et le SSH, et une méthode de transformation vectorielle, à savoir le VSH. Nous avons comparé leurs performances pour représenter les fonctions sphériques scalaires et vectorielles et sommes finalement convaincus que pour représenter avec précision et parcimonie des fonctions sphériques vectorielles telles que le FF ou son équivalent, l'ATF, il est préférable de recourir au VSH méthode.

Ensuite, la relation entre les variables aléatoires (représentant ces incertitudes aléatoires) et l'ATF parcimonieuse a été explicitement étudiée. Une approche déterministe canonique basée sur le principe de l'étude paramétrique a d'abord été proposée. Cette approche simple s'avère adaptée aux systèmes univariés ou au maximum bivariés, mais souffre d'une expressivité limitée pour les problèmes plus complexes où l'on considère un plus grand nombre d'entrées aléatoires et une plus grande gamme de variabilité.

Après cela, nous avons étudié une méthodologie statistique avancée basée sur le HLARS-PCE, qui est plus robuste et plus efficace sur le plan des calculs pour traiter les problèmes de gamme multivariée et de variabilité plus élevée. Cette approche a été appliquée à un dipôle déformable canonique (avec 3 paramètres d'entrée, à savoir l'étirement, la flexion et la torsion) pour démontrer son efficacité. Ensuite, la méthodologie a été encore améliorée/améliorée, notamment en prenant en compte le comportement en fréquence et en exploitant l'extrême parcimonie. L'approche améliorée a été testée sur une antenne patch textile réaliste (avec 4 paramètres aléatoires géométriques et la fréquence comme paramètre « aléatoire » supplémentaire) pour lesquels des métamodèles précis et robustes ont été obtenus, ce qui confirme son efficacité en termes d'efficacité, robustesse et évolutivité. Les métamodèles ainsi obtenus ont été mis en œuvre dans plusieurs environnements de propagation locaux classiques (réalisés avec le modèle WINNER2/+) pour démontrer leur utilité pratique pour la modélisation conjointe canal/antenne et l'analyse précise des liaisons radio.

Une méthodologie statistique a également été proposée pour modéliser le coefficient de réflexion en fonction de la fréquence des antennes variables. Cette approche vise à représenter de manière parcimonieuse le coefficient de réflexion au moyen de certaines techniques d'identification (par exemple, fitting polynomial, fonctions rationnelles), avant la modélisation statistique par le biais du HLARS-PCE. Cette approche a montré une bonne efficacité pour les antennes NB.

Nous pensons que notre méthodologie proposée peut être bénéfique pour différents types d'analyses, notamment lorsque les connaissances complètes (notamment la polarisation, l'amplitude et la phase du champ, ainsi que le coefficient de réflexion) sont obligatoires pour l'antenne étudiée. De tels contextes d'application comprennent, par exemple, la modélisation conjointe d'antennes et de canaux directionnels, les simulateurs asymptotiques enfichables dans l'antenne (par exemple, ray tracing), l'analyse de liaisons radio de bout en bout, la caractérisation de systèmes MIMO ou les conceptions de formation de faisceau, etc.

Perspectives

En ce qui concerne les perspectives de recherche, d'une part, nous étudions des antennes textiles plus flexibles. Cela comprend trois parties : premièrement, la technologie de fabrication, pour laquelle nous n'avons pas trop d'expérience, et nous testons maintenant certains matériaux textiles conducteurs disponibles dans le commerce, tels que les deux prototypes présentés par Figure 23; d'autre part, nous devrions développer des méthodes plus fiables pour la quantification de la distribution des paramètres aléatoires, en particulier lorsqu'il existe de fortes corrélations entre les paramètres aléatoires. Et nous devrions faire très attention lors de l'hypothèse sur la distribution conjointe, ce qui n'est évidemment pas

une tâche facile. Troisièmement, appliquer l'approche de modélisation statistique pour l'extraction du modèle de substitution.

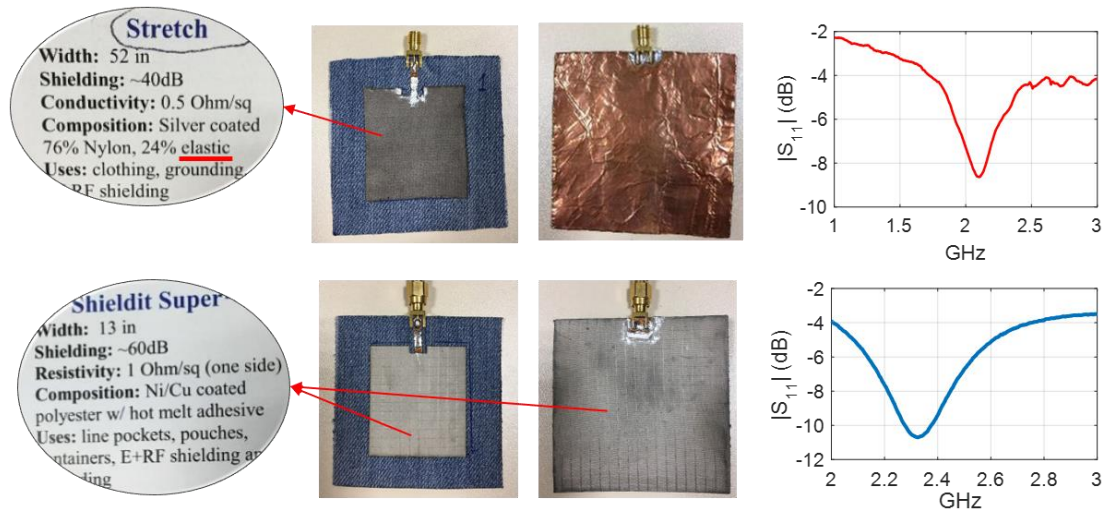


Figure 23: deux types d'antennes textiles sous investigation.

D'un autre côté, nous allons inclure les effets aléatoires de proximité corporelle dans notre modèle de substitution, ce qui est particulièrement indispensable pour les antennes à profil bas qui n'ont pas de plan de masse de protection, telles que les antennes IIFA, Figure 24.

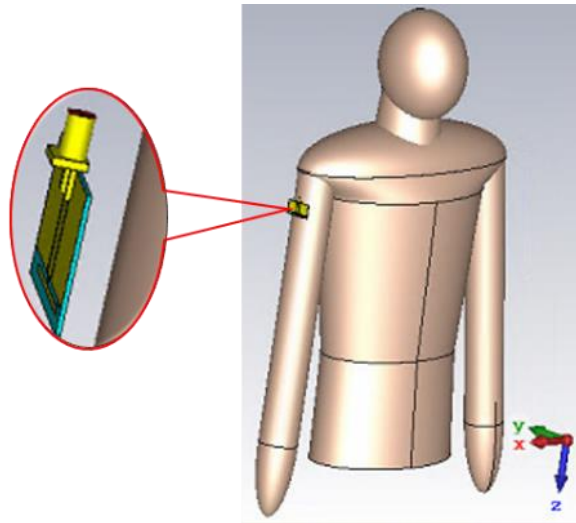


Figure 24: Modélisation de l'effet du corps sur une antenne de type IIFA.



Analyse et modélisation statistique d'antennes souples ou flexibles dans des conditions fluctuantes

RESUME : Avec le déploiement massif des électroniques flexibles dans le contexte de l'Internet des objets et des réseaux corporels sans fil, la demande d'antennes souples ou flexibles est amenée à se développer. Contrairement aux antennes traditionnelles non déformables ou clairement isolées dont les caractéristiques sont déterministes, les antennes souples/flexibles, en particulier lorsqu'elles sont mises en œuvre dans des conditions fluctuantes, sont sujettes à divers types de variabilité par essence aléatoires : déformations géométriques, variations dans les propriétés des matériaux, interactions avec l'environnement proche (par ex. le corps humain), etc. Ces incertitudes aléatoires peuvent perturber significativement les performances *in situ* des antennes et doivent être prises en compte quantitativement. La caractérisation de ces effets aléatoires ne peut être efficacement réalisée au moyen de l'approche conventionnelle de "simulation électromagnétique – prototypage – mesure" en raison de son coût très élevé (pour chacune de ces étapes). Dans ce contexte, des modèles de substitution qui permettent de prédire efficacement ces effets aléatoires avec une bonne précision sont excessivement utiles. Ce mémoire de thèse se concentre sur l'étude des méthodologies efficaces dédiées à la construction des modèles de substitution pour les antennes subissant des déformations aléatoires. Deux objectifs principaux sont visés. D'une part, décrire quantitativement et parcimonieusement le comportement *complet* des antennes, c'est-à-dire le champ lointain rayonné ainsi que le coefficient de réflexion. D'autre part, proposer des méthodologies efficaces, fiables et polyvalentes pour l'extraction de modèles d'antennes à partir d'un nombre limité de pré-évaluations. Notamment, une méthodologie statistique fondée sur le chaos polynomial a été proposée et son efficacité a été démontrée en l'appliquant tout d'abord à une antenne canonique subissant divers types de déformations, puis à une antenne imprimée sur substrat en tissu dans un cadre applicatif plus réaliste. L'intérêt des modèles de substitution ainsi développés est de pouvoir disposer de réponses « d'antennes aléatoires » pour un très faible coût de calcul. Du point de vue applicatif, cela permet de les utiliser dans divers types d'analyses de niveaux supérieurs telles que la modélisation conjointe antenne/canal, puis celle du lien radio, l'intégration des antennes dans les simulateurs asymptotiques (lancé ou tracé de rayons), la caractérisation des systèmes Multi-entrée & Multi-sortie, ou la formation de faisceaux.

Mots clés : antennes souples/flexibles, antennes déformables, modèles de substitution, modélisation statistique d'antennes, harmoniques sphériques vectorielles, polynômes de chaos.

Statistical analysis and modeling of soft or flexible antennas in fluctuating conditions

ABSTRACT: With the massive deployment of flexible electronics in the context of Internet of Things (IoT) and wireless body area networks (WBANs), the demand for soft or flexible antennas is substantially growing. Unlike traditional non-deformable or clearly isolated antennas whose characteristics are deterministic, soft/flexible antennas, especially when they are implemented in fluctuating conditions, are subject to various types of variability by essence random: geometric deformations, variations in the material properties, interactions with the surrounding environment (e.g. the human body), etc. These random uncertainties can significantly disturb the *in situ* performance of antennas and must be taken into account quantitatively. The characterization of these random effects cannot be effectively achieved using the conventional "electromagnetic simulation - prototyping - measurement" approach because of its very high cost (for each of these steps). In this context, surrogate models which can effectively predict these random effects with good precision are extremely useful. This dissertation focuses on the investigation of efficient methodologies dedicated to the construction of surrogate models for antennas undergoing random uncertainties. Two main objectives are targeted. On the one hand, describe quantitatively and parsimoniously the *overall* behavior of the antennas, that is to say, the *complete* radiated far-field (FF) as well as the reflection coefficient. On the other hand, propose efficient, reliable and versatile methodologies for the extraction of antenna models from a limited number of pre-evaluations. In particular, a statistical methodology based on polynomial chaos has been proposed and its effectiveness has been demonstrated by applying it firstly to a canonical antenna undergoing various types of deformations, then in a more realistic application framework, to an antenna printed on a fabric substrate. The benefit of the surrogate models thus developed is to have access to the responses of the "random antennas" at a very low calculation cost. From the application point of view, such surrogate models can be used in various types of higher-level analysis such as joint antenna/channel modeling, radio links analysis, antenna plugged-in asymptotic simulators (e.g. ray launching or tracing), Multi-Input & Multi-Output (MIMO) systems characterization, or beamforming.

Keywords: soft/flexible antennas, deformable antennas, surrogate models, statistical modeling, vector spherical harmonics, polynomial chaos.